Doctoral Dissertations

Fall 2006

Fluorescent enzymatic smart tattoos comprising hybrid silicate microparticles, metalloporphyrin complexes, and mass transport-limiting nanofilms

Erich Wayne Stein
Louisiana Tech University

FLUORESCENT ENZYMATIC SMART TATTOOS COMPRISING HYBRID

SILICATE MICROPARTICLES, METALLOPORPHYRIN COMPLEXES, AND

MASS TRANSPORT-LIMITING NANOFILMS

by

Erich Wayne Stein, B.S. Biomedical Engineering

A Dissertation Presented in Partial Fulfillment
of the Requirements for the Degree
Doctor of Philosophy

COLLEGE OF ENGINEERING AND SCIENCE
LOUISIANA TECH UNIVERSITY

November 2006

UMI Number: 3261295

INFORMATION TO USERS

The quality of this reproduction is dependent upon the quality of the copy submitted. Broken or indistinct print, colored or poor quality illustrations and photographs, print bleed-through, substandard margins, and improper alignment can adversely affect reproduction.

In the unlikely event that the author did not send a complete manuscript and there are missing pages, these will be noted. Also, if unauthorized copyright material had to be removed, a note will indicate the deletion.

UMI®

UMI Microform 3261295

Copyright 2007 by ProQuest Information and Learning Company.

All rights reserved. This microform edition is protected against unauthorized copying under Title 17, United States Code.

ProQuest Information and Learning Company
300 North Zeeb Road
P.O. Box 1346
Ann Arbor, MI 48106-1346

LOUISIANA TECH UNIVERSITY

THE GRADUATE SCHOOL

August 28, 2006
<div align="right">Date</div>

We hereby recommend that the dissertation prepared under our supervision
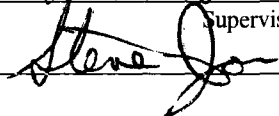
by Erich W. Stein

entitled   Fluorescent Enzymatic Smart Tattoos Comprising Hybrid Silicate Microparticles,

Metalloporphyrin Complexes, and Mass Transport Limiting Nanofilms

be accepted in partial fulfillment of the requirements for the Degree of

Doctor of Philosophy in Biomedical Engineering
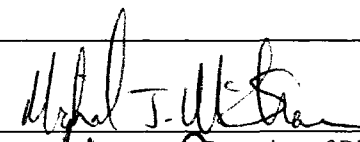
<div align="right">Supervisor of Dissertation Research</div>

<div align="right">Head of Department</div>

Biomedical Engineering
<div align="right">Department</div>

Recommendation concurred in:

Advisory Committee

Approved:

Director of Graduate Studies

Approved:

Dean of the Graduate School

Dean of the College

<div align="right">GS Form 13
(5/03)</div>

ABSTRACT

Diabetics are often required to self-monitor blood glucose levels to effectively deliver prescribed therapies. However, the pain and bother associated with traditional finger-prick measurements often result in decreased patient compliance and therefore poor disease management, which could result in the early-onset of complications. Enzymatic "smart tattoos" – implantable luminescent particles that may be transdermally interrogated with light – are being pursued as minimally-invasive diabetic monitoring devices, with hopes of increasing diabetic compliance by reducing excessive pain and bother associated with finger-prick measurements. These devices typically comprise an oxygen-quenched luminescent dye and glucose oxidase (GOx), an enzyme that catalyzes the oxidation of β-D-glucose. Under glucose-limited reaction conditions, local glucose concentrations can be extracted from oxygen-dependent emission spectra or luminescence lifetimes.

Previously, enzymatic smart tattoos comprising enzyme-doped alginate hydrogel microsphere sensors and ruthenium complexes as oxygen indicators were reported. In this dissertation, however, the integration of a more sensitive metalloporphyrin oxygen indicator, Pt(II) Octaethylporphine (PtOEP), and the reference probe, Rhodamine B Isothiocyanate (RITC), into enzyme-doped alginate-modified silica ("algilica") particles is presented. A particularly important feature of these sensors is the shift from traditional

ruthenium-based oxygen indicators to metalloporphyrin complexes, due in part to higher excitation wavelengths which reduce the effects of tissue scatter and absorption, increased photostability, and higher oxygen sensitivity. Using the novel algilica matrix and diffusion-limiting nanofilms, glucose sensitivities of two orders of magnitude greater than ruthenium-based enzymatic smart tattoos were achieved with porphyrin oxygen indicators. Of central importance was the demonstration that surface adsorbed polyelectrolyte nanofilms allowed glucose sensitivity and range to be controlled by modulating substrate flux into the sensor, resulting in sensitivities (change in intensity ratio) of $1 - 5$ %/mg dL^{-1} and upper range limits of $90 - 250$ mg/dL. Remarkably, it was shown that nanofilms only 12 nanometers thick could significantly affect response behavior, confirming theoretical predictions based on models of reaction-diffusion kinetics.

To approach clinical utility, implantable smart tattoos must maintain appropriate function for at least 6 months. Therefore, to examine the effects of long-term operation on sensor function, a mathematical model was developed and the output validated with experimental results. Both theoretical and experimental results demonstrated limited device lifetime ($\sim$ 90 % loss of sensitivity over 24 hours) due to enzyme inactivation resulting from hydrogen peroxide, a byproduct of glucose oxidation. To improve long-term stability, a first-generation bi-enzymatic smart tattoo prototype was constructed via the co-incorporation of catalase, an enzyme that consumes hydrogen peroxide, which enhanced response stability two fold over time. Furthermore, to design clinically viable implantation schemes, it is important to understand how individual sensors within a population contribute to overall response properties. Thus, an imaging technique was

developed to perform real-time ratiometric imaging of individual sensor function. The results indicated significant differences in sensor behavior depending on location within the sensor population and/or physical parameters, as expected. These findings demonstrate the feasibility of engineering highly sensitive enzymatic-based glucose sensors and lay the groundwork for developments of additional enzymatic analyte sensors.

APPROVAL FOR SCHOLARLY DISSEMINATION

The author grants to the Prescott Memorial Library of Louisiana Tech University the right to reproduce, by appropriate methods, upon request, any or all portions of this Dissertation. It is understood that "proper request" consists of the agreement, on the part of the requesting party, that said reproduction is for his personal use and that subsequent reproduction will not occur without written approval of the author of this Dissertation. Further, any portions of the Dissertation used in books, papers, and other works must be appropriately referenced to this Dissertation.

Finally, the author of this Dissertation reserves the right to publish freely, in the literature, at any time, any or all portions of this Dissertation.

Author _____

Date _____10 | 20 | 06_____

DEDICATION

To Amber, my loving wife, who has sacrificed so much to allow me to pursue my dream. To her, I am eternally grateful.

TABLE OF CONTENTS

LIST OF TABLES

LIST OF FIGURES

ACKNOWLEDGMENTS

I would like to thank my mentor, Dr. Michael J. McShane, for providing his students with an excellent atmosphere to grow professionally, as well as his selfless dedication in helping me reach my individual goals. Additionally, Drs. Patrick Grant, Huiguang Zhu, and Quincy Brown are thanked for their help and support throughout my years at Louisiana Tech. Dr. Grant is further acknowledged for developing the software used to run the dynamic testing apparatus. Dr. Zhu is also acknowledged for the initial development of algilica microparticles. Mr. Dustin Ritter is gratefully acknowledged for the design and fabrication of the microfluidic flow cell. Additionally, Mr. Scott Williams is acknowledged for his expertise in fabrication and arrangement of facility needs. I would also like to acknowledge financial support from the National Institutes of Health (RO1 EB000739-022). And last but certainly not least, I would like to thank my wife Amber, my parents Wayne and Valery Stein, brother Taylor, sister Lindsey, future brother-in-law Matthew Craig, parents-in-law Anthony and Amy Termine, brother-in-law Jared, and my sister-in-law Lauren, without whose continuous support this would have not been possible.

CHAPTER 1

INTRODUCTION

In the United States alone, it is estimated that 20.8 million or 7% of residents are afflicted with *diabetes mellitus*, a group of diseases characterized by hyperglycemia (blood glucose levels greater than 180 mg/dL) elicited from defects associated with insulin secretion, insulin action, or both.[1] Depending on the underlying cause of hyperglycemia, patients are diagnosed as either Type 1 or Type 2 diabetics.

Type 1 diabetes results from the progressive destruction of pancreatic beta cells – the cells responsible for producing insulin, the hormone responsible for regulating blood glucose levels. Beta cell destruction eventually results in absolute insulin deficiency, thus eliminating the body's natural ability to counteract elevations in glucose levels.[2] Approximately 5% of Type 1 diabetes results from idiopathic origins, conditions in which there is no known etiology for beta cell destruction.[2, 3] However, the most common form of Type 1 diabetes arises from autoimmune-mediated destruction of pancreatic beta cells. Since the peak incidence of Type 1 diabetes occurs in childhood and adolescence, it is commonly referred to as "juvenile-onset diabetes", and accounts for 5% to 10% of all diagnosed cases.[1] As with both classifications of Type 1 diabetes, afflicted individuals eventually become completely dependent on supplemental insulin for survival as the disease progresses.

1

The most commonly diagnosed type of diabetes mellitus is Type 2 diabetes, accounting for 90% to 95% of all cases.[1] Two common classifications of Type 2 diabetics exists: patients who have predominant insulin resistance with relative insulin secretion deficiency, and those with predominant insulin secretion deficiency with or without insulin resistance.[2] Although the exact cause of Type 2 diabetes is unclear, it is well documented that certain factors such as race, age, diet, physical activity, and family history play an important role in disease onset.[4, 5] Since the onset of Type 2 diabetes is commonly observed in adults, this classification is commonly referred to as "adult-onset diabetes"; however, an escalation in adolescent and childhood obesity has resulted in an increased frequency of Type 2 diabetes diagnoses in younger age groups.[6] Commonly, Type 2 diabetics can control their blood glucose levels by following a healthy lifestyle (e.g. healthy diet and exercise regime) and taking prescription medications; however, in some instances, supplemental insulin may be required.[7]

In both variants of diabetes, a clinical trial proved that proper care and management of blood glucose levels is critical in preventing or delaying the progression of complications, which include cardiovascular disease, stroke, hypertension, retinopathy, nephropathy, neuropathy, periodontitis, gingivitis, cataract formation, and pregnancy complications.[2, 8] Through proper management of diabetes, it is estimated that the patient will experience an additional 5 years of life, 8 years of sight, 6 years free of kidney disease, and 6 years free from amputations.[9] In 2002, it was estimated that diabetes costs in the United States alone totaled $132 billion – $92 billion attributed to direct medical costs and $40 billion attributed to indirect costs such as disability, work loss, and premature mortality – the majority due to complications.[10] Therefore, to reduce

complications, diabetics must effectively manage blood glucose levels using one or more of the following therapies: changing high-risk lifestyle habits, consuming prescription medications, and administering supplemental insulin.[7] However, to effectively manage therapy dosages, particularly supplemental insulin, patients must frequently and accurately assess blood glucose levels.

Currently, the gold-standard method for self-monitoring blood glucose levels is the "finger-prick" test, which involves lancing the skin and extracting a blood sample that is subsequently placed in a portable device to extract glucose levels. This method, although proven highly accurate, is both painful and bothersome for the patient, especially if the recommended testing frequency – at least 3 times per day – is practiced.[7] However, according to several studies, only 40% of diabetics requiring insulin therapy and 5% of diabetics requiring prescription medications monitor their blood glucose levels at least once per day, citing excessive pain and inconvenience as the principle reason for lack of compliance.[11-13] Therefore, it is reasonable to conclude that the development of a simple and painless method would increase patient observation of the recommended self-monitoring guidelines, which in turn would reduce overall complications. The development of a minimally or non-invasive technique which can provide continuous and spot measurements has long been considered one of the "holy grails" of diabetes research.[14] This dissertation is concerned with the development of a minimally-invasive device which could potentially be used to provide diabetics a means to painlessly monitor glucose levels while observing the recommended measurement frequency.

1.1 Current and Future Trends in Continuous Glucose Monitoring Technology

Traditional spot measurements using the standard finger-prick technique involve lancing the skin and collecting a small volume of blood for *ex vivo* analysis in a portable hand-held device that indirectly determines glucose levels through electrochemical or photometric analysis.[15] The blood is drawn into a test strip that contains the redox enzyme glucose oxidase (GOx), which catalyzes the oxidation of glucose into hydrogen peroxide and gluconic acid as indicated in the following reaction:

$$glucose + O_2 \xrightarrow{\text{GOx}} gluconic\ acid + H_2O_2$$
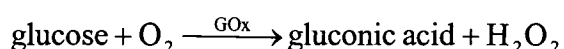
In electrochemical based systems, the redox current produced from glucose oxidation is measured by an electrode. Since the redox current is directly proportional to the concentration of glucose present, the measured current is easily converted into actual blood glucose levels and displayed on the device. In photometric monitoring systems, the oxidation of glucose is monitored through a colorimetric assay, whose proportional change in color intensity is used to determine glucose levels. Although the sensing schemes have been insignificantly changed throughout the last decade, current trends in measurement device technology center on minimizing the volume of blood needed to perform a measurement, allowing alternative site testing (forearm, thigh, and abdomen instead of the fingertip) and easing data interpretation with built-in databases and trend trackers.[16]

Minimally- or non-invasive monitoring techniques that completely replace finger-pricking are not yet commercially available; however, several manufacturers have introduced continuous monitoring systems which reduce lancing frequency.[17] Though these devices determine glucose levels via electrochemical or photometric analysis, they

employ minimally-invasive means to continuously extract interstitial glucose without frequent lancing. One class of these devices uses the principle of reverse iontophoresis, which drives the transdermal transport of uncharged molecules such as glucose from the interstitium into a wrist-worn monitoring system through the application of a small current.[18] Another class of continuous glucose monitoring systems involves the subcutaneous implantation of an electrochemical electrode into the abdomen. A redox current is continuously obtained from the electrode and sent to an external read-out device in which the glucose levels are continuously displayed. An additional class of minimally-invasive monitoring devices uses the principle of microdialysis to transport interstitial glucose to an external device. In this device, a microscale semipermeable membrane-bound container is implanted into the subcutaneous tissue. Over time, glucose diffuses from the interstitium into the membrane and is continuously transported by a fluidic current to an external device, where the glucose levels are electrochemically determined. Although these devices do indeed minimize lancing and provide useful information on metabolic trends, frequent calibrations rely on finger pricking to ensure continued accuracy; therefore, these devices are not intended to completely supplement traditional spot measurements. Additionally, all of the devices discussed above require a direct transdermal connection to the implant, thus providing a potential infection pathway as well as dermal irritation and constant replacement of the sensing element. Therefore, the current status of commercially available minimally-invasive technology leaves much to be desired.

On the other hand, optical monitoring techniques, including fluorescence,[19] absorbance,[20] raman,[21] and polarization spectroscopy[22] have been heavily researched as a

minimally-invasive means to measure glucose levels, but the high sensitivity and selectivity associated with fluorescence-sensing techniques have led to increased interest by many groups.[19] A particularly interesting technique which has the potential to provide both spot and continuous measurements of glucose levels are "smart tattoo" type sensors, which consist of micron-scale glucose-sensitive luminescent particles that could be implanted into the dermis and transdermally interrogated with light.[23-26] Most of the work in this field has primarily focused on the development of competitive binding-based assays, which rely on changes in fluorescence emission properties modulated by fluorescence resonance energy transfer (FRET) to optically transduce glucose levels.[27-31] FRET is driven through the competitive binding of a fluorescent ligand and analyte to receptor sites on lectins, glucose-binding proteins, or deactivated glucose-specific enzymes, such that the ligand is displaced from the receptor when in the presence of the analyte causing measurable changes in emission spectra.[32, 33] However, recent successes with enzymatic-based smart tattoo sensors have also been reported, and this work has aimed to further extend smart tattoo variants for use in diabetic monitoring.[26]

Enzymatic-based smart tattoo sensors are typically comprised of an oxygen-quenched luminescent dye and GOx entrapped within a microscale container. As glucose diffuses into the sensor, local oxygen levels are proportionally reduced through GOx-initiated catalysis. The glucose-dependent oxygen levels are then relayed through the fluorescence emission of the oxygen reporter, providing an indirect means to monitor glucose levels.[34] Although the integration of GOx into the sensing scheme provides innate selectivity to the sensor as well as reversibility, controlling the reaction-diffusion kinetics of both glucose and oxygen are key to the realization of optimized sensors.[35]

Initial work in this field was done using optical fibers with sensor components immobilized in transport limiting matrices.[36-38] While these devices exhibit desirable sensor properties, in practice they would require a permanent connection to external measurement devices, providing a potential infection pathway. Additional work showed that sensor components immobilized within nano-scale polyacrylamide particles reversibly responded to physiological glucose levels.[39] Brown et al. advanced the concept using calcium alginate hydrogel microspheres, which contained GOx, an oxygen-quenched ruthenium compound, and diffusion-limiting nanofilms adsorbed to the surface using layer-by-layer self-assembly.[26, 40, 41] By altering the physical properties of the nanofilms, the analyte transport properties into the microsphere could be altered, resulting in control of overall response characteristics, such as sensitivity and linear range.[41] Although the results reported to date are promising, the majority of work has focused on using phosphorescent ruthenium complexes as the reporter molecules, which have a lower sensitivity than other oxygen probes, such as phosphorescent metalloporphyrins.[37, 42, 43,44]

Since the overall response properties of enzymatic smart tattoo sensors depend upon the oxygen probe, it is hypothesized that the integration of a more sensitive Pt(II) porphyrin dye should result in an overall increase in sensitivity to glucose. To our knowledge there has only been one report utilizing Pt(II) porphyrins in enzymatic glucose sensors.[37] The lack of work with porphyrin indicators could be due to extreme hydrophobicity, causing difficulties in aqueous applications.[43] To overcome this difficulty, researchers have since developed immobilization matrices comprised of silicon, organic glassy, cellulose derivative, or fluoro-polymers, to which Pt(II)

porphyrins can be adsorbed, thereby allowing dissolved oxygen measurements in aqueous environments.[44, 45] It is well documented that the immobilization matrix can drastically affect the oxygen sensitivity and that silica-containing matrices produce high sensitivities, although the exact mechanisms are still debated.[42, 46] We recently developed a simple method to self-assemble mesoporous silicate particles comprised of homogeneously distributed hydrophilic and hydrophobic domains using a model hydrophilic polymer, sodium alginate. These particles have been developed as an immobilization matrix for enzymatic smart tattoo sensor components and will be used exclusively in this work. Therefore, *the central hypotheses of this work are that the co-immobilization of GOx and metalloporphyrin complexes into a silicate matrix would produce highly sensitive enzymatic smart tattoos, and the adsorption of polyelectrolyte nanofilm to the surface would allow sensor behavior to be controlled by modulating substrate flux into the catalytic region of the sensor.*

1.2 Objectives and Novel Aspects

This work represents an advancement of the technology required in the development of improved enzymatic-based smart tattoo sensors. In this dissertation, the design of enzymatic smart tattoos based on highly sensitive metalloporphyrin (PtOEP) oxygen indicators and novel silicate microstructures is presented. A simple method to self-assemble mesoporous silicate particles comprised of homogeneously distributed hydrophilic and hydrophobic domains, so-called hybrid structures, was developed for use as an immobilization matrix for GOx and PtOEP. Fluorescent nanofilms were adsorbed to the surface to provide an oxygen insensitive reference signal as well as to control analyte diffusion, allowing modulation of sensor response properties. The development

of this technology was pursued due in part to recent successes reported with a similar system utilizing less sensitive oxygen indicators and a hydrophilic matrix, [26] as well as the interesting and complex engineering required to produce a working prototype. This approach was also selected partly because of the innate selectivity and reversibility associated with an active enzymatic assay, avoiding early problems associated with affinity-binding FRET assays. Additionally, a straightforward approach to directly immobilizing enzymes to the sensor substrate can be utilized, whereas in affinity-binding assays, the assay components must be allowed to move relative to each other, thus complicating immobilization/encapsulation.

Therefore, the major objectives of this work include the development of immobilization strategies for PtOEP within algilica microspheres, characterization of oxygen sensitivity, development of co-immobilization strategies for PtOEP and GOx within algilica microspheres, characterization of glucose sensitive response properties, use of polyelectrolyte nanofilms to tailor glucose response properties, development of a mathematical model to simulate continuous sensor operation, the assessment of long-term sensor function, and development of an imaging technique to allow real-time imaging of sensor function.

For all the work described herein, Dr. Huiguang Zhu developed the initial protocol used to prepare the algilica microparticles and in conjunction with the author, assisted in modifying protocols to achieve the desired particle characteristics. Additionally, a substantial contribution was made by Dr. Patrick S. Grant in the development of custom software to efficiently control the testing apparatus used to perform dynamic glucose sensitivity experiments. Also, Mr. Dustin Ritter is credited for

microchannel fabrication used to conduct real-time ratiometric imaging of sensor function.

The novel contributions of this work to the field of engineering and science includes the co-development of the novel immobilization matrix used in this dissertation – algilica, whose unique properties readily allow immobilization of by hydrophilic and hydrophobic species. Additionally, this work demonstrates the ability to engineer device sensitivity and analytical range by simply adjusting the thickness of surface-adsorbed nanofilm coatings to modulate substrate transport. As a key concept, these results demonstrate the utility of polyelectrolyte nanofilms to control molecular transport properties, a concept which could be broadly applicable to situations requiring the precise regulation of transport, such as filtration systems. Also, the development of a mathematical model to simulate the effect of continuous operation on sensor lifetime was presented, the results of which could be applied to other catalytic systems by simply adjusting boundary conditions, geometries, and reaction kinetics. A technique was also developed to allow real-time observation of sensor operation using microfluidics and real-time ratiometric imaging, a tool which could prove to be useful for universal imaging applications.

It should be noted that the implications of this work extend well beyond that of glucose monitoring technology by laying the foundation for the development of additional highly sensitive biochemical monitors, which may be obtained by simply integrating other enzyme species specific to the target analyte. It is hoped that these devices may be integrated into minimally-invasive diabetic monitoring systems, allowing

diabetics to perform continuous and spot measurements of blood glucose levels without the pain and bother associated with "finger pricking."

1.3 Organization of Chapters

The chapters of this dissertation have been organized such that the disseminated material is presented in a clear and organized manner. Furthermore, several chapters are, of themselves, manuscripts that will be submitted for publication or are already in print. Chapter 2 gives an in-depth survey of currently available minimally-invasive monitoring devices as well as state-of-the art technologies still under development, with particular emphasis on optical-based sensing techniques, luminescent oxygen indicators, and mass transport limiting materials. Chapter 3 characterizes the performance of algilica-based metalloporphyrin oxygen sensors. Chapter 4 describes the development and characterization of glucose sensor prototypes. In Chapter 5, a mathematical model describing sensor deactivation kinetics is presented and the results subsequently compared with those experimentally obtained. Additionally, an alternative sensing scheme that could potentially increase sensor lifespan is presented. Chapter 6 describes the design and fabrication of a microfluidic flow cell to be used in the real-time ratiometric imaging of sensor function under dynamic conditions. Chapter 7 concludes the work presented in this dissertation and discusses the implications of this work in the context of the current state of the art, as well as detailing future work.

CHAPTER 2

BACKGROUND AND THEORY

In the work presented here, micro-scale glucose sensors are being pursued as a minimally-invasive diabetic monitoring technology. These devices function by optically reporting oxygen levels within the sensor as an indirect means to detect glucose levels. Ultimately, these devices are envisioned to be implanted into the dermis of diabetics, where transdermal optical interrogation/collection would allow painless acquisition of glucose levels, the so-called "smart tattoo." Given that these devices rely on knowledge of several major fields – namely optics, material science, and enzymatics – it is important to understand previous research contributions in the context of this work.

Therefore, in this chapter, a review of the operating principles of commercially available minimally-invasive glucose monitors is presented. More important, a review of current state-of-the-art optical monitoring technologies under development is given, with particular emphasis on enzyme-based fluorescence-sensing techniques. Also, the fundamentals of skin optics are presented, along with a detailed discussion on previously used diffusion-limiting materials and luminescent oxygen indicators.

12

2.1 Commercially Available Continuous Glucose Monitoring Systems

In this section, the literature on commercially available continuous glucose monitoring systems is reviewed and classified according to operating principle. This survey will consider only continuous monitoring systems classified by the FDA as minimally-invasive, which includes devices that breach the skin barrier but do not disrupt underlying vasculature.

2.1.1 Reverse Iontophoretic Sampling

To date, the only continuous monitoring system employing reverse iontophoretic sampling is the GlucoWatch® Biographer, a device worn on the arm or forearm of a patient and similar in appearance to a wrist watch. On the underside of the device lies an anode and cathode which upon application of a constant current source drives the convective transdermal transport of uncharged, polar species into the device.[18] More specifically, the applied potential causes the migration of positive counterions, namely Na^+, from the interstitium to the cathode. Cationic migration ultimately results in the convective flow (termed "electro-osmotic flow") of uncharged species such as glucose between the anode and cathode, such that the transdermal glucose flux is proportional to that in the interstitium (Figure 1).[47-49]
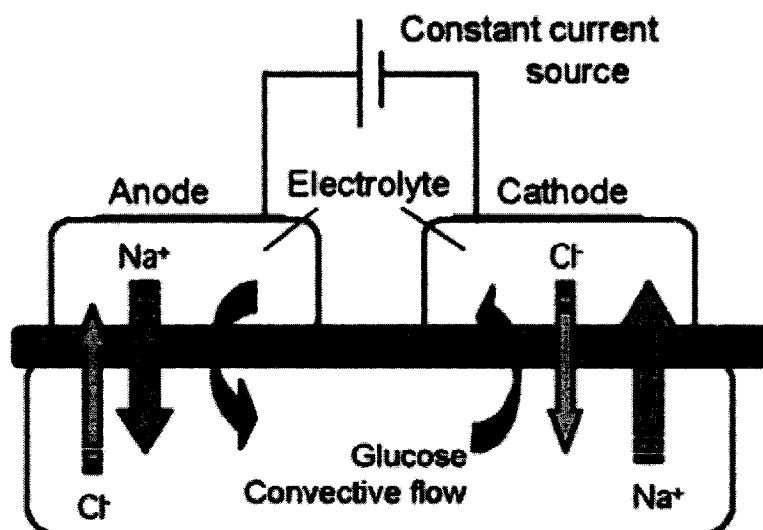
Figure 1. Transdermal extraction of glucose using reverse iontophoresis. Counterion ion transport induces convective flow of glucose into the cathode sampling chamber. Taken from Sieg et al.[47]

In this device, reverse iontophoresis is merely the sampling technique used to extract the interstitial fluid; therefore, a sensor is required to analyze glucose levels. Glucose levels are determined in the cathode sampling chamber, which houses a replaceable sensor. A glucose oxidase-coated platinum electrode comprises the replaceable sensor, whereby the redox current resulting from glucose catalysis is used to determine interstitial glucose levels.[48] It is noteworthy to state that the concentration of glucose extracted is in the μM range, approximately 3 orders of magnitude less than those observed in the interstitium; therefore, a highly sensitive detection assay is required and is supplied by the electrochemical sensor described above.[50]

The latest version of the GlucoWatch® Biographer, the G2, allows up to 13 hours of continuous monitoring, during which continuous measurements are displayed every 10 min – 3 min to extract the fluid and 7 min to determine glucose concentration. To ensure accuracy, it is recommended that the sensor be replaced every 13 hours and the device be

recalibrated with standard finger-prick measurements. Following sensor replacement, the device requires a 2 hour "warm up" period, during which residual glucose from the epidermis is removed.[51]

Several problems traditionally associated with electrochemical sensors are avoided in this device. Since glucose and oxygen are both required for glucose oxidation to proceed, the reaction must operate in a glucose-limited regime to obtain a signal directly proportional to glucose concentration. In this device, the sensor is exposed to atmospheric oxygen levels relatively greater than those of the interstitial fluid, allowing glucose-limited operation. Additionally, electrode fouling is greatly reduced since high molecular weight species, such as protein and other macromolecules, are prevented from contacting the sensing membrane by dermal filtering. Also, other electrochemically active components extracted are collected in the anode, thus preventing interference with glucose measurement, which occurs at the cathode.[47, 50]

Although this device has been shown to be fairly accurate (the mean error relative to standard measurements was determined to be 7%) and its technology indeed impressive, the diabetic community has not fully accepted it for the following reasons: (1) an extensive amount of data is generated, which could intimidate users; (2) frequent sensor replacements and blood-draw calibrations are necessary to achieve true continuous monitoring; (3) mild skin irritation can result from the applied current necessary to extract interstitial fluid; (4) excessive perspiration prevents operation; and (5) the expense of the device has severely limited its adoption to a select few. All these pitfalls, combined with reports that hypoglycemic events could be overlooked,[48] have severely limited the mass market appeal of the GlucoWatch® G2 Biographer. A device requiring

fewer finger-prick calibrations and sensing electrode replacements would be a substantial improvement.

2.1.2 Implanted Electrochemical Element

To date, most commercially available continuous monitoring systems use a subcutaneously implanted electrochemical sensor to relay glucose levels to an external device. The first FDA approved continuous monitoring system, the Continuous Glucose Monitoring System (CGMS®) Standard Gold produced by Medtronic, is one such device.[16] In this device, a healthcare provider inserts a needle-type electrochemical sensor into the subcutaneous layer of the abdominal wall. Glucose concentrations are extracted and subsequently stored in an external device.

The sensing element provides 72 hours of continuous operation before necessary replacement due to operational degradation resulting from biofouling. Glucose levels are continuously determined and averaged over subsequent 5 min intervals to provide a mean value. Although the sensor lifespan is indeed greater than that of the GlucoWatch®, the CGMS Standard Gold requires 12 blood-draw calibrations (4 per day) throughout the sensors operational lifespan to ensure accuracy.[51] This device also requires a 2 hour warm up period for reasons similar to those described above. Furthermore, reports have characterized suboptimal performance of the CGMS Standard Gold in accurately detecting hypoglycemic excursions.[52]

It is noteworthy to state that this device does not provide real-time measurements to the patient but instead stores them for future retrospective analysis that is performed by a healthcare professional. Therefore, this device is not intended to provide patients with real-time read-outs of glucose levels or completely supplement blood-draw

measurements, but is instead intended to "fill in the gaps" between traditional measurements and allow careful analysis of metabolic trends throughout the 72 hours of usage. Following the end of the testing period (72 hours), the patient returns to the healthcare provider, where the stored data are extracted and the trends analyzed.

In 2004, Medtronic was granted FDA approval to market the Guardian® RT, a doctor-prescribed, patient-owned device.[51] This device encompasses the exact sensing element as the CGMS® Standard Gold and therefore operates using the same electrochemical scheme.[52] However, several key features differentiate the Guardian® RT from the CGMS® Standard Gold. First, The Guardian® RT provides real-time glucose level read-outs to the patient and audible alarms to alert oncoming hypo- or hyperglycemic excursions, allowing the patient to take immediate corrective action. Additionally, the Guardian® RT employs a small external radiofrequency transmitter to wirelessly convey glucose levels to the monitor, reducing the possibility of inadvertent sensor removal. Although these advances do increase the user-friendliness of this system, the Guardian® RT shares similar shortcomings as the CGMS® system, including the requirement of frequent blood-draw calibrations, limited sensor lifetime, and a potential pathway for infection.

In summer 2006, Medtronic also made plans to release a complete closed-loop system, the Paradigm® REAL-Time system, comprised of a continuous glucose monitor and an insulin pump to deliver real-time insulin therapy for hyperglycemic correction.[53] As real-time glucose levels are extracted through the same sensor/transmitter utilized in the Guardian® RT, an insulin pump is used to continuously deliver the appropriate insulin therapy to reverse hyperglycemic excursions. However, similar shortcomings

described in the Guardian® RT and the CGMS® Standard Gold are inherent due to similar sensing elements.

The Diabetes Care division of Abbott Laboratories has currently applied for FDA approval of a minimally-invasive continuous monitoring system, the FreeStyle™ Navigator. The Freestyle navigator uses an electrochemical sensor implanted into the subcutaneous tissue of the upper arm and a wireless transmitter to convey real-time measurements to a pocket-sized device. Pending successful approval, which is anticipated, this device would allow patients to monitor glucose levels in real time for up to 3 days, a lifetime similar to systems previously described. However, with the FreeStyle™ Navigator, a single blood-draw calibration is required each time the sensor is replaced, a marked improvement over the 12 required for Medtronic systems. Additionally, the FreeStyle™ Navigator only requires a 1-hour warm up period, compared to previously described devices which require 2 hours,[51] but also suffers from inaccuracies in the hypoglycemic range.[54, 55]

Although these devices produced by Medtronic and Abbot Laboratories do represent technological advances in terms of continuous monitoring systems, there are indeed several significant shortcomings: (1) these devices are not designed to fully supplement blood-draw measurements but are marketed as a means to track metabolic trends; (2) limited lifetime of the *in vivo* sensor due to fouling requires replacement every 3 days; (3) a potential infection pathway is created through a transdermal connection to the sensor; and (4) inaccuracies plague monitoring of hypoglycemic events. It is clear that these devices leave something to be desired for a minimally-invasive monitoring system.

2.1.3 Microdialysis Sampling

A. Menarini Diagnostics produces the only FDA approved continuous monitoring system, the GlucoDay®, that utilizes microdialysis to constantly sample interstitial fluid.[56, 57] The microdialysis principle is based on the passive diffusion of substances across a semipermeable fiber implanted into the subcutaneous tissue of the abdomen. An isotonic solution (termed the perfusate) similar in ionic composition to the interstitial fluid is slowly pumped through the dialysis fiber allowing the perfusate to become enriched with analytes, such as glucose, due to diffusion. It is important to note that the perfusate flow rate must be such that a dynamic equilibrium between analytes within the dialysis fiber and interstitial fluid is observed (usually on the order of μL/min).[58] The analytes, including glucose, are subsequently transported to an external device housing an electrochemical sensor (Figure 2).
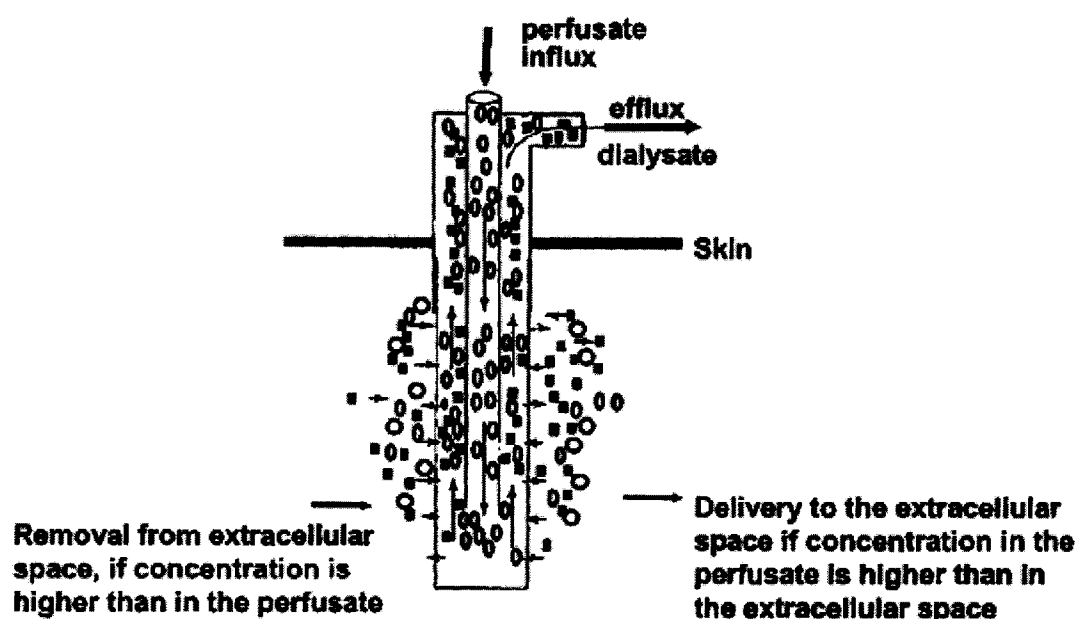
Figure 2. Interstitial fluid sampling using the microdialysis technique. Adapted from Heinemann et al.[58]

The GlucoDay® system provides up to 48 hours of continuous monitoring, requiring only a single calibration point, and audible alarms signaling the onset of hypo- or hyperglycemia.[51] Although the lifetime of the sensor is shorter than commercially available systems, the GlucoDay® requires no significant warm up period between flowing sensor replacement, making this device more of a "true" continuous monitoring system. Even though microdialysis techniques have been touted as having significant lag times between measured glucose levels and actual interstitial glucose levels,[14] studies conducted on the GlucoDay® system indicate that the perfusate takes an insignificant 11 seconds to reach the sensor and a total time of 1 minute to determine the subsequent glucose concentrations.[56] Nonetheless, this device provides a potential infection pathway inherent from the connection between the dialysis fiber and the detection device and would require frequent sensor replacement to continuously monitor trends. Again, it is reiterated that this device, along with all of the commercially available devices previously discussed, is not intended to replace blood-draw measurement but is instead meant to allow patients to closely observe metabolic trends.

2.2 Current Trends in Glucose Sensing

Although the currently available continuous systems described above do indeed increase the user-friendliness of diabetes management, there are significant limitations; therefore, it is no surprise that aggressive ongoing research is focused on developing non- and minimally-invasive glucose monitoring methods. In this section, a survey of techniques that are being pursued for continuous glucose monitoring is described.

2.2.1 Transdermal Extraction
Methods

Several methods are used in the transdermal extraction of glucose, one them previously discussed and incorporated into a commercially available system – reverse iontophoresis, employed in the GlucoWatch® Biographer by Cygnus. Although the sole application of these methods does not permit glucose sensing, they do present a means to extract interstitial fluid with minimal tissue disturbance to supply an external sensing device, and therefore merit a brief review.

2.2.1.1 Skin suction blister

The skin suction blister technique involves the application of a vacuum to the skin to purposely cause the formation of a blister between the epidermal-dermal junction. The vacuum is removed and the blister fluid sampled immediately, using a large gauge needle. Evidence of cell damage was observed as well as extensive dermal inflammation, leading the research community to ultimately conclude that this technique is no less invasive than traditional blood-draw methods.[47] Therefore, this technique has fallen out of favor with the biomedical research community.

2.2.1.2 Microporation

Microporation methods involve techniques to perforate the stratum corneum with microscale pores to allow efficient extraction of interstitial fluid. Common techniques used to form micron-sized ($<$ 100 μm) pores in the stratum corneum are laser- and thermal-mediated tissue ablation. The subsequent application of a mild vacuum to the perforated area extracts the interstitial fluid, which is electrochemically analyzed to determine the glucose levels.[47] Although this technique is classified as minimally-

invasive, no studies on the effects of long-term extractions have been reported, leaving the scientific community pessimistic about its overall feasibility.

2.2.1.3 Sonophoresis

Sonophoresis is a technique originally investigated as a method to enhance the efficiency of transdermal delivery.[59] In this technique, low-frequency ultrasound waves (~ 20 – 100 KHz) are applied to the skin surface. Several effects are induced, the most important of them believed to be cavitation. Cavitation results when gaseous inclusions within the skin expand and collapse at the applied frequency, which is believed to cause a reversible disruption of stratum corneum, resulting in the modulation of skin permeability.[60] Following ultrasound application, the application of a hyperosmotic agent enables the transdermal flux of interstitial fluid (order of magnitude greater than that achieved by reverse iontophoresis), which is subsequently used in the electrochemical determination of glucose levels.[47, 61] Although this extraction technique does show promise, it is unclear how a complete system would be miniaturized and packaged while maintaining a reasonable price tag. However, given the increased fluid extraction rate observed with sonophoresis, a device based on this technique may have the potential to provide continuous readings more rapidly than currently available systems like the GlucoWatch® G2. Nonetheless, a less invasive method would ultimately have greater appeal to the diabetic community.

2.2.2 Non-Invasive Glucose Sensing

A review of current progress in non-invasive glucose sensing, most of which employ various optical techniques, is presented in this section. Methods employing optical techniques in the direct transdermal probing of glucose levels are considered truly

non-invasive because methods do not involve the harvesting of body fluids to determine glucose levels. These technologies involve the direct interrogation of skin tissue with light and detect the subsequent changes in absorption, transmission, reflection, and scattering properties to determine glucose levels. Given that most of the work in the field of non-invasive glucose sensing is focused on optical interactions with tissue, a brief overview of skin optics along with how glucose affects optical characteristics is warranted.

Skin is a complex tissue having many non-homogeneously distributed components that absorb and scatter light in a complex fashion, which in turn attenuates the propagating light. Absorption occurs when the energy of the propagating photon is taken in by another molecule, resulting in an overall attenuation of intensity best described using the Beer-Lambert law. Scattering occurs when a propagating photon is forced to deviate from its trajectory by one or more non-uniformities in the medium, and the anisotropy factor is used to determine the directional probability of the photon's new trajectory. The absorption (σ_a) and scattering (σ_s) coefficients, as well as the anisotropy factor, describe light propagation through a medium – skin, in this case. Early work in the field of tissue optics observed a pronounced decrease in the scattering and absorption coefficients of the various skin layers with wavelengths above 600 nm (Figure 3).[62] The term "optical window" was subsequently coined as the wavelength region between 600 nm and 1300 nm, which allows increased light propagation by avoiding significant scattering and absorbing from tissue components (< 600 nm), while avoiding increased absorbance by water (> 1300 nm).
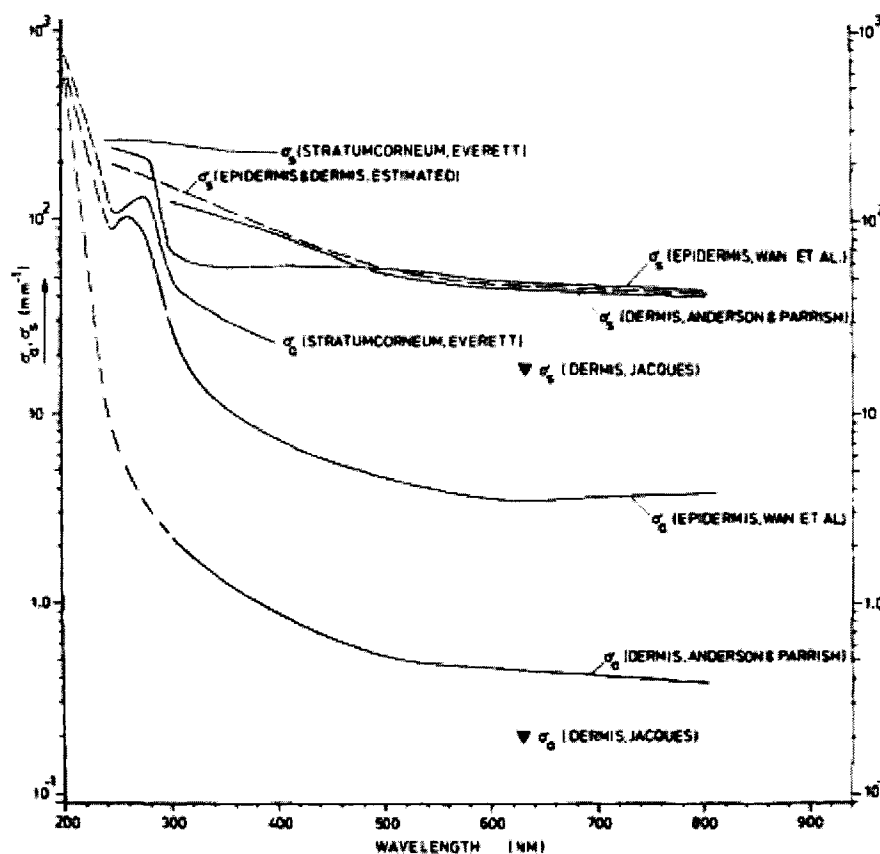
Figure 3. Experimentally determined scattering (σ_s) and absorption (σ_a) coefficients for the stratum corneum, epidermis, and dermis. Taken from Van Gemert et al.[62]

Researchers have focused an increasing amount of work on exploiting the optical window to probe glucose levels, most of them predicated on monitoring glucose-induced changes in scattering and absorption properties. In principle, glucose-induced changes in absorption properties are due to water displacement in the interstitium as glucose levels increase, while scattering properties are altered through refractive index changes from alterations in interstitial glucose levels.[63] However, the normal variations in physiological conditions such as skin temperature, hydration state, and even blood flow have been reported to affect the skin's optical properties, presenting a great challenge for the realization of reliable direct optical measurents.[64]

2.2.2.1 Infrared spectroscopy

Most of the work involving infrared probing of glucose levels employs near-infrared (NIR) radiation. NIR spectroscopy techniques are based on the premise that glucose-specific information embedded within the NIR spectral region (700 – 2500 nm) can be obtained and extracted using multivariate chemometric analysis techniques. Commonly, simple absorption and reflectance measurements have been performed to collect spectra over various regions of the body, including the tongue, upper and lower lip, nasal septum, and cheek. Although there has been much interest in the development of this technique, several disadvantages have challenged continued development. First, there has been considerable dispute over the measurement location, which has been observed to have a profound effect on results.[65] Additionally, several common analytes present within the skin share similar properties, making it difficult to determine spectral changes specific to changes in glucose levels (Figure 4).
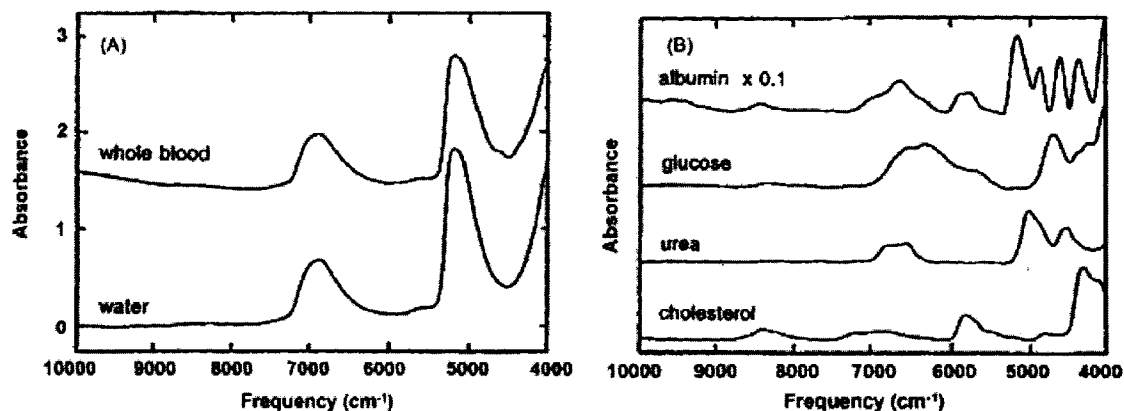
Figure 4. NIR absorbance of interfering species commonly present during glucose measurements. (A) whole blood and water (B) Common molecular species and glucose. Taken from Sieg et al.[47]

Given the complexity associated with extracting glucose measurements from convoluted spectra, a considerable amount of work in this field has been dedicated to multivariate analysis of the spectra. This complex undertaking involves characterizing a standard error of prediction, and a prediction's correlation coefficient, while preventing overfitting of the calibration data traditionally acquired using blood-draw methods. Recently, one report claimed that chance correlations in current models are present and suggested frequent blood-draw calibrations to solve this issue, which would ultimately detract from the non-invasiveness of this techniqe.[66] While there continues to be focus on developing analytical and consistent calibration models, it is still unclear how a portable device, packaged for home use, would be developed.[47] Nonetheless, sustained research programs are still pursuing NIR spectroscopy for the determination of interstitial glucose levels, despite the obvious limitations.[67]

Additional techniques using mid-infrared (MIR) radiation have also been explored. Techniques involving MIR spectroscopy are similar in principle to NIR techniques; however, glucose levels are determined by spectral signatures in the MIR spectral region, 2.5 – 50 μm (4,000 – 200 cm^{-1}). In this region, a more intense and detailed spectral signature for glucose is obtained, when compared to that of NIR measurements, allowing multiple peaks to be analyzed and concentrations extracted (Figure 5).
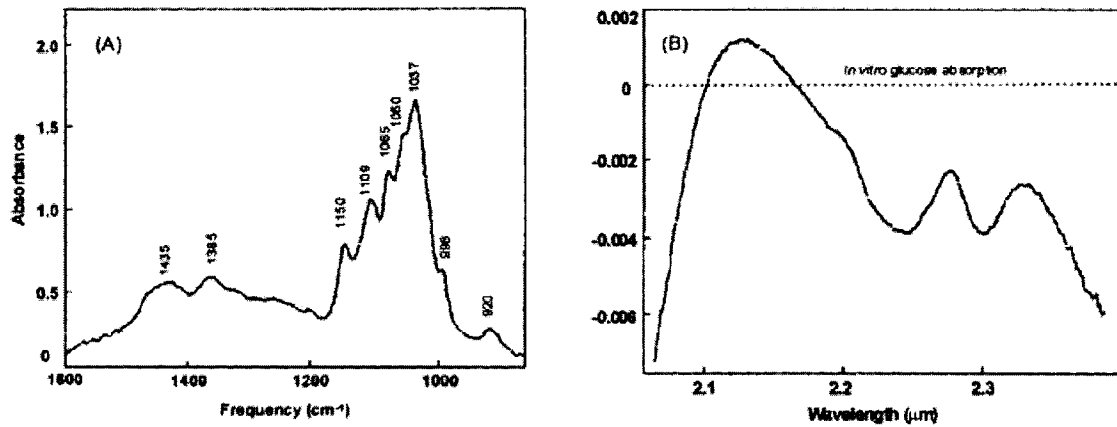
Figure 5. Optical absorption spectra of glucose in the MIR (A) and the NIR(B) regions. Taken from Sieg et al.[47]

However, by switching to the MIR region for analysis, a high background signal due to water absorption is often hard to account for in *in vivo* situations and severely limits the penetration depth of the propagating light.[63] As with NIR techniques, changes in skin optical properties measured via MIR spectroscopy could be non-specific, as reports have shown that varying physiological conditions can affect measurements.[64]

2.2.2.2   Light scattering

Light scattering techniques have been used in several aspects of non-invasive glucose monitoring. Several researchers have focused on using spatially resolved diffuse reflectance and NIR frequency domain reflectance techniques to directly measure changes in tissue scattering properties.[68-70] As glucose levels fluctuate, concentration differences in the interstitial fluid cause changes in the refractive index mismatch with other tissue components, thus causing alterations in measurable scattering properties. Work was done using light of various wavelengths to probe different tissue depths, while moving the external detector 1 – 10 mm from the skin surface.[68] Ultimately, the results indicated a substantial amount of drift that attributed to non-specific changes in scattering

properties. Also, this technique collects measurements across multiple skin compartments, and since individual compartments may have varying glucose transport dynamics, it is difficult to quantify results. Another report used a continuous microdialysis sampling technique in parallel with scattering measurements, to establish a calibration model. However, results showed that changes in scattering properties do not always correspond to glucose fluctuations, corroborating results from previous work.[69] Therefore, direct scattering measurements have been plagued by non-specific changes in scattering properties and lack of ability to specifically probe individual tissue compartments, both contributing to poor calibration models and lack of robustness.

In an attempt to monitor scattering properties of localized tissue compartments, occlusion spectroscopy was developed. In this technique, the vasculature of the measurement location (usually the finger tip) is occluded, resulting in the agglomeration of red blood cells (RBCs). This technique measures the changes in the refractive index mismatch between the agglomerated RBCs and the blood plasma, which contains glucose, with the premise that changes in glucose levels result in measurable changes in the refractive index mismatch.[71] Hence, occlusion spectroscopy allows probing of glucose levels within the vasculature and not the surrounding compartments, providing a localized measurement not obtainable with direct scattering methods. However, as with direct scattering measurements, non-specific changes in scattering properties due to blood proteins, analytes, and oxygenation levels make calibration difficult.[65]

Optical coherence tomography (OCT) is an imaging technique initially applied to the fields of ophthalmology and *in vivo* biopsies, but has found recent application in non-invasive glucose monitoring.[72] The principle on which OCT relies is low coherence

interferometry. The optical setup typically consists of an interferometer (typically Michelson type) with a low-coherence, broad-bandwidth light source used to illuminate the skin. The coherent light is split into and recombined from reference and probe beams, respectively. The combination of the backscattered light collected from the skin and the reference beam give rise to interference patterns, which are collected by a photodetector (Figure 6).[73]
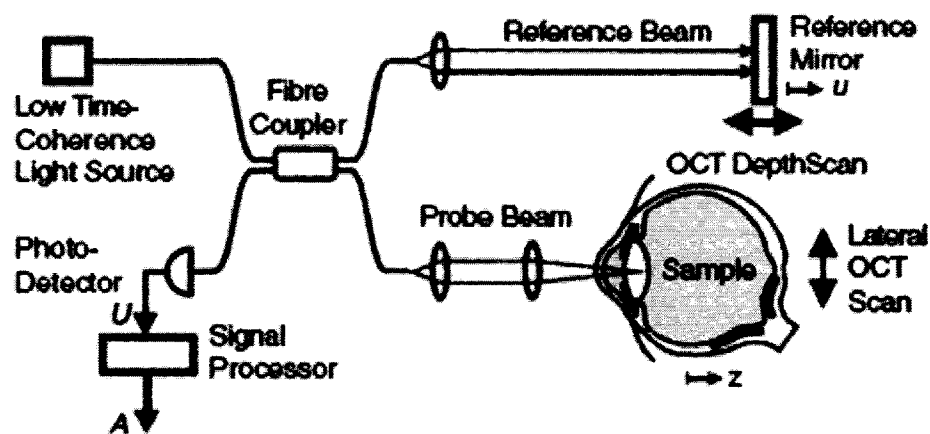
Figure 6. Components of an OCT scanning system. Taken from Fercher et al.[72]

By varying the position of the reference mirror, the scan depth can be altered, and if scanning optics direct the probe beam, axial image profiles can be obtained with micron precision and millimeter depth penetration.[72] For glucose detection, OCT is used to image individual skin compartments and determine changes in scattering properties brought about by fluctuations in glucose levels. Recent work has shown that by analyzing localized compartments, an accurate calibration model can be obtained (Figure 7).[65]
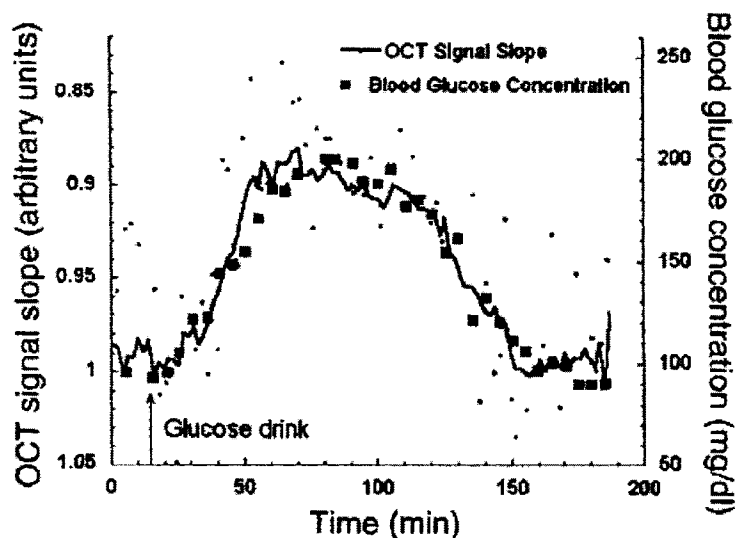
Figure 7. Comparison of OCT measurements to blood-draw calibrations. Taken from Khalil et al.[65]

Although this method is promising, it remains affected by non-specific changes in scattering properties when measurements are taken in environments that are not stringently controlled.[63]

Raman spectroscopy relies on infrared radiation, making this technique infrared by nature; however, this technique detects the molecular signatures of *scattered light*, justifying its discussion within this section. In this technique, samples are irradiated with monochromatic light, some of it absorbed or transmitted, but a portion of it scattered. Most of the scattered light will have the same frequency as the incident radiation; however, additional spectral signatures due to the vibrational and/or rotational energy of the scattering molecules can be detected. Since light energy is proportional to frequency, the frequency change of this scattered light must equal the vibrational frequency of the scattering molecules, an energy exchange process termed the Raman effect.[74] Like the infrared spectra collected by previously discussed techniques, highly specific spectral

features can be used to identify individual molecules. In comparison with the MIR techniques, which sufferes from water absorption interference, Raman techniques have fewer water overtones, easing measurement analysis.[63] However, due to a weak signal, researchers have searched for alternative testing sites, such as the anterior chamber of the eye.[75] While this work seems promising, safety and clinical efficacy remain to be addressed.

Although scattering based techniques are indeed non-invasive, making these techniques extremely attractive for diabetes management, several key limitations may jeopardize the future implementation in commercial devices: (1) a vast amount of physiological and environmental effects can influence the scattering and absorption properties of the skin, making extended calibrations very difficult; (2) extensive data-processing techniques complicate measurement analysis and introduce uncertainty into the final results; and (3) motion artifacts during measurements further complicate analysis.

2.2.2.3 Polarimetry

Polarimetry-based detection methods are predicated on tracking the optical activity of chiral molecules, in this case, glucose. When plane-polarized light is transmitted through a medium comprising optically active solutes, its polarization plane is rotated an angle, α, which is directly related to the concentration of the solute.[76] For this detection method to be truly non-invasive, radiation must pass through the medium and be collected before total depolarization occurs. Therefore, polarimetric measurements require low scattering mediums, making even minimal path length measurements (e.g., webbing between digits and external ear structures) through the skin

infeasible.[65] Therefore, researchers have commonly used this method to measure glucose levels in the anterior chamber of the eye, providing a low scattering medium.[76-79] To accomplish this task, incident radiation normal to the corneal surface is directed through the anterior chamber and the exit beam collected as shown in Figure 8.
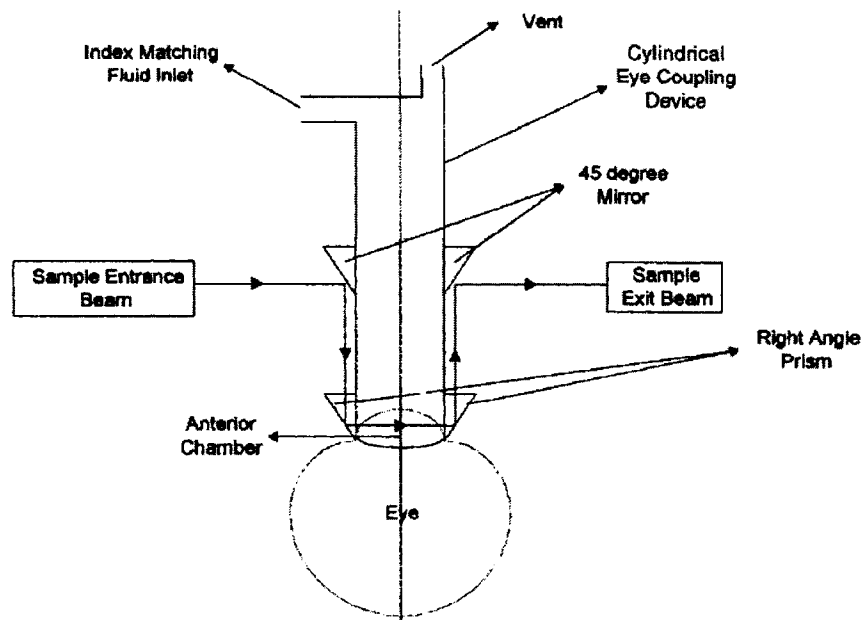
Figure 8. Depiction of a polarimeter used for anterior chamber glucose measurements. Taken from Cameron et al.[77]

Before this approach can be considered a viable *in vivo* glucose monitoring technique, several aspects must be addressed including (1) motion artifacts due to eye movement; (2) interference from additional optically active compounds; (3) lag times between glucose levels in the aqueous humor relative to blood and interstitial fluid levels; and (4) artifacts due to uncontrollable environmental and physiological factors.[65, 79]

2.2.2.4 Photoacoustic spectroscopy

Photoacoustic (PA) spectroscopy uses optically-induced ultrasonic waves to detect variations in interstitial glucose levels. Specifically, this analytical technique involves the conversion of optical energy into acoustic energy. Picosecond pulses of incident optical radiation (700 – 900 nm) are directed into the tissue, during which photon absorption leads to localized heating that leads to volumetric expansion of the region. This pulsating expansion creates ultrasonic pressure pulses which are subsequently measured by a piezoelectric detector.[80] The rise in temperature is characterized by the specific heat of the tissue. Increasing glucose levels decreases the specific heat, which in turn causes an increase in acoustic velocity. Therefore, glucose levels can be determined by monitoring relative changes in acoustic velocity.[65] MacKenzie et al. summarized several *in vivo* studies using PA spectroscopy to determine glucose levels, indicating that controlled calibration models could be obtained, but were not robust. Additionally, interfering species such as NaCl were identified as a contributing factor to unsustainable calibration models.[80] These limitations, along with minimal quantification of long-term affects from continued usage, have slowed commercial development.

2.2.2.5 Impedance spectroscopy

A particularly interesting non-optical approach that is capable of non-invasive monitoring is impedance spectroscopy (IS), a technique that measures the dielectric properties of the tissue. In this technique, a small alternating current is applied to the tissue, and the impedance of the tissue to the current flow is recorded as a function of frequency. Fundamentally, skin tissue is both resistive and capacitive in nature, and by

varying frequency, IS can separate individual resistive and capacitive contributions. Previous work has shown the utility of this technique to quantify transport properties and hydration of tissue.[47] Work by Heinemann's group significantly advanced applications towards glucose monitoring through the development of a wrist-worn prototype currently undergoing clinical evaluation.[81, 82] For glucose monitoring applications, the prototype device uses 1 – 200 MHz frequencies, allowing the interfacial membrane polarization of RBCs and other cell membranes to be studied. Since a modified membrane potential arises from the concentration-dependent interaction between glucose and RBCs, glucose levels can be determined. A reported change of 0.5 – 0.8 MΩ per mM of glucose was reported, with a total percent change of approximately 10% over the range tested and good correlation with standardized blood glucose levels, confirming that the device does track blood glucose levels (Figure 9).
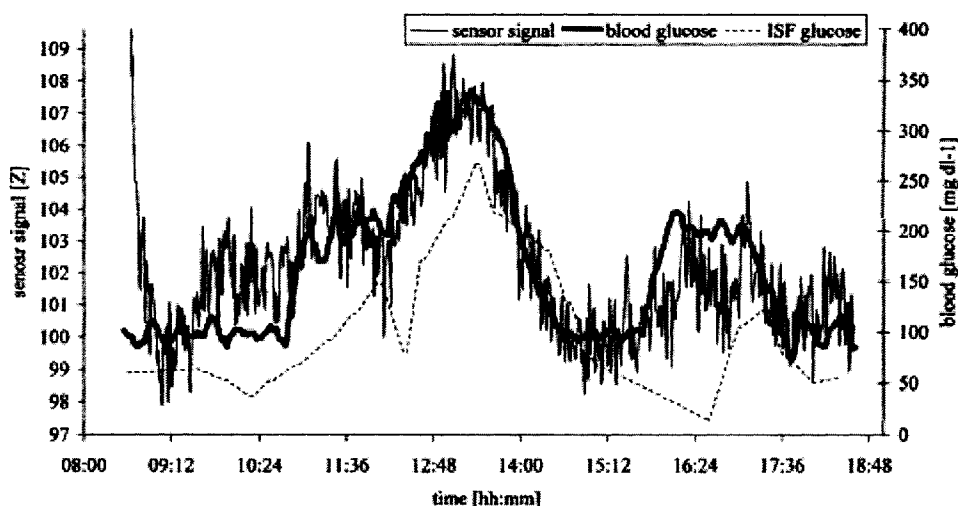
Figure 9. Comparison of IS measurements from a prototype sensor to standardized blood and interstitial fluid measurements. Taken from Caduff et al.[82]

To further extend the clinical efficacy of this test, extended clinical trials are underway; however, artifacts resulting from excessive sweating and motion, as well as temperature fluctuations, pose challenges in extracting accurate measurements over extended periods of time (> 2 days).[47]

2.2.3 Fluorescence-Based Glucose Sensing

Fluorescence is a phenomenon in which an excited molecule absorbs energy and subsequently releases energy in the form of a photon. For molecular detection, fluorescence-based techniques have proved to be highly sensitivity, even affording *single*-molecule detection.[83] Additionally, since fluorescence-sensing techniques rely on specific reporter molecules with unique optical properties to transduce analyte measurements, readings are highly specific, unlike previously reviewed optical techniques. Also, a variety of techniques can be used measure analyte concentration, providing researchers a means to develop an array of sensing schemes for a particular analyte of interest. Furthermore, given that fluorescence techniques are optically based, implantable devices could be developed to allow minimally-invasive monitoring of analytes. Thus, it is evident why an increasing amount of work has been focused on developing various methods to quantify glucose levels using fluorescence techniques.[19] In this section, direct and indirect glucose sensing schemes utilizing fluorescence transduction will be reviewed, including those based on naturally occurring and engineered glucose recognition molecules. Further, the work reviewed herein will be classified according to glucose-binding moiety.

2.2.3.1 Boronic acid based sensors

Boronic acid compounds form a reversible complex with *cis* 1,2- or 1,3- diols, such as the common biological carbohydrates glucose, galactose, and fructose. Since the complex is reversible, the integration of boronic acid derivatives as recognition elements in glucose sensors is being aggressively explored. Many systems are predicated upon the signaling of the diol binding event through modulation of fluorescence properties of the boronic acid compound, which are typically comprised of a binding moiety and a fluorescent signaling moiety.[84]

In the early 1990's, Yoon and Czarnik were the first to report on anthrylboronic acid-based fluorescent saccharide sensors, successfully showing saccharide binding could signal a change in fluorescence properties.[85] The high apparent pKa (~ 8.8) of the compound resulted in an emission intensity decrease with increasing saccharide concentration through a process termed "chelation-enhanced quenching." While this initial work was indeed an important "proof-of-concept," anthrylboronic acid was found to be more sensitive to fructose binding events than glucose. The Shinkai group advanced the concept through the integration of an amino group positioned between the boronic acid and anthracene. The amino group effectively increased the compound's saccharide binding affinity by lowering the pKa and enhanced photoelectron transfer, resulting in increased emission intensities with elevating saccharide levels (the opposite of which was seen with anthrylboronic acid).[86] However, as with Yoon's work, results showed preferential binding of fructose over glucose (approximately 50-fold selectivity for fructose at physiological pH).

In an attempt to further increase binding affinity and enhance glucose selectivity, Shinkai's group devised and initially reported bisboronic acid compounds.[87] In this work, sensing compounds were prepared with bisboronic acid configurations, and results showed that glucose selectivity can be enhanced by appropriately orienting the boronic acid compounds relative to the diol pairs on glucose. Further work showed that linker chain length (and type) between the boronic acid moieties greatly affects glucose selectivity, paving the way for the development of additional compounds with engineered affinity properties.[88] Using previous results as a guide, Karnati et al. prepared a derivative with a glucose selectivity 43-fold greater than that of fructose, demonstrating that boronic acid based sensors could indeed be designed for applications in glucose sensing.[89]

The James group further advanced the concept by demonstrating fluorophore choice could affect overall selectivity, stability, and sensitivity of the sensors, as well as using multiple pendant fluorophores to extend the emission wavelengths of the sensors through fluorescent resonance energy transfer (FRET) – a novel concept for boronic acid derivatives.[90] This system utilized a phenanthrene donor and pyrene acceptor, such that when excited with 299 nm light (the excitation maxima of phenanthrene) the entire system would emit at 417 nm (the emission maxima of pyrene).

To compensate for source fluctuations and variations in probe concentration, Heagy's group incorporated ratiometric functionality into boronic acid derivatives.[91] In this work 3-nitronaphthalic anhydride and 3-aminophenylboronic acid were used with various linker moieties to form a monoboronic acid sensor, where upon excitation with 377 nm light, bimodal emission spectra with peaks at 430 and 550 nm were observed. By

analyzing peak ratio (430/550) changes induced by variations in saccharide concentration, a response profile was generated (Figure 10).
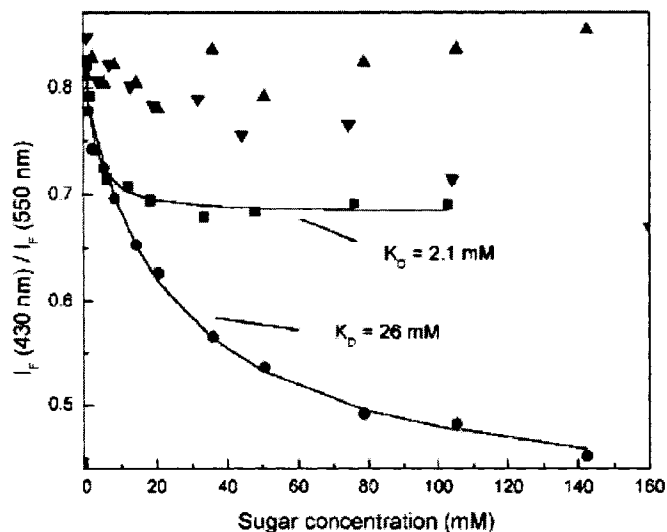
Figure 10. Titration curves against fructose (■), glucose (●), galactose (▲), and ethylene glycol (▼), measured in 0.1 M phosphate buffer, pH 8.0 at 25 °C. Taken from Cao et al.[92]

These results seemed to contradict earlier findings that demonstrated poor glucose selectivity with monoboronic acid derivatives. The authors suggest that competing factors may be simultaneously operating, such as conformational restriction between the phenylhydroxy-boronate:saccharide complex and its influence on the excited state, which could result in enhanced glucose selectivity.[92]

Another approach to designing glucose sensitive fluorophores was studied by Singaram, whose work is primarily focused on designing two-component boronic acid sensors. In previous work, single sensing moieties containing both receptor and fluorophores were studied; however, in Singaram's studies, the fluorophore – usually anionic in nature – is quenched by a physically separate boronic acid substituted viologen

receptor. As the saccharide binds with the receptor, the quenching efficiency of the

viologen is reduced, resulting in an increased emission intensity of the fluorophore

(Figure 11).
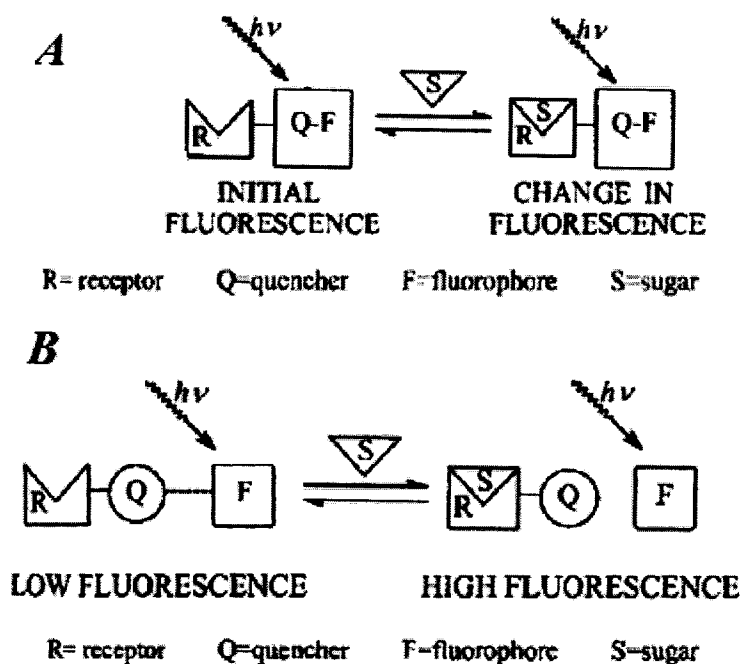
Figure 11. (A) One-component saccharide sensing system. (B) Two-component saccharide sensing system. Taken from Cordes et al.[93]

This facile approach readily allows the interchange of fluorophores without any

modification of the receptor, a considerable advantage since transformations can cause

unwanted changes in the photophysical dye properties. This work demonstrated that

sensitivity and selectivity as well as optical properties of the boronic acid derivatives can

be modulated by interchanging different viologens and fluorophores.[93, 94]

All previously described work on boronic acid derivatives has been performed in

solution phase; however, one group is investigating the feasibility of using boronic acid

derivative-doped contact lenses for continuous monitoring of glucose levels in tears.

Geddes and Lackowicz have shown that boronic acid derivatives could be successfully incorporated into an over-the-counter contact lens and still retain glucose sensitivity.[95-97] Contact lenses, typically composed of polyvinyl alcohol hydrogels, allow diffusion-facilitated loading of boronic acid derivatives. After incubation and removal of excess fluorophore, the fluorescence response to saccharide levels was characterized. Initially lenses loaded with stilbene, polyene, and chalcone derivatives were studied. However, results indicated a drastic difference in behavior of the doped lenses when compared with those obtained during solution phase testing. This discrepancy was attributed to pH differences between the testing environments – the local pH of the lenses was determined to be 6, whereas most of the solution phase testing was performed at pH 8. Therefore, the authors sought to design boronic acid derivatives containing various quinolinium moieties in an attempt to reduce the pKa of the probe to match the local pH of the sensing environment. One particular probe, N-(boronobenzyl)-6-methoxyquinolinium bromide (o-BMOQBA), was investigated and characterized accordingly (Figure 12).
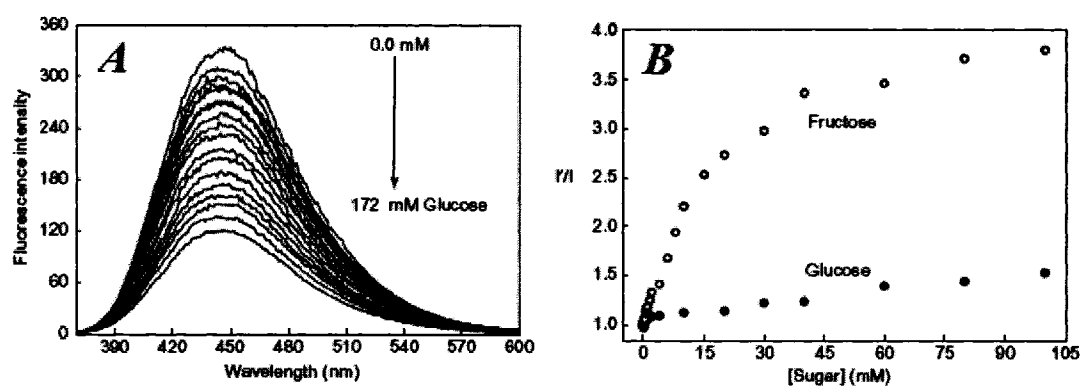
Figure 12. Spectral response (A) and calibration curve (B) of o-BMOQBA-doped contact lenses. Taken from Badugu et al.[96]

The results obtained from the o-BMOQBA-doped lenses clearly demonstrate saccharide sensitivity; however, glucose selectivity remains a significant obstacle. Although this work represents a novel attempt to construct minimally-invasive sensors, the development of a device to collect and analyze glucose levels has not been addressed. Additionally, the efficacy of using tears to manage diabetes has not been fully evaluated and sensor stability has yet to be demonstrated *in vivo* where uncontrollable conditions such as eye hydration may significantly affect measurements.

2.2.3.2 Competitive-binding based sensors

Competitive-binding assays for glucose, where signal transduction is typically based on resonance energy transfer (RET) mechanisms, are some of the most studied schemes for preparing fluorescent glucose sensors. RET occurs whenever the emission spectrum of a fluorophore, termed the "donor", overlaps with the excitation spectrum of another fluorophore, termed the "acceptor", such that the donor excited state is non-radiatively transferred to the acceptor, resulting in photon emission. RET efficiency (*E*) is highly dependent on the distance (*r*) between the donor and acceptor molecules as shown in the following equation:

$$E = \frac{R_o^6}{R_o^6 + r^6},$$

where R_o represents the Förster distance, the distance at which 50% efficiency is obtained (typically in the Å range).[98]

RET-based glucose transduction is driven through the competitive binding between a fluorescent ligand and glucose to receptor sites on lectins, glucose-binding proteins, or deactivated glucose-specific enzymes, such that the ligand (the donor) is

displaced from the receptor (the acceptor) when in the presence of glucose, resulting in measurable decreases in the acceptor emission intensity.[32, 33]

Concanavalin A RET systems. The inception of competitive-binding assays to monitor glucose levels was reported in the groundbreaking work of Mansouri et al., in which the glucose-binding protein Concanavalin A (Con A) was immobilized onto the lumen walls of a microdialysis fiber containing a high molecular weight fluorescein-labeled dextran (FITC-dextran) solution.[99] A single optical fiber (low numerical aperture) was used to deliver and collect photons from the solution within the dialysis fiber. When in the presence of glucose, FITC-dextran molecules are displaced and diffuse from the lumen walls into the core volume of the fiber, resulting in a rise in FITC emission intensity that could be correlated with glucose levels. Overall, a 60% change in intensity was observed over the range of 0 – 180 mg/dL of glucose; however, problems with drift occurred due to the lack of internal reference.

The same laboratory added ratiometric functionality by incorporating RET measurements between FITC-dextran and rhodamine-labeled Con A (TRITC-Con A) within microdialysis fibers.[100] In this scheme, a measurable decrease in RET efficiency was observed as glucose displaced FITC-dextran, resulting in a decreased acceptor emission intensity relative to donor emission intensity. Results indicated a linear correlation with glucose levels up to 200 mg/dL and 60% change in ratiometric intensity over the range of 0 – 900 mg/dL. The authors also noted problems with irreversible aggregation of Con A within a few hours, thereby restricting the development of this type of sensor.

A novel scheme was devised by Ballerstadt et al. to eliminate the need for Con A immobilization on the microdialysis fiber wall.[33] In this work, Sephadex beads comprising pendent glucose moieties and two highly absorbing dyes were used. Safranin O and Pararosanilin were selected as dyes to block the excitation spectrum of Alexa Flour® 488, the fluorophore used to label Con A (AF488-Con A). When in the absence of glucose, excitation light passing through the beads is preferentially absorbed by the Safranin O and Pararosanilin, resulting in poor emission from AF488-Con A. Upon glucose diffusion into the fiber, glucose-binding releases AF488-Con A from the beads, causing an increase in emission intensity that is well correlated with glucose levels. Additional efforts by the same lab were focused on extending the wavelengths into the NIR (to potentially make a system more suitable for transdermal applications) by using alternative fluorophores.[32] However, studies performed to evaluate long-term use of both systems indicated significant leakage over time, resulting in poor performance – mostly due to the lack of a reference signal – and ultimately proving that additional advances were necessary for future success.

Russel et al. showed that a Con A RET system could be encapsulated within polyethylene glycol spheres and retain functionality.[23] In this work, TRITC-Con A and FITC-dextran were entrapped within polyethylene glycol (PEG) millispheres, where the addition of glucose resulted in FITC-dextran displacement and alterations in RET efficiency. However, leaching of assay components, as well as long response times to changes in glucose, proved to be significant problems. This work represented the first reported attempt at a "smart tattoo" and will be further discussed in the later pages of this text.

The Lackowicz group was among the first to implicate that fluorescence lifetime measurements could potentially alleviate problems observed with intensity-based RET measurements.[101] Given that fluorescence lifetime – the average time at which the fluorophore remains in the excited state beforereturning to the ground state – is independent of fluorophore concentration and light scattering and absorption properties of the sample, this particular measurement is potentially promising for *in vivo* monitoring.[98] In this work, the assay is based on the decreased decay time of a donor fluorophore linked to Con A upon binding of acceptor-labeled α-D-mannoside. Upon introduction of glucose into the system, the displacement of the labeled sugars results in a decrease in energy transfer and an increase in the donor decay time. Results indicated that this assay scheme could be used with various donor-acceptor pairs, demonstrating the robustness and generality of this approach. Additional studies were performed on similar systems based on long lifetime fluorophores such as ruthenium complexes, reducing the need for high frequency light-modulation for phase-domain lifetime measurements.[102, 103]

Most recently, an *in vivo* investigation of a NIR Con A RET system was reported and the host response characterized.[104] In this work, Cy-7-labeled Con A and AlexaFluor® 647-labeled dextran system were entrapped with a hollow microdialysis fiber immobilized on the tip of an optical fiber. The device was characterized *in vitro*, the result of which indicated a response range of 2 – 25 mM. More important, the device was implanted *in vivo* and the response characteristics monitored throughout the course of 16 days. Results were promising, as the implant read-out retained a high degree of correlation with blood glucose fluctuations (as measured by blood-draw methods). The

authors noted that an increase in response time was observed at the end of the experimental period, citing fibrous encapsulation of the sensor as the cause. Additionally, the authors tested the cytotoxicity of Con A through direct administration to the animal. Results indicated that even at 10 times the amount of Con A present in the implant, that no significant toxicological or systemic response was observed.

Apo-enzyme RET systems. Recently, an alternative RET assay utilizing the inactive form of glucose oxidase (apo-GOx) as the target-binding molecule has been proposed, in an attempt to overcome the aforementioned difficulties associated with Con A based assays.[27, 105] In this work, a competitive-binding assay comprised of TRITC-apo-GOx and FITC-dextran was studied first in solution phase, then entrapped within hollow microscale polymeric containers. Apo-GOx provided high specificity for glucose binding as well as a high degree of reversibility, offering clear advantages over similar systems based on Con A. Results from both studies were promising, as the authors demonstrated high sensitivity (~ 3-fold greater than previous competitive-binding systems) and reversibility throughout physiologically significant glucose levels. Additional details concerning the behavior of the encapsulated assay as a smart tattoo concept will be given later in this text. More recently, the authors have transitioned to longer NIR wavelength dyes in efforts to reduce the effect of tissue scattering should a transdermal device be realized, the results of which are equally as promising.[106]

2.2.3.3 Reagentless protein-based sensors

In this section, current progress in fluorescent glucose sensors based on reagent transduction mechanisms is presented. While competitive-binding assays rely on binding interactions of both the ligand and the analyte of interest, reagentless mechanisms depend

upon a conformation change of the receptor induced through analyte binding and require only analyte binding for signaling to proceed. Environmentally sensitive fluorophores or intrinsic fluorescence properties of the receptor molecule are used to signal the binding event.

In the late 1980's, Wolfbeis' group reported that glucose-binding events triggered measurable changes in the intrinsic flavine fluorescence of GOx; however, significant changes were only observed with 1.5 – 2 mM glucose levels.[107] By labeling the enzyme with a fluorescein derivative, Castillo's group designed a RET system between the flavine group and fluorescein derivative, and demonstrated correlation between glucose levels and the time between glucose addition and fluorescence change.[108] Given the poor understanding of the underlying mechanism for Castillo's RET system, other groups worked on preparing reagentless sensors using apo-GOx.[29] In this work, apo-GOx was labeled with the environmentally sensitive fluorophore 8-anilino-1-anpthalene sulphonic acid (ANS). The binding of glucose to apo-GOx results in a conformational change such that the steady state intensity of ANS decreased 25% and the mean lifetime of ANS decreased about 40% from 10 – 20 mM glucose. This work showed that apo-GOx retained its high specificity and in many ways paved the way for advances in the development of a new biosensor genre.[27, 105, 106, 109] Additional work by the same group was performed on the apo- form of glucose dehydrogenase, where similar results were observed, thereby indicating the utility of deactivated enzymes as analyte recognition elements in optical sensors.[110]

In similar work done by Maity et al. using yeast Hexokinase (HEX), a 30% decrease in intrinsic tyrptophan fluorescence of HEX was observed during exposure to 12

mM of glucose.[111] The same group labeled HEX with an ANS derivative.[112] Contrary to experiments performed with ANS labeled apo-GOx, a decrease in sensitivity was observed. Recent work has shown that HEX-based transduction schemes are particularly vulnerable to excessive quenching when exposed to serum, indicating that a separation from the biological environment is necessary for *in vivo* applications.[19] With this concern in mind, Pickup's group immobilized HEX in a sol-gel matrix.[113] Results were promising, as a 20% change in intrinsic fluorescence was observed when immobilized HEX was exposed to saturating levels of glucose (~ 20 mM).

As the field of protein engineering advances rapidly, several researchers have adapted a glucose-binding protein (GBP) commonly found in the periplasmic space of *Escherichia coli* (*E. coli*) for use in glucose sensor applications. It has been shown that upon binding with glucose, a conformation change is induced in GBP. This glucose-initiated conformational shift was initially exploited by Marvin et al.[114] In this work, the authors incorporate allosterically-linked environmentally-sensitive fluorophores to the GBP binding site using cystene mutations to site-direct fluorophore linkage. Two fluorophores were used, both them showing an approximate change in fluorescence intensity of 80% at saturating levels of glucose. Tolosa et al. also used protein engineering to strategically place cystene residues within GBP for site-directed labeling with ANS. Results showed that ANS-GBP displayed a two-fold decrease in intensity when exposed to saturating levels of glucose, with a dissociation constant of ~ 1 µM.[115] The same report also showed that immobilization of ANS-GBP along with a long-lifetime ruthenium complex onto the surface of a cuvette could be successfully used in

low frequency phase-modulation lifetime measurements to predict bulk glucose levels within the cuvette.

More recently, the Schultz group reported on a RET-based GBP mutant created by fusing two fluorescent reporter proteins (green fluorescent protein as the donor and yellow fluorescent protein as the acceptor) to the C and N terminus, respectively.[116] In the case of a glucose-binding event, the spatial separation between the fluorescent proteins is altered, causing a change in RET efficiency. Given this group's previous experience with microdialysis fibers, a cellulose-based dialysis fiber was used to entrap the GBP RET assay. Upon exposure to solutions containing glucose, the emission intensity at 527 nm was reduced. The response was shown to be reversible; however, a maximum intensity change was observed at 20 µM, well below the physiological range (Figure 13).
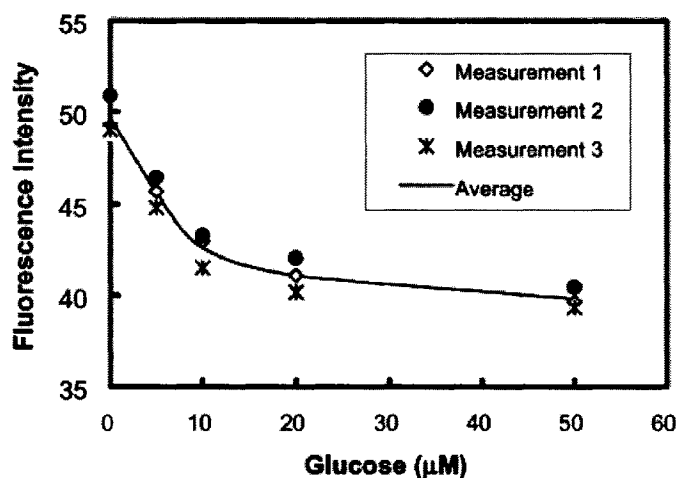
Figure 13. Glucose response of a GPB based RET assay entrapped within a microdialysis fiber. Taken from Ye et al.[116]

Although the majority of the sensors reported in this section show little or no sensitivity within the physiologically significant glucose range, future development in protein engineering techniques should further advances in engineered recognition molecules, making these approaches particularly attractive for future applications.

2.2.3.4 Enzymatic-based Sensors

There are many examples of fluorophores that can be directly used to monitor biological analytes such as Na^+, K^+, Ca^{2+}, Mg^{2+}, and Zn^{2+} through changes in fluorescence properties. To date, no reliable probes allow the direct monitoring of glucose over physiological levels, despite current efforts on boronic acid based sensors detailed in previous sections. Therefore, researchers have often integrated enzymes into glucose sensing schemes, where the co-consumption of non-glucose substrates and the generation of products are fluorescently tracked and used to indirectly determine glucose levels. One of the most widely researched enzymatic sensing schemes relies on GOx-catalyzed oxidation of glucose in the following reaction:

$$glucose + O_2 + H_2O \xrightarrow{\text{GOx}} gluconic\ acid + H_2O_2$$
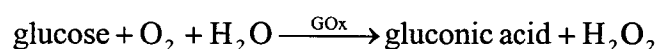
In this reaction, several schemes could be exploited to indirectly monitor glucose levels:

1. measurement of proton production (changes in pH due to gluconic acid formation)
2. measurement of hydrogen peroxide produced
3. measurement of oxygen consumed

In this section, sensors based on the above schemes will be discussed in detail. Before the review is undertaken, it is worth noting that enzymatic-based sensors are inherently very selective (enzymes contain highly specific binding sites), as well as reversible due to the catalytic nature of enzymes, making them ideal for use in biosensor applications. However, there are several drawbacks to using enzymatic schemes: (1) enzymes tend to spontaneously deactivate (denature) over time, leading to calibration drifts; (2) to obtain accurate indirect measurements of glucose, the reaction must remain glucose-limited, requiring control of reaction-diffusion kinetics; and (3) the consumptive nature of the enzyme could result in local depletion of glucose levels, leading to ambiguous readings, as well as possible tissue damage due to excessive consumption of glucose and oxygen.

Fluorescent pH transduction of glucose levels. This approach seems rather simple: add a pH-sensitive fluorophore to an assay containing GOx and monitor the decrease in pH due to GOx activity. However, this approach is inherently difficult because often the initial pH and the buffer capacity of the sample are unknown, making accurate calibrations difficult to obtain. Although little work has been done to develop this genre of glucose sensors, several significant contributions have been made.

In the late 1980's, Wolfbeis's group was the first to report a glucose sensor based on pH transduction.[117] In this work, GOx and a pH-sensitive dye (1-hydroxypyrene-3,6,8-trisulfonate, HPTS) were physically immobilized on the tip of an optical fiber. As the local pH was reduced by gluconic acid production, measurable changes in fluorescence were observed. Using flow-through measurements with buffer solutions of

various strengths, the optrode response time was determined to be 8 – 12 min, with a detection limit of 0.1 – 2 mM glucose and response saturation at 2 – 3 mM.

In the mid 1990's McCurley developed a fiber-optic-based glucose sensor that operated on the principle of pH-induced swelling.[118] In this device, a polyacrylamide gel was used to immobilize GOx and a rhodamine derivative fluorochrome on the tip of an optical fiber. During exposure to glucose, a reduction in local pH due to gluconic acid production caused the polyacrylamide hydrogel to swell by changing the ionization state of the amine groups. Since the concentration of the fluorophore remains constant while the surrounding hydrogel begins to swell, a measurable decrease in rhodamine emission intensity can be correlated with glucose concentrations up to 300 mg/dL. However, this sensor is not self-referencing and would require a direct connection to an optical fiber, providing a potential infection pathway; thus, this device would be unsuitable for sustained *in vivo* usage.

More recently, McShane's group reported on RET-based transduction of glucose-induced pH changes using chitosan microparticles.[119] In this approach, chitosan microspheres were prepared using an emulsion technique, followed by subsequent labeling of the spheres with TRITC and AlexaFluor 647® (AF647). Electrostatic differences between GOx and chitosan were exploited to attract and entrap GOx throughout the chitosan spheres. When the spheres are exposed to glucose, local decreases in pH cause the particles to swell. The swelling of the particles causes a separation of TRITC and AF647, thereby reducing RET efficiency. Although this work represents a "proof-of-concept" study, true feasibility will be judged when the prototypes are tested in increasing physiological (i.e., buffered) conditions.

Fluorescent H$_2$O$_2$ transduction of glucose levels. Using H$_2$O$_2$ as an indirect means to measure glucose levels has the advantage of minimal background interference because significant levels of hydrogen peroxide are not commonly found in body fluids.[120] However, most of these types of sensing assays require reaction coupling with peroxidase (POx). In such a system, hydrogen peroxide produced through glucose oxidation is then oxidized along with a non-colored substrate by POx, resulting in the formation of water and a colored/fluorescent product. By monitoring the resulting absorbance/fluorescence, correlations with glucose levels can be obtained. Given that these assays are non-reversible and somewhat complex, they have been commonly used in laboratory assay to determine glucose but have not been implemented in long-term monitoring applications. Therefore, for this technology to be considered further for long-term glucose monitoring, a reversible, reagentless probe for hydrogen peroxide would need to be developed.

In 2002, Wolfbeis's group reported the development of a reversible hydrogen peroxide probe that functioned independently of POx and used it to develop a fluorescent glucose sensing assay.[120, 121] This unique europium-based fluorochrome – europium (III) tetracycline (Eu$_3$TC) – is weakly fluorescent in an uncomplexed state; however, upon binding with hydrogen peroxide, a 15-fold increase in emission intensity is observed. Additionally, a 100% increase in decay time (from 30 μs to 60 μs in the presence of hydrogen peroxide) indicates that this probe could also be successfully implemented into lifetime measurements. While excited at 405 nm, a trimodal emission spectra with peaks centered at 577, 592, and 616 nm can be used to extract glucose concentrations. The results indicated a highly sensitive assay with a linear range of 2.2 – 100 μM as shown in Figure 14.
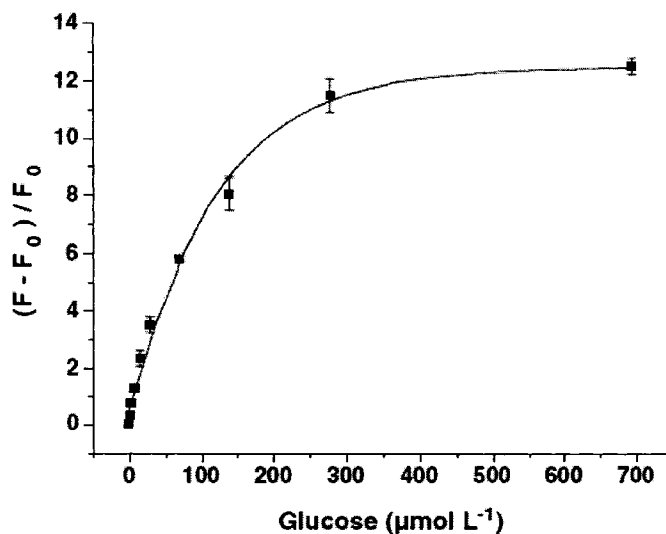
Figure 14. Eu₃TC assay response to varying glucose concentrations. Taken from Wu et al.[121]

More recently, the same group introduced a GOx-based glucose sensor using Eu₃TC.[122] In this work, Eu₃TC and GOx were immobilized within a polyacrylonitrile-co-polyacrylamide (Hypan) polymer matrix. The doped polymer was exposed to varying concentrations of bulk glucose, while continuously monitoring fluorescence emission at 616 nm (400 nm excitation light was used). Results indicated a high degree of reversibility with sensitivity to glucose in the range of 0.1 – 5 mM concentrations; however, approximately 3000 sec were required for the sensor to equilibrate following a 2 mM glucose step (Figure 15).
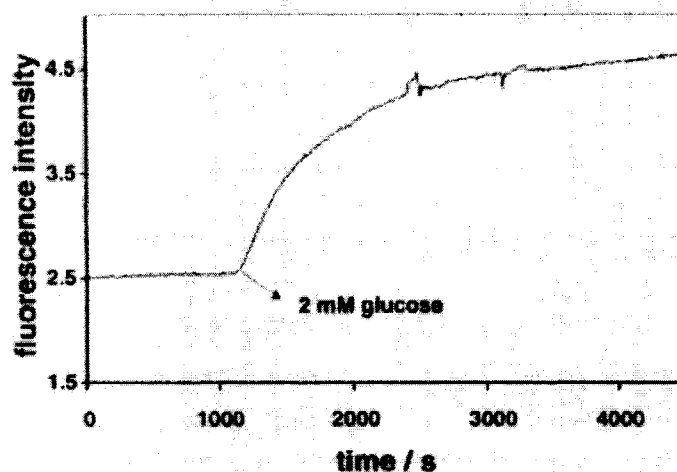
Figure 15. Real-time response of a Eu₃TC based glucose sensor to a 2 mM glucose step. Taken from Duerkop et al.[122]

Therefore, should additional advancements be made such that response time is significantly reduced and the analytical range extended, this technology could potentially be implemented into diabetic monitoring devices.

Fluorescent O_2 transduction of glucose levels. Unlike hydrogen peroxide based transduction schemes, there are many reliable O_2 sensitive probes to choose from. Additionally, O_2 transduction is dependent only on a single variable, unlike pH transduction, which is dependent on buffer capacity as well as ionic strength. However, because oxygen levels form a high background in physiological systems, a glucose sensor based on O_2 transduction could become oxygen-limited if not properly designed.

While the earliest known report of using oxygen to indirectly determine concentrations of glucose, lactate, and alcohol was reported in 1983,[123] it was the introduction of longer wavelength oxygen indicators that renewed interest in this type of sensor.[122] One of the first successful reports of optically transduced glucose sensing via indirect oxygen monitoring was in 1988, where GOx and decacyclene were immobilized

within a nylon membrane, and glucose-limited consumption of oxygen was measured via fiber optic bundles.[124] As bulk glucose levels increased, local concentrations of oxygen deceased, allowing indirect monitoring of glucose concentration via decacyclene emission. Experiments were performed in a flow chamber where air-equilibrated buffer with varying glucose levels were exposed to the membrane. Results were promising, as a response time of 1 – 6 min and an analytical range of 20 mM were demonstrated; however, since the excitation and emission properties of decacyclene (385/500 nm) are not conducive transdermal applications, no further discussion will be given on decacyclene-based devices.

Following the development of ruthenium-ligand complexes, which demonstrated longer excitation/emission wavelengths than those of decacyclene a surge of work was focused into developing oxygen-transduced glucose sensors. Again, Wolfbeis' group reported on one of the first glucose sensors to utilize a ruthenium compound [tris(1,10-phenanthroline)-ruthenium(II)].[125] The ruthenium compound was incorporated into a silica gel, which was then placed onto the tip of an optical fiber. Oxygen sensitivity experiments performed on the optrode show sensitivity over 0 – 750 torr. A layer of immobilized GOx was added onto the ruthenium-doped silica gel. To optically insulate the system, a surface coating of carbon black was adsorbed before testing in a flow chamber. The fiber was indeed sensitive to glucose concentrations up to 1mM, with response times around 6 min. Although these results were promising, the operation range would need to be greatly extended for this design to be useful in diabetic monitoring.

Additional work was done using luminescent porphyrin compounds (Pb and Pt) as probes in glucose sensitive fibers.[37] In this work, porphyrin probes were selected as

oxygen indicators due to higher sensitivity to oxygen than ruthenium compounds, leading to the hypothesis that a system with superior sensitivity over ruthenium-based systems could be developed. In this system, a porphyrin-doped polystyrene membrane was adsorbed to the surface of an optical fiber, onto which GOx was directly immobilized. Glucose sensitivity tests were performed by dipping the optrode into air-equilibrated solutions of glucose while monitoring the spectroscopic response in real-time. The authors observed a 400% increase in porphyrin emission intensity at saturating levels of glucose, which were unfortunately below (1 mM saturation) the physiologically relevant range. *A probable reason for the poor analytical range is that the authors did not incorporate diffusion limiting layers over the enzyme to modulate reaction-diffusion kinetics; therefore, local oxygen levels were rapidly depleted, resulting in a low glucose sensitive range.*

Walt's group developed a method to precisely deposit distinct regions of analyte-sensitive dye onto an imaging bundle.[126] To accomplish this goal, the distal surface of the fiber was silanized to functionalize the fiber surface with polymerizable acrylate groups. A thin film of poly(hydroxyethyl methacrylate) doped with a pH-sensitive fluorescein derivative was deposited onto the functionalized fiber surface using a spin-coating method. Using spot-directed UV illumination through individual fibers, selected regions were photopolymerized, and upon rinsing, revealed a pH-sensitive optical array. This ingenious approach was further applied to the area of glucose sensing, where Li et al. described an optical fiber capable of monitoring glucose and oxygen continuously.[127] In this work, oxygen sensitive optical arrays were prepared by mixing Ru(4,7-diphenyl(Ph)-1,10-phen)$_3$Cl$_2$ (Ru(Ph$_2$phen)$_3{}^{2+}$), a oxygen-quenched ruthenium

compound, in a siloxane copolymer. Before photopolymerization, the tip of the optical fiber was silanized. With the silianized fiber submerged in the $Ru(Ph_2phen)_3^{2+}$ siloxane copolymer solution, site-directed UV polymerization was applied such that four siloxane polymer cones were deposited onto the fiber surface. To prepare glucose sensitive assays, GOx was mixed with poly(hydroxyethyl methacrylate) (HEMA), and an aliquot placed over two siloxane cones. Illumination times were varied such that different thickness of the GOx-HEMA was polymerized to the siloxane cones. The additional two cones were coated with HEMA containing no GOx, to allow the measurement of local oxygen levels. Glucose sensitivity experiments were performed under various bulk oxygen concentrations, and the results showed that glucose sensitivity and operational range could be affected – higher bulk oxygen levels extended the operational range since the sensor became oxygen-limited at higher glucose levels. Response experiments showed sensitivity over the range of 0.6 – 20 mM glucose, with a response time of approximately 20 sec. Additionally, the authors found a dramatic difference in step response properties of the sensing arrays with varying GOx-HEMA layer thicknesses (Figure 16).

However, it is unclear whether this change in response is generated by the presence of a thicker diffusion barrier or the increase in enzyme concentration associated with the thicker GOx-HEMA layer. The implications of this study are profound for enzymatic smart tattoo applications, as they depict how enzyme concentration and/or membrane thickness, along with bulk oxygen levels, could drastically affect sensor response properties.
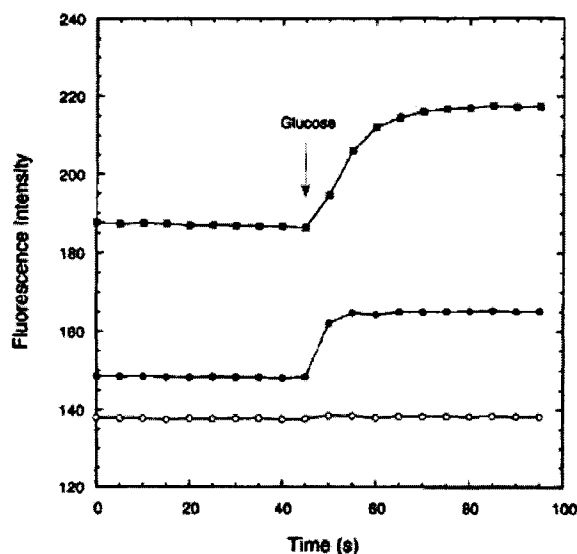
Figure 16. Response time curves of glucose sensors with thicker (■) and thinner (●) poly-HEMA layers compared to oxygen reference (○). Taken from Li et al.[127]

Significant work was done by Rosenzweig and Kopelman to further the development of glucose sensitive optical fibers, by examining the dependence of response properties on enzyme concentration and sensor size.[38, 128, 129] In this work, optical fibers with tip diameters ranging from 0.1 – 50 μm were prepared through the precise application of tension to the fiber, while the tip was heated with a CO_2 laser. The tips were acrylate-functionalized through a silanization procedure. The functionalized fibers were dipped into a polyacrylamide cocktail containing $Ru(Ph_2phen)_3^{2+}$ and varying concentrations of GOx. UV illumination was used to crosslink the polymer matrix containing the sensing components to the fiber tip. To quantify the affect of GOx concentration within the polymer cocktail, 10 μm sensors were exposed to 10 mM glucose and the response allowed to equilibrate. The final $Ru(Ph_2phen)_3^{2+}$ intensity was normalized to the intensity obtained in glucose-free buffer and plotted against the GOx

dilution used to prepare the polymer matrix (GOx stock solution was 225 units/mg) as

shown in Figure 17.
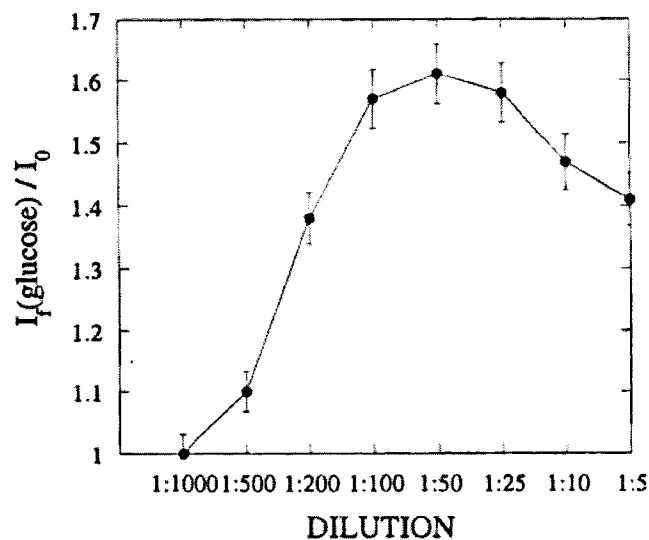
Figure 17. Effect of GOx concentration within the polyacrylamide cocktail on sensor response. Taken from Rosenzweig et al.[38]

Results indicate an optimized response was observed when a 1:50 dilution of GOx

to polyacrylamide was used during sensor fabrication. The data show and increase in

response until a 1:100 dilution was obtained. In this region of operation, glucose

oxidation is kinetically limited, therefore the glucose and oxygen consumption is directly

proportional to the concentration of GOx within the polymer matrix. From 1:100 to 1:25,

the reaction kinetics are governed by mass transport of analytes from the bulk into the

sensor; therefore, an increasing concentration of enzyme has no effect on response

properties since the reaction is now *diffusion-limited*. The authors explain that at higher

GOx concentrations (> 1:25), the buffering capacity of the sensor is overcome, resulting

in a local decrease of pH, which in turn decreases enzymatic activity. This explanation is

indeed possible; however, a more plausible explanation would be that the high levels of enzyme rapidly consume glucose on the outer boundary of the sensor, resulting in an insufficient decrease in oxygen levels within the sensors and subsequently, a loss of sensitivity. It is important to state that a separate report showed a similar trend when the effect of enzyme concentration on device sensitivity within spherical sensors was examined.[41]

A similar experiment was performed using fiber diameter as the independent variable. In this experiment, fibers with diameters ranging from 0.1 – 50 μm were exposed to 5 mM glucose and the response allowed to equilibrate. The final $Ru(Ph_2phen)_3^{2+}$ intensity was normalized to the intensity obtained in glucose-free buffer and plotted against fiber diameter (Figure 18).
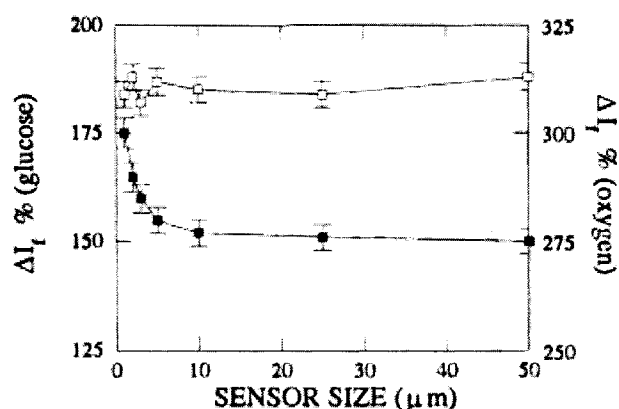
Figure 18. Dependence of sensor response on the fiber diameter of glucose (■) and oxygen (□) sensors. Taken from Rosenzweig et al.[38]

The results indicate that the oxygen response of the sensors is independent of diameter; however, clearly the glucose response is dependent on sensor diameter. An approximate 20% increase in intensity is observed when the fiber diameter is decreased

from 5 to 1 μm. The authors attribute the intensity increase to an increase in enzymatic activity per GOx molecule. For sensor diameters > 10 μm, the authors state that enzymes trapped within the inner core of the sensors only become "active" after enzyme molecules toward the sensors' surface become deactivated. However, the authors fail to show that enzyme concentration was held constant throughout the experiments investigating the size effect, making their results somewhat questionable. Nonetheless, the authors successfully iterate that sensor size and enzyme concentration can significantly influence sensor properties, concepts indeed applicable to the work presented in this dissertation.

Thus far, glucose sensors based on oxygen transduction with optical fiber substrates were reviewed. These reports demonstrate the first successful attempts in developing this type of sensor; however, for *in vivo* minimally-invasive monitoring, a system with a decoupled sensor and excitation/collection apparatus is desired. Numerous reports have demonstrated the ability to prepare functional glucose sensors by immobilizing GOx and an O_2 indicator within various species of gel slabs and use external excitation/collection to monitor sensor kinetics.[130] However, Xu et al. was the first to report on preparing nanoscale spherical particles comprising GOx and O_2 indicators for use in intracellular monitoring of glucose.[39] In this work, a glucose-sensitive variant of their PEBBLE[131, 132] (Probes Encapsulated By Biologically Localized Embedding) type sensors is prepared through a microemulsion polymerization technique. The polyacrylamide based PEBBLES are polymerized in the presence of GOx, a sulfonated version of $Ru(Ph_2phen)_3^{2+}$ (a water soluble compound used to enhance loading in the polyacrylamide hydrogel), and an oxygen-insensitive fluorophore, resulting in sensors with a mean diameter of 45 nm. The incorporation of an oxygen-

insensitive fluorophore allows ratiometric intensity measurements of sensor response, eliminating spectral artifacts caused by source fluctuations or changes in particle concentration. Several variants of glucose-sensitive PEBBLES were prepared: one variant with Texas Red as the reference dye for excitation-based ratiometric measurements and one variant with Oregon Green as the reference for emission-based ratiometric measurements. The sensors showed a dynamic range of 0.3 – 8 mM, with a linear deviation occurring at glucose levels greater than 5 mM. The sensors exhibit an approximate 100% change in ratiometric intensity from glucose depleted to saturated conditions. Additionally, the authors demonstrate that the sensors have an approximate response time of 100 sec. Although this initial work is promising, there is one particular shortcoming worth noting. Response properties were determined in a standard cuvette, and it is unclear whether bulk oxygen levels were controlled throughout the experiment; therefore, it is possible that spectral changes could have been influenced by changes in bulk oxygen levels as well as glucose. If bulk oxygen levels are not fully replenished, as glucose and oxygen are consumed locally within the sensors, the depletion of local oxygen levels could be due to decreasing bulk oxygen levels from glucose oxidation, resulting in erroneous observations. Nonetheless, this work represents an important step in the development of an enzyme/oxygen indicator transduction scheme for glucose that is decoupled from an excitation/collection apparatus.

In 2005, a significant advancement in the development of an enzyme/oxygen indicator transduction scheme was described by Brown.[133] This work represented the first report in which a continuous bead-based fluorescent sensor for glucose designed for transdermal implantation was demonstrated. In this work, calcium alginate hydrogel

microspheres doped with GOx were prepared using an emulsion technique. Following particle preparation, GOx was covalently bound to the alginate matrix using EDC/NHSS catalyzed amide bond formation. Ruthenium-tris(4,7-diphenyl-1,10-phenanthroline)dichloride (Ru(dpp)) was subsequently loaded into the spheres using a controlled precipitation technique. A novel feature of this work entails the used of fluorescent nanofilms deposited via the Layer-by-Layer (LbL) self-assembly technique to provide a reference signal (provided by AF488) as well as control substrate mass transport properties. Sensor response was quantified using a flow chamber apparatus, which allowed bulk oxygen levels to be stringently controlled while acquiring real-time response data. Results were indeed promising because these sensors exhibited a highly reversible and linear response to glucose over 0 – 600 mg/dL range. However, a 10% maximum percent change over the operation range was observed, leaving something to be desired in terms of device sensitivity.

2.2.3.5 The "smart tattoo" concept

The smart tattoo concept is predicated upon the entrapment of a fluorescent glucose assay within microscale containers, which are subsequently implanted into the dermal region of the skin. The carriers are designed such that small molecular weight molecules like glucose are able to freely diffuse into the container, while permanently compartmentalizing the sensing assay. The tattoos freely interact with interstitial fluid, and upon transdermal interrogation, emit glucose sensitive spectra that are collected and analyzed to reveal interstitial glucose levels to the patient in a continuous or spot fashion (Figure 19).[26]
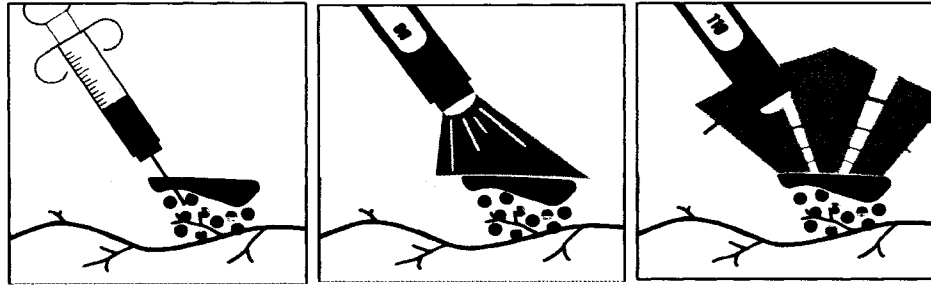
Figure 19. Schematic of the "smart tattoo" concept: implantation, interrogation, and readout. Taken from McShane.[26]

Ultimately, this approach could completely supplement the current standard blood-draw measurement technique, with hopes of increasing management compliance among diabetics. In this section, a brief history of the smart tattoo will be given, with particular interest given to the encapsulation method, as well as transduction scheme. Additionally, a brief summary of how the smart tattoo configuration addressed in this work represents a significant advancement of the concept will be given.

These sensors extract glucose levels from the interstitial fluid; therefore, before additional discussion, the relationship between glucose concentration in the interstitial fluid and blood should be addressed. Traditional glucose monitoring techniques and subsequent therapies are based on blood measurements, thus the relevance of interstitial measurements depends on the existence of a correlation between the two fluids. Under normal physiological conditions, changes in the glucose levels within the interstitial fluid and blood are highly correlated, given free mass transfer of glucose occurs between the two compartments. Therefore, with the exception of a slight lag time (~ 5 min) reports have shown a high correlation with glucose levels in the blood and interstitial fluid, particularly within close proximity of capillaries. [47, 48] Additionally, all FDA-approved minimally-invasive devices currently available extract glucose levels through sampling of

the interstitial fluid; thus, for the duration of this report, glucose measurements by means of analyzing interstitial fluid will be considered an accurate method by which to manage diabetic therapies.

Given that the success of smart tattoos is based on the ability to transdermally interrogate and collect light, optical properties of the skin must also be considered. This topic was briefly covered in an earlier section during which the wavelength dependencies of absorption and scattering properties were discussed (Figure 3); however, additional detail concerning light propagation as a function of tissue depth was not covered and is essential for understanding the location at which the implants should be placed. As light enters the skin, an initial 4% is specularly reflected as a result of the refractive index mismatch between the air and epidermis.[62] The remaining 96% enters the tissue, where it is attenuated due to successive absorption and scattering events, which contribute to diffusing the incident beam. The scattering and absorption properties of skin are highly dependent upon the wavelength of the incident light, such that light at UV (< 300 nm) and IR (> 1000 nm) wavelengths are strongly absorbed, while wavelengths in between tend to be strongly scattered (Figure 3).[62] The scattering and absorption events attenuate the light intensity as it propagates through the various skin layers (Figure 20). Therefore, long wavelength fluorophores should be considered during sensor preparation.
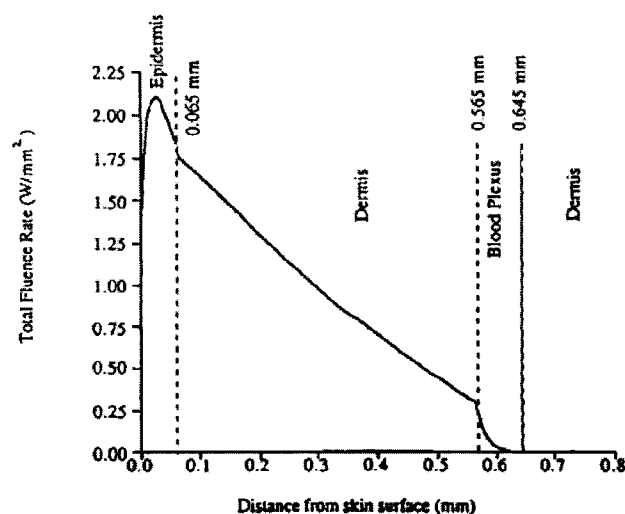
Figure 20. Total fluence rate as a function of skin depth. (577 nm incident radiation) Taken from Van Gemert et al.[62]

The question then arises: which location within the dermis is best suited for implantation such that sensor performance is maximized? To answer this question, a brief description of the microcirculation within the skin is necessary.[134]

Blood flow is supplied to the skin through two plexuses: the upper and lower horizontal plexuses. The upper plexus is approximately 1 – 2 μm below the epidermis, while the lower horizontal plexus is at the dermal–subcutaneous junction. Ascending arterioles and descending venules are paired because they connect the two plexuses. Ascending from the upper plexus is a series of arterial capillaries that form the dermal papillary loops, which represent the main supply of nutrients to the skin. Sphincter-like smooth muscle cells are at the capillary-arteriole junction of the upper horizontal plexus, serving as a means to regulate the microcirculation. At the dermal–subcutaneous junction, the upper plexus directly connects to the lower plexus, which supplies nutrients to other structures in the skin such as hair follicles or sweat glands. A schematic of the skin circulation can be seen in Figure 21.
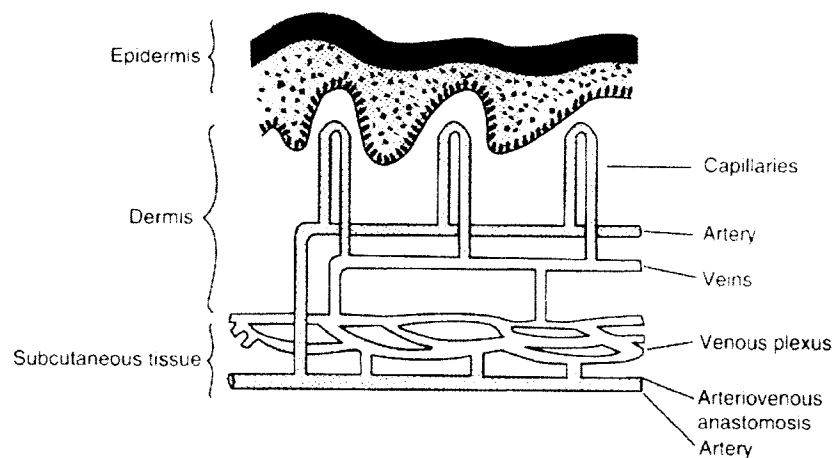
Figure 21. Skin circulatory system. Taken from Guyton and Hall.[134]

Oxygen is supplied to the dermal tissue through uptake from the atmosphere, as well as through oxygen transported through the capillaries.[135] Recent work has shown the contribution of oxygen from the atmosphere and the blood supply is highly dependent upon depth within the dermis. In this work, the authors produced a depth dependent profile of intracutaneous oxygen levels assuming 90 μM and 0 μM (vasculature occlusion) oxygen within the hematogenic supply and 277 μM (air-equilibrated oxygen levels) oxygen at air-skin interface (Figure 22).
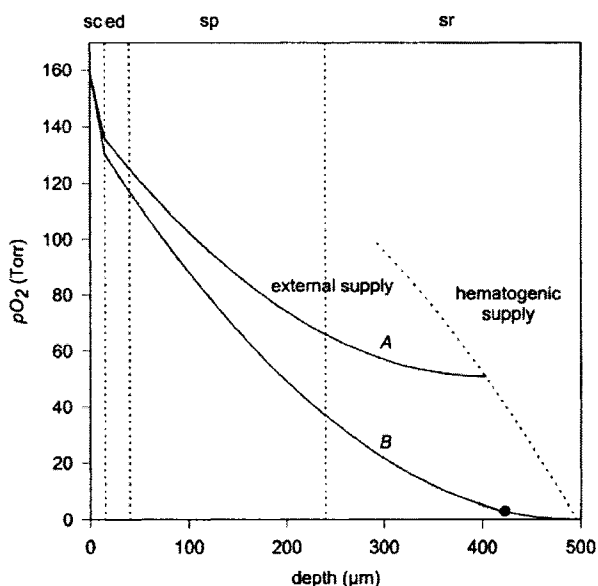
Figure 22. Theoretical estimation of the intracutaneous PO_2 profile. Sc: stratum corneum; ed: epidermis; sp: papillary dermis; sr: reticular dermis. Taken from Stücker et al.[135]

By simulating the oxygen profile in the case of an occlusion within the vasculature, the authors determined that tissue as deep as 400 μm receives a portion of its oxygen supply from the atmosphere (Figure 22, trace B). However, at depths greater than 230 μm a substantial portion of the oxygen is supplied by the vasculature. It is additionally important to note that oxygen levels within the dermis are highly depth-dependent, such that oxygen levels at the epidermal-dermal junction are approximately 215 μM, in contrast to the oxygen levels at the papillary-reticular dermis junction, which are approximately 115 μM (overall, an approximate 50% variation). Given that the smart tattoos addressed in this dissertation are based on indirect measurements though oxygen transduction, bulk oxygen levels must be considered when selecting the appropriate oxygen probe as well as when analyzing sensor performance (local oxygen levels ultimately determine when the devices become *oxygen-limited*). These concepts are

critical to the success of the work presented in this dissertation and will be revisited in later chapters.

Therefore, in an attempt to maximize the efficiency of excitation and collection efficiency of the tattoos, while at the same time placing the tattoos in close proximity of capillaries (so that chemical concentrations within the interstitial fluid closely match those in the blood), it is proposed that such systems be implanted in the papillary dermis at a depth of 150 – 200 μm below the skin surface, as suggested by previous work on similar systems.[23, 133]

History of the smart tattoo. The first known attempt at preparing smart tattoo type sensors was in 1999.[23] In this work, Russell et al. described the encapsulation of FITC-dextran and TRITC-Con A within millimeter sized PEG hydrogel spheres for use in a RET-based glucose biosensor. Before sphere formation, a PEG hydrogel precursor solution was prepared by chemically conjugating TRITC-Con A to the PEG monomers. This precursor solution, along with FITC-dextran, was then extruded through a 21-gauge syringe into a bath of mineral oil, resulting in spheres with an approximate diameter of 2 mm. The spheres were subsequently photopolymerized using UV illumination, then separated and allowed to hydrate overnight.

Glucose sensitivity experiments were performed, and the percent change in relative fluorescence at 514 nm was used to compare various sensor formulations. The authors demonstrated that the maximum percent change in fluorescence was obtained when a TRITC-Con A/FITC-dextran ratio of 100:1 was used during particle preparation. Additional experiments also determined that the absolute concentration of the binding pairs significantly affected device sensitivity. The authors used a 500:1 TRITC-Con

A/FITC-dextran ratio, which demonstrated optimum performance (i.e., highest relative percent change), to construct an additional set of sensors. Results were promising because the sensors were shown to linearly respond to glucose levels up to 600 mg/dL. At elevated glucose concentrations, non-linearities in the response profile were due to the displacement of the majority of FITC-dextran molecules and concentration quenching by free FITC-dextran molecules. The forward response time of these systems was approximately 10-12 min; however, the reverse response time was significantly longer (~ 20 min). Although leaching of FITC-dextran molecules over time as well as elevated response time could prevent this system from being used in *in vivo* diagnostics, this work represents an ingenious first attempt in smart tattoo development.

Additional work from the same group was focused on developing a software package to simulate photon propagation through skin tissue.[25] In this work, McShane et al. used Monte Carlo simulation techniques to track excitation photons as they propagate through the skin. Following the generation of a fluorescence event, the software tracks the propagation of the fluorescence photons throughout the tissue, ultimately producing a spatial distribution of sensor fluorescence at the skin surface, to aid in the design of an excitation/collection apparatus. Simulation results pointed out that several factors ultimately dictated transdermal excitation/collection efficiency: (1) geometrical properties of the sensors and/or implanted sensor population, (2) depth at which the sensors were implanted, and (3) the separation distance between the excitation and collection optics. Ultimately, the package only simulates the propagation of 488 and 520 nm photons, restricting applications. Nonetheless, simulation results did indeed indicate

that transdermal excitation and collection of the implanted systems reported by Russel et al.[23] was feasible.

The Coté group eventually tested the efficacy of exciting and collecting emission data from PEG hydrogel sensors implanted in an *in vivo* rat model.[136] Transdermal emission spectra were successfully collected from sensors implanted approximately 500 μm below the skin surface. Additionally, a bolus injection of glucose into the tail vein resulted in measurable spectral changes. This important developmental step ultimately proved that the smart tattoo concept could provide a feasible mean to fabricate minimally-invasive glucose sensors.

More recently, Ibey et al. reported on a longer wavelength competitive-binding assay, with hopes of reducing the low signal-to-noise ratio observed in previous work.[31, 136] In this work, a RET system based on AlexaFluor® 647 labeled Con A (AF647-Con A) and a fourth-generation polyamidoamine (PAMAM) glycodendrimer labeled with AlexaFluor 594 (AF594-dendrimer), which is hypothesized to increase assay sensitivity to glucose was developed. The authors report that the alkalinic nature of the dendrimers could ultimately cause pH-induced spectral fluctuations, resulting in artifacts; however, no such artifacts were observed when using the reported fluorophores. Characterization results indicated that the assay responded linearly to glucose up to 20 mM concentrations, while responding to step changes in approximately 5 min. A total percent change of approximately 100% was observed over the operational range of the assay, a considerable improvement over the sensitivity observed with the TRITC-Con A/FITC-dextran system. However, the assay was only characterized in solution phase; whether or not behavioral changes will be observed when the assay is encapsulated has yet to be reported, but the

authors indicate that encapsulation of the AF647-Con A/ AF594-dendrimer within a PEG

hydrogel is in progress.

Chinnayelka et al.[27] recently reported on a novel competitive-binding assay based

on the deactivated form of GOx, apo-GOx, as the binding molecule. In this work, a RET

assay based on the competitive-binding between FITC-dextran and glucose with TRITC-

apo-GOx (TAG) is reported, a schematic of which is given in Figure 23.
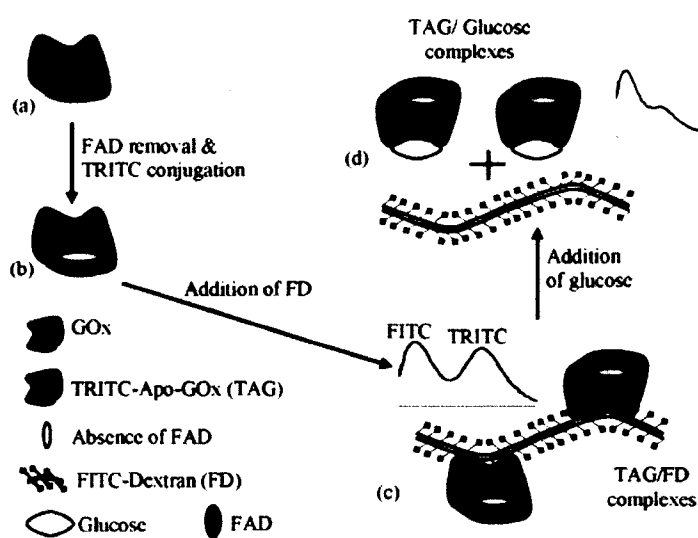
Figure 23. Schematic of a RET assay based on the competitive-binding between dextran and glucose. Taken from Chinnayelka et al.[27]

A distinguishing feature of this work is the encapsulation of the sensing assay

within *hollow* microscale capsules, thereby allowing the free movement of the ligand,

receptor, and analyte within the capsule during competitive displacement. To prepare the

capsules, a degradable $MnCO_3$ was used as a sacrificial template to which alternating

layers of PAH (a cationic polymer) and PSS (an anionic polymer) were adsorbed using

the LbL self-assembly technique. Additional multilayers comprised of PSS and DAR (a

photocrosslinkable resin) were subsequently adsorbed to the particle surface. The core template was removed through an acid treatment, resulting in hollow polymeric capsules with semi-porous walls. The capsules were loaded with the assay using simple diffusion, after which a brief exposure to UV radiation crosslinked the DAR and PSS molecules, permanently entrapping the assay within the capsule. In this report, several key results were emphasized, the most notable of them is that the molecular weight of the dextran used in the assay, the FITC-dextran/TAG ratio, as well as the sensor concentration all greatly affected the sensitivity and glucose dissociation constant, allowing the response properties of this system to "tuned." Also, the author reported a 5-fold increase in sensitivity over previously reported competitive-binding systems, as well as high reversibility. Additionally, unpublished work using NIR-emitting fluorophores were equally as impressive.[106] All the work reported by Chinnayelka was completed using steady-state fluorimetric analysis; however, future work includes dynamic testing as well as lifetime analysis of the system prior to *in vivo* analysis.

Most recently, the first smart tattoo based on enzymatic transduction was demonstrated by Brown.[133, 137] In this work, GOx was entrapped within calcium alginate microspheres by the emulsion-conjugation technique.[35] In this technique, GOx is initially mixed with an alginate solution to form a precursor. Through an emulsion process, GOx-doped alginate spheres are prepared and stabilized with Ca^{2+} crosslinking. A covalent amide linkage was formed between GOx and alginate, to stabilize the entrapment. A methanol-induced controlled precipitation process was used to entrap the ruthenium derivative, tris(4,7-diphenyl-1,10-phenanthroline)ruthenium(II), $Ru(dpp)_3^{2+}$ throughout the spheres. Additionally, a series of fluorescent nanofilms were adsorbed to the particle

surface using the LbL technique, the purpose of which is two-fold: to provide an oxygen-insensitive reference signal (AF488) and arguably more important, to provide a means by which to control the substrate mass transport properties. The authors point out that enzymatic sensors provide high selectivity as well as specificity, but require strict control over reaction kinetics to ensure that the sensors operate in a glucose-limited regime.

Testing of the enzymatic smart tattoos was accomplished in a flow chamber apparatus that allowed complete control of oxygen concentration in the testing solution. Sensors were exposed to buffer, followed by exposure to a glucose step, during which real-time emission data were collected. Results indicated that the sensors responded linearly up to 600 mg/dL of glucose, with a sensitivity of 0.02 % change per mg/dL (approximately 10% change observed at saturation). The report details that approximately 50% of the ratiometric signal was lost due to photobleaching within the first hour of continuous illumination, requiring extensive data processing techniques to extract usable calibration profiles. Even though excessive photobleaching and poor sensitivity were observed with these concepts, this work represents a significant contribution in the development of enzymatic smart tattoos.

Smart tattoo configuration addressed in this work. In this work, an enzymatic smart tattoo sensor based on oxygen transduction is presented. Specifically, GOx and platinum porphyrin oxygen indicators are immobilized within mesoporous hybrid silica particles. The hybrid silica particles are prepared through the sol-gel technique using an alginate-modified silanol as the precursor. Fluorescent nanofilms are implemented to provide a reference signal as well as to control substrate transport, a technique proven crucial in the success of similar systems.[41, 133, 137] Although previously reported results on these similar

systems will serve as the basis of comparison for many results detailed throughout this dissertation, a brief review on the following topics will indeed be useful for depicting why the materials used in this work were selected: materials used to control substrate diffusion and oxygen-sensitive fluorophores.

2.2.4 Mass Transport Controlling Materials

In enzymatic glucose sensing schemes, mass-transport controlling materials can ultimately dictate whether or not a particular design is successful. These sensor types operate on the principle of glucose-limited oxygen consumption within the local environment of the sensor. As glucose diffuses into the sensor, oxygen is consumed and rapidly replaced, allowing indirect glucose monitoring through an oxygen reporter. To achieve this fundamental condition, the relative diffusion rate of oxygen into the sensor must be greater than that of glucose; therefore, the local oxygen levels within the sensor are in excess and the sensor is operating in a glucose-limited regime. As bulk glucose levels are increased, the rate of glucose delivery into the sensor begins to eclipse the rate of oxygen replenishment, preventing the relative recovery of oxygen levels within the sensor. In this state of operation, the sensor response begins to deviate from linearity, thus implicating the onset of oxygen-limited glucose consumption. Further increases in glucose levels elicit no sensor response, due to complete internal depletion of oxygen levels (oxygen is readily consumed upon diffusion into the sensor). This condition is elicited by the surplus of local glucose within the sensor and signifies absolute oxygen-limited catalysis and response saturation. Therefore, mass-transport limiting materials could effectively control the operational range of enzymatic-based sensors.

Previously, researchers have employed several mechanisms by which to control substrate transport. One of the simplest methods involves the use of thin films, which can be comprised of a variety of synthetic or naturally occurring polymer materials. Wolfbeis' group made use of a simple dialysis membrane to construct a sensor, whose sensitivity was quite unimpressive (1.5 – 2 mM).[107] Others have used the so-called "sandwich conformation" to control diffusivities, where GOx was entrapped between two membranes; however, results implicated that product buildup within the enzyme layer led to rapid sensitivity losses under continuous operation.[138] As previously reviewed, Rosenzweig et al. used a polyacrylamide thin film to control substrate diffusivities and achieved notable results.[38] Additional work by other researchers have shown that sol-gel derivatives could be implemented as diffusion-limiting films.[139-141] All this work has proved successful, but to an extent, these techniques do not provide a *highly* precise means to control substrate transport.

Thin films fabricated using LbL self-assembly allow the construction of complex nanocomposites through simple adsorption of oppositely charged molecules in a sequential fashion. In this technique, a charged substrate is introduced to oppositely charges molecules that electrostatically self-assemble on the substrate surface, forming a nanometer scale thin film. Subsequent molecular layers are adsorbed in a similar fashion, ultimately resulting in a film with the desired molecular arrangement (Figure 24).
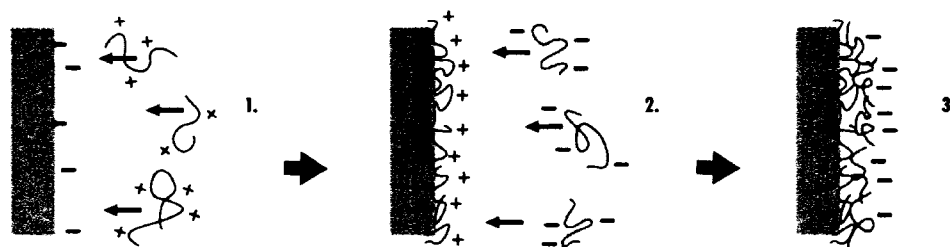
Figure 24. Layer-by-Layer nanofabrication process. Taken from McShane.[26]

This general technique has been applied to various charged species, including linear polyions, proteins, viruses, ceramics, lipid tubules, lipids, and charged nanoparticles.[142] Therefore, this technology affords a practically endless variety of nanocomposite materials to be constructed through an extremely simple procedure. Through the careful selection of materials and deposition conditions, precise nanometer-scale thin films can be deposited in a regular, consistent fashion. This technique has also allowed the realization of complex microscale three-dimensional structures, namely microcapsules.[143] Polymeric microcapsules are obtained through the sequential adsorption of polyelectrolyte multilayers onto sacrificial spherical templates (inorganic or organic). After the desired film architecture is obtained, the core templates are dissolved, resulting in stable *hollow* polymeric microcapsules comprised of nanocomposite walls. Such containers have already been exploited to successfully prepare RET-based smart tattoo sensors.[27, 106]

The Bruening group published a series of manuscripts studying the transport of various molecular species through polyelectrolyte multilayers.[144-149] In one report, the transport of uncharged solutes such as glucose, glycerol, and sucrose through polyelectrolyte multilayer with various film architectures was explored.[144] In this work, multilayers comprised of PSS and PAH were deposited onto porous alumina substrates

and the diffusivities of the uncharged solutes through the films determined. Results demonstrated that the glucose diffusivity through 7 bilayers of PSS/PAH [demarked (PSS/PAH)$_7$] was 9.87 x 10^{-14} m^2 sec^{-1}, a decrease in *four orders of magnitude* when compared to the glucose diffusivity in water (6.9 x 10^{-10} m^2 sec^{-1}), proving that polyelectrolyte films could adequately be applied as diffusion-limiting coatings. This result is remarkable, given that a typical (PSS/PAH)$_7$ film has an approximate thickness of *28 nm* (4 nm per PSS/PAH bilayer).

Brown and McShane devised a model based on reaction-diffusion kinetics to simulate how polyelectrolyte films would influence the performance of enzymatic smart tattoos.[41] In this work, the authors present a mathematical model of previously reported sensors concepts,[137] in which a ruthenium derivative and GOx were encapsulated within calcium alginate microspheres coated with polyelectrolyte multilayers to control substrate diffusivity. Various simulations were used to observe the effect of sensor parameters, such as sphere diameter, film thickness, and enzyme concentration. By varying nanofilm thickness through simply adjusting the amount of bilayers adsorbed onto the surface, the diffusivity of glucose relative to oxygen is modulated, thereby adjusting the average steady-state oxygen levels observed within the sensor (Figure 25).
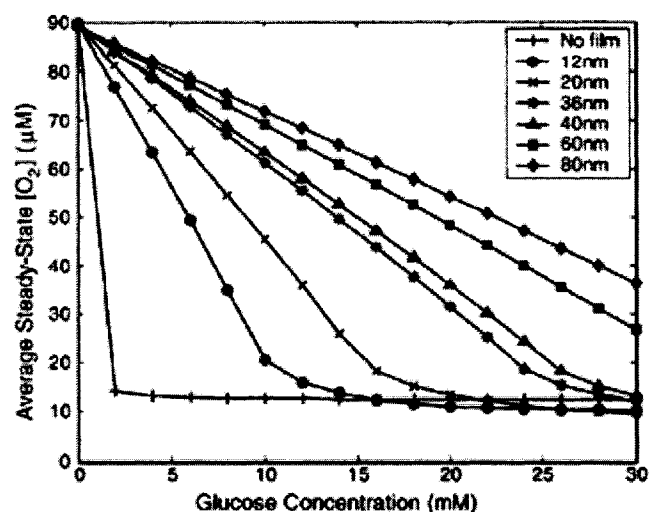
Figure 25. Average oxygen concentration at steady-state within alginate enzymatic smart tattoo sensors with varying glucose levels and nanofilm thicknesses. Taken from Brown et al.[41]

The authors highlight that these nanofilms drastically affect the sensor response, such that 12 nm nanofilms deposited onto the surface can significantly improve device response when compared with uncoated sensors. However, it is important to note that the model used in this work assumed that the substrate diffusivities throughout the nanofilms were independent of thickness, an assumption that is not likely to hold in reality. Nonetheless, the utility of these nanofilms in engineering the response properties of enzymatic smart tattoos cannot be understated. Further simulations using experimental parameters were performed and the output directly compared to experimentally determined results. Excellent agreement between simulated response and the experimental response were observed, further validating the accuracy of the model (Figure 26).
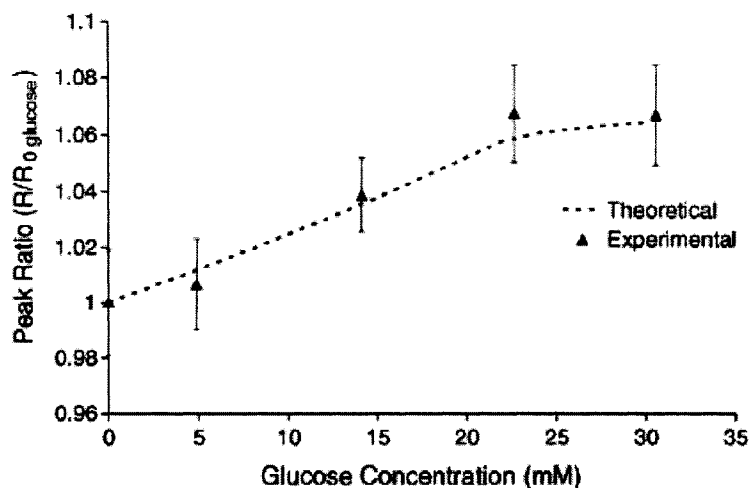
Figure 26. Comparison of simulation output and experimentally determined date. Taken from Brown et al.[41]

Therefore, the high precision and controllability afforded by LbL films, as well as the proven ability to successfully modulate substrate diffusivities in similar enzymatic sensors (as proven in experimental and simulation studies [41, 133, 137]), make this technique highly attractive for the work presented in this dissertation.

2.2.5 Luminescent Oxygen Indicators

Oxygen is one of the best known collisional quenchers of fluorescence. In collisional quenching, the quencher contacts the fluorophores while in the excited state, returning the fluorophore to ground state without photon emission.[98] The process of collisional quenching is typically characterized by the Stern-Volmer equation:

$$\frac{F_0}{F} = \frac{\tau_0}{\tau} = 1 + k_q \tau_0 [Q] = 1 + K_D [Q]$$

In this equation, F_0 and F are the fluorescence intensities in the absence and presence of the quencher, τ_0 and τ are the lifetimes of the fluorophore in the absence and presence of

the quencher, k_d is the biomolecular quenching constant, and *[Q]* is the concentration of the quencher (in this case, molecular oxygen). The Stern-Volmer quenching constant is K_D, and is calculated as the product of k_d and τ_0. The Smoluchowski equation describes the biomolecular quenching constant, k_d, and is given by:

$$k_q = 4\pi Np(D_f + D_q) \cdot 10^3,$$

where D_f and D_q are the diffusion coefficients of the quencher and fluorophore, respectively, N is Avogadro's number, and p is the probability of collision. Therefore, for oxygen indicators to be sensitive to low concentrations of oxygen, long lifetimes in the absence of the quencher (τ_0) must be exhibited (most oxygen indicators typically exhibit lifetimes greater than 100 ns). In the context of this dissertation, the indicators will be physically immobilized; thereby, the diffusion of oxygen through the immobilization matrix will to some degree affect sensitivity. This concept will be revisited later in this section.

There are two main classes of luminescent oxygen indicators: organic luminescent probes and organometallic compounds.[150] The first class includes polycyclic aromatic hydrocarbons and decacyclene compounds; however, most of these fluorophores require high UV excitation, making transdermal applications difficult and will therefore not be considered for further review in this text. Additional reading on organic luminescent probes can be found in the recent review by Amao.[150]

The majority of research in luminescent oxygen probes has focused on organometallic compounds, comprised of transition metal complexes and metalloporphyrins. Metal ligand complexes (MLCs) refer to transition metal (Ru^{2+}, Re, Os^{3+}, and Ir^{3+}) complexes containing one or more diimine ligands.[98] These compounds

are rendered fluorescent through electron promotion from the metal to the ligand – the so-called metal-to-ligand charge transfer transition (MLTC) state upon photon absorption, where an intersystem crossing from the singlet to the lowest-energy triplet state (requiring an electron-spin inversion) proceeds. Given that the conversion from the triplet state to the ground state requires an additional electron-spin flip, the triplet state of MLCs has an intrinsically long lifetime prior to photon emission.[98]

Upon contact with molecular oxygen (while in the excited triplet state), the energy of the MLC is non-radiatively transferred to oxygen, resulting in the formation of singlet oxygen. This highly reactive form of oxygen can either spontaneously return to ground state or consume oxygen from another molecule (oxidation). Should this occur to the MLC itself, irreversible damage can result (termed "photo-oxidation").

Of the transition metal complexes, ruthenium metal ligand complexes have been extensively researched for applications in biosensors.[38, 103, 129, 137, 151-153] Of the various ruthenium complexes, ruthenium(II)-2,2'-bipyridine and tris(4,7-diphenyl-1,10-phenanthroline)ruthenium(II) and have been studied the most. Both these compounds exhibit lifetimes in the low μs range and are excited with approximately 450 nm light, with subsequent emission around 590 – 605 nm. This relatively long Stokes shift allows a reference fluorophore with emission in the 500 – 570 nm range (and excitation in the range of 450- 500 nm) to be readily incorporated into the optical transduction scheme.[137] Although biosensors utilizing ruthenium complexes have been successfully demonstrated, metalloporphyrins typically have longer lifetimes and are therefore more sensitive to oxygen levels than ruthenium complexes.[44]

Metalloporphyrins, like MLCs, have unique electron transfer properties, resulting in luminescent properties. Typically porphyrin molecules have three distinct absorption peaks, the first of these is the Soret band, which results from the electronic excitation from the ground state to a vibration level of the second excited state. Two additional absorption bands (usually between 500 and 600 nm) result from the promotion of ground state electrons to the lowest vibration state level of the first excited singlet state and one moment of vibrational energy at the first excited singlet state.[44] Therefore, porphyrin molecules tend to have a variety of excitation options, allowing more versatility when designing optical transduction schemes, but the highest relative excitation efficiency is observed with UV excitation. Upon contact with molecular oxygen, a similar photo-oxidation schemes unfolds; however, porphyrins undergo different electron orbital transitions when compared to ruthenium complexes.

Two of the more popular porphyrin compounds are Pt(II) and Pd(II) octaethylporphines, both of which exhibit lifetimes on the order of 100 µs, with excitation peaks at ca. 375, 500, and 535 nm and emission at 640 – 660 nm.[46] For the application described within this dissertation, Pd(II) porphyrin complexes will not be further considered due to lack of sensitivity over dermal physiological levels described earlier. Pt(II) complexes are highly sensitive over physiological oxygen levels in the dermis (as will be detailed later in this text); however, these complexes are poorly soluble in water, making aqueous application difficult. To overcome this difficulty, surface adsorption to a carrier, usually silicon, organic glassy, cellulose derivatives, or fluoropolymers is common practice; in these cases, the immobilization matrix has been shown to significantly affect O_2 sensitivity.[44, 45] Generally, researchers agree that the

difference in sensitivities observed in various immobilization media are due to the solubility and diffusivity of oxygen in the host matrix.[46] Given this observation, the highest O_2 sensitivities with Pt(II) complexes been reported with Pt(II) porphyrin adsorption onto silica-containing matrices.[42, 46] It is theorized that oxygen molecules adsorb to the surface substrate then rapidly diffuse across the surface, the so-called Langmuir-Hinshelwood, and silica containing substrates exhibit high oxygen binding affinities and surface diffusion rates.[45, 46] Thus, silica containing matrices often excel as platforms upon which highly-sensitive oxygen sensors are built.

This result was observed in the work of Koo et al., where and oxygen-sensitive variant of optical PEBBLE nanosensors was presented.[42] In this work, organically-modified silicate nanoparticles containing Pt(II) octaethylporphine (PtOEP) as the oxygen indicator and octaethylporphine (OEP) as the oxygen-insensitive reference were prepared through the sol-gel process. Using the percent change in PtOEP/OEP peak ratio observed at oxygen depleted and saturated conditions, the authors calculated the overall sensitivity. A sensitivity of 97% was calculated, significantly greater that those observed for ruthenium-based sensors. A similar sensitivity was observed using a ketone-modified variant of PtOEP. Table 1 details the findings of the authors in terms of a comparison of sensitivities observed with ruthenium based schemes immobilized in various matrices:

Table 1. Comparison of sensitivities (Q_{DO}) of Pt(II) porphyrin and ruthenium complexes immobilized in various silica-containing matrices. Taken from Koo et al.[42]

probe	sensor type	Q_{DO} (%)
$[(Ru(dpp)_3]^{2+}$	silica film	30
$[(Ru(dpp)_3]^{2+}$	ormosil film	56–80
$[(Ru(dpp)_3]^{2+}$	silica nanoparticle	80
PtOEP	ormosil nanoparticle	97
PtOEPK	ormosil nanoparticle	97

Therefore, for the work detailed in this dissertation, highly sensitive Pt(II) porphyrin complexes immobilized within silica-containing matrices will provide highly sensitive oxygen sensors as platforms for enzymatic smart tattoos.

In summary, many methods have been employed in an attempt to provide sustained minimally- and non-invasive glucose monitoring techniques. Techniques based on fluorescence-sensing schemes have advantages (high sensitivity, as well as selectivity) over other techniques, but challenges to realize *in vivo* diagnostic devices may be faced. Recent work in the area of enzymatic smart tattoos has indeed been promising,[26, 133] but problems with sensitivity and photodegradation have raised efficacy questions. In the following chapters, a similar approach (enzymatic transduction) will be employed utilizing highly sensitive oxygen-sensitive indicators dyes and silicate immobilization matrices in an attempt to produce more sensitive, photostable devices. These devices could potentially be integrated into a transdermal glucose monitoring system to provide continuous and spot monitoring to diabetics, with hopes of increasing compliance with suggested monitoring frequencies.

CHAPTER 3

PORPHYRIN-BASED SPHERICAL OXYGEN

SENSORS AS PLATFORMS FOR

ENZYMATIC SMART TATTOOS

3.1 Introduction

Optical glucose sensors[19, 154] particularly "smart tattoo" type sensors[23-26] –

implantable luminescent particles that may be transdermally interrogated with light – are

being pursued as minimally-invasive diabetic monitoring devices. While work in this

field has primarily focused on systems exploiting competitive-binding assays,[28-30, 155, 156]

critical steps toward realizing enzymatic smart tattoos have also been reported.[26]

Enzymatic smart tattoos are typically comprised of an oxygen-quenched phosphorescent

dye and glucose oxidase (GOx), an enzyme which specifically catalyzes the oxidation of

β-D-glucose. Under conditions where this reaction is glucose-diffusion-limited, local

glucose concentrations can be extracted from O_2-dependent emission spectra or

luminescence lifetimes.[34] Therefore, overall performance of such sensors is directly

related to oxygen sensing properties. For this reason, long-lived oxygen-quenched

phosphorescent heavy metal ligand complexes are commonly used for such

applications.[43] Most work in this area has focused on using ruthenium complexes as the

reporter dye.[36, 153, 157] However, metalloporphyrin-based sensors, particularly Pt(II)

86

complexes, exhibit significantly greater sensitivity to O_2,[44] due in part to a longer fluorescence lifetime; however, these have received only minimal attention for biosensing applications.[37]

Pt(II) porphyrin complexes are poorly soluble in water, making aqueous application difficult. To overcome this difficulty, surface adsorption to a carrier, usually silicon, organic glassy, cellulose derivatives, or fluoropolymers is common practice; in these cases, the immobilization matrix has been shown to significantly affect O_2 sensitivity.[44, 45] Overall, the highest O_2 sensitivities have been observed with porphyrin adsorption onto silica-containing matrices.[42, 46]

An additional consideration when attempting to combine the oxygen indicator with an enzyme is the need for co-immobilization of these two active elements. For GOx, the immobilization environment is preferably hydrophilic, and the enzyme must further be accessible to both oxygen and glucose. We recently introduced a facile approach to produce mesoporous silicate particles comprising homogeneously distributed hydrophilic and hydrophobic domains using sol-gel-induced self-assembly. These hybrid structures are being studied as a platform for optical enzymatic biosensor technology.[158] The hybrid functionalities allow simple homogeneous adsorption of both hydrophobic and hydrophilic species like dyes and enzymes, respectively; however, maintaining sufficient functionality of the immobilized materials is paramount. Thus, the effect of this carrier material on the immobilized O_2 indicator must first be evaluated. As a first step in designing highly sensitive glucose-sensitive materials, we report on the immobilization of a Pt(II) porphyrin complex, namely Pt(II) octaethylporphine (PtOEP),

onto hybrid mesoporous silicate particles and characterization of the O_2-induced quenching effect.

3.2   Experimental Details

3.2.1   Materials

Sodium alginate (low viscosity, 250 cps, MW 12-80 kDa), (3-glycidyloxypropyl) trimethoxysilane (GPTS), and ammonium hydroxide were obtained from Sigma and used for the synthesis of mesoporous alginate-silica particles. Platinum(II) octaethylporphine (PtOEP, Frontier Scientific) and tetrahydrofuran (THF, Fluka) were used to prepare PtOEP-doped alginate-silica particles. Poly(allylamine hydrochloride) (PAH, MW = 70 kDa, Aldrich), poly(sodium 4-styrene sulfonate) (PSS, MW = 70 kDa, Aldrich), and sodium chloride (Sigma) were used during the deposition of multilayer thin films. Additionally, rhodamine B isothiocyanate (RITC, Aldrich) was conjugated to PAH and used in thin film deposition. O_2 (Air Liquide), N_2 (Air Liquide), and phosphate-buffered saline (PBS, Sigma) were used during testing. All necessary titrations were performed using 1.0 M HCl and 1.0 M NaOH, which were obtained from Fluka. All chemicals listed above were reagent grade and used as received. Throughout all experimental procedures, ultra pure water with a resistivity of greater than 18 MΩ was used. Unless otherwise stated, all experimental processes were conducted at 25 °C.

3.2.2   Preparation of Mesoporous
Alginate-Silica Particles

Alginate-silica ("algilica") particles were prepared using a procedure similar to that which was previously reported.[35, 159] Briefly, the precursor was prepared by stirring a solution comprised of 1.5 wt% aqueous alginate solution and glycidyl silane (GPTS) in a 1:1 volumetric ratio for at least 4 hours, resulting in an alginate-modified silanol.

While stirring, 2 mL of the precursor silanol was added to 3 mL of water. To initiate the sol-gel process, 1.25 mL of 10 M NH$_4$OH was added and stirred for 20 min, followed by the addition of 10 mL of water and an additional stirring time of 40 min. An extra 40 mL of water was added and the suspension stirred for at least an additional 4 hours. The resulting particle suspension was rinsed with DI water using four sequential centrifugation cycles and diluted to a total aqueous suspension volume of 1.5 mL. A Beckman Coulter counter (Z2) equipped with a 100 μm aperture was used to obtain the mean diameter and concentration of particles comprising the stock suspension.

3.2.3 Preparation of PtOEP-Doped Particles

Approximately 250 μL of stock particle suspension was placed in a microcentrifuge tube, the supernatant removed via centrifugation, and 250 μL of a 750 μM PtOEP solution prepared in THF was added. The container was sealed to prevent volatilization of THF and stirred for 30 min, after which 30 μL of water was added and the suspension stirred for an additional 30 min. The water added to the suspension initiated a solvent-mediated controlled precipitation of PtOEP into the mesoporous particles, a technique used in previous reports to aid in the immobilization of desired molecules.[160] The suspension was subsequently rinsed with DI water four times.

3.2.4 Adsorption of Nanofilm Surface Coatings

RITC was conjugated to PAH (PAH-RITC) according to a standard amine conjugation protocol.[161] Before multilayer film deposition, respective solutions of PSS, PAH, and PAH-RITC were prepared in 0.2 M NaCl at a concentration of 2 mg/mL. The supernatant of the particle suspension was removed and the particles were resuspended in

PAH-RITC. Following a 15 min adsorption time, during which the particles were continuously shaken using a Vortex Genie-2 (Fisher Scientific) and protected from light with aluminum foil, the particles were rinsed three times with DI water and subsequently resuspended in PSS solution. To determine the overall number of PAH-RITC/PSS bilayers to be deposited on the particle surface, fluorescence emission spectra were acquired using the sample chamber detailed in the following section after each bilayer deposition. When the PtOEP emission maxima (645 nm) was approximately 75% of the RITC emission maxima (580 nm), which in this case was three bilayers of PAH-RITC and PSS (denoted {PAH-RITC/PSS}$_3$), PAH-RITC deposition was halted. The completed oxygen sensors were imaged using confocal microscopy with 543 nm He/Ne excitation and a 63x oil immersion lens.

3.2.5 Testing Apparatus

A custom-designed software suite (LabVIEW, National Instruments) and testing apparatus was developed to monitor changes in sensor response to varying levels of dissolved oxygen (Figure 27).
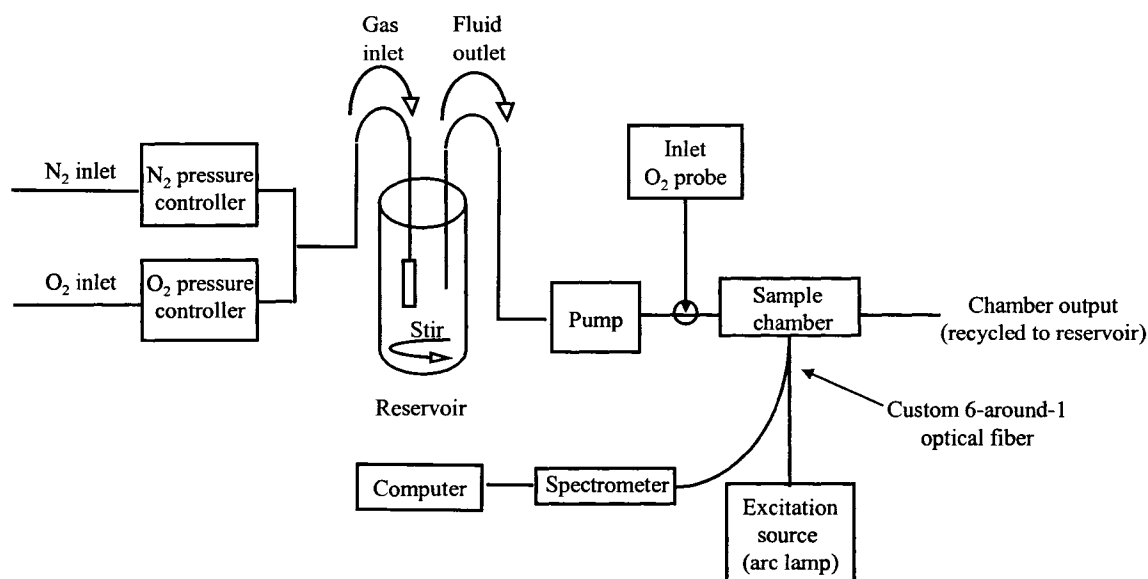
Figure 27. Schematic of testing apparatus used to quantify oxygen response properties of self-referenced oxygen sensors.

This system allows control of bulk oxygen concentration by means of regulated mixing of oxygen and nitrogen through a pair of individually addressable pressure controllers (Model 00122QA, Cole-Parmer Instrument Company) entering the buffer reservoir. Equilibration of oxygen levels within each reservoir was hastened with a gas diffuser (ChemGlass, fine frit) and magnetic-assisted stirring (Dylastir, VWR). A peristaltic pump (MasterFlex L/S 7550 pump drive with MasterFlex Easy Load 3 pump heads) extracted the oxygenated buffer from the reservoir and into the sample chamber. Prior to entering the sample chamber, the dissolved oxygen level of the solution was recorded using an in-line oxygen microelectrode and picoammeter (OX 500 and PA2000, Unisense). The sample chamber consists of a custom-designed garolite flow cell, which accepts a standard microscope slide (25x75x1 mm, VWR) with the sensors immobilized to the surface. Additionally, the reaction chamber contains a port to interface the sample slide with a custom optical fiber. The optical fiber probe was comprised of one delivery

fiber (400 μm multi-mode, ThorLabs) and six collection fibers – a so-called "6-around-1" fiber – and delivered excitation light from a Hg-Xe arc lamp (Model 68811, Oriel) containing a 530 ± 5 nm interference filter (ThorLabs). Sensor emission was subsequently delivered to a diode array spectrometer (USB 2000, OceanOptics) through the collection bundle. Following passage through the sample chamber, the solution was recycled into the reservoir vessel. Tubing (Norprene® , MasterFlex) in direct contact with solution exhibited negligible oxygen permeability, thereby minimizing convective-induced changes in oxygen levels as the solution traveled through the apparatus. It is noteworthy to state that all of the equipment, except the stir plates, used in the testing apparatus are either individually addressable (i.e., directly controlled) or report (i.e., output collected and processed in real-time) through the custom software suite, allowing increased user-control of the experimental environment and minimized data processing times. Details on experimental parameters, including sample preparation techniques, will be detailed in the next section.

3.2.6 Oxygen Sensitivity Testing

The testing apparatus was set up to pump buffer (0.01 M PBS, pH = 7.4) into the sample chamber (Figure 27). To prepare a sample for testing, double-sided pressure-sensitive polyacrylate adhesive (3M) was placed onto the surface of a standard microscope slide, followed by the addition of 10 μL ($\sim 10^6$) of sensors onto the adhesive surface. The sample was dried under streaming N_2 and fixed into the sample chamber. Randomized oxygen levels ranging from oxygen depleted to oxygen saturated conditions were obtained by bubbling O_2 and N_2 at varied partial pressures into the buffer reservoir. With the solution flow rate set at 4 mL/min, the oxygen-dependent emission spectra of

the sensors were collected when the oxygen level at the reaction chamber inlet reached steady-state, as indicated by the in-line oxygen microelectrode.

3.3 Results and Discussion

3.3.1 Sensor Fabrication

To allow compensation for instrumentation fluctuations and changes in illuminated particle numbers, it is common practice to include an O_2-insensitive reference probe, allowing ratiometric analysis of sensor response. To provide such a reference signal, rhodamine isothiocyanate (RITC)-tagged nanofilms were deposited onto the particle surface using electrostatic layer-by-layer assembly,[40] a technique allowing multilayer polyelectrolytes to be deposited with nanometer precision on three-dimensional structures. Following deposition of RITC-doped nanofilms, the emission spectrum of the dissolved oxygen sensors was acquired using the testing apparatus detailed in the above section (Figure 28). Additionally, it is important to state that these data were collected at air-equilibrated conditions.
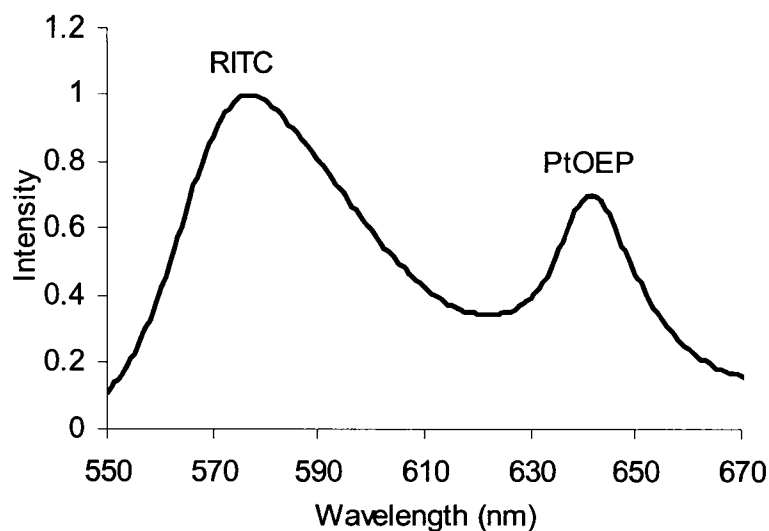
Figure 28. Emission spectrum of self-referenced dissolved oxygen sensors acquired using 530 nm excitation.

From inspection of the emission spectrum of the sensors, it is clear that a bimodal distribution exists. Upon 530 nm excitation, both RITC and PtOEP are efficiently excited and emit with maxima around 580 nm and 645 nm for RITC and PtOEP, respectively. A schematic of this concept is given in Figure 29, where $h\nu_{ex}$, $h\nu_{RITC}$, and $h\nu_{PtOEP}$ represent the 530 nm excitation and simultaneous emission of RITC and PtOEP, respectively.
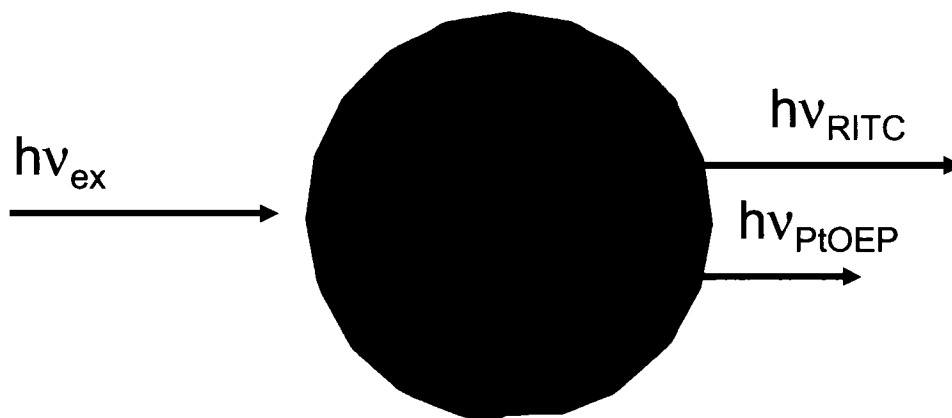
Figure 29. Schematic of single-excitation/dual-emission ratiometric oxygen sensor.

The spatial distribution of dyes within the particles was analyzed using confocal microscopy with 543 nm HeNe excitation and emission collection over 560-600 nm and 630-660 nm for RITC and PtEOP, respectively (Figure 30). Line scan analysis of the acquired images indicated PtOEP adsorption was uniform throughout the particle, while RITC was limited to the surface, as expected (Figure 30).
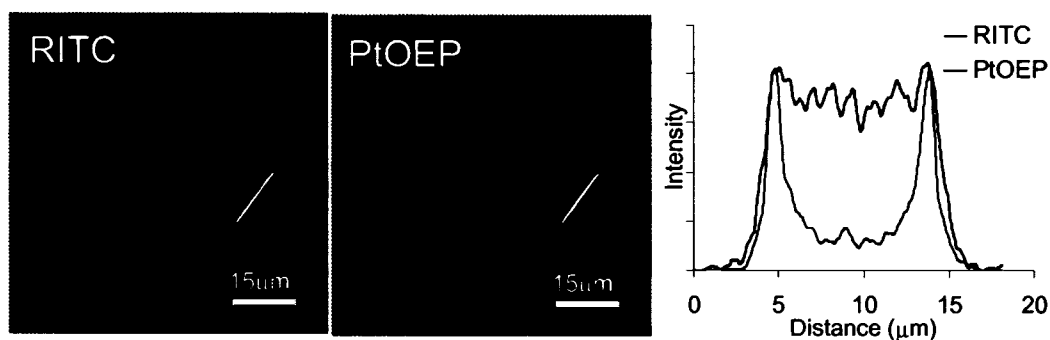
Figure 30. Confocal images of self-referenced oxygen sensors with corresponding line scan data depicting the spatial distribution of RITC (red) and PtOEP (blue).

3.3.2 Oxygen Response Properties

Characterization of the O_2-quenched properties of the particles was performed using steady-state fluorimetric analysis with particles immobilized in a custom flow-through chamber. Upon 530 nm excitation with a filtered arc lamp, intense stable emission spectra were acquired (Figure 28). The steady-state response of the sensors was obtained by pumping buffer from a reservoir set at a desired oxygen concentration, in random order. Spectral measurements were performed in parallel with measurements collected from a calibrated O_2 microelectrode. The ratiometric response was obtained by normalizing the corrected intensity spectra to the RITC maximum at 575 nm (Figure 31), where the 645 nm peak decreased with increasing oxygen concentration. The PtOEP peak ratio vs. O_2 concentration was plotted to determine regions of high sensitivity (Figure 31 – inset). Before ratio calculations, the PtOEP peak ratio (645/575 nm) was corrected for spectral overlap from the reference peak, which was determined to be approximately 17%.
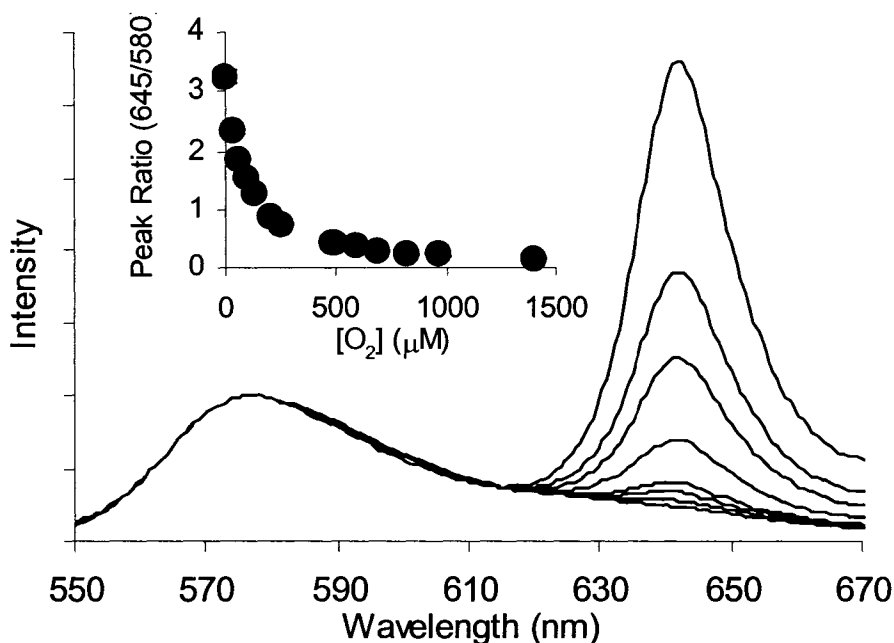
Figure 31. Oxygen-dependent emission spectra of sensors, depicting strong decrease in emission at 645nm when moving from oxygen depletion to saturation. Inset: Peak ratio vs. O_2 concentration.

An important feature of these nanocomposite materials is the high sensitivity to oxygen levels between O_2 depleted and atmospheric (277 μM) levels, such that 95% of the total change in ratiometric intensity per μM of O_2 occurs for O_2 concentrations less than 277 μM. Given the reported intradermal O_2 level of 90 μM,[162] these sensors would be highly sensitive in the physiologically relevant range. *For enzymatic smart tattoo applications, high sensitivity to O_2 within this region is critical, as reported reaction-kinetic simulations of enzymatic smart tattoo behavior show that local O_2 levels within the sensor can be reduced to 10 μM when elevated blood-glucose levels (350 mg/dl) are present.*[41]

It is well-known that environmental properties can influence the quenching properties of luminescent oxygen probes, affecting the Stern-Volmer relationship, which

relates fluorescence intensities in the absence and presence of the quencher, F_0 and F, respectively, to the quencher concentration. Other reports have observed a downward curvature in the Stern-Volmer relationship, attributed to indicator exposure to multiple environments of varying O_2 diffusivity.[163, 164] However, we observed highly linear quenching behavior (Figure 32), indicating that PtOEP is distributed within a highly homogeneous environment throughout the immobilization matrix, such as has been noted in other silica-based systems.[42]
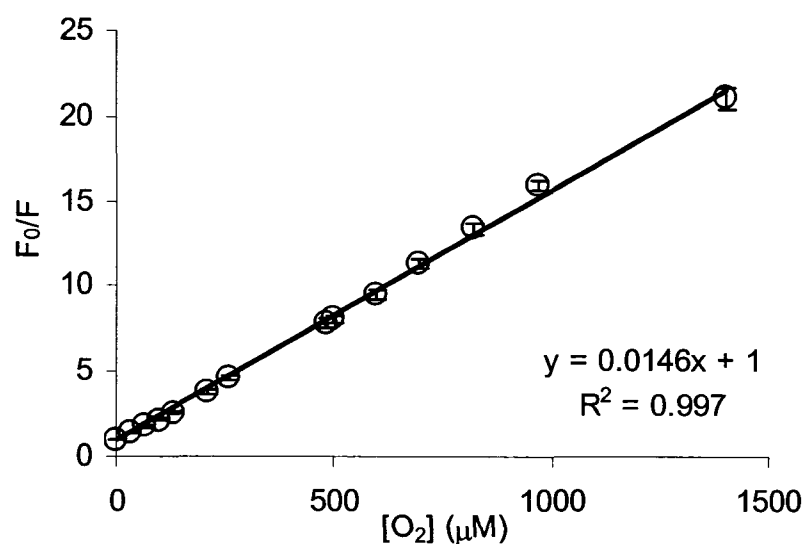
Figure 32. Stern-Volmer plot for ratiometric PtOEP sensors, including linear fit. Error bars indicate one standard deviation (n=3).

Additionally, it is common to quantify sensitivity by calculating the overall quenching response to dissolved oxygen (Q_{DO}) using the following equation:

$$Q_{DO} = \frac{R_{deoxy} - R_{oxy}}{R_{deoxy}} \times 100 ,$$

where R_{deoxy} and R_{oxy} represent the PtOEP peak ratio during exposure to oxygen depleted and saturated conditions, respectively. The sensitivity was determined to be 95%, among the highest reported sensitivity for luminescent dissolved-oxygen sensors reported to date.[42] High oxygen sensitivity, coupled with the protein-friendly amphiphilic mesoporous immobilization matrix, makes these systems ideal for enzymatic smart tattoo development.

3.4 <u>Conclusion</u>

Highly sensitive, internally-referenced phosphorescent oxygen sensors using hybrid mesoporous silicate microparticles were prepared, in which homogenous adsorption of PtOEP was achieved throughout the particle structure, while reference emission was localized to the surface. The sensors respond linearly to oxygen concentration while exhibiting 95% sensitivity. These results form a basis for development of enzymatic glucose sensors for use in diabetic monitoring by integrating glucose oxidase into the reported oxygen-quenched system. Thus, in the next chapter, the co-immobilization of PtOEP and GOx is presented and the glucose sensitive response properties evaluated.

CHAPTER 4

PORPHYRIN-BASED ENZYMATIC

SMART TATTOO SENSORS

4.1 Introduction

In the previous chapter, a ratiometric oxygen sensor comprising algilica matrices, platinum porphyrin indicators and fluorescent nanofilms was described. The results indicated high oxygen sensitivity within the expected range of operation (< 90 µM); therefore, algilica matrices and PtOEP indicators provide a platform upon which to develop smart tattoo type sensors. In this chapter the feasibility of co-immobilizing PtOEP and glucose oxidase within algilica matrices to produce glucose sensitive devices is explored, with particular emphasis on using fluorescent nanofilm coating to modulate response characteristics, namely sensitivity and range. Ultimately, devices with a high degree of controllability would be an attractive solution to provide diabetics with monitoring technology customized to their individual needs.

In the United States alone, it is estimated that 20.8 million residents (7% of the population) are afflicted with diabetes mellitus, a group of diseases characterized by hyperglycemia elicited from defects associated with insulin secretion, insulin action, or both.[1] A recent clinical trial proved that proper care and management of blood glucose

100

levels is critical in preventing or delaying the progression of complications, which include cardiovascular disease, stroke, hypertension, retinopathy, nephropathy, neuropathy, periodontitis, gingivitis, cataract formation, and pregnancy complications.[2, 8] Proper disease management is centered around effective control of blood glucose levels using one or more of the following therapies: changing high-risk lifestyle habits, consuming prescription medications, and administering supplemental insulin.[7] However, to effectively manage therapy dosages, particularly supplemental insulin, patients must frequently evaluate blood glucose levels. Currently, the gold-standard method for self-monitoring blood glucose levels is the "finger-prick" test, which involves lancing the skin and extracting a blood sample that is subsequently placed in a portable device to extract glucose levels. This method, although proven highly accurate, is both painful and bothersome for the patient, especially if the recommended testing frequency – at least 3 times per day – is practiced.[7] However, according to several studies, only 40% of diabetics requiring insulin therapy and 5% of diabetics requiring prescription medications monitor their blood glucose levels at least once per day, citing excessive pain and inconvenience as the principle reason for lack of compliance. [11-13] Therefore, it is reasonable to conclude that the development of a simple and painless method would increase patient observation of the recommended self-monitoring guidelines, which in turn would reduce their overall complications. The development of such a minimally- or non-invasive technique which can provide continuous and spot measurements has long been considered one of the "holy grails" of diabetes research.[14]

Optical monitoring techniques, including fluorescence,[19] absorbance,[20] raman,[21] and polarization spectroscopy[22] have been heavily researched as a minimally-invasive

means to measure blood glucose levels. However, the high sensitivity and selectivity associated with fluorescence-sensing techniques have led to increased interest by many groups.[19] A particularly interesting technique which has the potential to provide both spot and continuous measurements of glucose levels are "smart tattoo" type sensors, which consist of micron-scale glucose-sensitive luminescent particles that could be implanted into the dermis and transdermally interrogated with light.[23-26] Most of the work in this field has primarily focused on the development of competitive-binding based assays, which rely on changes in fluorescence emission properties modulated by fluorescence resonance energy transfer (FRET) to optically transduce glucose levels.[27-31] FRET is driven through the competitive binding of a fluorescent ligand and analyte to receptor sites on lectins, glucose-binding proteins, or deactivated glucose-specific enzymes, such that the ligand is displaced from the receptor when in the presence of the analyte causing measurable changes in emission spectra.[32, 33, 165] However, recent successes with enzymatic-based smart tattoo sensors have been reported.[26, 166]

Enzymatic-based smart tattoo sensors typically entail of an oxygen-quenched luminescent dye and glucose oxidase (GOx) entrapped within a microscale container. As glucose diffuses into the sensor, local oxygen levels are proportionally reduced through GOx-initiated catalysis. The glucose-dependent oxygen levels are then relayed through the fluorescence emission of the oxygen reporter, providing an indirect means to monitor glucose levels.[34] Although the integration of GOx into the sensing scheme provides innate selectivity to the sensor as well reversibility, controlling the reaction-diffusion kinetics of both glucose and oxygen are key to the realization of optimized sensors.[35] Initial work in this field was done using optical fibers with sensor components

immobilized in transport limiting matrices.[36, 37, 167] While these devices exhibit desirable sensor properties, in practice they would require a permanent connection to external measurement devices, providing a potential infection pathway. Additional work by Kopelman's group showed that sensor components immobilized within nano-scale polyacrylamide particles reversibly responded to physiological glucose levels.[39] Brown et al. advanced the concept using calcium alginate hydrogel microspheres, which contained GOx and an oxygen-quenched ruthenium compound, and diffusion-limiting nanofilms adsorbed to the surface using layer-by-layer self assembly.[26, 40, 41] By altering the physical properties of the nanofilms, the analyte transport properties into the microsphere could be altered, resulting in control of overall response characteristics, such as sensitivity and linear range.[41] Although the results reported to date are promising, most work has focused on using phosphorescent ruthenium complexes as the reporter molecules, which have a lower sensitivity than other oxygen probes, such as phosphorescent metalloporphyrins.[37, 42, 43,44]

Since the overall response properties of enzymatic smart tattoo sensors are dependent on the oxygen probe, *it is hypothesized that the integration of a more sensitive Pt(II) porphyrin dye should result in an overall increase in sensitivity to glucose.* To our knowledge only one report has used Pt(II) porphyrins in enzymatic glucose sensors.[37] The lack of work with porphyrin indicators could be due to extreme hydrophobicity, causing difficulties in aqueous applications.[43] To overcome this obstacle, researchers have since developed immobilization matrices comprised of silicon, organic glassy, cellulose derivative, or fluoro-polymers, to which Pt(II) porphyrins can be adsorbed, thereby allowing dissolved oxygen measurements in aqueous environments.[44, 45] It is

well documented that the immobilization matrix can drastically affect the oxygen sensitivity and that silica-containing matrices produce high sensitivities, although the exact mechanisms are still debated.[42, 46]

We recently introduced a simple method (performed at room temperature and independent of surfactants) to self-assemble mesoporous silicate particles comprised of homogeneously distributed hydrophilic and hydrophobic domains, so-called hybrid structures, for use as a platform technology.[35] One application of this technology is the use as an immobilization matrix for enzymatic smart tattoo components. As a first step in preparing enzymatic smart tattoos, Pt(II) octaethylporphine (PtOEP) was adsorbed to alginate-modified mesoporous silica particles, followed by characterization of the oxygen-induced quenching effect, as detailed in Chapter 3.[159] As a continuation of that work, this report focuses on the adsorption of both GOx and PtOEP into alginate-modified mesoporous silica particles subsequently coated with fluorescent nano-films using the LbL technique. The loading characteristics of the sensor components into the mesoporous substrate were characterized using confocal microscopy and fluorescence spectroscopy. The response dynamics – stability, response time, reversibility, sensitivity, and analytical range – of the sensors to varying bulk glucose levels were characterized using a custom flow chamber. Potentially, these systems or similar systems may be integrated into minimally-invasive diabetic monitoring devices, allowing diabetics to perform continuous and spot measurements of blood glucose levels without the pain and bother associated with "finger pricking". More important, this work lays the foundation for the development of additional highly sensitive biochemical monitors, which may be obtained by simply integrating other enzyme species specific to the target analyte.

4.2 Experimental Details

4.2.1 Materials

Sodium alginate (low viscosity, 250 cps, MW 12-80 kDa), (3-glycidyloxypropyl) trimethoxysilane (GPTS), and ammonium hydroxide were obtained from Sigma and used for the synthesis of mesoporous alginate-silica particles. Platinum(II) octaethylporphine (PtOEP, Frontier Scientific), tetrahydrofuran (THF, Fluka), glucose oxidase (GOx, type VII from *Aspergillus niger*, 198 k units/g solid, Sigma), N-(3-dimethylaminopropyl)-N'-ethylcarbodiimide hydrochloride (EDC, Fluka), N-hydroxysulfosuccinimide sodium salt (NHSS, Toronto Research Chemicals Inc.), and sodium bicarbonate (Sigma) were used to prepare PtOEP/GOx-doped alginate-silica particles. Poly(allylamine hydrochloride) (PAH, MW = 70 kDa, Aldrich), poly(sodium 4-styrene sulfonate) (PSS, MW = 70 kDa, Aldrich), and sodium chloride (Sigma) were used during the deposition of multilayer thin films. Additionally, rhodamine B isothiocyanate (RITC, Aldrich) was conjugated to PAH and used in thin film deposition. β-D-glucose (MP Biomedicals, Inc.), O_2 (Air Liquide), N_2 (Air Liquide), and phosphate buffered saline (PBS, Sigma) were used during dynamic testing. All necessary titrations were performed using 1.0 M HCl and 1.0 M NaOH, which were obtained from Fluka. All chemicals listed above were reagent grade and used as received. Spectroscopic grade potassium bromide (KBr, Thermo Electron) was used to prepare infrared spectroscopy samples. Throughout all experimental procedures, ultra-pure water with a resistivity of greater than 18 MΩ was used. Unless otherwise stated, all experimental processes were conducted at 25 °C.

4.2.2 Particle Preparation and Characterization

Alginate-silica ("algilica") particles were prepared using a procedure similar to that which was previously reported.[35, 159] Briefly, the precursor was prepared by stirring a solution comprised of 1.5 wt% aqueous alginate solution and glycidyl silane (GPTS) in a 1:1 volumetric ratio for at least 4 hours, resulting in an alginate-modified silanol. While stirring, 2 mL of the precursor silanol was added to 3 mL of water. To initiate the sol-gel process, 1.25 mL of 10 M NH$_4$OH was added and stirred for 20 min, followed by the addition of 10 mL of water and an additional stirring time of 40 min. An extra 40 mL of water was added and the suspension stirred for at least an additional 4 hours. The resulting particle suspension was rinsed with DI water using four sequential centrifugation cycles and diluted to a total aqueous suspension volume of 1.5 mL. A Beckman Coulter counter (Z2) equipped with a 100 μm aperture was used to obtain the mean diameter and concentration of particles comprising the stock suspension. Fourier transform infrared spectroscopy (FTIR, Nexus 470) was used to characterize the chemical makeup of the particles. Samples for FTIR analysis were prepared by using a hand press with accompanying die and anvil (Thermo Electron) where approximately 1 mg of dried particles were mixed with 15 mg of KBr and pressed into pellet form. After the spectrometer was purged with N$_2$, IR spectra were acquired using the prepared pellets.

4.2.3 pH Effect on GOx Immobilization

For use in fluorescence imaging, FITC labeled GOx (FITC-GOx) was prepared using 1:1 molar ratio during the labeling reaction, which was performed using a standard amine labeling protocol.[161] The final solution was diluted to a final concentration of 2

mg/mL in 0.05 M sodium acetate. Separate FITC-GOx solutions were titrated to the following pH values: 3.0, 4.0, 5.0, and 6.0, using an electrochemical pH meter (270 A+, Thermo Orion) to monitor the titrations. Approximately 5 mg of dried alginate-silica particles were added to 250 μL of the respective FITG-GOx solutions. Solutions were allowed to equilibrate overnight before analysis. Samples were prepared for image analysis by placing 10 μL of each particle suspension onto a coverslip (24x60 mm No. 1.5, VWR). Image analysis was performed on a Leica TCS 2 (Leica Microsystems) confocal imaging system equipped with a 63x HCX PL APO oil immersion lens (1.4 – 0.60 NA) and 488 nm Ar/Kr excitation.

4.2.4 Preparation of PtOEP and GOx-Doped Particles

Approximately 250 μL of stock particle suspension was placed in a microcentrifuge tube, the supernatant removed via centrifugation, and 250 μL of a 750 μM PtOEP solution prepared in THF was added. The container was sealed to prevent volatilization of THF and stirred for 30 min, after which 30 μL of water was added and the suspension stirred for an additional 30 min. The water added to the suspension began a solvent-mediated controlled precipitation of PtOEP into the mesoporous particles, a technique used in previous reports to aid in the immobilization of desired molecules.[160] The suspension was subsequently rinsed with DI water four times. Following the last rinse cycle, the supernatant was removed and 300 μL of 35 mg/mL GOx prepared in 0.05 M sodium acetate (pH = 4.0) was added and the pH value experimentally determined from the results obtained in the previous section. The suspension was stirred for 1.5 hours, followed by two rinsing cycles with DI water. The supernatant was subsequently

removed and replaced with 250 µL of solution comprised of 30 mg/mL and 10 mg/mL of

EDC and NHSS in 0.05 M sodium acetate (pH = 5.0) to catalyze amide bond formation

between amine and carboxylic acid functionalities on GOx and alginate, respectively.[35]

Finally, the suspension of PtOEP/GOx-doped particles was stirred for 4 hours then rinsed

two times with DI water. The Lowery method was used to determine the concentration

of GOx immobilized in the particles,[168] indicating that approximately 720 µM of GOx

per particle was immobilized. For imaging purposes, a separate batch of PtOEP/GOx-

doped particles were prepared using FITC-GOx and imaged using the confocal scanning

system detailed above, set in sequential scanning mode with 488 nm Ar/Kr and 543 nm

He/Ne excitation, respectively.

4.2.5 Adsorption of Nanofilm
Surface Coatings

RITC was conjugated to PAH (PAH-RITC) according to a standard amine

conjugation protocol.[161] Before multilayer film deposition, respective solutions of PSS,

PAH, and PAH-RITC were prepared in 0.2 M NaCl at a concentration of 2 mg/mL. The

supernatant of the PtOEP/GOx-doped particles was removed and the particles were

resuspended in PAH-RITC. Following a 15 min adsorption time, during which the

particles were continuously shaken using a Vortex Genie-2 (Fisher Scientific) and

protected from light with aluminum foil, the particles were rinsed three times with DI

water and subsequently resuspended in PSS solution. To determine the overall number of

PAH-RITC/PSS bilayers to be deposited onto the particle surface, fluorescence emission

spectra were acquired using the sample chamber detailed in the following section after

each bilayer deposition. When the PtOEP emission maxima (645 nm) was approximately

75% of the RITC emission maxima (580 nm), which in this case was three bilayers of

PAH-RITC and PSS (denoted {PAH-RITC/PSS}₃), PAH-RITC deposition was halted. An additional seven PAH/PSS bilayers were deposited using the same protocol, making the total film architecture deposited on the PtOEP/GOx-doped particles [{PAH-RITC/PSS}₃/{PAH/PSS}₇] and completing sensor fabrication. The complete sensors were imaged using confocal microscopy with 543 nm He/Ne excitation.

4.2.6 Dynamic Testing Apparatus

A custom-designed software suite (LabVIEW, National Instruments) and dynamic testing apparatus were developed to monitor real-time changes in sensor response (Figure 33). The system allows control of bulk oxygen concentration by means of regulated mixing of oxygen and nitrogen through a pair of individually addressable pressure controllers (Model 00122QA, Cole-Parmer Instrument Company) for the buffer and glucose reservoir, respectively. Equilibration of oxygen levels within each reservoir was hastened with gas diffusers (ChemGlass, fine frit) and magnetic assisted stirring (Dylastir, VWR). Peristaltic pumps (MasterFlex L/S 7550 pump drive with MasterFlex Easy Load 3 pump heads) extract glucose and buffer from the reservoirs at a relative rate that when mixed prior to entering the reaction chamber, the glucose concentration was equivalent to a user-defined value. Prior to entering the reaction chamber, the bulk oxygen level of the glucose solution was recorded using an in-line oxygen microelectrode and picoammeter (OX 500 and PA2000, Unisense).
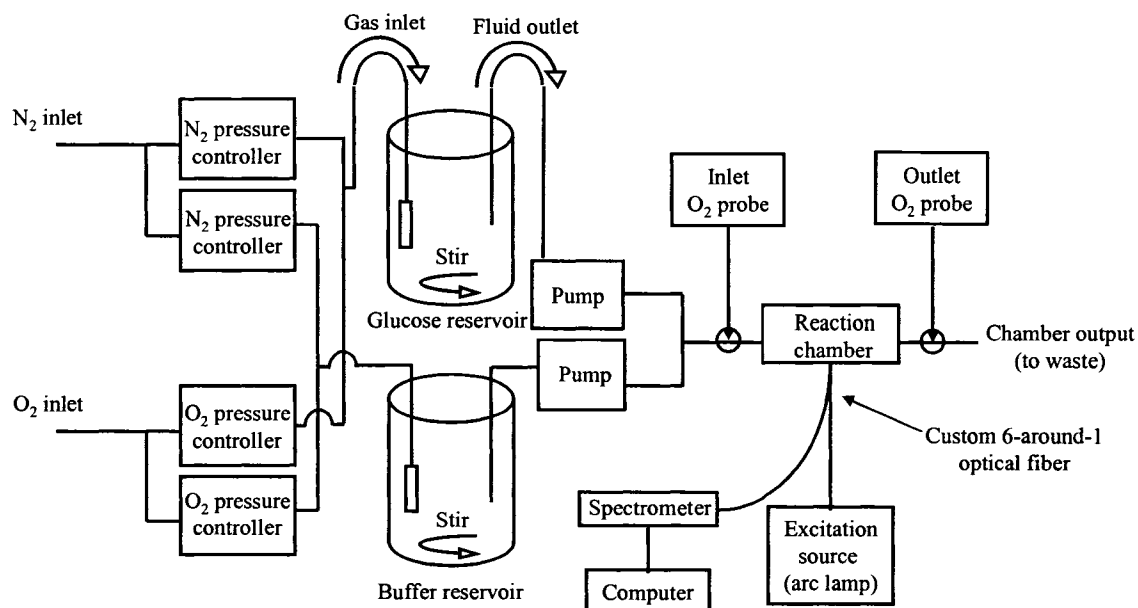
Figure 33. Schematic of dynamic testing apparatus used to quantify sensor response properties.

The reaction chamber consists of a custom-designed garolite flow cell, which accepts a standard microscope slide (25x75x1 mm, VWR) with the sensors immobilized to the surface. Additionally, the reaction chamber contains a port to interface the sample slide with a custom optical fiber. The optical fiber probe had one delivery fiber (400 μm multi-mode, ThorLabs) and six collection fibers – a so-called "6-around-1" fiber – and was used to deliver excitation light from a Hg-Xe arc lamp (Model 68811, Oriel) containing a 530 ± 5 nm interference filter (ThorLabs). Sensor emission was subsequently delivered to a diode array spectrometer (USB 2000, OceanOptics) through the collection bundle. Following passage through the reaction chamber, outlet solution oxygen levels were recorded using an additional in-line microelectrode chamber prior to being collected as waste and discarded. Tubing (Norprene® MasterFlex) in direct contact with solution exhibited negligible oxygen permeability, thereby minimizing

convective-induced changes in oxygen levels as the solution traveled through the apparatus. It is noteworthy to state that all of the equipment, with exception of the stir plates, used in the testing apparatus are either individually addressable (e.g. directly controlled) or report (e.g. output collected and processed in real-time) through the custom software suite, allowing increased user-control of the experimental environment and minimized data processing times. Details on experimental parameters, including sample preparation techniques, will be detailed in the next section.

4.2.7 Oxygen Sensitivity Testing

The testing apparatus was set to pump only buffer (0.01 M PBS, pH = 7.4) into the reaction chamber (Figure 27). To prepare a sample for testing, double-sided pressure-sensitive polyacrylate adhesive (3M) was placed onto the surface of a standard microscope slide, followed by the addition of 10 μL ($\sim 10^6$) of sensors onto the adhesive surface. The sample was dried under streaming N_2 and fixed into the reaction chamber. Randomized oxygen levels ranging from oxygen-depleted to oxygen-saturated conditions were obtained by bubbling O_2 and N_2 at varied partial pressures into the buffer reservoir. With the solution flow rate set at 4 mL/min, the oxygen-dependent emission spectra of the sensors were collected when the oxygen level at the reaction chamber inlet reached steady-state, as indicated by the in-line oxygen microelectrode.

4.2.8 Dynamic Glucose Sensitivity
Testing

Large volume reservoirs (4 L) supplied the testing apparatus with buffer and glucose, respectively. The buffer reservoir contained 0.01 M PBS (pH = 7.4), while the glucose reservoir contained 600 mg/dL of β-D-glucose dissolved in 0.01 M PBS (pH = 7.4). The oxygen levels in both reservoirs were equilibrated to air saturated conditions.

Sample preparation was performed as described above. Random triplicate glucose levels, ranging from 25 mg/dL to 300 mg/dL in 25 mg/dL increments, were flowed through the reaction chamber at a rate of 4 mL/min for approximately 8 min, which was experimentally predetermined to allow response equilibration. To show reversibility of the sensors and assess baseline stability, buffer was flowed at the same rate between the glucose step changes for the same time allotment. Spectral data were collected in real-time throughout the course of the experiments.

4.2.9 Glucose Response at Various Bulk Oxygen Levels

Using the setup described in the previous section, sensor response to glucose was evaluated at different bulk oxygen levels. Dissolved oxygen levels were varied through the adjustment of nitrogen and oxygen pressures of the gas mixture used to aerate the glucose and buffer reservoirs. Dissolved oxygen levels were monitored at the reaction chamber inlet, and upon stabilization, glucose sensitivity testing proceeded as described above. Additionally, it is noteworthy to state that the same sample was used throughout this experimental procedure.

4.3 Results and Discussion

4.3.1 Preparation of Algilica Particles

Following particle fabrication, the infrared spectrum of the particles were acquired using FTIR spectroscopy, and compared to previously reported spectra.[35] As expected, the spectrum confirmed alginate-GPTS conjugation indicated by absorbance bands present at 1630 cm^{-1} – contributed by the carboxylic acid groups on alginate – and 1730 cm^{-1} – contributed by the conversion of carboxylic acid groups into ester bonds

during the conjugation. Additionally, the particle spectrum showed a very strong Si-O

bond absorbance band between 1100 and 1000 cm^{-1}, confirming successful condensation

of the silanol and formation of the silicate structure.

4.3.2 Sensor Component Immobilization

With enzymatic smart tattoos, it is important to have a uniform distribution of the

enzyme and indicator dye so that a homogeneous sensing environment is achieved. For

the reported case, that involved achieving a uniform distribution of GOx and PtOEP

throughout the microparticle matrix. During preliminary experimentation, the pH of the

GOx loading solution was observed to have a profound effect on whether or not the

enzyme was uniformly distributed throughout the particle. To characterize this effect,

GOx immobilization within algilica particles was performed at various pH levels and

imaged using confocal microscopy (Figure 34).
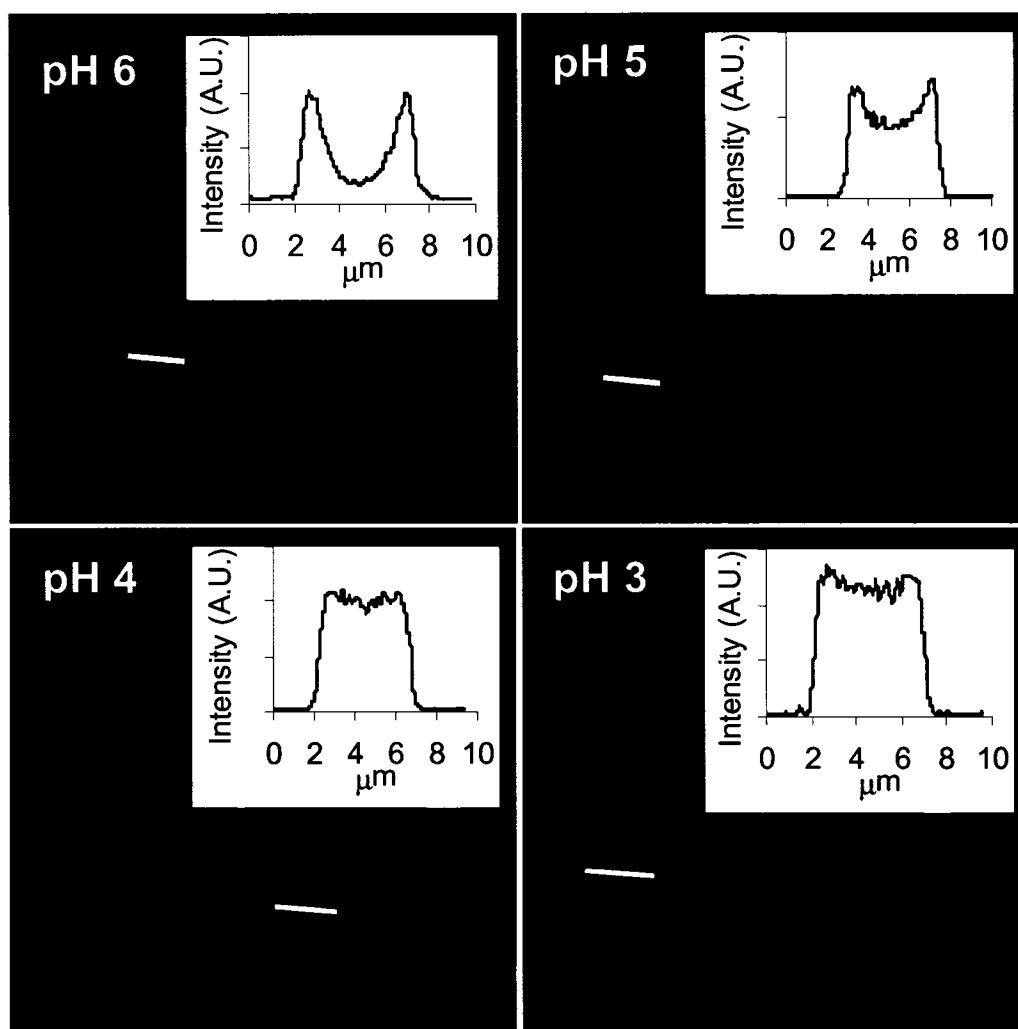
Figure 34. Confocal micrographs of GOx loading at different pH levels. Insets for the respective micrographs depicts the intensity profile along the given line. Note that bars used for line scan analysis represent 10 μm.

The distribution profile of GOx within the particles was obtained through line scan analysis of the confocal micrographs (Figure 34– insets). By inspecting the relative fluorescence intensities of the line scan data corresponding to the particle center and comparing those with the intensities at the surface, one sees that the solution pH does influence whether GOx is uniformly (Figure 34, pH 3 and 4) or non-uniformly (Figure 34, pH 5 and 6) distributed within the microparticle. However, to quantifiably compare

the distribution profiles, the following equation was introduced to calculate a distribution

index, D_r.

$$D_r = \frac{\bar{\upsilon}}{\frac{1}{2}(\bar{\alpha} + \bar{\beta})}, (1)$$

where $\bar{\upsilon}$ is the average fluorescence intensity of the center 10% of the particle and $\bar{\alpha}$

and $\bar{\beta}$ are the average fluorescence intensities of the outer 10% of the distribution

profile, located at the right and left boundaries of the particle surface, respectively. As

the value of D_r approaches unity, GOx is uniformly distributed throughout the particle,

and as D_r approaches zero, the distribution of GOx becomes inhomogeneous, with bias

toward the surface boundaries. The calculated D_r values were plotted versus solution pH

(Figure 35).
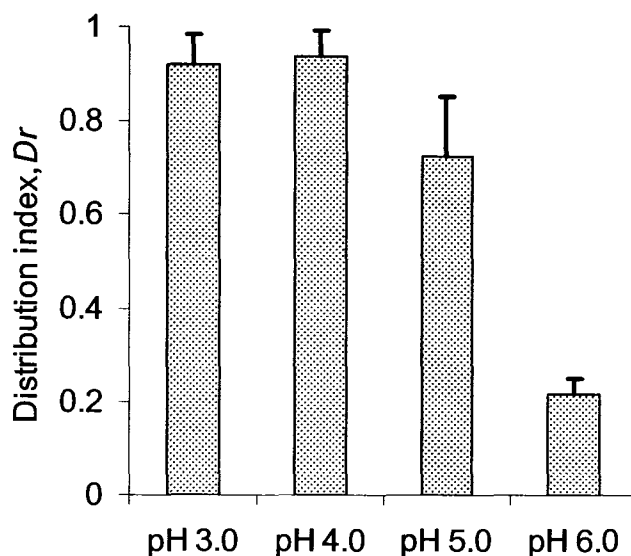
Figure 35. Distribution indices calculated for GOx loading at various bulk pH levels. Error bars donate one standard deviation of three measurements.

D_r values close to unity were observed for pH 3.0 and 4.0 with no statistical difference (Student's t-test, with $\alpha = 0.1$) between the two, indicating that uniform distributions were obtained when GOx was loaded under these conditions. Conversely, the D_r values significantly decreased when the bulk pH was increased to 5.0 and 6.0, respectively, signifying an increased bias for GOx adsorption to the outer surface of the particle. This observed trend could be explained through pH-induced modulation of attractive and repulsive electrostatic forces. As the solution pH is reduced below the pI of GOx (4.2)[169] and above the algilica pI (estimated to be 2 from reports on similar organically-modified silicates).[170-172] GOx exhibits a cationic surface potential, while the net surface potential of algilica remains anionic. Opposite surface potentials elicit attractive electrostatic forces between GOx and algilica, allowing GOx to readily penetrate and adsorb throughout the microparticle. Such behavior was observed at bulk pH levels of 3.0 or 4.0. However, as bulk pH values are elevated above the GOx pI, the surface potential of both GOx and algilica become increasingly anionic, inducing an increased electrostatic repulsion. These repulsive forces incrementally reduce GOx penetration throughout the particle, while progressively confining adsorption to the particle surface, as seen in loading solutions of pH 5.0 and 6.0, respectively. Similarly, other reports have observed the same phenomenon and have used pH-induced electrostatic loading as a means to immobilize enzymes.[173] Therefore, to obtain a uniform distribution of GOx within the sensors, a pH 4.0 loading solution was used. Additionally, it is important to note that post-loading exposure to elevated pH levels resulted in no significant changes of the GOx distribution profile.

Following the controlled precipitation of PtOEP, algilica particles were doped with GOx, and subsequently imaged using confocal microscopy (Figure 36A and B).
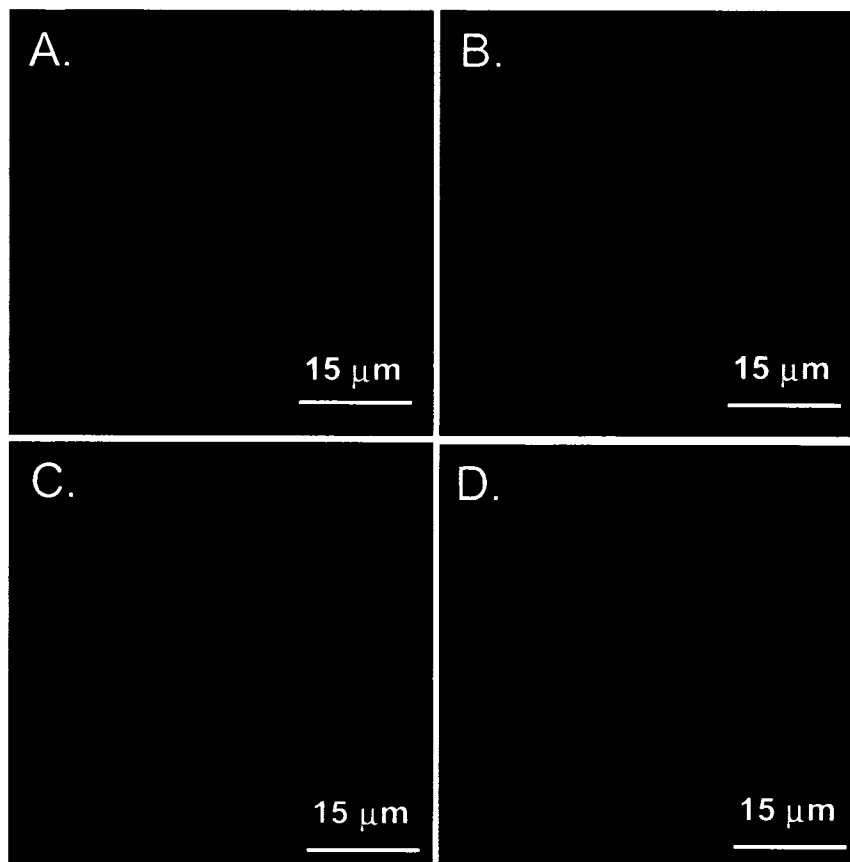
Figure 36. Typical confocal micrographs of algilica particles loaded with FITC-GOx (A) and PtOEP (B) and complete self-referenced sensors comprising RITC-doped nanofilms (C), PtOEP (D), and unlabeled GOx.

D_r values calculated for GOx (Figure 4A) and PtOEP (Figure 4B) were 0.87 ± 0.11 and 0.86 ± 0.08, respectively, suggesting that the precipitation technique used to adsorb PtOEP has no significant effect on GOx immobilization. We also observed that the distribution profiles of GOx and PtOEP remained unchanged if the order of immobilization was reversed (i.e., GOx loaded before PtOEP). The ability to obtain uniform immobilization of both GOx and PtOEP is due in part to the unique chemical

and structural properties of the mesoporous algilica matrix, comprised of a homogeneous arrangement of hydrophilic and hydrophobic functionalities that provide thermodynamically stable environments for both GOx and PtOEP.[35]

In fluorescence-sensing application, it is common to incorporate a reference dye which is non-sensitive to the measured analyte into the sensor, allowing a ratiometric read-out. Ratiometric monitoring of sensor response provides a signal independent to instrumental drift, namely light source fluctuations, and the number of sensors interrogated. To provide a reference signal, RITC-doped multilayer nanofilms were adsorbed to the outer surface of the GOx/PtOEP-doped particles using the well established layer-by-layer technique. The completed ratiometric sensors were imaged using confocal microscopy (Figure 36C and D), and the resulting line scans used to calculate D_r. The D_r value calculated for the RITC-nanofilms was 0.22 ± 0.03, confirming surface limited adsorption of the nanofilms.

4.3.3 Component Immobilization Stability

The stability of component immobilization is of utmost importance when designing sensors of this type. A loss of PtOEP over time would cause negative drift (decrease) in the PtOEP signal over time, which would in turn affect the ratiometric response via increased noise and gradual loss of sensitivity. To determine the immobilization stability of PtOEP, sensors were prepared without nanofilm coatings and placed in an aqueous suspension. Fluorescence measurements were made by removing the supernatant after the particles precipitated via centrifugation and normalizing the PtOEP emission maxima to a separate RITC standard to account for source fluctuations.

The supernatant was subsequently replaced and the measurement repeated again every 24

hours. The data obtained are presented in Figure 37.
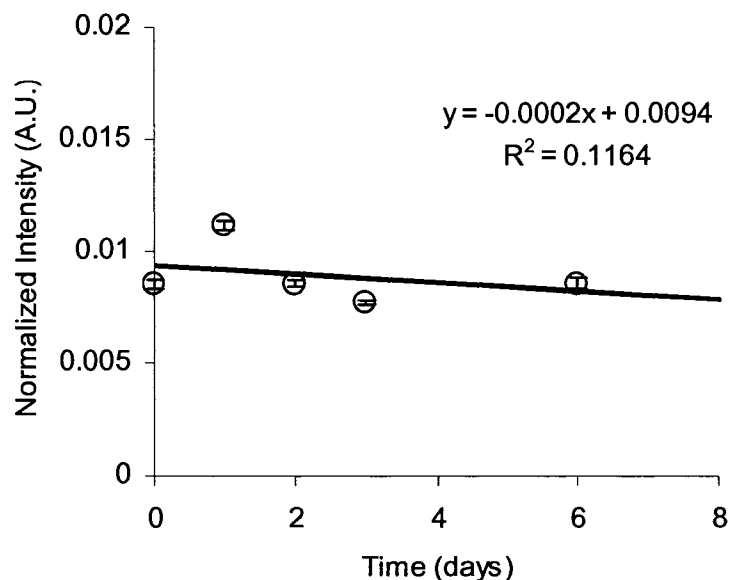
Figure 37. PtOEP leaching profile. Error bars denote one standard deviation of triplicate measurements.

Upon analysis of these data, no statistically significant trend depicting an increase

in normalized PtOEP emission with time is observed, indicating that an insignificant

amount of PtOEP leaches from the particles during this time period. This result is

expected, given the hydrophobic nature of PtOEP. Following the controlled precipitation

procedure used to immobilize PtOEP, the particles are suspended in aqueous solution

from that point on, deterring PtOEP leaching.

Leaching of GOx over the lifetime of the smart tattoo would also have a drastic

affect on sensor dynamics. Should GOx leach from the sensors, fewer enzymes would be

available to consume oxygen and glucose, thereby causing less of a change in the average

steady state oxygen level within the sensor for a given glucose concentration, leading to decreased sensitivity over time. The leaching properties of GOx were monitored via a similar experiment, but in this case FITC-GOx was used and an Oregon-Green solution, which has similar excitation and emission properties, was employed as a separate intensity reference. The leaching data obtained over 6 days are presented in Figure 38.
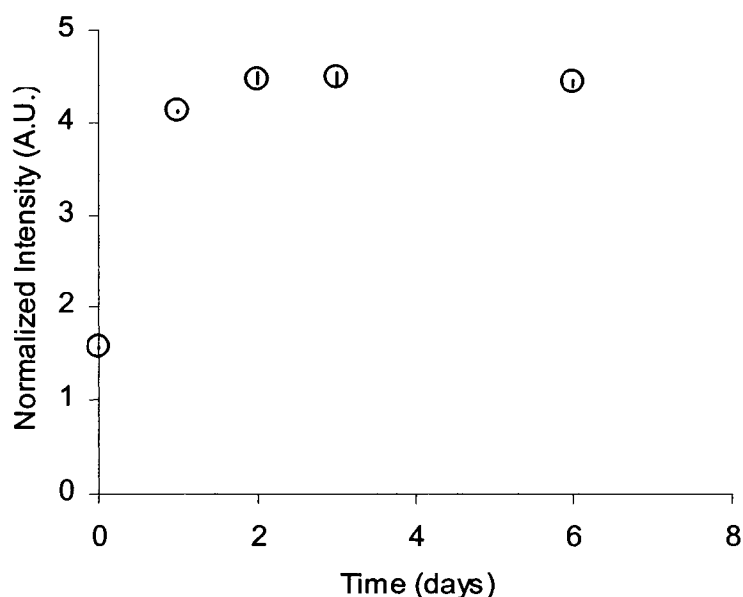
Figure 38. GOx leaching profile. Error bars denote one standard deviation of triplicate measurements.

The data presented in Figure 38 indicate that over the first 24 hours, weakly-immobilized GOx does leach from the sensor. GOx is soluble in aqueous solution; therefore, some degree of leaching can be expected from enzyme molecules not covalently bound to the algilica matrix. It is also important to note that previous work on enzyme immobilization within alginate hydrogels shows covalent attachment of GOx to alginate moieties (via amide linkages) provides a stable system with minimal leaching.[35]

Additionally, these experiments were performed without nanofilm coatings, which have been shown to stabilize encapsulation;[35] therefore, these data represent a "worst case" scenario. Since all the data presented in this work were obtained at least 48 hours after GOx immobilization, including the experiments to determine the concentration of GOx immobilized per particle, it can be concluded that GOx leaching is negligible in the experiments presented herein. Therefore, calibrations to determine the percent of initial immobilized GOx leached from the microparticles were not performed.

4.3.4 Sensor Response to Bulk Oxygen Changes

The reported sensors indirectly measure local glucose levels by monitoring changes in local oxygen levels elicited through GOx-catalyzed glucose oxidation. Therefore, it is critical to quantify the oxygen response characteristics of the sensors before performing glucose sensitivity experiments. To quantify the oxygen response, the dynamic testing apparatus (Figure 27) was used to vary bulk oxygen levels and collect emission spectra after the establishment of concentration equilibrium. To depict the oxygen-induced quenching effect observed at extreme oxygen levels (oxygen and nitrogen saturated conditions, respectively) with air saturated conditions as a reference, selected spectra normalized to the RITC emission maxima at 585 nm are presented in Figure 39.
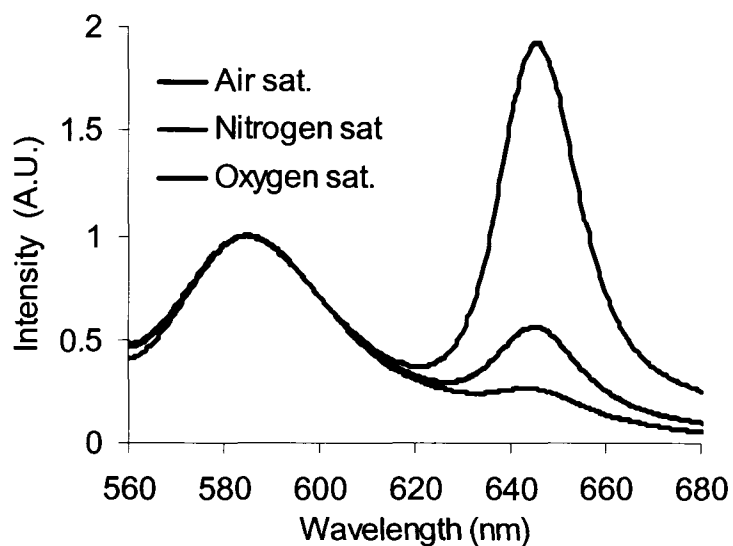
Figure 39. Sensor response to variations in bulk oxygen levels: spectral response to air, nitrogen, and oxygen saturated environments.

A more concise view of the oxygen-quenching effect is demonstrated by plotting the PtOEP/RITC peak ratio, obtained by normalizing the intensity observed at the PtOEP maxima (645 nm) to that of the RITC maxima (585 nm), versus bulk oxygen concentration Figure 40.
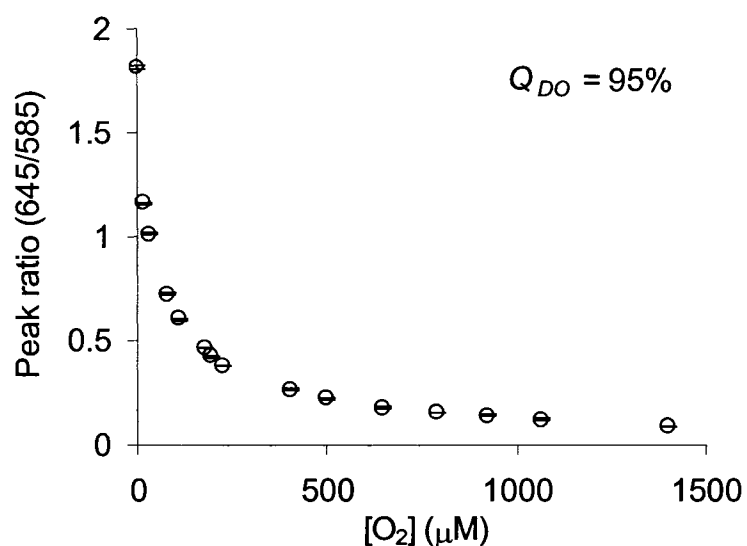
Figure 40. Peak ratio response to randomized oxygen levels ranging from oxygen depleted to oxygen saturated conditions. Error bars denote one standard deviation from triplicate measurements.

These data suggest the sensors are highly sensitive to oxygen levels between depleted and atmospheric (277 µM) levels, such that approximately 95% of the total change in ratiometric intensity per µM of oxygen occurs within this region. For enzymatic smart tattoo applications, high oxygen sensitivity within this region is critical to optimal sensor performance. Reported reaction-kinetic simulations of similar systems under physiological conditions show that local oxygen levels within the sensor can be reduced to 10 µM (assuming intradermal oxygen levels of 90 µM) when elevated blood glucose levels (350 mg/dL) are present.[41, 162]

To quantify the sensitivity of the overall oxygen-induced quenching response (Q_{DO}), the following relationship is commonly used:

$$Q_{DO} = \frac{R_{N_2} - R_{O_2}}{R_{N_2}} \times 100, \quad (2)$$

where R_{N_2} and R_{O_2} are the PtOEP/RITC peak ratios observed under nitrogen and oxygen saturated conditions, respectively. Surprisingly, Q_{DO} was calculated as 95%, a sensitivity equivalent to that observed with algilica based dissolved oxygen sensors, which did not contain GOx, as reported in Chapter 3. *This result indicates that GOx adsorption does not function as an impenetrable barrier that prevents fractal diffusion of oxygen and quenching of PtOEP, but allows oxygen to readily diffuse throughout the matrix.* Although the steady-state transport of oxygen is not affected by GOx adsorption, current studies are underway to examine whether or not the transport *rate* of oxygen is affected. Additionally, a linear Stern-Volmer relationship ($R^2 = 0.99$) was observed (Figure 41), confirming PtOEP adsorption within a homogeneous environment, a characteristic also observed in our previous work.[42, 159]
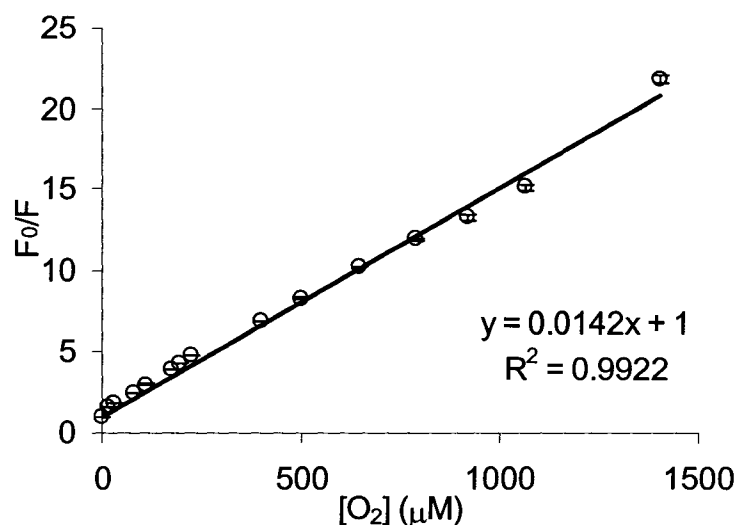
Figure 41. Stern-Volmer quenching characteristics. Error bars denote one standard deviation from triplicate measurements.

These data show high sensitivity to oxygen levels within predicted sensor operation limits, while exhibiting linear quenching characteristics.

4.3.5 Sensor Response to Bulk Glucose Changes

Although the reported system demonstrated high sensitivity to oxygen, a response to glucose is not inherent. Since the sensors are designed to indirectly measure glucose levels through monitoring glucose-limited consumption of local oxygen, the system must adequately control glucose diffusion relative to that of oxygen to be glucose responsive. The glucose response characteristics were monitored using the dynamic testing apparatus (Figure 33), which allowed real-time monitoring of sensor performance as step changes in bulk glucose levels were introduced. In this report, dynamic testing was used to efficiently evaluate critical sensor characteristics such as stability, response time, reversibility, sensitivity, detection limit, and analytical range.

Dynamic response data collected during sensor exposure to random bulk glucose levels ranging from 0 to 300 mg/dL are shown in Figure 42. It is important to note that the data displayed in Figure 42 are only of the initial 150 min of the experiment, which totaled 500 min. The data shown in Figure 42 are the respective peak intensities of RITC and PtOEP, displayed to highlight the advantages of ratiometric monitoring. The data presented in Figure 42 depicts three key properties about the sensor fluorimetrics: (1) step changes in glucose concentration elicit a significant increase in PtOEP emission (Figure 42, demarked "Glucose step"), (2) flushing the system with buffer (Figure 42, demarked "Buffer flush") caused the PtOEP intensity to return to the baseline value, and (3) RITC emission intensity remains independent of modulations in glucose concentration.
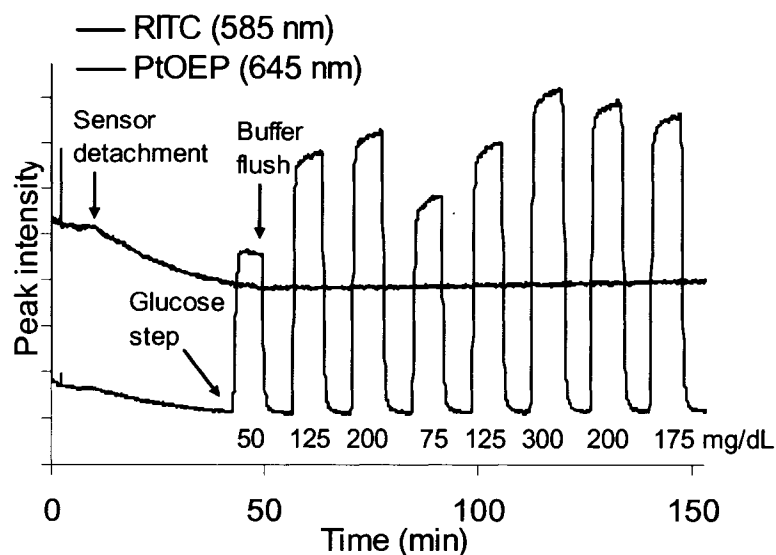
Figure 42. Dynamic sensor response data shown in raw intensity units.

Using ratiometric analysis, it is possible to account for source fluctuations and changes in sensor concentration. One such case can be observed in Figure 42, where after 10 min had elapsed, the peak intensities of PtOEP and RITC began to decline as a result of sensor detachment (Figure 42, demarked as "Sensor detachment"), causing a decrease in sensor concentration; however, after normalizing the peak intensities, the concentration-dependent artifact is eliminated and the baseline prior to glucose step introduction ($t = 0 - 45$ min) becomes stable (Figure 43). Additionally, it is noteworthy that after approximately 50 min, the RITC peak becomes stable (Figure 42), signifying the removal of weakly adhered sensors.
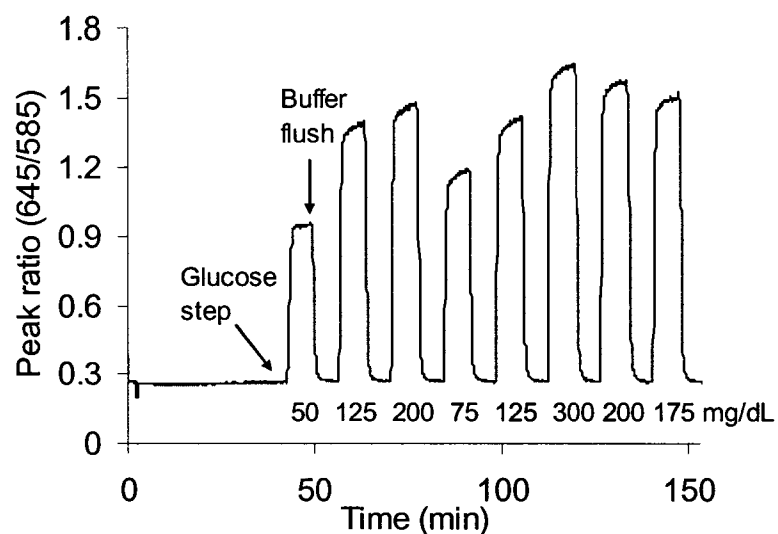
Figure 43. Dynamic sensor response data shown in ratiometric intensity.

4.3.6 Sensor Stability

In this report, the sensors were immobilized on a glass slide and continuously illuminated for approximately 500 min, during which approximately 5000 spectra were acquired. The power density of the excitation source at the sample was measured to be 36 mW cm^{-2}. Baseline values were defined as the average ratiometric intensity values occurring at 0 mg/dL glucose throughout the experiment. A statistical comparison of the baseline values indicate insignificant drift ($p < 0.1$) had occurred throughout the course of the experiment.

Photostability of the sensors was subsequently characterized via continuous exposure of the sensors to the excitation source over approximately 4 days. It is noteworthy to state that this experiment was performed in the dynamic testing apparatus with continuous buffer flow (4 mL/min). A profile of the ratiometric intensity versus time is given in Figure 44.
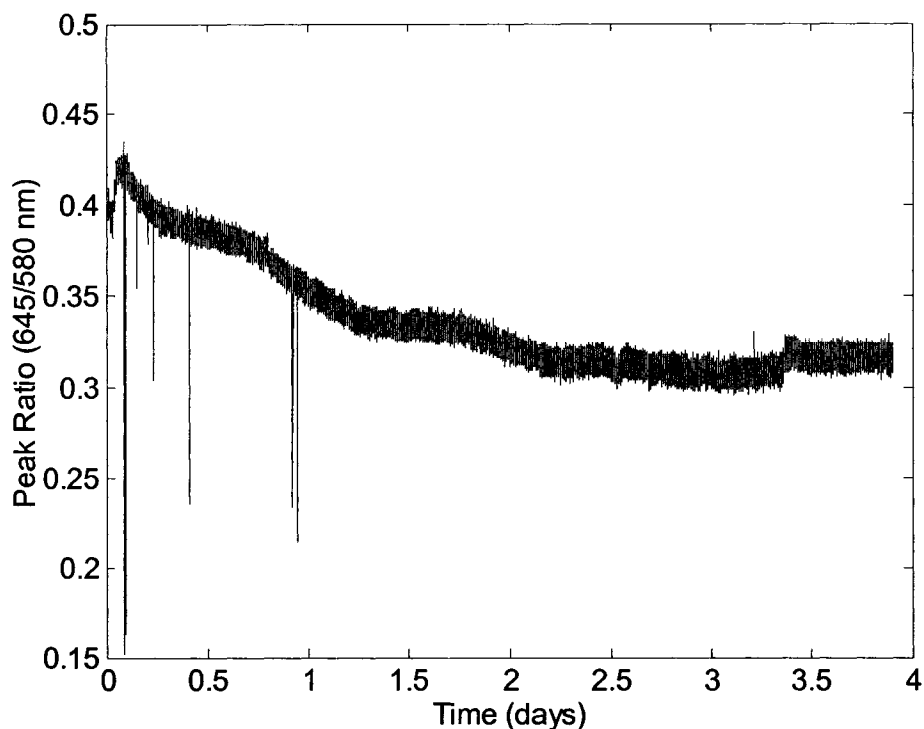
Figure 44. Photobleaching of sensors under air-equilibrated conditions.

These results indicate an approximate 30% loss in ratiometric intensity over the course of 4 days of continuous illumination (~ 7.5% per day). Over the course of this experiment approximately 162,000 spectra were obtained, one every 3 seconds. In light of this observation, photobleaching seems to be insignificant, since in a practical setting, relatively few measurements will be acquired each day. To put these data into perspective, let us assume that in a clinical setting, the average of three measurements will be used to determine an average glucose value and glucose levels will be monitored 6 times/day; therefore, the sensors will be optically interrogated on average 18 times per day. Assuming that it would require approximately 3 seconds to record each measurement, the sensors would be irradiated for a total of 54 seconds per day — it would take 24.5 *years* to degrade the ratiometric intensity by 30%. However, additional effects

like fluctuations in oxygen levels (elevated oxygen levels increase photodegradation) and exposure to sunlight would be expected to greatly contribute to photodegradation. More specifically, the bulk oxygen concentration was kept at air-equilibrated conditions (277 μM), but in physiological conditions, bulk oxygen levels are expected to be significantly lower (approximately 90 μM). Additionally, when in the presence of normoglycemic levels (> 70 mg/dL and < 180 mg/dL) oxygen levels within the sensors would be expected to be further reduced to approximately 60 μM.[41] Under these conditions, it is expected that the affects of photodegradation would be *further reduced*, given that less oxygen present would result in less singlet oxygen produced, which would in turn reduce the probability of photoxidation.[98] Thus, to obtain a more accurate photostability profile, a similar experiment should be performed with continuous exposure to a normal physiological glucose level. Nonetheless, as a point of comparison, the photodegradation rate of similar enzymatic smart tattoo concepts was reported to be 2.3% per hour, approximately 10x's greater than the RITC/PtOEP based concepts.[133, 166] Therefore, the current RITC/PtOEP based enzymatic smart tattoos show great promise as being highly photostable systems.

4.3.7 Response Time and Reversibility

Response time is a critical figure of merit for diabetic monitoring, as sensors must respond within the physiological time scale of glucose fluctuations to ensure accuracy. Using the dynamic data acquired, sensor response time was defined as the time required for the PtOEP/RITC peak ratio to reach 95% of its maximum value in response to a step change in glucose concentration. The average response time was determined to be 86 ± 12 seconds, making these sensors adequate to monitor fluctuations in blood glucose,

which usually occur over a period of 30 min.[174] Upon comparison, the measured response time is similar to other systems based on optical oxygen transduction of glucose levels.[39] It is noteworthy that in Chapter 6, the response time for individual sensors was determined to be approximately 30 seconds less than that observed in the dynamic testing apparatus. This observation indicates that the response time determined with the dynamic testing apparatus may be due a combination of fluidic latency and equilibration time within the immobilized sensor population.

Reversibility is a figure of merit that assesses baseline change before and after exposure to the analyte. Reversibility was quantified by flushing the reaction chamber with buffer before subsequent glucose step changes, then calculating the baseline variation. Figure 45 shows sensor response to several step changes in glucose concentrations.
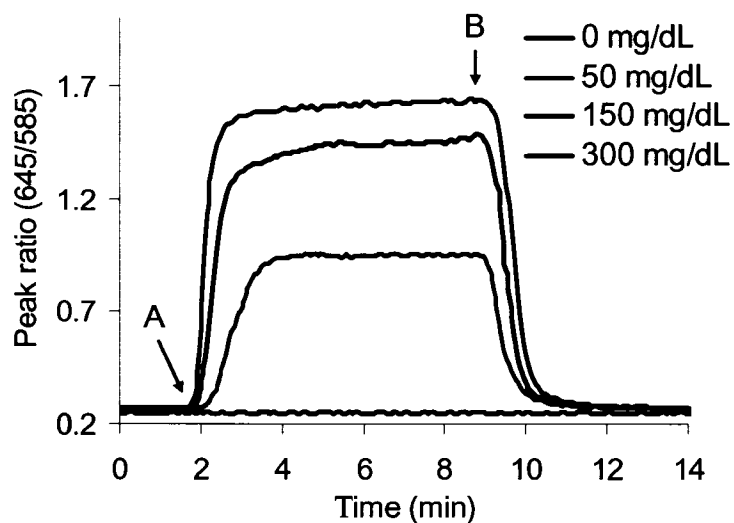
Figure 45. Sensor response to step changes in glucose concentration. Sensors were exposed to a step change in glucose at (A) and the chamber subsequently flushed with buffer to remove glucose (B). Notice the peak ratio returns to initial values following glucose removal.

It is important to note that after glucose is flushed from the bulk solution (Figure 45, marked "B"), the PtOEP/RITC peak ratio returns to the baseline value observed prior to the glucose step (Figure 45, marked "A"). The average percent change in the baseline value before and after a step change in glucose concentration was determined to be 0.75 ± 0.6%, indicating a high degree of reversibility. This result is not surprising, as enzymatic-based sensors usually display a high degree of reversibility due to consistent analyte consumption.[26, 39]

4.3.8 Sensitivity

Sensitivity is a critical sensor performance characteristic that characterizes the change in analyte signal with a corresponding change in analyte concentration. A sensitivity curve was generated by plotting the percent change in PtOEP/RITC peak ratio versus bulk glucose concentration (Figure 46), using the following equation to calculate percent change:

$$\% \ Change = \frac{R - R_o}{R_o} \times 100,$$

where R and Ro are the PtOEP/RITC peak ratio obtained at incremental glucose levels and 0 mg/dL glucose, respectively.

600
500
% Change 400
300
200
100
0

Analytical range

$y = 4.1608x$
$R^2 = 0.9696$

0   100   200   300
[Glucose] (mg/dL)
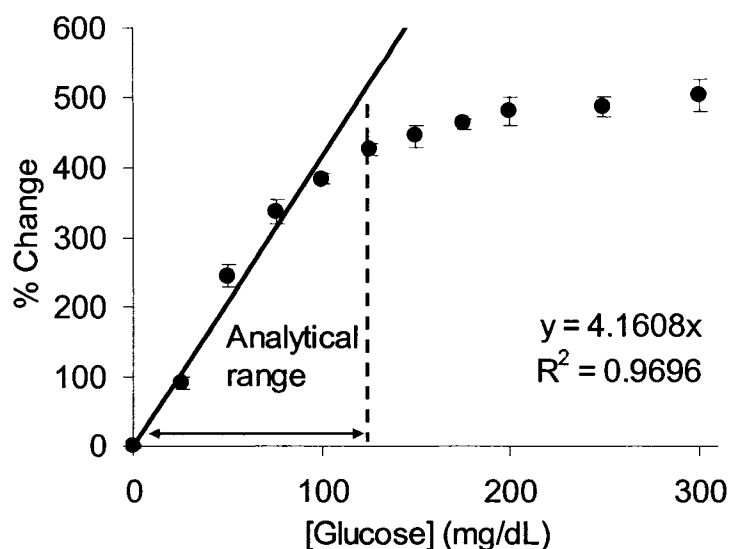
Figure 46. Percent change in PtOEP/RITC peak ratio values following step changes in bulk glucose levels. Regression line used to depict linear operation range, while analytical range demarks a 10% response deviation from linearity. Error bars denote one standard deviation of random triplicate measurements.

The response sensitivity was determined by taking the slope of the linear region, which was defined as the region within the sensitivity curve that exhibited an R^2 value greater that 0.95. Using linear regression, with the y-intercept forced to 0, the response sensitivity was determined to be 4.16 ± 0.57 % change / mg dL^{-1} (assuming 95% confidence bounds, Figure 46), which is greater by at least one order of magnitude than those of similar systems.[27, 37, 39] However, it should be noted that high sensitivity is often associated with a reduction of the analytical range; therefore, the sole objective is not high glucose sensitivity, but to obtain the highest sensitivity while staying within the confines of the desired analytical range. Additional discussion on the analytical range and how multilayer thin films can be used to tailor the response sensitivity will be given later.

4.3.9 Detection Limits

Detection limits are used to quantify the lowest concentration of analyte that can be readily detected. Several types of detection limits commonly characterize sensor performance; the first of them is the limit of detection, which is the lowest analyte concentration that is detectable (assuming 66% certainty). The identification limit is the lowest analyte concentration that can be detected with a reasonable degree of certainty, commonly 83%. For this work, the detection limit used is the quantification limit, which is defined as the lowest analyte concentration in which there is at least 90% certainty that the analyte is present. The quantification limit, C_{QL}, is defined as

$$C_{QL} = \frac{10\sigma_{baseline}}{S}, \quad (2)$$

where $\sigma_{baseline}$ is the standard deviation of the baseline (e.g. glucose concentration equal to 0 mg/dL) and S is the response sensitivity defined above. C_{QL} was determined to be 1.5 ± 0.2 mg/dL. The low C_{QL} is a result of the high signal-to-noise ratio, which was determined to be 175, and the high response sensitivity of the sensors. Given that hypoglycemic comas are commonly observed when blood glucose levels drop below 30 mg/dL,[175] the low detection limit of these devices are not advantageous for diabetic monitoring devices; however, other applications requiring low detection limits could find this characteristic useful.

4.3.10 Analytical Range

The analytical range is one of the most critical figures of merit when evaluating the feasibility of a sensor. The analytical range was defined as the concentration range over which glucose levels can be statistically differentiated. Typically the lower limit of the analytical range is defined as C_{QL}, while the upper limit is the analyte concentration

observed when the response profile deviates 10 % from linearity (Figure 46), making this figure of merit a function of response sensitivity (for the upper limit) and baseline noise (for the lower limit). Using this definition, the analytical range of the sensors was determined to be 2 – 120 mg/dL of glucose, which does not cover the entire accepted range of 40 – 350 mg/dL for self-testing systems.[176] However, the reported system could adequately monitor hypoglycemic events (blood glucose levels below 70 mg/dL), which according to one report, is the most critical aspect of diabetic care.[177]

The fundamental operating principles of the sensors can be described through further analysis of Figure 46, in conjunction with Figure 47.
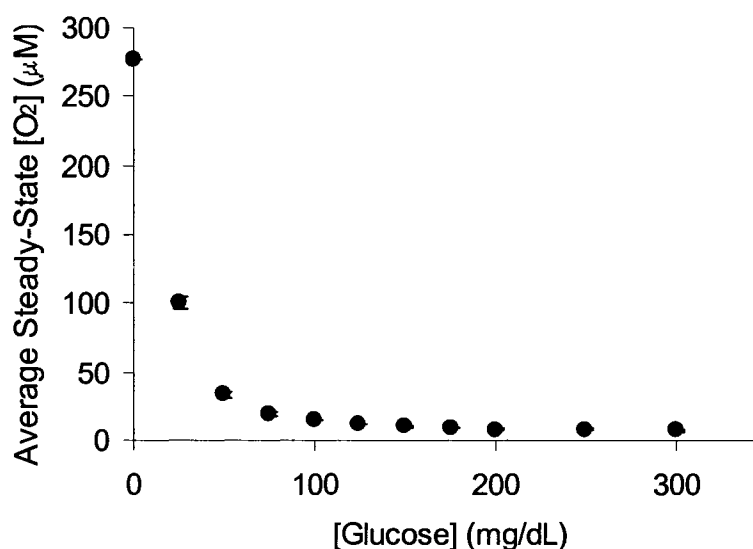
Figure 47. Average steady-state oxygen concentration within the sensors as a function of bulk glucose concentration.

It should be noted that these data were obtained by using the calibration data relating oxygen concentration to PtOEP/RITC peak ratio, as presented in Figure 40. Prior to analysis it is important to note that linear ranges of the data presented in Figure

46 and Figure 47 differ significantly, arising from the nonlinear relationship between PtOEP/RITC peak ratio and oxygen concentration. Given that oxygen sensitivity increases as oxygen levels approach 0 μM, slight changes in reduced local oxygen levels result in significant changes in ratiometric intensity increasing the glucose sensitive range of the sensors, as described in the following text.

As previously mentioned, these sensors operate on the principle of glucose-limited oxygen consumption within the smart tattoo. As glucose diffuses into the sensor, oxygen is consumed and rapidly replaced, allowing indirect glucose monitoring through an oxygen reporter. To achieve this fundamental condition, the relative diffusion rate of oxygen into the sensor must be greater than that of glucose, such that local oxygen levels within the sensor are in excess, resulting in glucose-limited oxygen consumption. This condition can be observed in the linear response region ([glucose] < 90 mg/dL, Figure 46), where peak ratio changes resulting from the depletion in steady-state oxygen levels are proportionally reduced in response to increasing bulk glucose levels. As bulk glucose levels are increased, the rate of glucose delivery into the sensor begins to eclipse the rate of oxygen replenishment, preventing the relative recovery of oxygen levels within the sensor. In this state of operation, the sensor response begins to deviate from linearity with bulk glucose levels between 90 and 150 mg/dL (Figure 46), thus implicating the onset of oxygen-limited glucose consumption. With additional increases in glucose levels above 150 mg/dL, the sensor does not respond to changes in bulk glucose concentrations (Figure 46). This phenomenon is due to internal depletion of oxygen levels, such that oxygen is readily consumed upon diffusion into the sensor, a condition elicited by the surplus of local glucose within the sensor and signifies absolute oxygen-

limited catalysis and response saturation. Therefore, to extend the analytical range to cover both hypoglycemic and hyperglycemic events, the mass transfer properties of oxygen and glucose must be altered to limit the glucose delivery rate into the smart tattoo. Limiting glucose diffusion allows oxygen levels within the sensor to remain relatively elevated, allowing the sensor to operate under glucose-limited conditions over a greater range of bulk glucose levels.[41]

To control glucose flux relative to oxygen, previous work on enzyme-based sensors have found that mass transfer limiting surface coatings could successfully modulate sensor response properties.[166, 178] In our approach, we utilize surface-immobilized multilayer nanofilm technology to control the analyte mass transfer and induce glucose-limiting kinetics. This technology allows exquisite control over substrate diffusivities through nanoscale changes in film thickness.[5, 26, 41, 147] We hypothesize that the analytical range of these sensors can de tuned by simply altering the thickness of the nanofilms, the results of which will be presented later in this chapter.

4.3.11 Accuracy

Accuracy is arguably the most critical figure of merit of sensor performance and ultimately clinical efficacy. For this work, accuracy is defined as the degree of conformity of the predicted (measured) glucose level to the actual value. To quantify accuracy, a set of standards must be initially determined. For this exercise, the calibration standard was determined to be the first and last PtOEP/RITC peak ratio values obtained at each glucose concentration (three measurements at each glucose concentration were obtained during each dynamic testing experiment). The average and standard deviation was obtained, and glucose concentration was related to the mean

PtOEP/RITC peak ratio and plotted (Figure 48). Since this is a not an attempt to model any physiological process (i.e., a model describing the underlying physical and chemical mechanisms), the data were fitted to a model yielding the highest correlation coefficient, which in this case was a rational function of the following form:

$$[\text{glucose}] = \frac{(a + b \cdot PR)}{1 + c \cdot PR + d \cdot PR^2},$$

where PR is the PtOEP/RITC peak ratio and a, b, c, and d are fitting coefficients determined through a least-squares fitting algorithm. Given that the same form of this model will be used to fit additional data, the exact values of the fitting parameter will not be given. The resulting fitted data were plotted and compared with the experimental data (Figure 42).
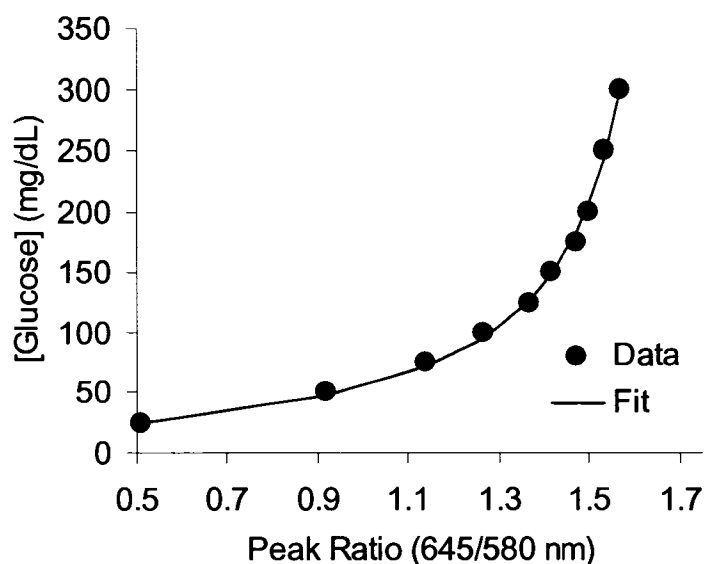
Figure 48. Experimental data and rational function fit used to construct calibration model.

Upon comparison of the experimental and fitted data, Figure 48 shows that the rational function provides a good prediction of glucose concentration when the PtOEP/RITC peak ratio is used as input ($R^2 > .99$).

Using the rational model, the experimentally determined peak ratio data were used to predict glucose concentration. The predicted values were then compared with actual values assigned by the calibration standards. The "unknown" sample was considered to be the second mean PtOEP/RITC peak ratio obtained at each glucose concentration, and was subsequently used to predict glucose concentration using the same rational model, followed by comparison to the calibration standards. These data are presented in Figure 49.
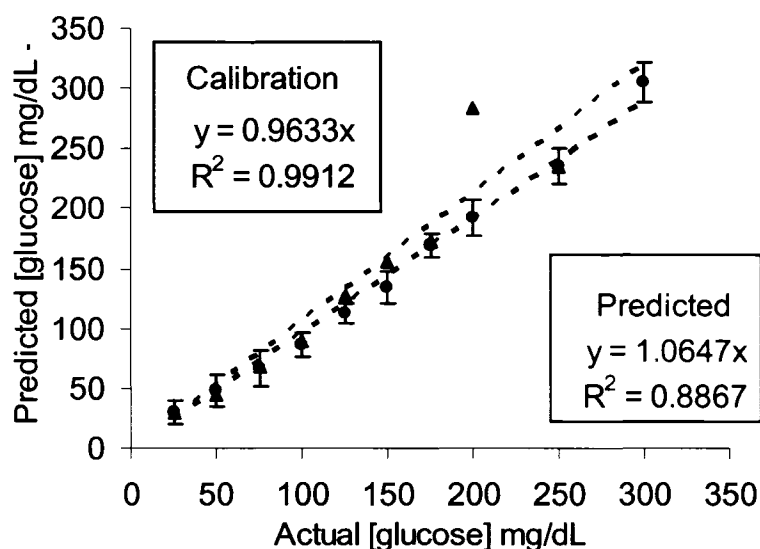
Figure 49. Calibrated comparison of sensor accuracy using first and third mean PtOEP/RITC peak ratios obtained at each glucose concentration as calibration standards.

When analyzing these data, it is common to include a linear regression fit (with the y-intercept forced to 0) to the data so that the slope, which related the predicted and

actual glucose levels, can be analyzed. As the slope approaches 1 and the correlation coefficient approaches 1, the sensors are highly accurate as actual and predicted glucose levels are statistically the same. As the slope deviates from 1, several insights on sensor behavior can be extrapolated. For instance, the data having a slope greater than 1, indicates that the sensor over predicts or overshoots the actual analyte concentration. On the other hand, when the slope decreases below 1, the sensor under shoots the actual analyte concentration. A high correlation between the actual and predicted glucose levels is expected in the calibration model, since these data were used to define actual glucose levels, and that is indeed what is observed in Figure 49 ($m = 0.96 \pm 0.035$). Additionally, the "unknown" sample depicted in Figure 49 as "predicted" also exhibits a high degree of accuracy ($m = 1.06 \pm 0.154$).

As an additional exercise, a second calibration was performed, this time using the first and second mean PtOEP/RITC peak ratios obtained at each glucose concentration as calibration standards, and the third mean PtOEP/RITC peak ratios obtained at each glucose concentration as the unknowns. In both cases, the data were fitted to the rational function previously discussed. The data obtained are presented in Figure 50.
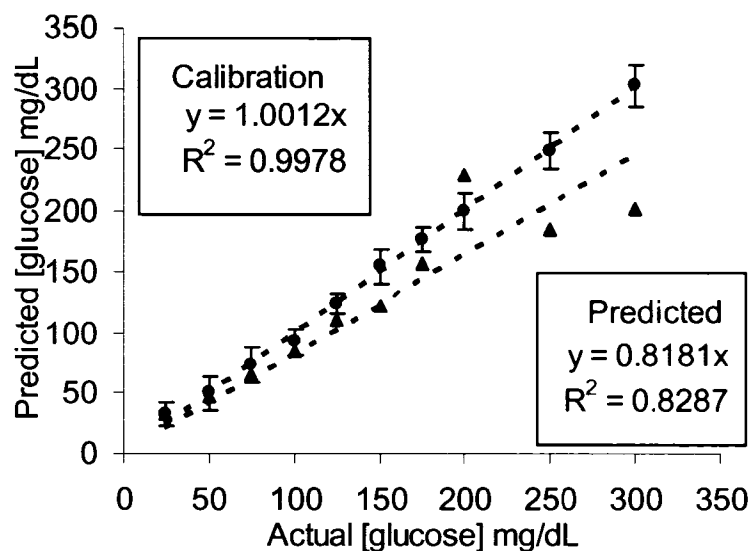
Figure 50. Calibrated comparison of sensor accuracy using first and second mean PtOEP/RITC peak ratios obtained at each glucose concentration as calibration standards.

As expected, the calibration data show a high degree of accuracy ($m = 1.00 \pm 0.018$). On the other hand, the unknown sample shows significantly lower accuracy ($m = 0.8181 \pm 0.128$), indicating a loss of sensitivity (~ 20% deviation of accuracy) over time. It is again important to note that these data were acquired in a random triplicate fashion to eliminate hysteresis. When preparing the calibration standard using the average peak ratios obtained during the first and third glucose measurements, time-based fluctuations were averaged; however, in the later case, these fluctuations were exposed. There are several explanations for the loss of sensitivity over time, one of which is leaching of the enzyme; however, earlier in this chapter, data were presented indicating that after the initial day of immobilization, GOx is stably immobilized within the particle (Figure 38). A second and more likely scenario would be the temporal deactivation of GOx. This well-known phenomenon can spontaneously occur over time, or could be poison-induced by reaction byproducts, namely hydrogen peroxide and hydronium ions.[179, 180] This

scenario will be reviewed in depth later in this dissertation through the careful examination of response properties obtained continuously over several days.

4.3.12 Response Stability over Extended Periods of Time

To assess response stability over extended periods of time, dynamic response experiments were performed on samples obtained from the same stock suspension of sensors over a period of 21 days. The sensor suspension was stored in glucose-free buffer at 3 °C until needed. It is important to note that these data do not reflect response stability under a *continuous mode of operation*. Upon completion of the experiment, the temporal response profiles were used to determine sensitivity over the examined time range, the results of which are presented in Figure 51.
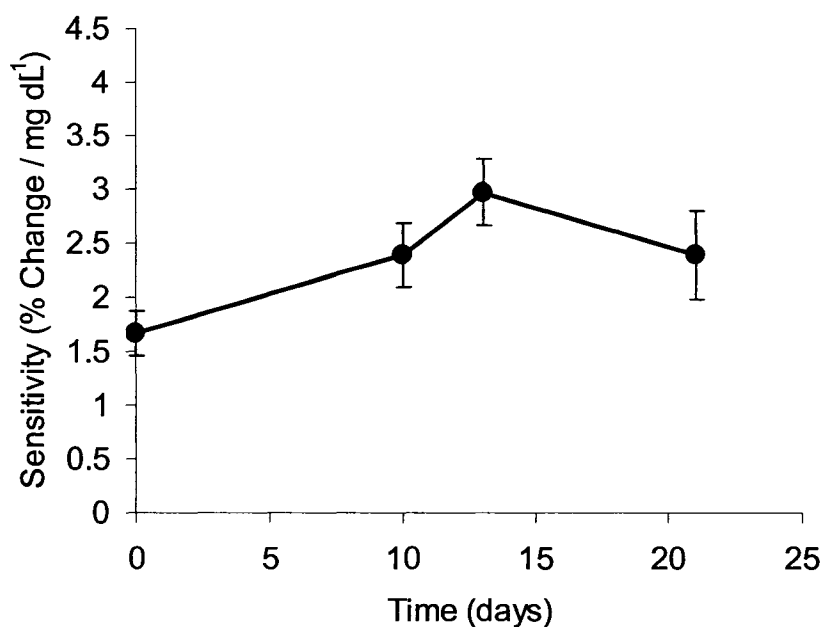
Figure 51. Stability of device sensitivity over time. Note that these data were not collected under a continuous mode of operation.

These data indicate a somewhat erratic stability profile. Interestingly, the last three data points (collected at 10, 13, and 21 days after sensor fabrication) indicate no statistical difference, revealing that no significant change in sensitivity over this given time period is observed. However, a statistical difference lies between the first and the last three data points, indicating that a slight increase in sensitivity is observed after the initial week of preparation. This seemingly improbable occurrence could be explained in the variation of the samples themselves, which could in turn influence the response profiles collected. Although great care is taken to ensure that a similar concentration of sensors is used throughout the sample preparation procedure, it is difficult to maintain a consistent number of immobilized sensors through out each experiment. Inevitably, sensors will be detached by the shear force exerted by the flowing bulk solution, a parameter difficult to keep constant throughout all prepared samples. This topic will be covered in great depth in the later section of this chapter.

It is important to state that a stable response (i.e. sensitivity vs. time) was expected given the experimental conditions. Previously in this chapter, it was shown that in the days following GOx immobilization, insignificant leaching was observed, indicating the enzyme was stably immobilized within the sensor (Figure 38). Additionally, it was also shown that PtOEP immobilization was stable (Figure 37). Therefore, the possibility that the sensors would lose sensitivity due to component leaching was deemed insignificant. Given that the sensors were stored in ambient conditions (i.e. no glucose), the enzymes were assumed to be dormant, thus eliminating the possibility of poisoning due to peroxide and/or pH drop (no glucose present = no production of byproducts). Given these assumptions, the most obvious path by which

sensitivity reduction could occur would be the spontaneous deactivation of the enzyme over time, but given that the sensors were stored at near-freezing temperature, the deactivation rate would be reduced substantially. Additionally, the rigid structure of the algilica particles could provide structural support[181] to the enzyme such that the rate of spontaneous denaturing (i.e. unfolding) and denaturing due to byproduct poisoning is reduced. In a report on the stabilization of creatine kinease within a sol-gel matrix, it was found that the enzyme retained 50% activity 10 times longer than that of free enzyme, attributing the decreased inactivation to the rigid structural support of the matix.[182] It is also noteworthy to state that a more accurate assessment of response stability would be to repeat the experiment using a *single* sample, thus removing error due to sample variations. To reduce drift associated with spontaneous enzyme inactivation, the immobilized sensors should be stored in buffer at refrigerated temperatures. Additionally, a more practical exercise would be test stability at normal physiological temperatures over extended periods of time, as the results of which would provide insight on how the spontaneous deactivation of GOx would affect sensor performance.

4.3.13 Effect of Bulk O_2 Variations on Glucose Response

As mentioned in Chapter 2, the local oxygen supply within the dermis has been shown to be highly dependent on atmospheric conditions as well as depth, with concentration fluctuation from 215 μM (near the epidermis-dermis junction) to 90 μM (near vasculature).[135] Therefore, it is informative to examine the overall effect of sensor performance when exposed to varying bulk oxygen levels. Following stabilization of bulk oxygen levels at oxygen levels below, at, and above atmospheric concentration,

sensors were exposed to random step changes in bulk glucose levels. The response data obtained are presented in Figure 52.
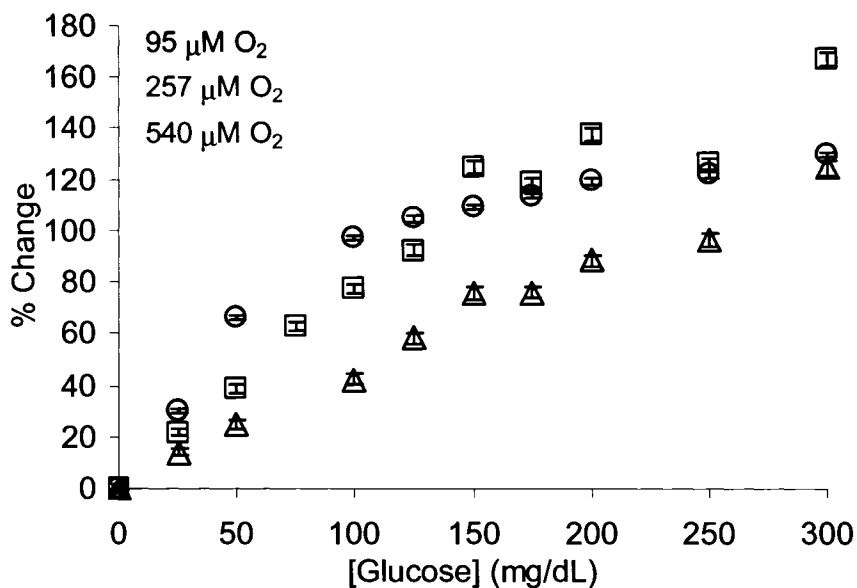
Figure 52. Sensor response to glucose at various bulk O₂ concentrations. Error bars denote one standard deviation of random triplicate measurements.

These data do indeed indicate a significant shift in sensitivity. To enhance clarity of the effects of bulk oxygen concentration on sensor performance, the sensitivity and analytical ranges were calculated for each sample set (Figure 53).
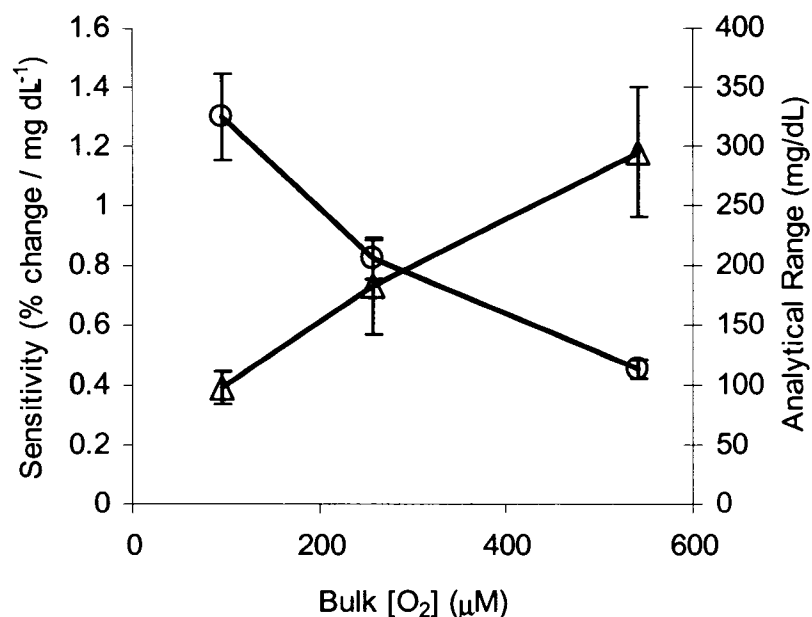
Figure 53. Effect of bulk O2 levels on sensitivity and analytical range of glucose response.

As expected, these data suggest that the glucose response significantly varies with fluctuations in bulk oxygen levels, a observation noted in similar enzymatic systems.[127, 183] First, it is important to note that these data indicate reaction-limited consumption is not obtained, such that at higher bulk oxygen levels, the glucose-limited rage is extended when compared to that obtained with 95 μM bulk oxygen. Additionally, at oxygen levels above atmospheric, in this case 540 μM, the sensors exhibit a sensitivity and analytical rage of 0.455 ± 0.03 % change / mg dL^{-1} and 295 ± 55 mg/dL, respectively. When compared to the response properties obtained at 95 μM − 1.3 ± 0.145 % change / mg dL^{-1} and 98 ± 14 mg/dL − an approximate 65% decrease in sensitivity and a 200 % increase in analytical range is observed. This occurrence can be simply explained by variations in local oxygen levels induced by changes in the bulk. At elevated bulk oxygen levels, the average steady-state oxygen concentration within the sensors is elevated;[41] therefore,

higher incremental glucose levels are required to significantly reduce the elevated average oxygen level within the sensor. This occurrence ultimately results in an extension of glucose-limited range, which in turn results in decreased device sensitivity and increased analytical range as shown in Figure 53. A more physiologically relevant demonstration would be to compare response properties acquired at 95 μM and 257 μM oxygen levels. Under air saturated conditions, response properties were determined to be 0.826 $\pm$ 0.07 % change / mg dL^{-1} and 182 $\pm$ 40 mg/dL, which when compared with those obtained at 95 μM, represent a 36% decrease in sensitivity and a 54% increase in analytical range. These findings, although expected, indicate the importance of having an internal oxygen reference to monitor bulk oxygen levels. Such a reference would determine absolute changes in oxygen levels within the sensor that are directly due to glucose oxidation, allowing for the compensation of response artifacts due to fluctuations in bulk oxygen levels. Therefore, for this approach to ultimately be successful in *in vivo* applications, direct oxygen monitoring functionality will need to be incorporated to allow compensation for fluctuations in bulk oxygen levels within the dermis. This topic will be revisited later in the text.

4.3.14   Effect of Sensor Concentration on Glucose Response

Additionally, it is a constructive exercise to examine the effect of sensor concentration on overall response properties, as this understanding would enhance the ability to design clinically viable implantation schemes (implants would ultimately be comprised of a population of sensors, not a single sensor). In this series of experiments, suspensions of various sensor concentrations were used during sample preparation. After drying, the samples were subjected to dynamic testing. The following data represent

sensor response profiles acquired from samples prepared with various concentrations (Figure 54).
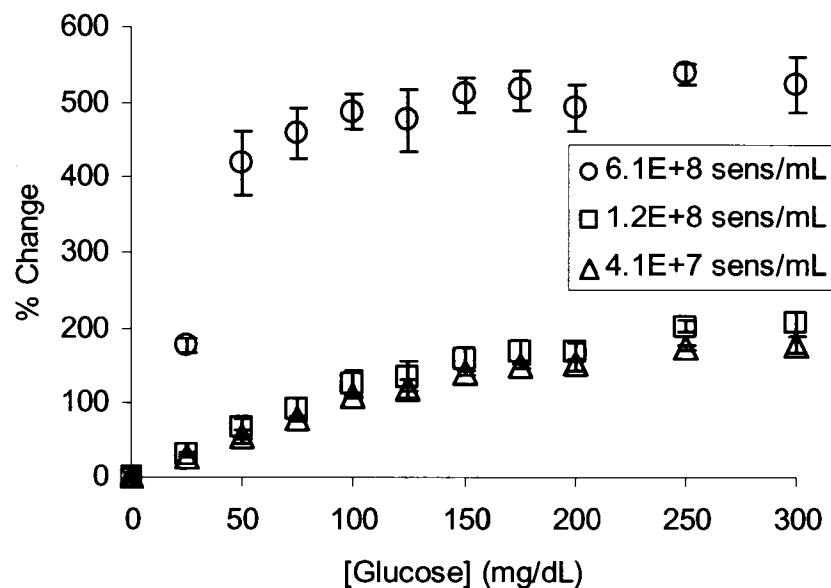
Figure 54. Sensor response profiles acquired with varying sensor concentrations.

Remarkably, samples prepared with a high concentration, in this case 6.1×10^8 sensors/mL, exhibit a total percent change of over *two fold* greater than those with lower concentrations. Additionally, samples prepared with concentrations below 6.1×10^8 sensors/mL exhibit lower sensitivities and increased ranges when compared with those obtained with 6.1×10^8 sensors/mL (Figure 55).
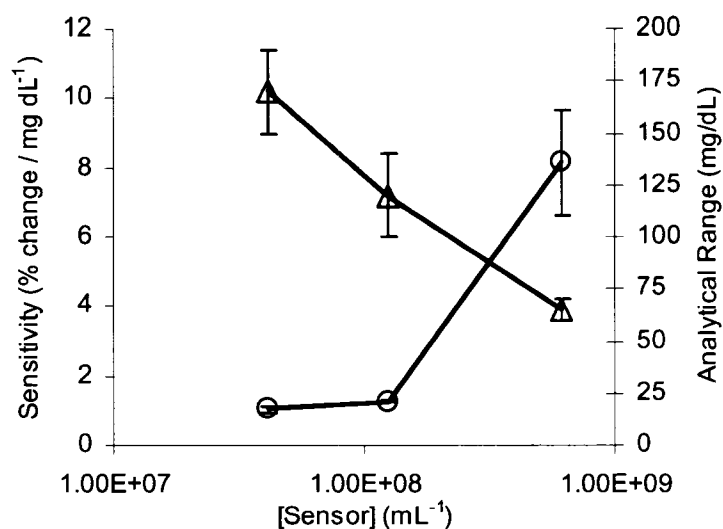
Figure 55. Sensor concentration effect on overall sensitivity and analytical range.

These observations can be explained through careful analysis of the environmental conditions surrounding individual sensors. For this discussion, the environment around a single sensor will be initially considered, followed by increasing sensor concentration in a packed-bead fashion. For a single-sensor scenario, the sensor is surrounded by solution containing a supply of glucose and oxygen, and since the solution is continuously replaced (replenishment is greater than consumption), it is assumed that the sensor *surface* is exposed to a constant supply of both substrates. As glucose diffuses into the sensor, glucose and oxygen are consumed (oxygen is rapidly replenished), resulting in a decrease in the steady-state level of oxygen within the sensor; however, the steady-state concentration of oxygen within the sensor is dependent on the oxygen concentration within the bulk. Higher bulk oxygen levels result in higher steady-stale levels within the sensor and vise versa with lower bulk oxygen levels, which in turn affect sensor dynamics (as described in the previous section). As the particle concentration is increased, the sensors become tightly packed together (small interparticle

distances), and the environment surrounding individual sensors becomes drastically different than that of the single sensing microsphere. At greater sensor concentrations, a higher rate of substrate consumption would be expected, such that substrate concentrations at the sensor surface may be considerably less than those in the bulk. Lower substrate levels at the sensor boundaries would affect sensor performance. Therefore, it is hypothesized that this phenomenon is not due solely to increased concentration but due instead to decreased interparticle distances associated with increased sensor concentrations.

The experimental data presented in Figure 54 and Figure 55 seem to corroborate the above scenarios. At the highest concentration tested (6.1 x 10^8 sensors/mL), the analytical range was determined to be 65 ± 5 mg/dL, indicating early onset of an oxygen-limited regime. This result could be explained by reduced oxygen levels at the sensor surface due to rapid consumption by the sensor population (consumption from the sensor population is greater than replenishment from the bulk); therefore, average steady-state oxygen levels within the sensors are reduced such that oxygen-limited catalysis occurs at relatively low glucose levels. This event would also explain the high total percent change obtained with 6.1 x 10^8 sensors/mL, as decreasing oxygen levels would result in an increased percent change from baseline. As the concentration is reduced by a factor of 5 (1.2 x 10^8 sensors/mL), the sensor population consumes bulk substrates at a lower rate, thereby allowing more rapid replenishment of substrates at the sensor surface than compared with those of the highest concentration. This reduction in sensor concentration results in an extending the glucose-limited operation range, effectively increasing the analytical range. The same observation was observed with a 15x dilution, resulting in a

concentration of 4.1 x 10^7 sensors/mL, such that the analytical ranges and sensitivities were similar (Figure 55). This observation indicates that substrate diffusivities within the bulk solution were able to overcome substrate consumption of the sensor population at a similar rate to those of the 1.2 x 10^8 sensors/mL sample set.

To further analyze this situation, changes in bulk oxygen levels at the entrance and exit of the reaction chamber were monitored during the experimental procedure (Figure 56).
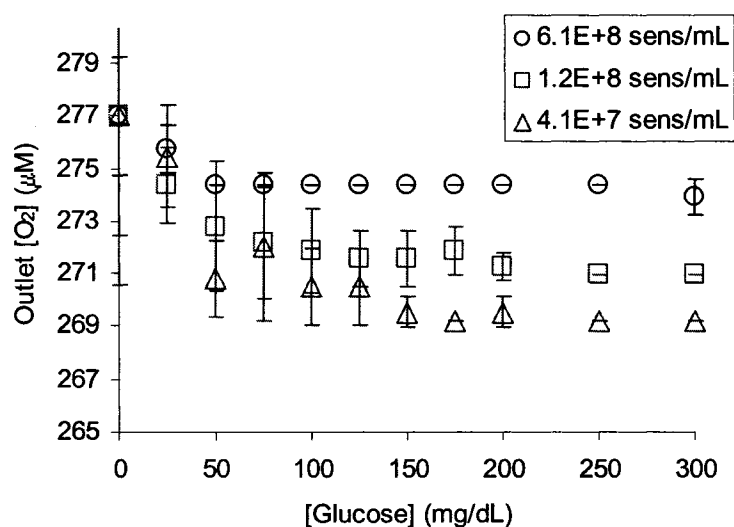
Figure 56. Bulk oxygen levels at sample chamber outlet for various sensor concentrations.

These data indicate that there is indeed a mean reduction of oxygen levels at the chamber outlet; however, the oxygen level fluctuations observed under 0 mg/dL glucose make statistical conclusions difficult. In an attempt to account for fluctuations of oxygen at the chamber inlet, the absolute difference between the inlet and the outlet was calculated (Figure 57).
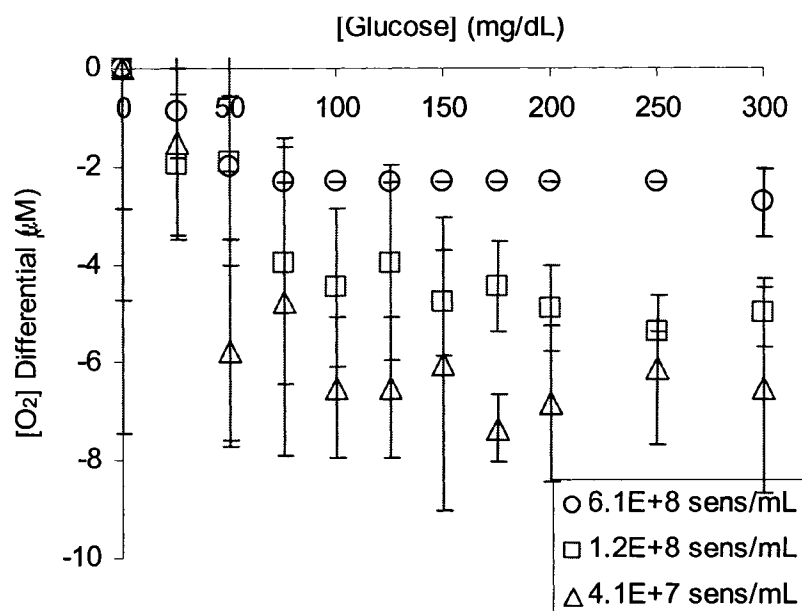
Figure 57. Oxygen differential between chamber inlet and outlet versus sensor concentration.

Correction for fluctuations of bulk oxygen at the chamber did not enhance statistical viability of the data, given the standard deviations observed at 0 mg/dL of glucose are not statistically different than measurements acquired over non-zero glucose levels. Statistical significances aside, it is noteworthy to point out that the *mean* changes in bulk oxygen levels observed with the lowest particle concentration (4.1 x 10^7 sensors/mL) are *greater* that those observed with the highest tested concentration. These data seem counterintuitive, as it would be expected that samples prepared with a higher concentration of sensors would consume more oxygen and would therefore result in a greater oxygen differential. In an attempt to explain this anomaly, a closer inspection of the sample preparation technique was warranted. As detailed in the methods section of this chapter, 10 μL of the sensor suspension are placed on double-sided pressure-sensitive

polyacrylate adhesive and dried under streaming nitrogen. After testing, the samples were

removed, dried under streaming nitrogen, and imaged using a SEM (Amray 1830, 20kV).
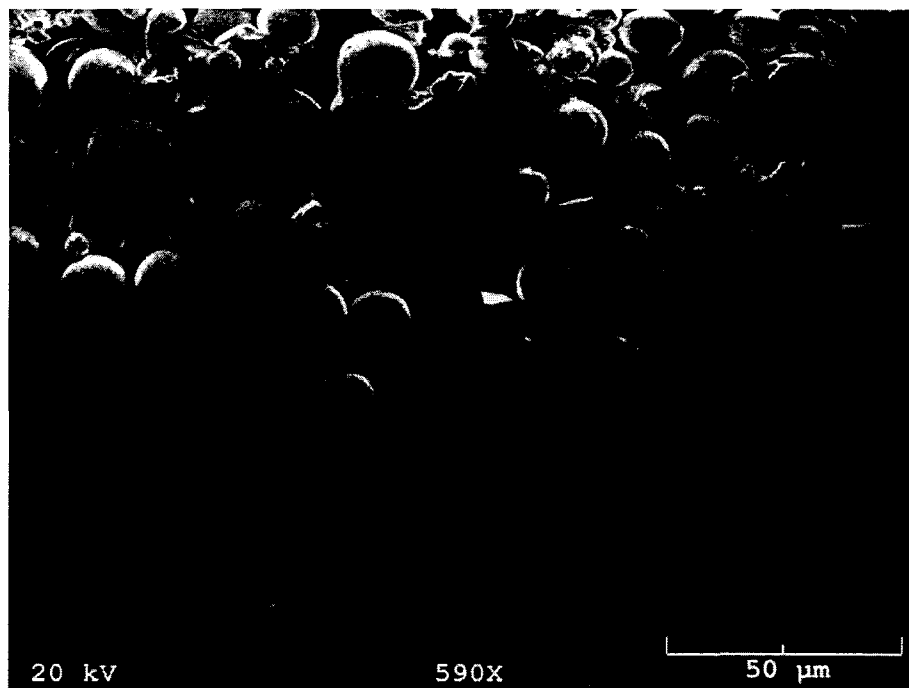
**Figure 58 Scanning electron micrograph of immobilized sensor sample prepared
with 6.1 x 10^8 sensors/mL.**

From this image, it is apparent that multiple sensor layers (approximately 3)

comprise the tested sample. Thus, it is plausible that underlying sensor layers "see"

different substrate concentrations at their respective surfaces. It is important to note that

the non-spherical matter could be due to salt crystal formation as a result of PBS presence

during the drying process.

Additionally, tested samples were examined on a more global scale using UV

illumination (BlackRay), while collecting PtOEP emission with a digital camera (Figure

59).

Figure 59. Images of sample with varying concentration after testing – left (6.1 x 10^8 sensors/mL), middle (1.2 x 10^8 sensors/mL) and right (4.1 x 10^7 sensors/mL). Sensors are identified by red/pink color.

Shear forces exerted at the sample-solution interface removed weakly adhered sensors (red/pink color), resulting in immobilization patterns observed in Figure 59. When compared with an image of a sample obtained before testing, a significant difference between the immobilization patterns can be observed (Figure 60).

Figure 60. Image of sample prior to dynamic testing (6.1 x 10^8 sensors/mL).

These images indicate that the distribution profile of the sensors can significantly change as the shear forces are exerted on the sensors (this event takes approximately 45 min to equilibrate as shown in Figure 42). Therefore, the initial number of immobilized sensors can not be assumed to be constant throughout the experimental procedure, but it

is apparent that the absolute quantity of sensors immobilized when using 6.1×10^8 sensors/mL is indeed greater than that observed for the two lower concentrations. Therefore, there is no current explanation as to why mean decreases in bulk oxygen levels are greater for a lower number of sensors present on a sample. It is believed that lowering the flow rate would result in an increased amount of oxygen consumed from the bulk, which should exaggerate the oxygen differential and possibly reduce the noise observed in Figure 56 and Figure 57, allowing statistically significant measurements of the oxygen differential between glucose-containing solution and buffer. Additionally, it is important to recognize that the sample geometry tested is similar to that of a disk, where in *in vivo* situations, the sensor implant geometry may more closely resemble that of a sphere. Nonetheless, it is a practical concept to consider when designing the *in vivo* functionality of the system.

4.3.15   Effect of Flow Rate on Glucose Response

A critical variable of the testing apparatus used in this work is flow rate. It was hypothesized that the solution flow rate through the reaction chamber could indeed cause changes in the dynamic response properties of the sensors. An experiment was devised during which a sample was exposed to varying glucose levels at several flow rates. Data were collected and the % change in PtOEP/RITC peak ratio was plotted versus glucose concentration (Figure 61).
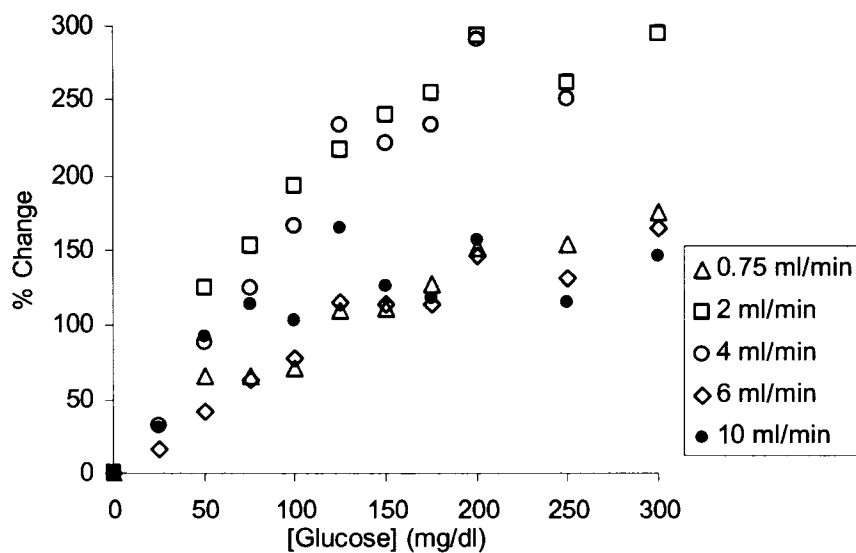
Figure 61. Effect of solution flow rate on mean sensor response.

It should be noted that since the same sample was used throughout this experiment, that random duplicate exposures to each glucose concentration were performed (as opposed to triplicates in the previous experiments), with the samples being exposed to random flow rates. These data indicate that solution flow rate does have an effect on the response properties of the sensors. In order to further interpret the data in Figure 61, the sensitivity and analytical ranges determined for each flow rate were calculated.
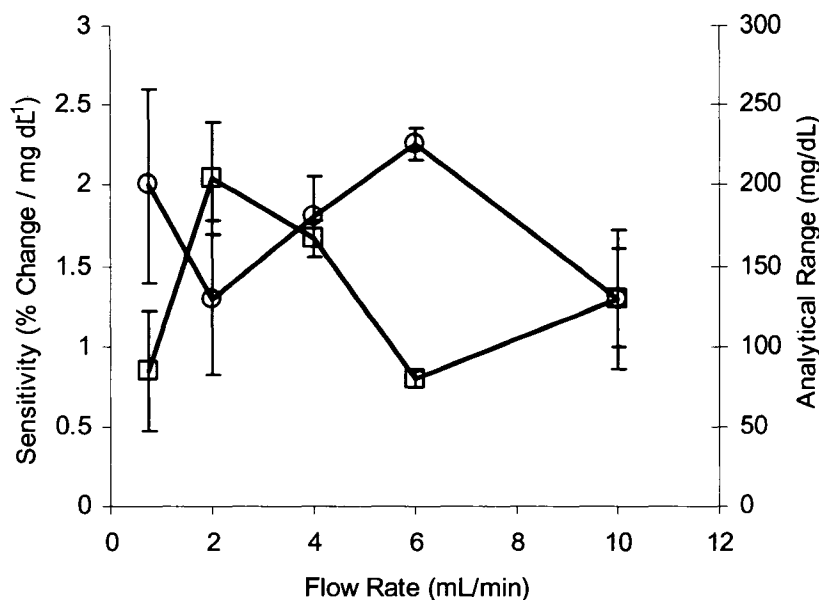
Figure 62. Flow rate effect on sensor sensitivity and analytical range.

In contrast to previous data sets, there is no clear trend (i.e. continuously increasing or decreasing) of how flow rate affects sensitivity and analytical range. For instance increasing the flow rate from 0.75 mL/min to 2 mL/min results in an increase in sensitivity, but increasing the flow rate from 2 mL/min to 4 mL/min results in a subsequent decrease in sensitivity. Given that these data are indeed more chaotic than previous data detailing a parameter's effect on sensitivity and analytical range of the sensors, conclusions are more difficult to draw. Therefore, it is desirable to formulate a *quantitative relationship between device sensitivity and analytical range* such that a single coefficient is extracted and compared with those obtained from other values of the independent variable, in this case, flow rate. To relate device sensitivity and analytical range, the following "fitness" function (F) is introduced:

$$F(m, R^2) = \cfrac{1}{1 - \left(A * m * \cfrac{\max \Delta_{glu}}{\max \Delta_{\%Change}} + B * R^2 \right)}$$

The fitness value is obtained from the overall sensitivity (m) and linearity (R^2) of the response. It should be noted that in this case, the sensitivity is not defined as before (the slope of the linear region of the response), but is defined as the overall sensitivity (average slope, m) of the *entire* response, which is obtained by simply performing a least-squares linear regression to the entire response profile. The overall sensitivity was subsequently normalized to the maximum possible slope over the range of interest. The overall linearity of the response is defined as the correlation coefficient obtained through the linear regression; this R^2 value is synonymous with analytical range, such that as R^2 approaches 1, the linearity (i.e., range) of the response over the range of interest is increased. It is noteworthy to state that the fitness function assigns weights to m and R^2 given by A and B, respectively, allowing one to assign varying levels of importance to either parameter. It should be noted that summation of the weighting factors is equal to unity. For the work presented in this section, an equal weighting of 0.5 was assigned to each variable (i.e., sensitivity and linearity are of equal importance). Before instating this function to analyze the data, presented in Figure 61 and Figure 62, it is a useful exercise to examine how profiles with varying sensitivity and range affect the fitness. To compare the effect steady-state response profiles on fitness values, several sets of dummy response profiles were generated and a fitness value calculated for each case (Figure 63).
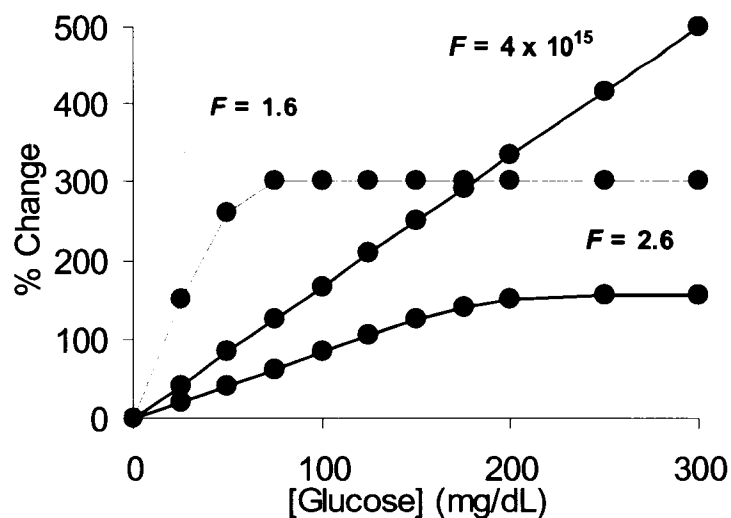
Figure 63. Response profile effect on fitness value (*F*). Note that these data were not experimentally determined.

The data presented in the black trace represent the "ideal" response, with the highest obtainable sensitivity and linearity over the defined response range (0 – 300 mg/dL), thereby warranting the "infinite" fitness value of 4×10^{15}. The data presented in the red and blue traces represent similar deviations in sensitivity and linearity, respectively, such that the resulting fitness values are similar in magnitude. Therefore, elevated fitness values represent increasing conformity of the response data to the "ideal" response.

Using this approach, the fitness values were calculated for each response profile obtained at various flow rates (Figure 61) and displayed in Figure 64.
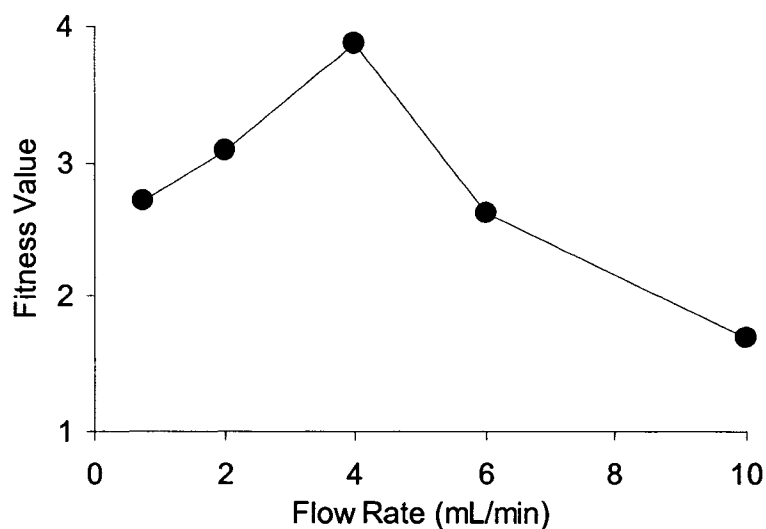
Figure 64. Fitness value versus flow rate.

The first noteworthy point is that flow rate can indeed affect the glucose response of the sensors. Additionally, these data indicate a "sweet spot" between sensor response and flow rate, as observed by the maximum fitness value occurring at 4 mL/min. This result is not surprising, as at low flow rates (0.75 mL/min), it is possible that substrate replenishment from the bulk cannot match consumption of the sensors. As flow rate is increased, more rapid delivery of substrates allows extension of the oxygen limited response, resulting in an increased fitness value. However, at extreme flow rates (i.e. 10 mL/min), forced mass transfer due to convection may occur, resulting in sensitivity loss and a reduced fitness value. Under the premise that oxygen has a greater diffusivity than that glucose through the nanofilm coatings,[144] convection would result in elevated average steady-stage oxygen levels within the sensor, causing decreased sensitivity similar to that observed in Figure 52 (540 μM sample set). It is also important to state that normal physiological interstitial fluid flow rates are on the order of mL/hour, significantly lower than those obtainable with the current experimental setup.[184] When

tested under physiological flow conditions it is expected the response will exhibit a poor analytical range due sensor consumption being greater than bulk replenishment; therefore, changes in sensor concentration, as well as nanofilm thickness (as discussed in the next section), may be required to obtain a desirable clinically viable response properties.

4.3.16 Effect of Nanofilm Thickness on Glucose Response

One of the key hypotheses of this dissertation is that modulation of substrate diffusivities into the sensor would result in alterations of response properties, namely sensitivity and analytical range. More specifically, limiting glucose diffusivity (relative to oxygen) would decrease the drop of steady-state oxygen levels within the sensors for a given bulk glucose level, ultimately reducing sensitivity and extending the glucose sensitive range of the sensors.[41] Previously, substrate transport was controlled via component immobilization within diffusion limiting polymer supports,[38] sol-gel derivatives, [139-141] and dialysis membranes.[107] Although these reports have shown successful response properties to glucose, a simple means to modulate response properties (i.e. customize sensitivity and analytical range) is difficult to achieve with the reported fabrication techniques.

In this work, the surface adsorption of thin films fabricated using LbL self-assembly has been selected as substrate diffusion limiting membranes in part due to the ability to create complex nanocomposite thin films through the sequential adsorption of oppositely charged molecules. This general technique has been applied to various charged species, including linear polyions, proteins, viruses, ceramics, lipid tubules, lipids, and charged nanoparticles, [142] thus providing a means to engineer a practically

endless variety of nanocomposite materials via an extremely simple procedure. Previous work has shown that glucose diffusivity through PAH/PSS thin film (the film architecture used in this work) could decrease glucose diffusivity by *four orders of magnitude* when compared with the glucose diffusivity in water, proving that LbL films could indeed provide diffusion limiting capabilities.[144] This result is indeed remarkable, given that a typical (PSS/PAH)$_7$ film has an approximate thickness of *28 nm* (4 nm per PSS/PAH bilayer).

Additionally, a reaction-diffusion model was developed to examine the effect of physical parameters on enzymatic smart tattoo function, comprising LbL nanofilms as a substrate diffusion barrier.[41] By varying nanofilm thickness (through simply adjusting the number of bilayers adsorbed to the surface), the authors demonstrated that the diffusivity of glucose relative to oxygen could be modulated, thereby adjusting the average steady-state oxygen levels observed within the sensors. Additionally, optimal response properties (sensitivity and range) were obtained with 9 PAH/PSS bilayers adsorbed to spherical immobilization matrix in which the oxygen diffusivity is approximately 6-fold greater than that of the glucose diffusivity. Given that theoretical predictions of sensor dynamics showed excellent agreement with experimental observations, the utility of these nanofilms in preparing successful enzymatic smart tattoo concepts was demonstrated, making LbL films a model thin film technology to use in an attempt to engineer smart tattoo response properties.[41, 133, 137]

To examine the effect of nanofilm thickness on sensor response properties, sensors with varying numbers of PAH/PSS bilayers were prepared as previously

described, and the response properties acquired using the dynamic testing apparatus

(Figure 65).
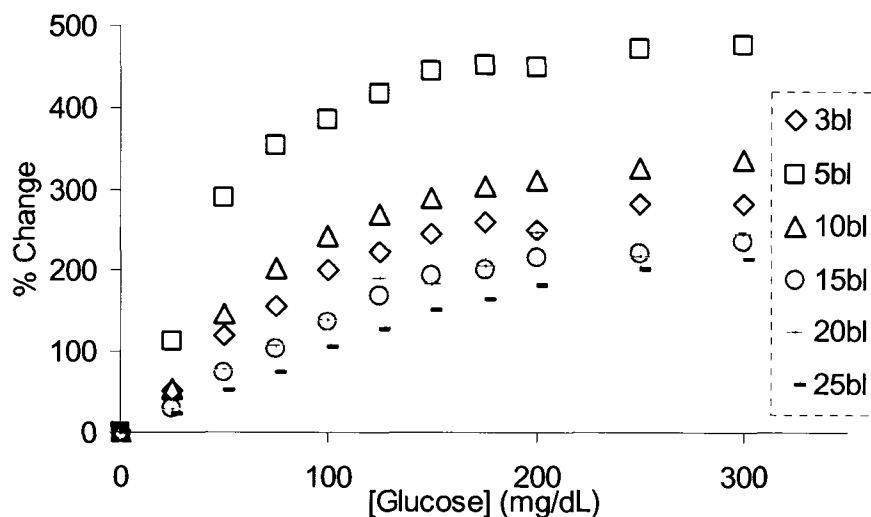
Figure 65. Effect of the number of PAH/PSS bilayers on glucose response properties.

From these data, it is apparent that the number of PAH/PSS bilayers (i.e.,

thickness of the PAH/PSS film) can effect the response sensitivity and analytical range.

To quantify the effect of nanofilm thickness on response properties, the sensitivity and

analytical range were determined for each sample set and presented in Figure 66.
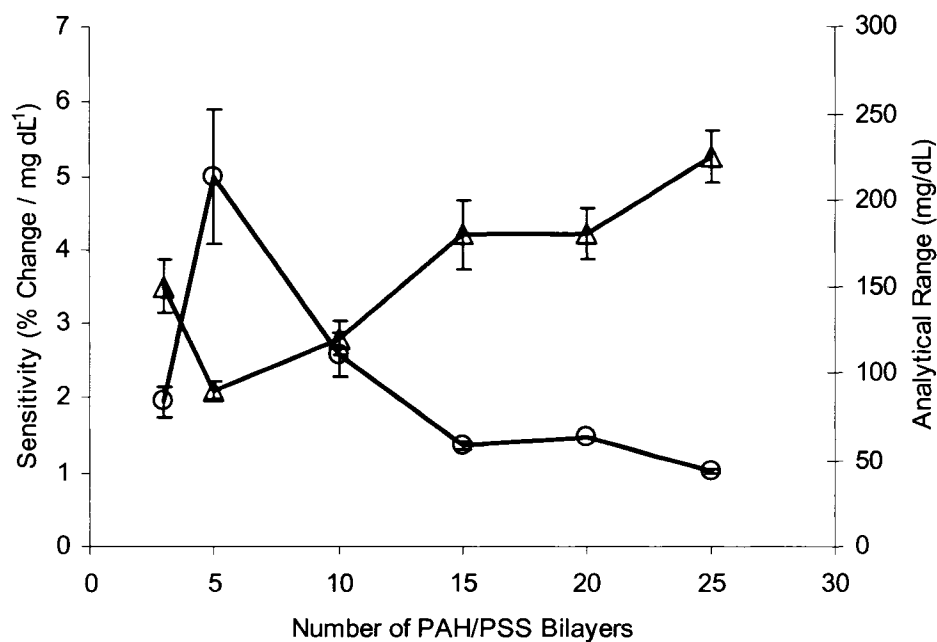
Figure 66. Effect of PAH/PSS bilayer number on device sensitivity and analytical range.

To begin this discussion, the increase in sensitivity observed between sensors coated with {PAH/PSS}₃ and {PAH/PSS}₅, respectively, will be considered. This observation is indeed unexpected, as it was hypothesized that sensors comprised of a lower number of PAH/PSS bilayers would exhibit a higher relative sensitivity. This hypothesis stems from the ideology that films comprised of a low number of bilayers would provide an insufficient barrier to glucose; hence, steady-state glucose levels within the sensors would be greater than those observed with a higher number of bilayers for a given bulk glucose level. This phenomenon would in turn elicit increased oxygen consumption within the sensor, resulting in decreased steady-state oxygen levels that would ultimately cause the rapid onset of an oxygen-limited reaction scheme (i.e. high device sensitivity and low analytical range) when compared with that of sensors with a greater number of bilayers. Nonetheless, the opposite behavior is observed between

{PAH/PSS}$_3$ and {PAH/PSS}$_5$ coated sensors. One potential explanation for this occurrence could be that the algilica matrix itself provides an efficient diffusion limiting effect, allowing the sensor to operate in an extended glucose-limited range. Given that this explanation ignores the contribution of the LbL film, it is somewhat controversial; however, it has been documented that several bilayers of LbL films are necessary to ensure complete surface coverage, [185] suggesting the possibility that {PAH/PSS}$_{3-5}$ may not be sufficient to achieve complete coverage of the sensor. With a "leaky" diffusion barrier, the reaction-diffusion kinetics would be governed to a greater extent by the algilica matrix.

Given that the transport properties of glucose and oxygen through the algilica matrix remain unknown, extensive speculation is impractical. However, it is well known that silica-containing matrices exhibit glucose diffusivities similar to those observed in water, while having increased oxygen diffusivities (approximately 2 order of magnitude greater) when compared with hydrogel matrices, whose oxygen diffusivities are similar to that of water.[170, 186] Should the algilica matrix have similar diffusivities to that of mesoporous silica, it is plausible that the rapid replenishment of oxygen with respect to glucose could result in a glucose-limited response without the aide of diffusion limiting coatings. Nonetheless, this finding indicated that surface adsorption of 20 nm thin films (typical bilayer thickness of a PAH/PSS film is 4 nm) could drastically influence the behavior of these sensor prototypes.

Following the initial increase in sensitivity between {PAH/PSS}$_3$ and {PAH/PSS}$_5$ coated sensors, the hypothesized trend (i.e. decreased sensitivity with increased nanofilm thickness) becomes apparent. To emphasize the effect of

polyelectrolyte films on device sensitivity as well as analytical range, the percent change

of these figures of merit observed in sensors comprising greater than five PAH/PSS

bilayers was determined (Figure 67).
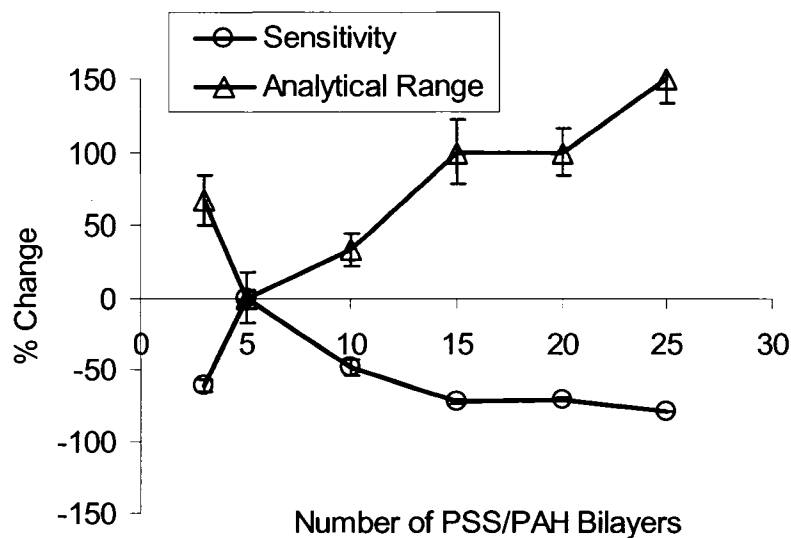
Figure 67. Percent change in sensitivity and analytical range resulting from an increasing in nanofilm bilayers.

The first point of note is that these data indicate the remarkable ability of

PAH/PSS nanofilms to control device response properties. Overall, the sensitivity was

reduced by approximately 80% and the range extended approximately 150% through the

adsorption of $\{PAH/PSS\}_{25}$ coatings to the particle surface. It is important to highlight

that there is an approximate linear relationship between the percent change in sensitivity

and analytical range observed with sensors comprising 5, 10, and 15 PAH/PSS bilayers.

By performing linear regression between these data sets, it was determined that the

percent change in sensitivity per bilayer was -7.26 ± 0.3% and the percent change in

analytical range was 10 ± 0.35% - a total percent change of 70 and 100%, respectively.

However, this trend was significantly dampened between sensors coated with 15, 20, and 25 bilayers, such that sensitivity was only reduced by approximately a 10% change (~ 0.7% per bilayer). This result can be explained by the incremental reduction of glucose flux (relative to oxygen) observed with 5, 10, and 15 bilayer coatings, such that the sequential adsorption of 5 bilayer increments linearly retards glucose flux into the catalytic region of the sensor. However, after the adsorption of 15 bilayers, the transport rate of glucose into the sensing region of the sphere begins to be less affected by the nanofilms, resulting in a dampened response, as predicted in previous work.[41] Given this analysis, it is hypothesized that a further increase in the number of nanofilm bilayers would continue to reduce the sensitivity and increase the analytical range, albeit at a less effective rate. Nonetheless, it is important to restate that the sequential adsorption of PAH/PSS films onto the particle surface does allow the sensitivity and the analytical range of these devices to be tailored using an extremely simple technique. Additionally, future applications are not limited to PAH/PSS nanofilms, but a variety of nanocomposite films could be applied to this platform, such that more dense films could reduce the thickness (i.e. number of bilayers) needed to obtain a similar response.

Following the analysis of bilayer effect on sensor response properties, it is only logical to speculate about the number of PAH/PSS bilayers required to obtain an optimum response. To determine the optimum number of bilayers, the fitness function (as described earlier in this chapter) is employed. As previously stated, the fitness function allows the relative importance of sensitivity and linearity of the response to be assigned through weighting factors over a designated range of operation. As an initial exercise, the glucose range over which the fitness values were calculated was varied from

0 – 300 mg/dL to 0 – 150 mg/dL assuming equal weighting of sensitivity and linearity (Figure 68).
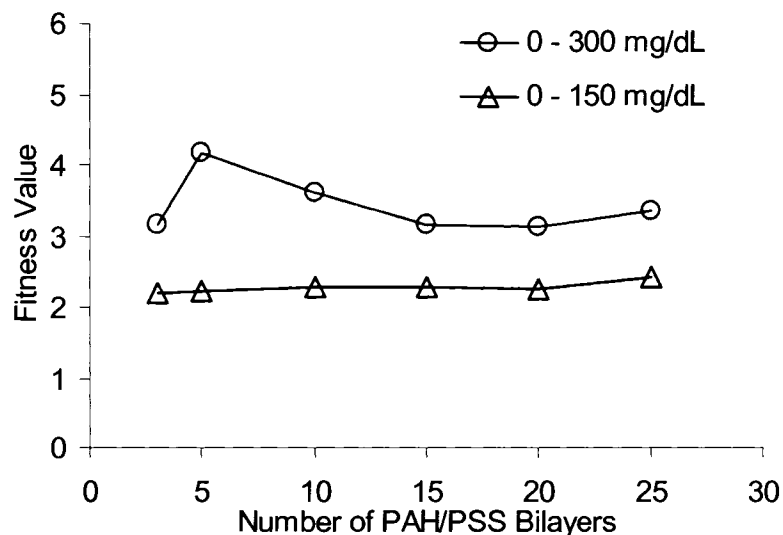
Figure 68. Fitness of sensor response versus number of PAH/PSS bilayers at various ranges of interest. Note that these data were obtained with equal weighting of sensitivity and linearity.

These data indicate that by decreasing the range of interest to 0 – 150 mg/dL, the fitness values of the sample set are similar, in part due to the high linearity of the sample sets in this range, whereas, when using 0 – 300 mg/dL as the range of interest, sensors comprising 5 nanofilm bilayers (range = 90 ± 5 mg/dL) produce the highest valued response. Although this exercise is somewhat impractical (undoubtedly a glucose monitor with such a limited range would not be viable), it is nonetheless interesting to examine the effect of varying the analytical range of interest on the calculated fitness value.

A more practical exercise would be to study the effect of the weighting factors on the fitness output. In Figure 69 the fitness values with equal and unequal weighting factors were calculated for the sensor response properties given in Figure 65.
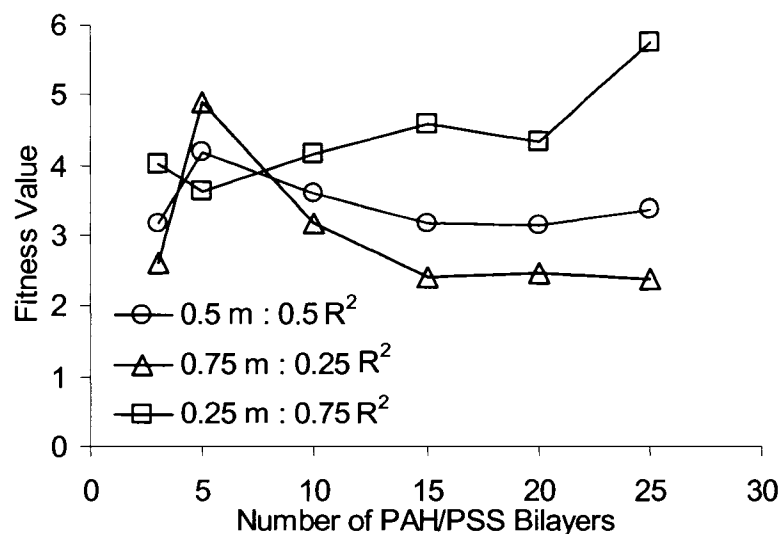
Figure 69. Fitness of sensor response versus number of PAH/PSS bilayers at various sensitivity (m) and linearity (R^2) weightings, assuming a 0 – 300 mg/dL range of interest.

As expected, these results indicate that weighting factors can influence the fitness of response. The red trace yields the fitness values obtained when equal weighting ($A=B=0.5$) was used, and indicated that the optimum response (given by the largest fitness value) is obtained through the adsorption of {PAH/PSS}$_5$ to the particle surface. If the weighting values are skewed such that more importance is given to sensitivity ($A=0.75$ and $B=0.25$), the resulting fitness values place more emphasis on {PAH/PSS}$_5$ as the optimum bilayer number. The analytical range of sensors with {PAH/PSS}$_5$ coatings was determined to be 90 ± 5 mg/dL, which does not cover the accepted range (up to 350 mg/dL) of monitors for home use.[176] Hence, it can be said that these devices are too

sensitive (greater than those of similar systems by at least one order of magnitude).[27, 37, 39]

Therefore, more importance was assigned to response linearity (A = 0.25 and B = 0.75).

These data are depicted in the blue trace and indicate that the optimum response is

obtained with {PAH/PSS}$_{25}$ coatings, which provided the greatest analytical range (225 ±

15 mg/dL) of all tested sample sets. Although these sensors do indeed have an extended

range when compared with sensors coated with a lower number of PAH/PSS nanofilm

bilayers, the analytical range is still not within clinical standards. It is hypothesized that

films with increased resistance to glucose diffusion (as compared to PAH/PSS

nanofilms), such as self-assembled lipid bilayers would allow a more efficient means to

extend the glucose sensitive range of these devices.[187]

4.3.17 Response Properties of Uncoated Particles

As shown in the previous section, a precise means to modulate sensitivity and

analytical range of these sensor prototypes is to adsorb polyelectrolyte multilayer films of

varying thickness to the sensor surface. By modulating the flux of glucose relative to

oxygen, the glucose-limited range can be engineered. However, it is interesting to

consider sensor function without surface-adsorbed nanofilms. In the previous section, it

was hypothesized that uncoated algilica particles would have a glucose-sensitive

response, since reports have shown that silica based matrices have greater oxygen

diffusivities than that of glucose by approximately 2 orders of magnitude. [170, 186] This

hypothesis was tested by preparing sensors without fluorescent nanofilm coatings and

tracking the change in PtOEP intensity as a function of bulk glucose concentration over

time.

It is important to note that in these data, no reference signal was used; therefore, the data had to be corrected for any drift resulting from source fluctuations and decreases in sensor concentration. Figure 70 depicts the raw data and the curve fit used to correct baseline drift.
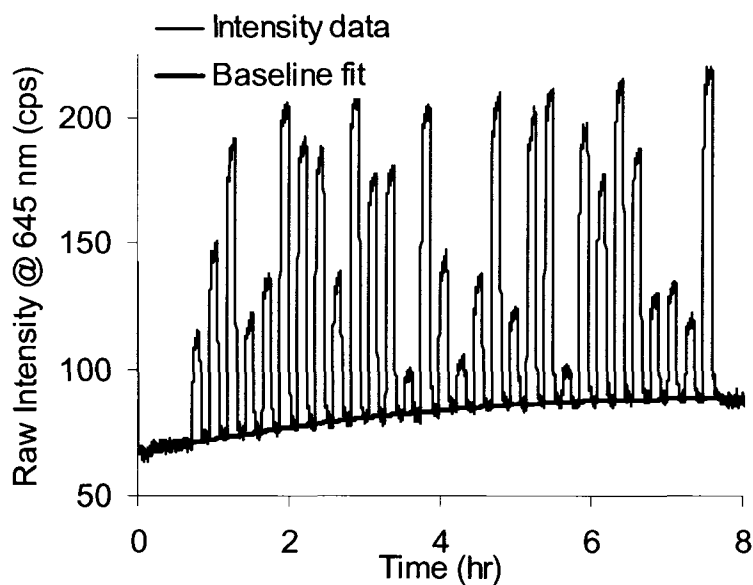
Figure 70. Raw PtOEP peak intensity obtained during dynamic glucose testing of sensors without nanofilm surface coatings and baseline fit used to correct for signal drift over time.

It should be noted that to obtain the baseline fit, the dynamic sensing data obtained at 0 mg/dL were fitted to a second-order polynomial. After the data were corrected for drift by subtracting the baseline drift, the profile in Figure 71 was obtained.
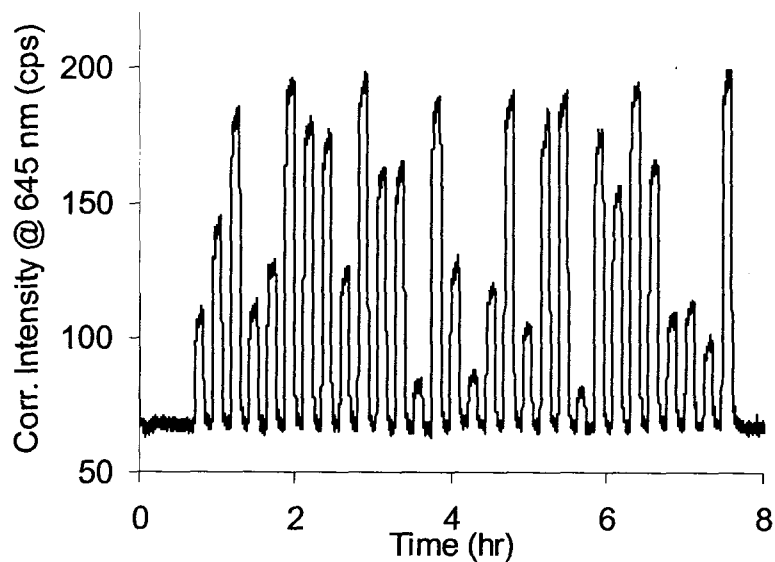
Figure 71. Corrected PtOEP peak intensity obtained during dynamic glucose testing of sensors without nanofilm surface coatings.

From these data, it evident that a stable baseline was obtained through the baseline correction procedure. The corrected data were then used to obtain the following response profile.
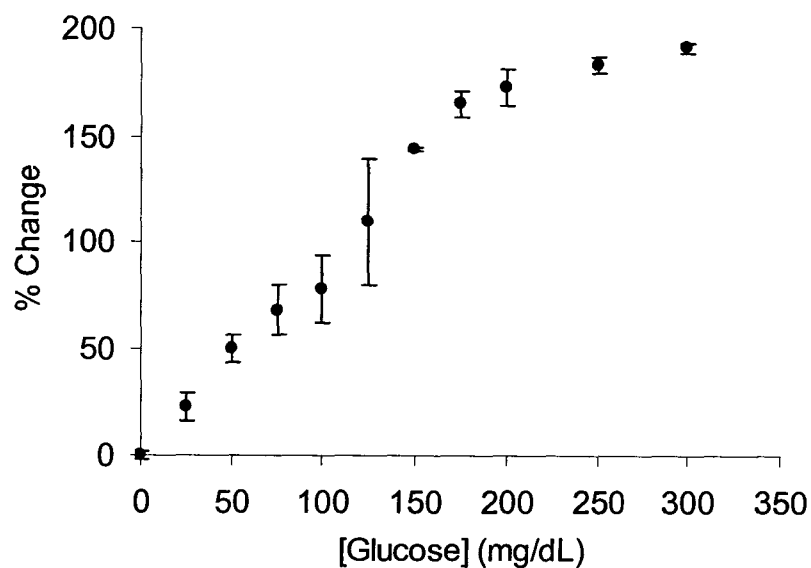
Figure 72. Glucose response profile of uncoated sensors.

The first point of note is that the uncoated sensors are indeed sensitive to changes in bulk glucose levels. Using the data presented in Figure 72, the sensitivity and analytical range of the uncoated sensors can be obtained and subsequently integrated into the data presented in Figure 66 to create the graph in Figure 73.
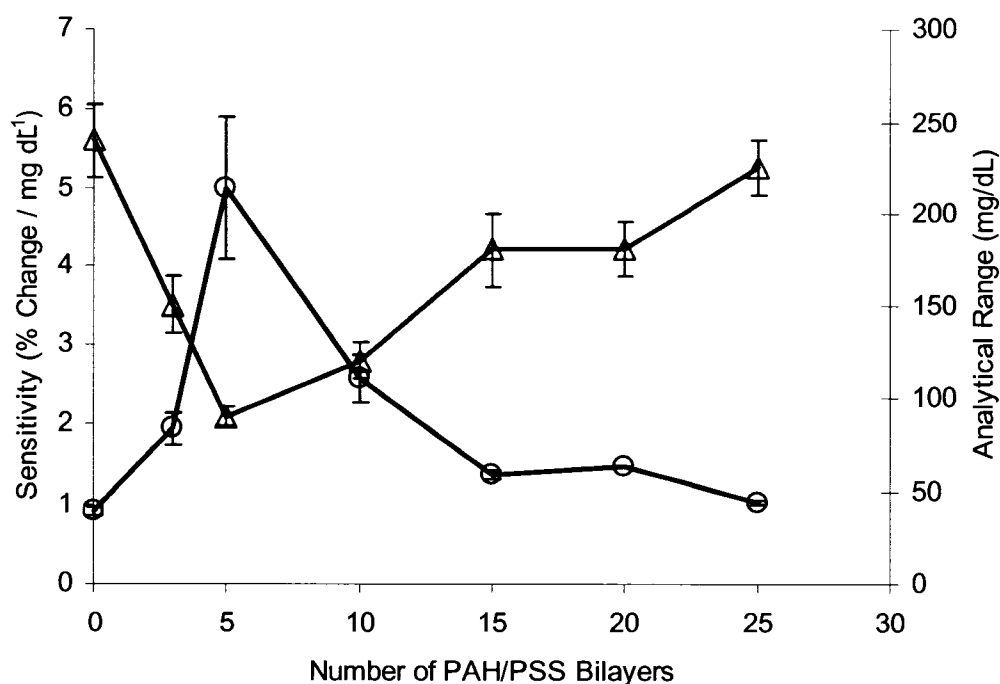
Figure 73. Comparison of uncoated to coated sensor response properties.

It should be noted that the behavior responsible for the decrease in sensitivity observed with sensors coated with {PAH/PSS}$_{5-25}$ was discussed in the previous section; therefore, the discussion here will focus on the increasing sensitivity trend observed with sensors comprising {PAH/PSS}$_{0-5}$.

One explanation for the initial increase in response sensitivity could lie in the hindrance of oxygen adsorption to the algilica surface by the incomplete surface coverage

of initial nanofilm bilayers. In previous reports, it is hypothesized that the rapid oxygen diffusivity observed in silica based matrices occurs due to surface adsorption of dissolved oxygen followed by diffusion across the surface.[46] Thus, if incomplete polyelectrolyte multilayers are deposited to the surface, it is possible that glucose diffusion may be minimally effected, but oxygen adsorption to the algilica surface and subsequent diffusion may be significantly hindered. This phenomenon would ultimately decrease oxygen flux relative to that of glucose entering the catalytic region of the sensor. As a result, the rate of oxygen replenishment would be eclipsed by the rate of glucose supplied from the bulk, resulting in increased sensitivity and reduced analytical range, as shown in the transition from 0 to 3 nanofilm bilayers. If the adsorption of additional bilayers fails to provide a significant barrier for glucose but provides additional hindrance to oxygen surface adsorption, the effect would be compounded, resulting in a sequential increase in sensitivity and decrease in analytical range, as seen in the transition from 3 – 5 nanofilm bilayers. Additional support for this theory could be found by analyzing the response profile of sensors coated with 0, 3, and 5 nanofilm bilayers, respectively (Figure 74).
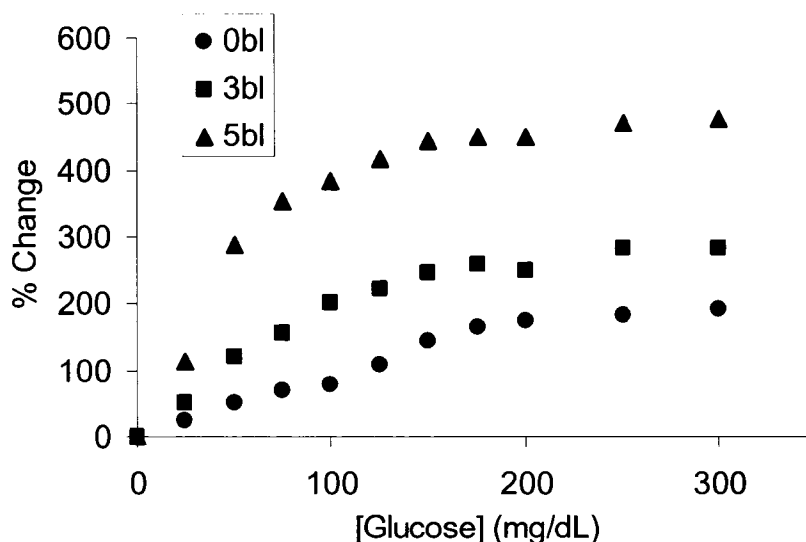
Figure 74. Glucose response profile comparison of sensors coated with 0, 3, and 5 PAH/PSS bilayers.

If oxygen flux (relative to glucose flux) is reduced by the deposition of 3 nanofilm bilayers, then the internal oxygen levels would be expected to be lower for a given bulk glucose concentration, when compared with those sensors without nanofilm coatings. This event would result in an increased percent change in the PtOEP/RITC peak ratio (less oxygen = increased PtOEP emission) for a given bulk glucose level when compared with those obtained with uncoated sensors, which is indeed what is observed in Figure 74. The adsorption of an additional 2 nanofilm bilayers (5 total) also results in an increased percent change in peak ratio for a given bulk glucose level, when compared with those of 0 and 3 nanofilm bilayers, respectively. These data support the theory that the initial 5 nanofilm bilayers have a profound effect on the oxygen flux, while additional nanofilm bilayers dominantly affect the flux of glucose into the sensor. Further experimental work investigating the oxygen response may provide additional support for this theory. More specifically, examining oxygen response time of the sensors versus the

number of nanofilm bilayers may allow the quantification of relative differences in oxygen flux throughout the sphere.

The lack of some details on the underlying phenomena not withstanding, these data indicate that glucose-sensitive prototypes using algilica matrices can be obtained without polyelectrolyte nanofilms, a stark contrast to theoretical simulation using alginate as the immobilization matrix, the results of which indicated that nanofilms were a critical aspect in obtaining a glucose sensitive response.[41, 133] It is of critical importance to state that *although nanofilm coating are not required to obtain a glucose-sensitive response for algilica matrices, they are indeed useful in providing a means to regulate device sensitivity and analytical range, thus allowing these prototypes to be engineered to individual specifications.* Therefore, the efficacy of polyelectrolyte nanofilms in this application cannot be understated.

4.4 Conclusion

A highly sensitive microparticle-based enzymatic glucose sensor technology has been demonstrated. As a first step, techniques were developed to allow the homogeneous immobilization of GOx and PtOEP within algilica microspheres, following which, fluorescent nanofilms were deposited onto the particle to provide a reference signal and obtain glucose-limited oxygen consumption within the sensor by controlling glucose transport. The oxygen-dependent response of the sensors was quantified, indicating linear quenching characteristics and high sensitivity to oxygen within the expected range of physiological operation. Upon the addition of glucose, these self-referencing systems rapidly responded (t_{95} = 84 sec) to step changes in glucose concentration, while exhibiting excellent baseline stability, photostability, and reversibility between alterations

of bulk glucose levels. It was found that these systems are highly sensitive to glucose, with sensitivities approximately an order of magnitude greater that those of similar systems. As a key point of this work, it was shown that through the subsequent adsorption of polyelectrolyte multilayers, the reaction-diffusion kinetics within sensors could be modulated, ultimately resulting in the ability to control the sensitivity and analytical range and design a sensor sensitive within a range of interest. These results are undoubtedly promising indicators of the efficacy of these sensors as potential implants for diabetic monitoring. However, given that the response properties are highly dependent on bulk oxygen concentration, as well as the concentration of immobilized sensors, these factors need to be addressed to enhance the practicality of the systems for *in vivo* use. Future work will investigate the feasibility of incorporating bulk oxygen sensors into the implanted sensor population to correct for fluctuations in oxygen levels seen under normal physiological conditions, as well as oxygen fluctuations due to substrate consumption from the enzymatic smart tattoo population. Additionally, the effect of polyelectrolyte nanofilms on the oxygen diffusivity through algilica should be investigated, as additional insight could enhance future designs. Moreover, a critical aspect of clinical viability remains to be characterized – long-term response properties. Thus, in the following chapter, a mathematical model describing the effect of long-term operation on sensor function is presented and the output compared to experimentally determined results.

CHAPTER 5

MODELING AND EXPERIMENTAL VALIDATION

OF ENZYME DEACTIVATION

KINETICS

5.1 Introduction

In the previous chapter, the preparation and characterization of enzymatic smart tattoo concepts were successfully demonstrated. These sensors rely on the co-immobilization of glucose oxidase and platinum porphyrin complexes to indirectly report glucose levels through changes in local oxygen levels resulting from glucose consumption. A particularly novel feature of these concepts is the use of fluorescent polyelectrolyte nanofilms to provide an internal reference signal, as well as to modulate substrate transport into the catalytic region of the tattoo. A schematic of the sensor prototype, as well as confocal micrographs of actual prototypes are given in Figure 75.

177
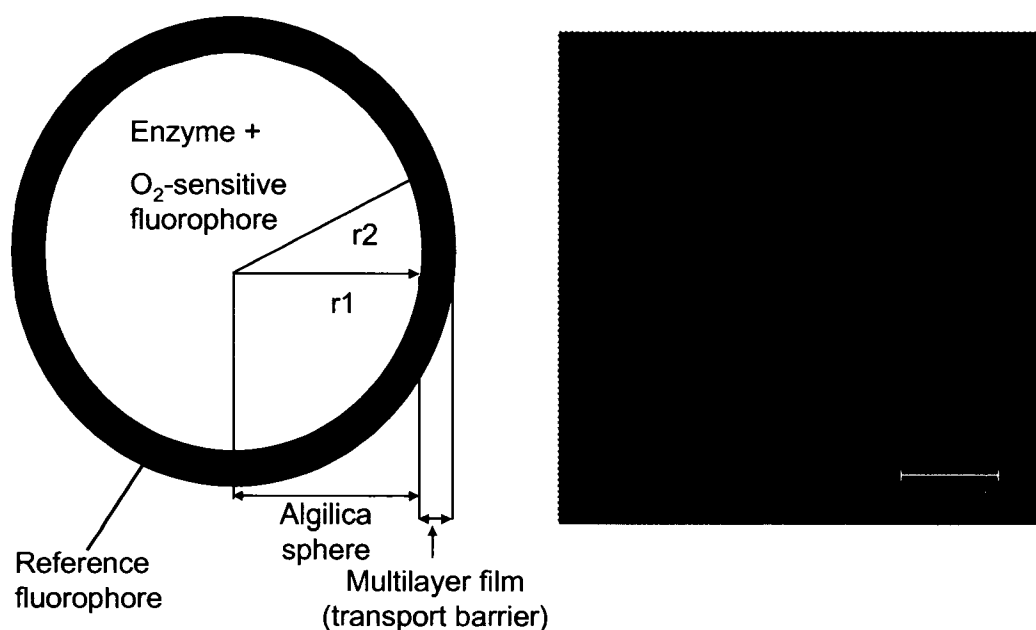
Figure 75. Schematic of enzymatic smart tattoo sensor and accompanying confocal micrograph depicting indicator (blue) and reference (pink) dye location.

While the results reported thus far are undoubtedly promising, sensor performance under extended periods of continuous operation has yet to be characterized. Since the ultimate goal of this work is to provide a clinically viable technology to enhance the quality of life for diabetic patients, it is desirable for these transdermal devices to exhibit long lifetimes (> 6 months). Constant removal/replacement of the tattoos, as well as increased calibrations required to ensure readout accuracy would ultimately detract from the "minimal invasiveness" of this technology and potentially eliminate application in long-term situations. Although previously reported in Chapter 4, photodegradation of fluorophores could also contribute to decreased sensor life span, but has been shown to be minimal over the projected sensor lifetime.

It is also important to recognize that host-mediated inflammatory responses could potentially be detrimental to sensor longevity.[188] Inflammation serves to contain,

neutralize, reduce, and wall off the foreign body. Through the initial steps of this process, the implant would be attacked by the host immune system, with full attention focused on removing the implants via oxidative processes or phagocytosis, ultimately resulting in a loss of implant function over time. However, it should be noted that this phenomenon is most likely dependent on surface structure and chemistry, and may be controlled via the deposition of different surface coatings, as previous work suggests.[189] Additionally, fibrous capsule formation around the implants may prove more detrimental to long-term function stability, as most likely the substrate mass transport properties through the capsule would be significantly less that those in the subcutaneous space. This phenomenon may lead to increased lag times[104] as well as performance alterations due to variations in the bulk conditions "seen" by the implants. Additionally, the fibrous capsule is expected to alter the excitation and collections efficiency of transdermal irradiation, making the spectral acquisition more challenging. However, the detailed consideration of these factors is out of the scope of this work.

Additionally, one particular phenomenon which could greatly influence the long-term response properties of enzymatic smart tattoos is the temporal deactivation of glucose oxidase. Loss of enzymatic activity would ultimately result in decreased device sensitivity over time, causing diminished accuracy and ultimately requiring device replacement. Being that GOx is used in a broad range of applications, a copious amount of work has been dedicated to understanding its kinetic properties, as well as factors affecting kinetic properties.[179, 190-193] In these reports, several key factors that affect the long-term stability of GOx have been determined, including inactivation due to time, temperature, pH, and hydrogen peroxide poisoning. Of these factors, inactivation

(unfolding) resulting from hydrogen peroxide poisoning has been shown to be the most grave, such that one report showed > 95% loss of enzymatic activity after 50 hours of continuous operation, while other factors such as pH and thermal inactivation have been reported to have little effect on enzyme activity at physiologically regulated values.[179, 190, 193] Despite the understanding of GOx deactivation kinetics, there has been little effort in integrating inactivation kinetics into a spatio-temporal reaction-diffusion model, possibly due to the computationally intensive processes required to obtain a solution. Even so, one report proposed a dimensionless model to investigate the effect of GOx deactivation on glucose-sensitive response properties of planar electrochemical glucose sensors.[179] Although simulation results were not experimentally validated, model output predicted significant loss of device sensitivity (~ 45%) due to enzyme inactivation after only ten days of continuous operation. Nonetheless, a dimensional model with spherical coordinates is desired to describe the devices detailed in this work (Figure 75). More recently, a model describing the reaction-diffusion kinetics within spherical enzymatic smart tattoos was proposed.[166] However, the model proposed in this report was solely used to examine the effect of physical parameters on sensor response properties to prepare functional first-generation prototypes; therefore, drift in response properties due to enzyme inactivation was not considered.

Given that functional prototypes have been demonstrated in the previous chapter, emphasis is shifted to engineering sensors with sustainable response properties. Hence, *there is a need to combine these efforts to develop a spatio-temporal reaction-diffusion model which includes the ability to monitor long-term operation, while considering the effect of enzyme inactivation on device function.* Such a model could be used to examine

the effect of physical properties on long-term sensor function, providing a tool to rationally design enzymatic smart tattoos for optimal response over extended periods of continuous operation, thus alleviating the need for frequent calibration and/or replacement. The scope of this chapter is to develop such a mathematical model, while experimentally validating the results.

5.2 Methods

5.2.1 Instrumentation

A numerical solution of the sensor model was obtained with the PDEPE function, which solves initial-boundary value problems for systems of parabolic and elliptic partial differential equations in one space variable and time, in MATLAB 7.0 (Mathworks). Stand-alone C applications were created using MATLAB compiler v3.0 and executed on a Windows XP Professional-equipped workstation with dual 2 GHz Xenon$^{®}$ processors and 2 GB of RAM (Dell).

5.2.2 Theory

Glucose oxidation as catalyzed by glucose oxidase in the presence of oxygen can be described by the following reaction scheme:

$$E_o + G \underset{k_1,k_{-1}}{\overset{}{\longleftrightarrow}} X_1 \overset{k_2}{\longrightarrow} E_r + P \tag{1}$$
$$E_r + O_2 \underset{k_3,k_{-3}}{\overset{}{\longleftrightarrow}} X_2 \overset{k_4}{\longrightarrow} E_o + H_2O_2$$
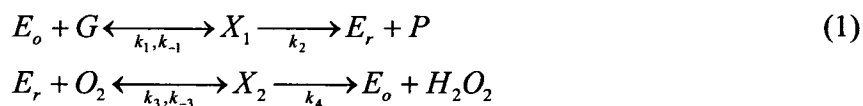
where G and O_2 represent the reactants, glucose and oxygen, respectively, while P and H_2O_2 represent the products, gluconic acid and hydrogen peroxide, respectively. The oxidized and reduced forms of the enzyme are represented by E_o and E_r, and the enzyme-substrate complexes are given by X_1 and X_2. The forward and reverse reaction rate

constants are given by k_1, k_{-1}, k_2, k_3, k_{-3}, and k_4. Additionally, the following scheme describes the first-order inactivation kinetics due to hydrogen peroxide poisoning:

$$E_o + H_2O_2 \xrightarrow{K^1} IE_o$$
$$X_1 + H_2O_2 \xrightarrow{K^2} IX_1 \qquad (2)$$
$$E_r + H_2O_2 \xrightarrow{K^3} IE_r$$
$$X_2 + H_2O_2 \xrightarrow{K^4} IX_2$$
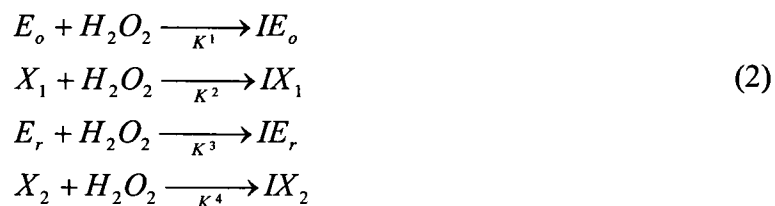
where K^1, K^2, K^3, and K^4 represent the inactivation rate constants of the respective enzyme forms, and IE_o, IX_1, IE_r, and IX_2 represent the inactivated enzyme forms.

Applying a mass balance in the r direction to a spherical shell averaged in ϕ and θ, seven equations describing the reaction-diffusion kinetics within an individual spherical sensor are obtained:

$$\frac{\partial G}{\partial t} = D_G \frac{\partial^2}{\partial r^2}(r^2 G) + r^2(-k_1 G E_o + k_{-1} X_1)$$

$$\frac{\partial O_2}{\partial t} = D_O \frac{\partial^2}{\partial r^2}(r^2 O_2) + r^2(-k_3 O_2 E_r + k_{-3} X_2)$$

$$\frac{\partial H_2 O_2}{\partial t} = D_H \frac{\partial^2}{\partial r^2}(r^2 H_2 O_2) + r^2 k_4 X_2 \qquad (3)$$

$$\frac{\partial E_o}{\partial t} = r^2(-k_1 E_o G + k_{-1} X_1 + k_4 X_2 - K^1 E_o H_2 O_2 - K^0 E_o)$$

$$\frac{\partial X_1}{\partial t} = r^2(k_1 E_o G - (k_{-1} + k_2) X_1 - K^2 X_1 H_2 O_2 - K^0 X_1)$$

$$\frac{\partial E_r}{\partial t} = r^2(k_2 X_1 - k_3 E_r O_2 + k_{-3} X_2 - K^3 E_r H_2 O_2 - K^0 E_r)$$

$$\frac{\partial X_2}{\partial t} = r^2(k_3 E_r O_2 - (k_{-3} + k_4) X_2 - K^4 X_2 H_2 O_2 - K^0 X_2)$$

where the diffusivities of glucose, oxygen, and hydrogen peroxide are given by D_G, D_O, and D_H, respectively. It should be noted that K^0 represents the spontaneous deactivation rate constant for each enzyme form and was assumed

$$K^0 = 0.25 K^T,$$

where K^T is the total spontaneous inactivation rate constant, stating the respective enzyme forms spontaneously inactivate at an equivalent fraction of the total rate constant. Additionally, the total active enzyme concentration, E_T, at any time t and space r is defined as

$$E_T(r,t) = E_o(r,t) + X_1(r,t) + E_r(r,t) + X_2(r,t),$$

where E_o, X_1, E_r, and X_2 represent the concentration of the *active* enzyme forms.

Therefore, the simultaneous solution of the above series of partial-differential equations with boundary and initial conditions appropriate for the structure of Figure 75 would result in the spatio-temporal profile of reaction substrates within the sensor, while considering the effect of enzyme inactivation. Thus, the effect of enzyme inactivation on sensor function over extended periods of continuous-operation could be predicted, as well as the effect of varying physical parameters to minimize response drift. Simulation output could provide critical information in the development of sensor prototypes with sustainable response properties.

5.2.3 Assumptions

Using the schematic in Figure 75, the model assumes homogeneous distribution of active enzyme and indicator within the algilica particle, from $0 < r < \text{r1}$. It should be noted that near-homogeneous distributions of enzyme and indicator dye were achieved in the previous chapter and depicted in Figure 36, validating a shell balance averaged ϕ and

θ. Given the stable immobilization of enzyme within the sensor after 24 hours (Figure 38), the enzyme components were assumed to have respective diffusivities of zero (i.e. non-mobile). It is also assumed that the nanofilms are homogeneously adsorbed to the particle surface from r1 < *r* < r2, and substrate diffusivities through the nanofilms remain constant irrespective of film thickness. Additionally, for model output to describe a population of implanted sensors, it must be assumed that individual sensors within a population are exposed to the same bulk conditions regardless of the sensor concentration (the model simulates the reaction-diffusion kinetics within a single sensor). It should be noted that this assumption will not hold under all conditions (i.e. high particle concentration and small interparticle distances); however, given the intense computation processes required to solve the model, this simplification is warranted for the work presented herein.

The following assumptions are applied for the initial and boundary conditions:

1. The oxygen concentration in the bulk for all *t* remains constant at 90 μM, the accepted value for intradermal oxygen tension near a constant hematogenic source.[135] Similarly, glucose and hydrogen peroxide concentrations within the bulk remain constant for all *t*. No enzyme is present in the bulk.

2. At time *t* = 0, the concentrations of glucose and oxygen are equivalent to those in the bulk for all *r*. Additionally, the initial enzyme concentration is 1 mM and there is no hydrogen peroxide for all *r* at time *t* = 0.

3. Glucose, oxygen, hydrogen peroxide, and enzyme concentrations remain constant for all *t* at *r* = r2.

4. There is no component flux at *r* = 0 for all *t*.

The mathematic description of these conditions is summarized in the following table.

Table 2. Initial and boundary conditions for sensor model.

$G(r,0) = G(\text{bulk})$ $O_2(r,0) = 90\ \mu\text{M}$ $H_2O_2(r,0) = 0\ \text{mM}$ $E_T(r,0) = 1\ \text{mM}$	Initial Conditions
$G(r2,t) = G(\text{bulk})$ $O_2(r2,t) = 90\ \mu\text{M}$ $H_2O_2(r2,t) = 0\ \text{mM}$ $E_T(r2,t) = 0\ \text{mM}$	Boundary Conditions
$\dfrac{\partial}{\partial t}G(0,t) = 0$ $\dfrac{\partial}{\partial t}O_2(0,t) = 0$ $\dfrac{\partial}{\partial t}H_2O_2(0,t) = 0$ $\dfrac{\partial}{\partial t}E_T(0,t) = 0$	

5.2.4 Simulations

The model described herein predicts the effect of enzyme inactivation on long-term sensor function and determine if alterations in physical parameters could enhance sensor longevity. In a typical simulation, a step increase in glucose concentration is generated at time $t = 0$, and the temporal and spatial distribution of reaction substrates (namely glucose and oxygen) and active enzyme components within the sensor are tracked. It should be noted that the initial conditions assume that the glucose and oxygen levels within the sensor are equilibrated with bulk levels, such that at time $t = 0$, the enzyme is activated and substrate consumption is initiated. This condition allows the

time required for the sensor to operate in steady-state (i.e. a balance between substrate consumption and replenishment within the sensor) to be determined. After the achievement of steady-state operation, the true average oxygen levels within the sensor can then be used to indirectly monitor bulk glucose levels. To determine the true average oxygen concentration, $\overline{O_2}$, within the sphere, a weighting operation is performed on the oxygen concentration calculated at each r, as previously described.[41]

$$\overline{O_2} = \sum_{r=0}^{r1} \frac{[O_2]_r \cdot V_{shell}}{V_{sphere}},$$

where the parameters $[O_2]$, V_{shell}, and V_{sphere}, represent the oxygen concentration at r, the shell volume with boundaries r and $r + \Delta r$, and the total volume of the sphere at $r = r1$, respectively. It should be noted that this operation is necessary to obtain the true average oxygen concentration within the sphere, since at greater r (i.e., r approaches r1) the shell volume is larger and thus contains more oxygen indicator molecules, which inherently contributes more to the overall fluorescence signal.

In these simulations, the effects of enzyme inactivation due to spontaneous inactivation, hydrogen peroxide poisoning, and the combined effects of both on sensor function (i.e. sensitivity) over time were characterized. The effect of enzyme inactivation on sensor function was characterized through analysis of predicted device sensitivity over time, which was defined as the average slope of $\overline{O_2}$ versus bulk glucose concentration at each time t. Table 3 contains the model input parameters, which were experimentally determined or obtained in previous work describing glucose oxidase, mesoporous silica, and polyelectrolyte multilayers.[41, 144, 170, 179, 180, 186] It should be noted that the diffusivities for hydrogen peroxide through algilica ($0 < r < r1$) and the polyelectrolyte nanofilms (r1

$< r <$ r2) were estimated, as values were unreported in the literature. These values were estimated by comparing previously published diffusivities for glucose and peroxide.[194] Additionally, glucose and oxygen diffusivities for algilica were assumed to be equal to those of mesoporous silica, an assumption requiring additional experimental work to validate.

Table 3. Input parameter values used in simulations.

Parameter	Value (unit)
k_1	10^5 (M^{-1} · sec^{-1})
k_{-1}	3×10^3 (sec^{-1})
k_2	300 (sec^{-1})
k_3	10^6 (M^{-1} · sec^{-1})
k_{-3}	150 (sec^{-1})
k_4	50 (sec^{-1})
K^0	9.2×10^{-8} (sec^{-1})
K^1	6.8×10^{-5} (M^{-1} · sec^{-1})
K^2	1.97×10^{-2} (M^{-1} · sec^{-1})
K^3	2×10^{-2} (M^{-1} · sec^{-1})
K^4	7.6×10^{-1} (M^{-1} · sec^{-1})
O_2(bulk)	90 (μM)
G(bulk)	0:2:30 (mM)
$E_T(r,0)$	1 (mM)
$r1$	10 (μm)
t_{film}	32 (nm)
D_{G-S}	2.5×10^{-11} (m^2 · sec^{-1})
D_{O-S}	2×10^{-7} (m^2 · sec^{-1})
D_{H-S}	5×10^{-10} (m^2 · sec^{-1})
D_{G-F}	9.87×10^{-14} (m^2 · sec^{-1})
D_{O-F}	1.15×10^{-10} (m^2 · sec^{-1})
D_{H-F}	4.15×10^{-10} (m^2 · sec^{-1})

Unless otherwise stated, the parameter values given in Table 3 were used in all simulations herein.

5.2.5 Fluorescence Predictions and Experimental Validation

In the previous chapter, the oxygen response of the enzymatic smart tattoos was characterized by exposing the sensors to buffer of various oxygenation levels and recording the corresponding PtOEP/RITC peak ratios, the results of which provided calibration curves (Figure 40 and Figure 41). Using these calibration data, the average oxygen concentration within the sensor, as given in the model output, was converted to predicted fluorescence peak ratio values, allowing direct comparison to experimental data.

Sensors comprising 10 PAH/PSS bilayers were prepared as described in Chapter 4 and used during continuous operation experiments. Characterization of sensor performance under continuous operation was performed with the dynamic testing apparatus (Figure 33), where sensors were exposed to random glucose levels, ranging from 50 mg/dL to 300 mg/dL in 50 mg/dL increments, for approximately 25 min each, with buffer flushing between each glucose step. This process was repeated continuously over a period of 4.5 days, while the sensors were subjected to continuous irradiation. Results obtained were subsequently compared to model output.

5.3 Results and Discussion

5.3.1 Steady-State Response to Step Input of Glucose

Before analyzing the effect of inactivation on sensor performance, it is a useful exercise to consider sensor performance ignoring enzyme inactivation, as these data will serve as a baseline to which additional results are compared. The averages oxygen

concentration with the sensor for different step concentrations in bulk glucose is given in

Figure 76.
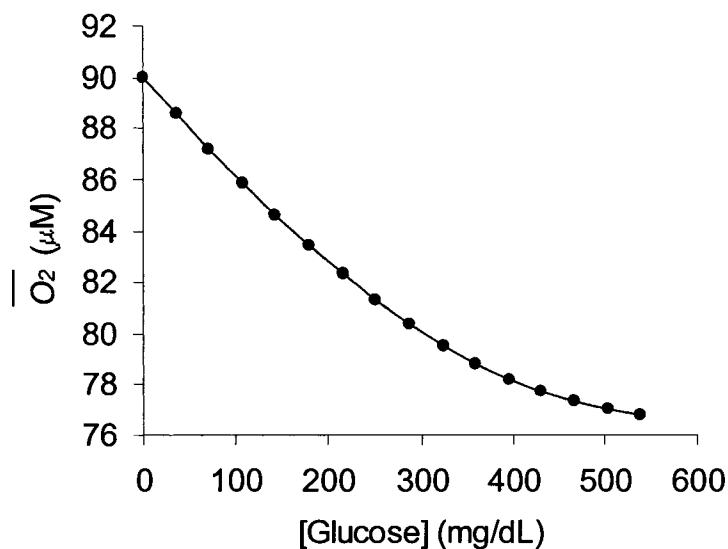
Figure 76. Average steady-state oxygen concentration within the sphere versus step glucose concentration.

From these data, the fundamental operating principles of enzymatic tattoos can be determined by analysis of Figure 76. At glucose concentrations ranging from 0 to 300 mg/dL, steady-state oxygen levels are linearly reduced in response to increasing bulk glucose levels, indicating the sensor is operating in an absolute diffusion-limited regime. A deviation from linearity is observed with increasing bulk glucose levels (300 – 600 mg/dL), resulting from an increased rate of glucose delivery (higher concentration gradient) into the sensor. Given that significant levels of oxygen remain within the sensor, this deviation from linearity may be attributed to the onset of reaction-limited consumption as opposed to the onset of oxygen-limited consumption.

A particularly useful activity afforded by model output is to convert internal average steady-state oxygen levels into ratiometric values using experimentally determined calibration data. Given the experimental data presented in the previous chapter, the predicted ratiometric values can be simply converted into the expected percent change of the PtOEP/RITC peak ratio and plotted against bulk glucose levels Figure 77.
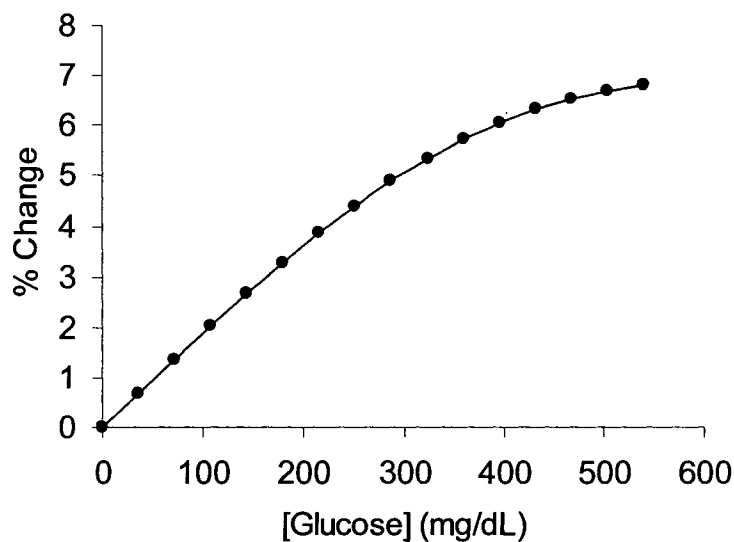
Figure 77. Predicted percent change in PtOEP/RITC peak ratio for different bulk glucose levels.

These data can then be directly compared to experimental results presented in Figure 46, yielding the following plot.
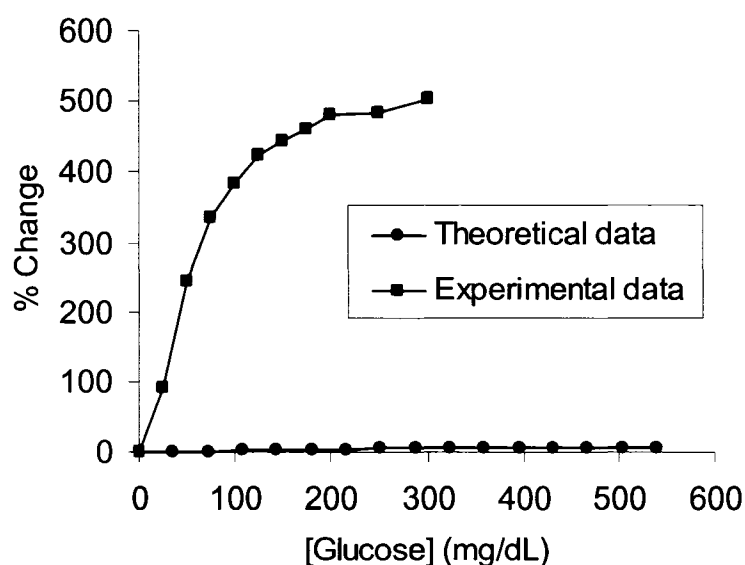
Figure 78. Comparison of model output to experimental data.

From the data presented in Figure 78 it is apparent that the sensor model grossly underestimate actual response characteristics, as the percent change at 300 mg/dL is predicted to be approximately 5, while experimental observations show approximately 500. Given that excellent agreement between theoretical predictions and experimental outcomes were achieved using a similar model, it is logical to contemplate the discrepancy observed in Figure 78.[41] In previous unpublished work, it was shown that the diffusivities of glucose and oxygen through the sensor immobilization matrix can greatly affect the predicted response properties of the sensor.[133] Such an insight is indeed expected, and indicates the importance of knowing the substrate diffusivities through all sensor components to produce a more accurate model. Nonetheless, the substrate diffusivities through algilica were estimated to be equivalent to those of mesoporous silica, but given that algilica is a unique material containing hydrophilic and hydrophobic domains, known substrate diffusivities through more hydrophilic media were used as input parameters and compared with experimental data:
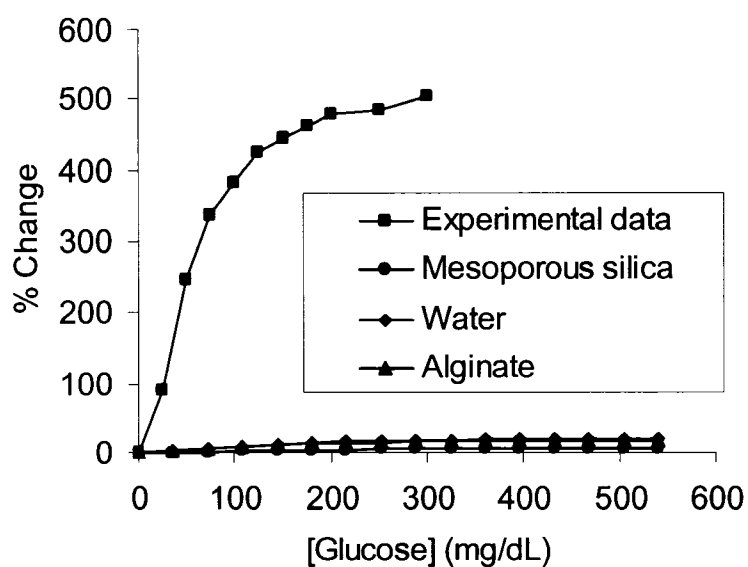
Figure 79. Comparison of theoretical and experimental results assuming sphere diffusivities of several materials.

The data presented in Figure 79 indicate that by changing the substrate diffusivities from those of mesoporous silica to alginate ($D_{G-S} = 4 \times 10^{-10}$ and $D_{O-S} = 2.45 \times 10^{-9}$ $m^2 \cdot sec^{-1}$) and water ($D_{G-S} = 6.9 \times 10^{-10}$ and $D_{O-S} = 2 \times 10^{-9}$ $m^2 \cdot sec^{-1}$), little improvement in theoretical-experimental agreement is observed. An effort was made to "fit" algilica substrate diffusivities to experimental data in an attempt to extract reasonable values that produced better agreement (Figure 80).
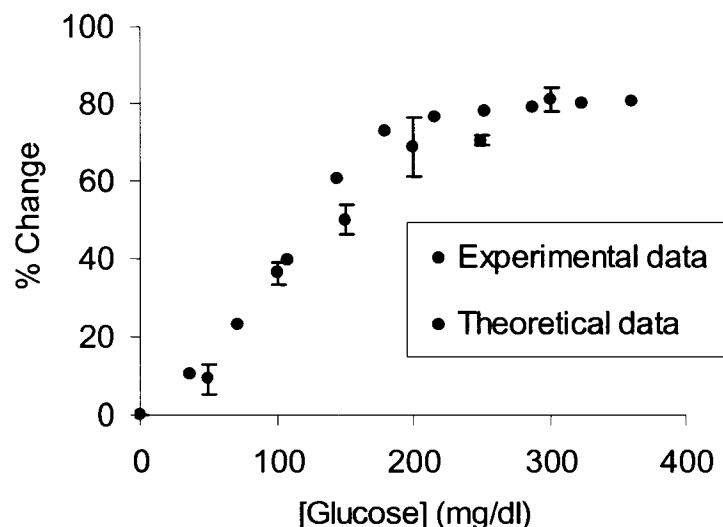
Figure 80. Comparison of model agreement to experimental data using fitted values for substrate diffusivities through algilica.

The glucose and oxygen diffusivities used to obtain these data were 8.81×10^{-13} and 2×10^{-11} m$^2 \cdot$ sec^{-1}, respectively. Although good agreement was observed with this particular experimental data set (Figure 52, 540 μM O$_2$), it is difficult to speculate whether or not these values are reasonable.

Despite the lack of understanding of substrate diffusivities through algilica, it is paramount to restate *that the sensor model only simulates the reaction-diffusion kinetics within a single sensor and assumes constant bulk substrate concentration at the sensors surface.* As multiple sensor are immobilized, as is the case with this work, a higher rate of substrate consumption from the bulk would be expected (more sensors = more consumption); therefore, the substrate concentrations at the sensor surface may be considerably less than those in the bulk. Lower substrate levels at the sensor surface would affect sensor performance by decreasing the average steady stale levels within the sensor, ultimately affecting sensor dynamics, as shown in Figure 54. Of important note is

that if the experimental data are scaled to allow comparison to the theoretical profiles (Figure 81), it is apparent that the theoretical predictions (regardless of the sphere diffusivities) do not represent the experimental profile.
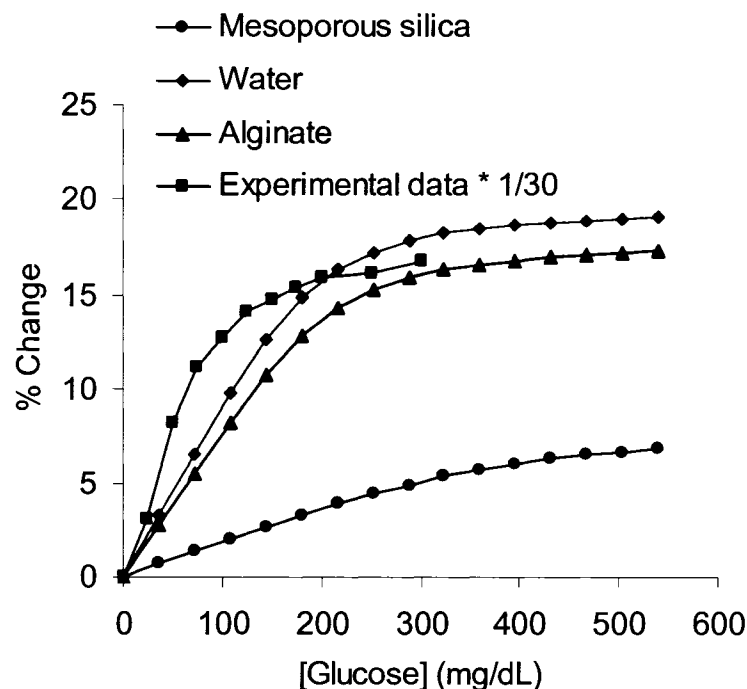
Figure 81. Comparison of experimental (scaled by 1/30) and theoretical response profiles using sphere diffusivities of various media.

Given that the model profiles are reaction-limited, while the experimental profiles are oxygen-limited (as was proven in 4.4.13), it may be inferred that the kinetic constants used as input parameters, which were derived from solution-phase experiments, are significantly lower than those of the immobilized enzyme. A comparison of immobilized and free enzyme kinetics was reported in a recent study, where enzymes immobilized within mesoporous silica exhibited a 2 fold greater activity per mass than those in solution phase.[195] The authors attributed this observation to the increase in structural

support provided by the mesoporous silica matrix. Thus, additional experiments should be performed to examine kinetic parameters of GOx immobilized within algilica substrates, as such may improve the correlation between simulation and experimental data. Moreover, it is hypothesized that an additional and perhaps more considerable reason for the disagreement of the theoretical and experimental results may be due to disregarding the global effects of multiple sensors in the current model. A particularly interesting paper detailing the derivation of a sorption kinetic model used to describe a population of polydispersed particles may be of particular use in expanding "group functionality" to the current model and possibly improve theoretical-experimental agreement.[196]

5.3.2 Effect of Spontaneous Inactivation on Sensor Function

It is a well known phenomenon that over time, enzymes will unfold, resulting in a loss of activity. This phenomenon is sometimes referred to as spontaneous inactivation, time-dependent inactivation, or substrate-independent inactivation and should be considered when utilizing enzyme-based devices for extended periods of time. In order to examine the individual effects of spontaneous inactivation on sensor function, simulations were first executed by assuming K^1, K^2, K^3, and K^4 were equal to zero. Thus, the only inactivation component was K^0, the rate constant for time-dependent inactivation (i.e. independent of reaction substrates). The following surface plots show the spatial distribution of active enzyme components within the sensor exposed to various bulk glucose levels over time.
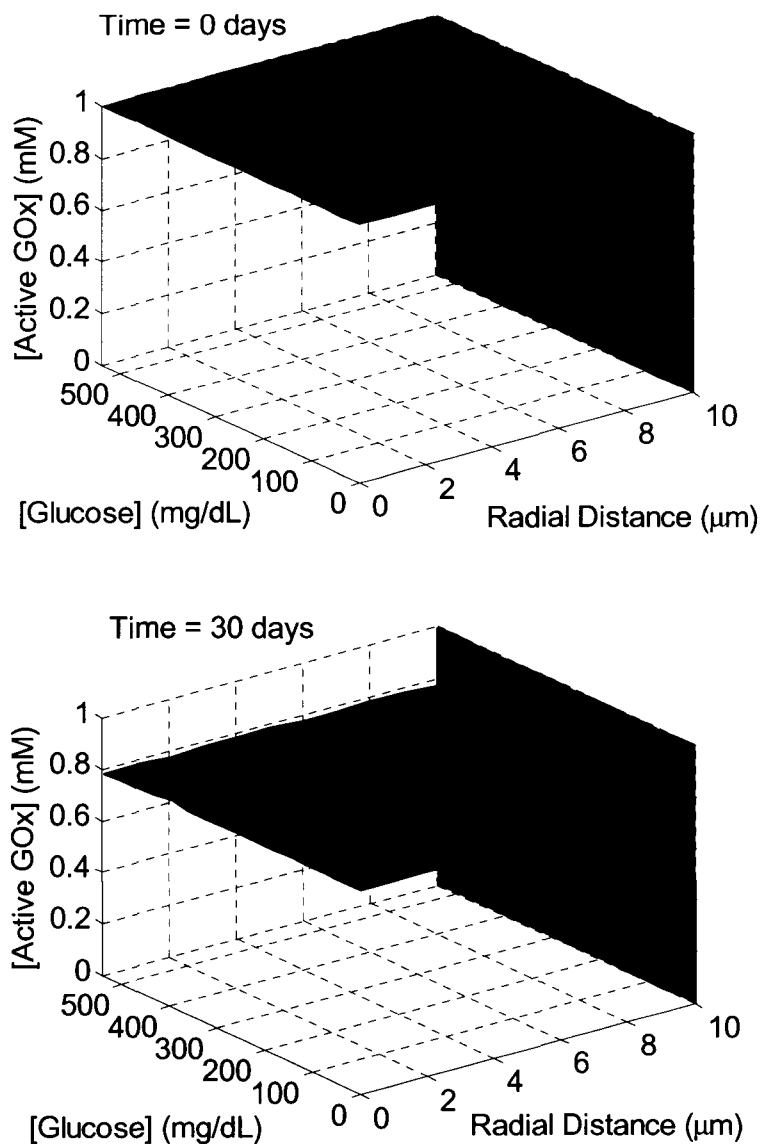
Figure 82. Surface plots depicting the distribution of active GOx as a function of time, space, and bulk glucose concentration. Note the respective figure titles, indicating the time of continuous operation.

From these plots, it is important to note two key features, the first of which is that enzyme inactivation is independent of glucose concentration, as well as location within the sphere. This result is expected, given that spontaneous-inactivation is solely based on operation time. Also, for r1 < r < r2, the active enzyme remains at the initial value of 1

mM. This occurrence is a result of assuming homogeneous enzyme distribution throughout the sensor (0 < r < r2), but assuming *no reaction occurs within the nanofilm layer* (r1 < r < r2). Therefore, enzymes within the nanofilm layer are assumed to be dormant and thus have no consequence on substrate concentrations within the sensor or on calculation determining the average active enzyme concentration within the sensor (0 < r < r1). The average active enzyme concentration, $\overline{E_T}$, was calculated through a weighting operation similar in form to that used to determine the average oxygen concentration within the sphere and plotted against time (Figure 83).
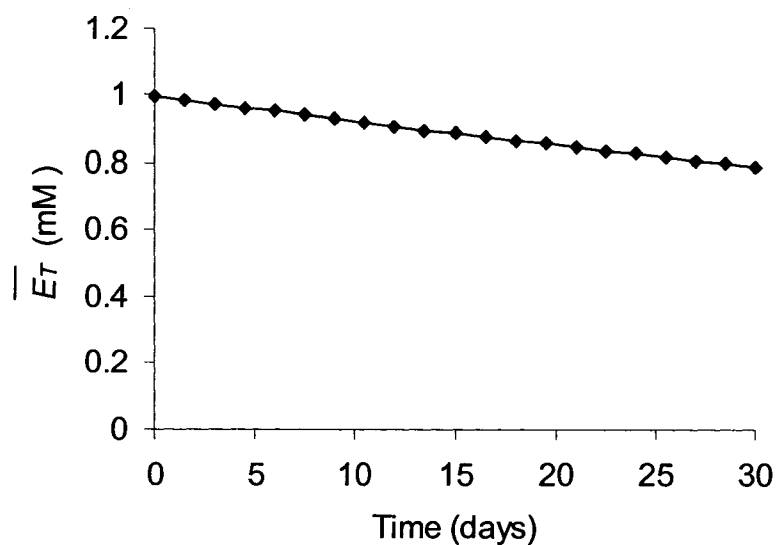
Figure 83. Average active enzyme concentration within the sphere versus operational time.

From these data, it is shown that over 30 days of continuous operation, 21% of the initial enzyme population within the sensor is deactivated. The following figure shows the effect of spontaneous inactivation on sensor performance.
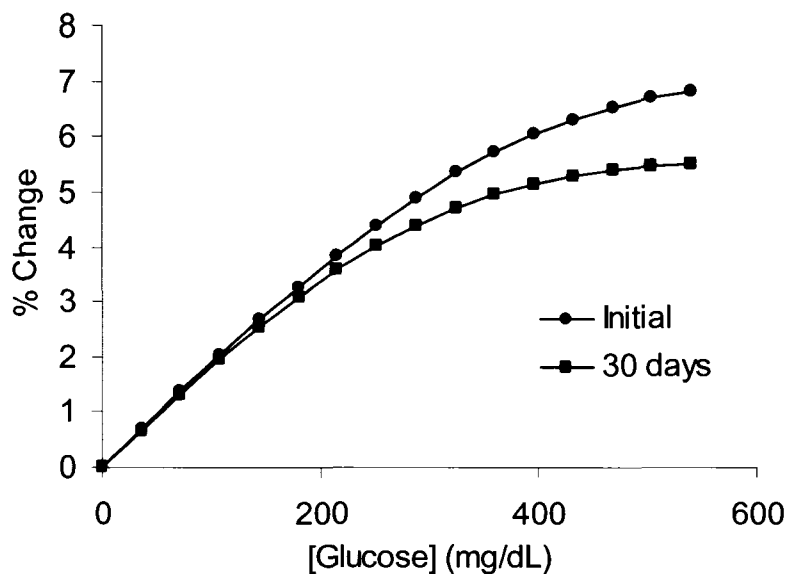
Figure 84. Predicted effect of spontaneous inactivation on sensor steady-state behavior after 30 days of continuous operation.

From these data, it is important to note that as the active enzyme concentration decreases over time, the steady-state oxygen levels for a given bulk glucose concentration are increased, as a result of decreased consumption of substrates within the sphere. This event ultimately leads to decreased device sensitivity, as shown in Figure 84. A perhaps more pertinent exercise would be to examine the change in overall sensitivity over the operational period.
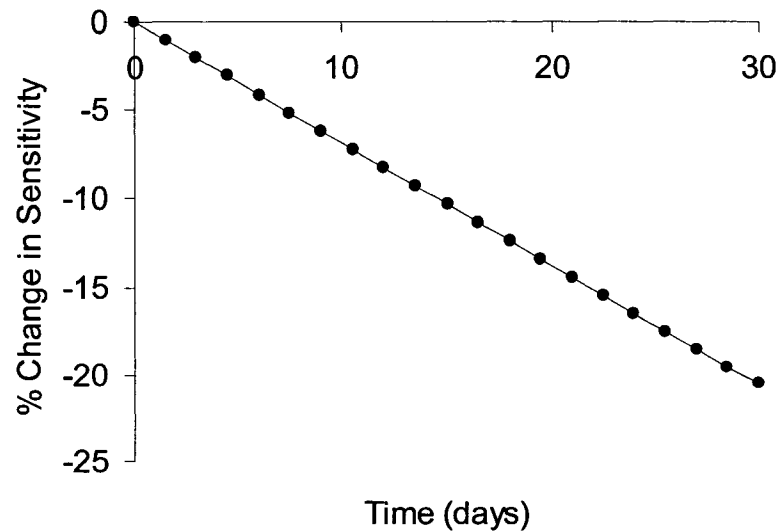
Figure 85. Predicted percent change in device sensitivity over time arising from spontaneous inactivation.

Before data analysis, it is important to note that the *overall sensitivity* is defined as the average slope of the *entire response*, thereby allowing the overall decrease in maximum percent change to be accounted for. These data indicate a near-linear decrease in sensitivity over the operational time period. A useful exercise would be to compare the predicted change in sensitivity to that which was experimentally determined (Figure 51). It is important to note that the data presented in Figure 51 were obtained by testing device sensitivity over storage time (i.e., no contact with substrates). To directly compare these data, it is important that the calculations used to determine sensitivity are equivalent. In the previous chapter, sensitivity was defined as the slope of the linear operation range, whereas in this chapter, the overall sensitivity is defined as the slope of the entire response. Using the sensitivity (not overall sensitivity) calculation, the loss in sensitivity over a 21 day period was determined to be 3%. When comparing this value to the change in sensitivity experimentally observed (44 ± 27%), it is difficult to determine

if the experimental data and the theoretical predictions agree, given fluctuations in the experimental data due to sample variations. Nonetheless, the experimental and theoretical data indicate that sensor function is not completely compromised by spontaneous inactivation (over a 30 day operational period), such that periodic calibrations could potentially be used to account for sensitivity drift.

5.3.3 Effect of Combined Inactivation on Sensor Function

Of more practical importance is the combined effect of enzyme inactivation resulting from hydrogen peroxide poisoning and spontaneous inactivation on the operational stability of the sensor.[179] In these simulations, input parameters given in Table 3 were used, and the resulting spatial and temporal substrate profiles used for analysis. The following surface plot depicts the active enzyme profile at a function of radial distance and step glucose concentration. It is important to note that this profile was obtained after only 24 hours of operation.
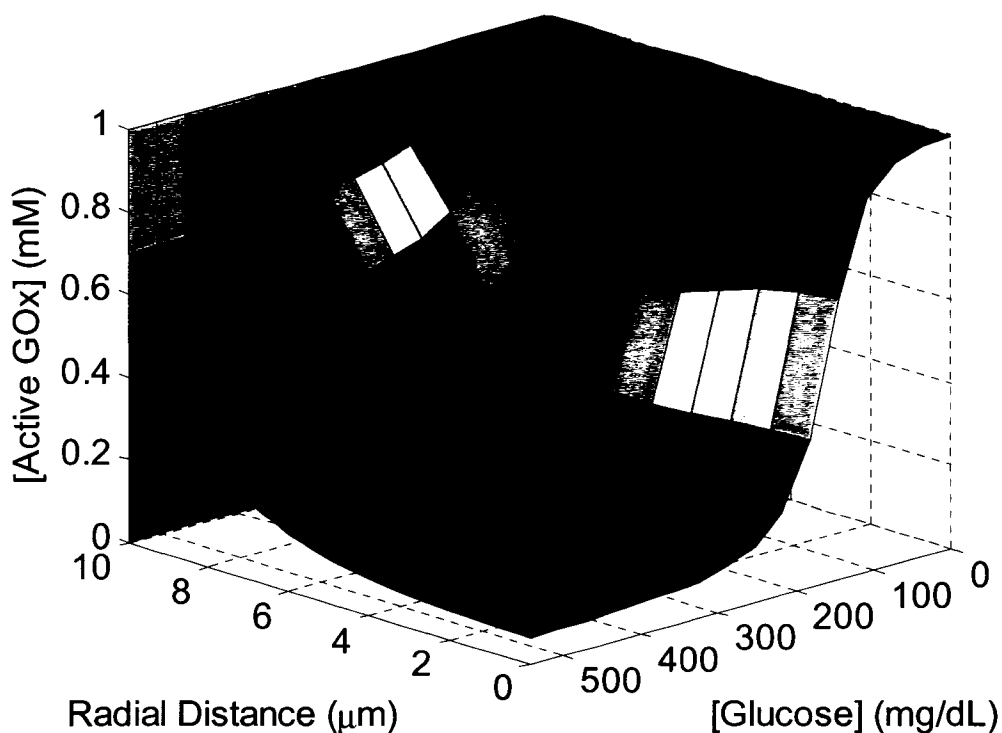
Figure 86. Distribution of active GOx as a function of space and bulk glucose concentration after 24 hours of operation.

Although it is quite obvious, it is important to highlight that enzyme inactivation due to peroxide poisoning is much more dominant than spontaneous inactivation (Figure 82, $t = 30$ days). Therefore, the combined inactivation effects on sensor function were investigated simultaneously. The first point of note is that the distribution of active enzyme is a function of time, space, and substrate concentration, as expected. Of more importance is that for bulk glucose concentrations greater than 100mg/dL, the vast majority (> 85 %) of enzyme molecules within 8 μm of the origin are denatured. This distribution profile is a result of hydrogen peroxide buildup within the center of the sphere, hastening the inactivation of enzyme located within that region. Additionally, while peroxide production is highest near the sphere-nanofilm interface (where substrates

first contact active enzyme), less inactivation is observed due to peroxide diffusion from the sensor into the bulk. This behavior was observed in previous work, and may be experimentally validated using a similar procedure reported by Stein et al.[179, 197] It is also important to note that at bulk glucose levels less than 100 mg/dL, this effect is not observed. In these cases, the bulk concentration of glucose is such that glucose consumption occurs outside the sphere origin, resulting in peroxide buildup within the region of 6 μm < r < 8 μm and the observed active enzyme "trough." The active enzyme concentration at the surface remains the highest due to peroxide diffusion into the bulk, as does for all bulk glucose levels (except 0 mg/dL).

Given that these sensors rely on enzymatic consumption of glucose and oxygen to indirectly monitor bulk glucose levels, it is important to know the *active* enzyme concentration within the sensor for a given time. The following plot shows the average active enzyme concentration, $\overline{E_T}$, within the sensor versus time for a given bulk glucose concentration.
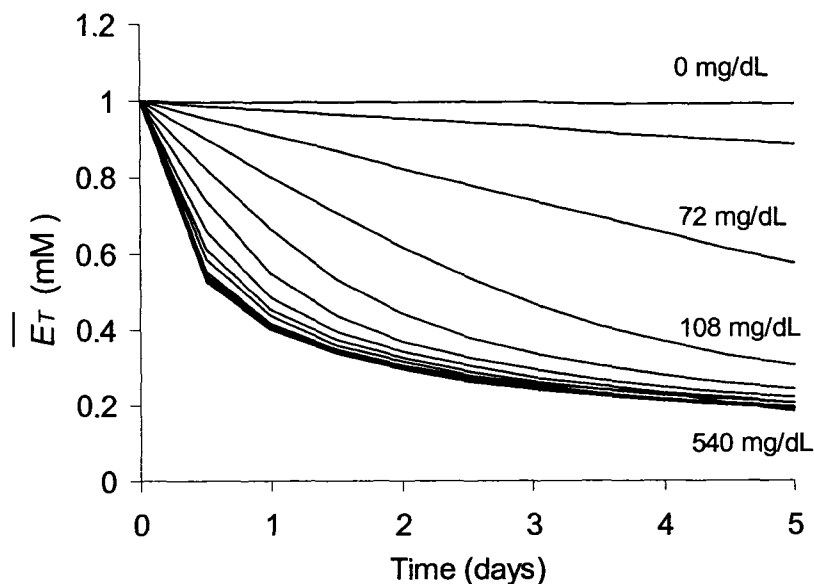
Figure 87. Average active enzyme concentration within the sphere with respect to time and bulk glucose level.

The first point of note is that enzyme inactivation occurring at 0 mg/dL bulk glucose is due to spontaneous inactivation. Of more importance, this plot indicates quite dire results, such that for normoglycemic levels (glucose levels in between 70 and 180 mg/dL) at least 40% of the initial enzyme concentration is rendered inactive after only 5 days of operation. It is also important to note that after 5 days of continuous exposure to hyperglycemic conditions (> 180 mg/dL), approximately 80% of immobilized enzymes are rendered inactive. It is indeed quite obvious that this level of inactivation would have a tremendous effect on the glucose dependent reduction of steady-state oxygen levels within the sensors, as observed in Figure 88.
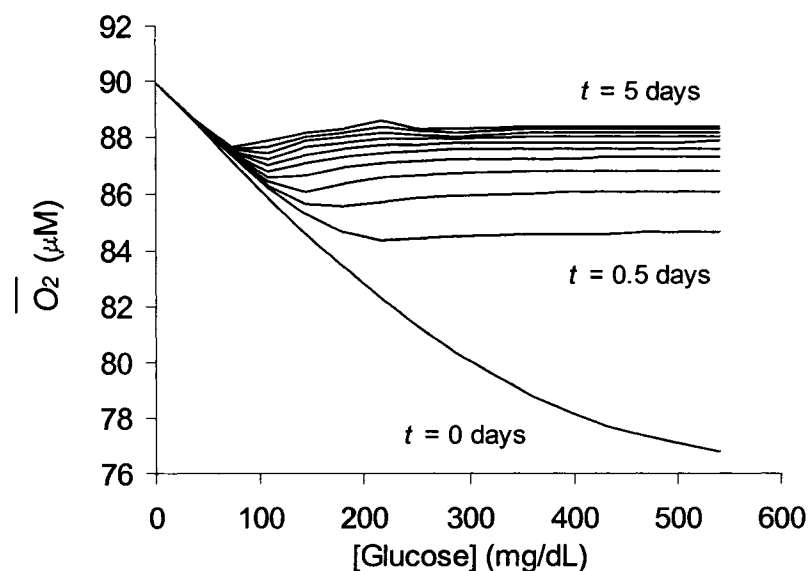
Figure 88. Effect of inactivation of the average steady-state oxygen levels within the sensor for a given bulk glucose concentration.

Before analysis, it is important to state that the time increments given in Figure 88 represent the total time at which the sensor was exposed to *each* bulk glucose level. The first point of note is that following 12 hours of operation, as a result of enzyme inactivation, the sensors ability to reduce the average local oxygen levels in response to increasing bulk glucose levels is severely compromised. It is important to highlight that at bulk glucose concentrations below 100 mg/dL (for all t), that the reduction in $\overline{O_2}$ is comparable to the initial response. With low bulk glucose levels, the drop in $\overline{O_2}$ is expected to be low relative to those expected with increasing glucose levels. Therefore, even though a significant amount of enzyme is inactivated over 5 days of continuous operation, the remaining enzyme population is capable of supplying the necessary catalytic requirements, such that a response comparable to that of the initial is obtained (i.e. the response remains glucose-limited). As more enzyme is deactivated through

exposure of higher bulk glucose levels, the rate of change in $\overline{O_2}$ versus bulk glucose levels begins to decrease, as shown from 100 – 200 mg/dL (t = 0.5). Eventually, the enzyme inactivation is such that no change in $\overline{O_2}$ is observed for a given range of bulk glucose (225 – 250 mg/dL, t = 0.5). More seriously, for elevated ranges of glucose (> 250 mg/dL, t = 0.5), inactivation is so severe that it results in an *increase* in $\overline{O_2}$. As the operational time is increased, this effect is compounded, such that the glucose level at which increases in $\overline{O_2}$ are observed begins to occur at progressively lower bulk glucose levels (due to progressive enzyme inactivation), until $\overline{O_2}$ approaches that of the bulk (90 μM).

Using the data presented in Figure 88, the predicted percent change in spectral peak ratio was determined (Figure 89).
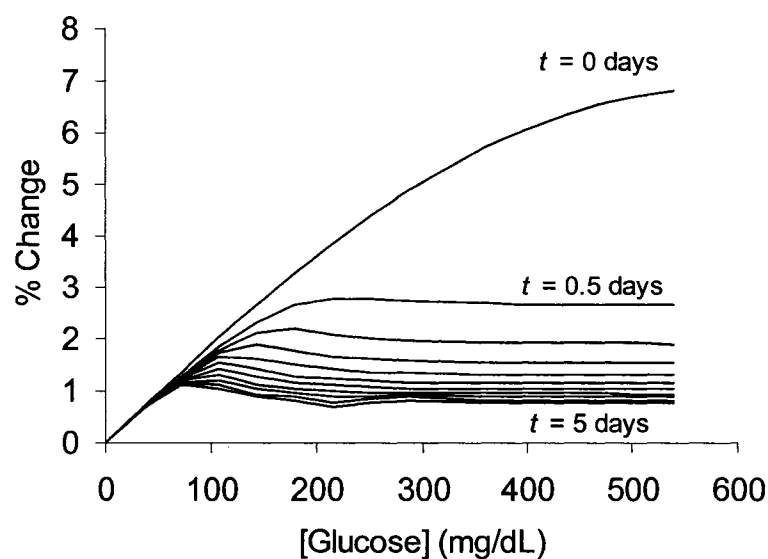
Figure 89. Predicted effect of inactivation on the percent change in PtOEP/RITC peak ratio.

Similar to the data presented in Figure 88, it is important to note that a decrease in active enzyme concentration results in increased $\overline{O_2}$ levels, ultimately eliciting decreased percent changes in PtOEP/RITC peak ratios with respect to increasing glucose concentration and time of operation (Figure 89). Although it is quite obvious that after 12 hours of operation, the overall device sensitivity has been severely reduced, it is important to quantify the percent change in sensitivity over time.
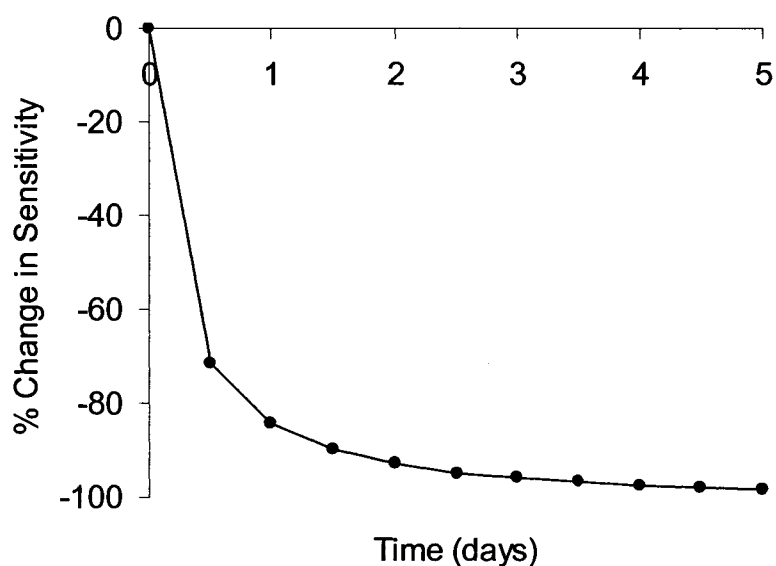
Figure 90. Predicted loss of overall device sensitivity resulting from enzyme inactivation.

Figure 90 indicates that after 12 hours of continuous operation, the sensitivity of the devices is decreased by 75%. After two days, the loss of sensitivity approaches 90%, until day 5, when a loss of 98 % sensitivity arising from enzyme inactivation is observed. Clearly, these data indicate that the current design would be unacceptable for long-term use. It is also important to note that these simulations do not include inflammatory

responses such as biodegradation and bioremediation, which may cause additional sensitivity losses. However, it is important to state that the inactivation rate constants used were derived from experiments in which enzyme-doped membranes were prepared via glutaraldehyde crosslinking within a collagen membrane.[193] There are some significant differences between this enzyme-doped membrane and the mesoporous silicate microstructures used in the current work, most notably the rigid structure of the algilica particles, which could provide structural support to the enzyme such that the rate of spontaneous denaturing (i.e., unfolding) and denaturing due to byproduct poisoning is reduced.[181] In a report on the stabilization of creatine kinease within a sol-gel matrix, it was found that the enzyme retained 50% activity 10 times longer than that of free enzyme, attributing the decreased inactivation to the rigid structural support of the matix.[182] Therefore, it is plausible that the inactivation rate constants for algilica may be *lower* that than the input parameters used, resulting in a theoretical overestimation of the inactivation effect. Additionally, it is important to reiterate that the hydrogen peroxide diffusivities through the nanofilms, as well as algilica, were estimates. Therefore, it is possible that actual values may differ. Should the actual diffusivities be greater, then peroxide diffusion from the sensor into the bulk would be more *rapid*, indicating that the model would exaggerate inactivation effects. On the other hand, if actual diffusivities are lower that those used in the simulation, then hydrogen peroxide diffusion from the sensor into the bulk would be retarded, thus increasing the onset of inactivation and indicating *underestimation* of inactivation effects by the model. Therefore, further experimental work to extract hydrogen peroxide diffusivities through algilica and polyelectrolyte nanofilms, as well as investigate enzyme inactivation kinetics within algilica supports,

could provide more accurate model input parameters, which in turn may increase the correlation between experimental and theoretical results.

5.3.4 Experimental Validation

In the previously described simulation, influence of enzyme inactivation on device sensitivity over time was demonstrated, the results of which indicated that after 12 hours of continuous operation, approximately 75% of initial sensitivity was loss. In order to determine whether or not the simulation output could adequately describe experimental observations, sensors were exposed to bulk glucose fluctuations for a period of approximately 4.5 days, while simultaneously collecting real-time ratiometric data. The data obtained are presented in Figure 91.
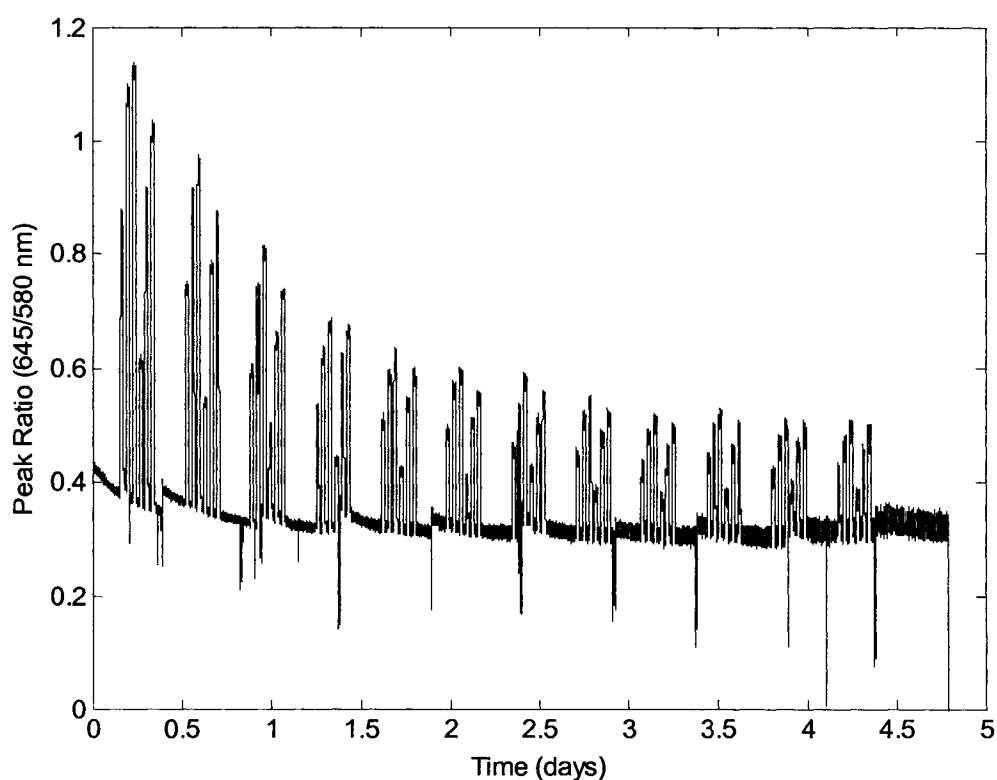
Figure 91. Glucose response under continuous operation.

It is important to state that there is a progressive increase in noise throughout the experiment and is a direct result of incremental detachment of the adhesive anchoring the sensors to the slide surface, such that the collected intensities were decreased but the peak ratio remained unchanged. Also, the sensors were exposed to the same array of glucose concentrations for 12 times over the course of this experiment, with each glucose step totaling 25 minutes in duration. Given that continuous operation is the total time at which the sensors were exposed to a particular step concentration, it can be said that over the course of this experiment, sensors were continuously exposed to step changes in bulk glucose levels for a total of 5 hours (25 min/step * 12 steps) per concentration. For reference, throughout the experiments detained in the previous chapter, sensors were exposed to random triplicate glucose steps for 7 min, totaling 21 minutes of continuous operation per glucose concentration.

Using the 12 repose profiles obtained over 4.5 days (Figure 91), the respective sensitivities were determined.
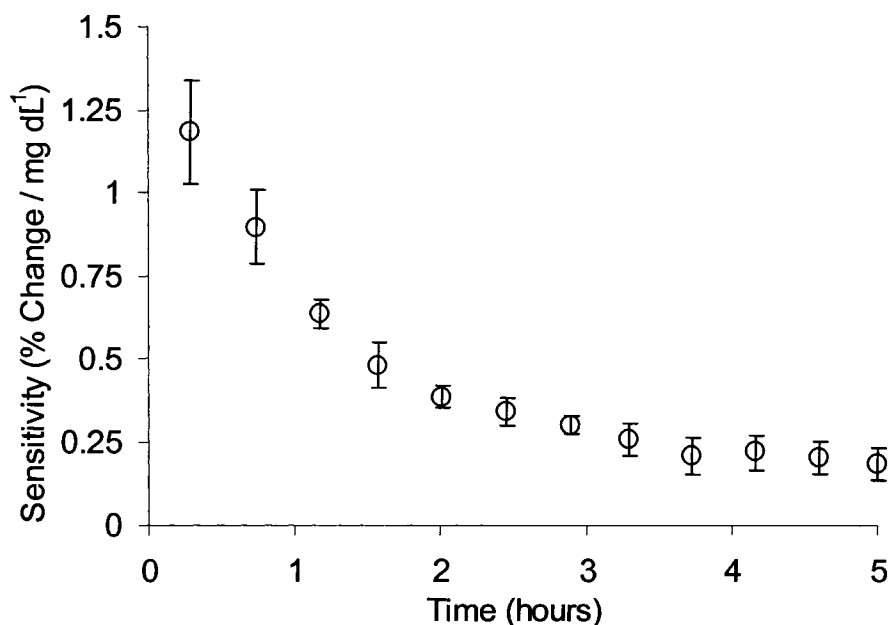
Figure 92. Experimentally determined loss of device sensitivity versus time of continuous operation.

These data indicate that approximately 80% of device sensitivity is lost over 5 hours of continuous operation. It is indeed intuitive to question the source of this sensitivity loss. Earlier it was shown that enzyme and indicator immobilization was stable over time (Figure 37 and Figure 38), and from the data presented in Figure 92, it is apparent that a baseline shift is not responsible. Therefore, it is assumed that enzyme inactivation mainly contributes to the observed decline in device sensitivity. A particularly useful exercise would be to compare these experimental data with those produced by the sensor model. Using the values given in Table 3, the following substitutions were made: $E_T = 720$ μM , O_2(bulk) = 277 μM, and $t_{film} = 40$ nm; the percent change in sensitivity was determined and directly compared with experimental results. It is important to note that E_T was experimentally determined using the Lowery method, as described in Chapter 4.
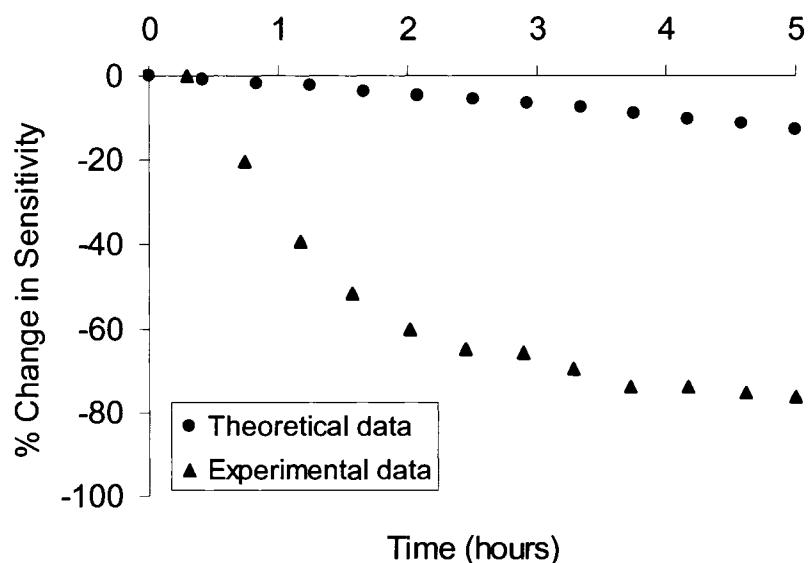
Figure 93. Experimental-theoretical comparison of inactivation induced changes in device sensitivity.

Upon comparison of experimentally and theoretically obtained data, it is quite obvious that significant disagreement is observed. Interestingly, the theoretical data underestimates the inactivation effect, such that after 5 hours of continuous operation, 10% of sensitivity is lost, while the experimental data indicate an 80% loss in sensitivity. It is hypothesized that this discrepancy arises from the boundary conditions used in the model, which state that peroxide concentration at the sensor-bulk interface remains at 0 μM. In experimental conditions, this condition is not expected to hold, despite testing in a flow chamber where the bulk solution is continuously replaced. As the sensor population is exposed to glucose, hydrogen peroxide is produced and diffuses into the bulk, which may result in an increase in hydrogen peroxide concentration at neighboring sensor surfaces, thereby reducing the concentration gradient of hydrogen peroxide from the sensor into the bulk. This event would ultimately result in elevated hydrogen

peroxide levels within the sensors, thus yielding increased inactivation of the enzymes and ultimately causing the sensors to lose sensitivity more rapidly than predicted. This provides yet another example for the need of a model that accounts for the contributions of a sensor population on response properties. Nonetheless, regardless of theoretical-experimental disagreement, it is important to reemphasize that 80% of device sensitivity was observed after only 5 hours of continuous operation, a considerable discouragement for devices which would ideally exhibit sustained sensitivity for at least 6 months. To accentuate how this loss of sensitivity would impact change in device accuracy over the continuous operation period, an accuracy profile using the initial response profile as the calibration standard and the final response profile as the unknown was constructed (Figure 94).
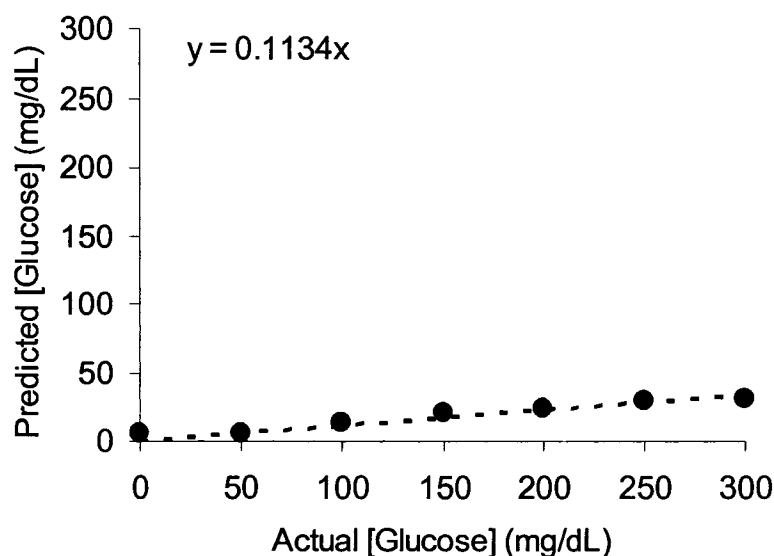
Figure 94. Accuracy profile of sensors after 5 hours of continuous operation.

It is somewhat difficult to use these data in a practical example given that a patient would be expected to be in a hyperglycemia-induced coma with blood glucose

levels below 30 mg/dL,[198] but it is important to note that the loss of sensitivity shown in Figure 92 would result in a 90% decrease in accuracy, such that the sensor readout would grossly underestimate true glucose levels. Additionally, it is common to evaluate the significance of clinical device inaccuracies using error grid analysis (EGA).[54, 199] EGA assigns clinical outcomes arising from device accuracies by defining regions on a plot similar to Figure 94. Using the data presented in Figure 94, EGA indicates that clinical action resulting from device inaccuracies could have "significant and/or dangerous medical consequences."[199] Hence, it is quite obvious that the *current sensing scheme would be overlooked for use in long-term diabetic monitoring situations*.

Therefore, a significant change in the sensor design is indeed warranted. It is hypothesized that increasing the immobilized enzyme concentration would increase response stability over time, albeit at a cost of initial sensitivity. It is expected that a drastic increase in enzyme concentration (> 10x's) would cause an initial decrease in sensitivity, due to rapid substrate consumption near the sensor-bulk interface, resulting in a lower $\overline{O_2}$ per bulk glucose level and extended linear range. However, this parameter is indeed experimentally limited, such that once the sensor matrix is saturated with enzymes, it is difficult to achieve concentrations above the saturation point while maintaining stability. Also, the sensor radius could be altered, but it is important to note that great effort was focused into developing a protocol to produce monodispersed algilica particles of radii greater than 20 μm, but little success was made. Nevertheless, increasing the sphere radius would allow a greater magnitude of enzymes to be entrapped, which should retard the inactivation effect, while increasing initial sensitivity (increased volume over which $\overline{O_2}$ can be reduced). Additionally, the nanofilm thickness

could be increased, which would decrease the glucose flux (relative to oxygen) for entering the catalytic region of the sensor for a given bulk glucose concentration. This would undoubtedly decrease the initial sensitivity, but may increase response stability over time. Although these modifications may reduce the complications of enzyme inactivation, the problem source (hydrogen peroxide) is not directly addressed, making these proposed modifications more of a "patch" to slow down inactivation. Therefore, a means to eliminate hydrogen peroxide would be ideal in *directly* combating the effects of enzyme inactivation.

5.3.5 Incorporation of Catalase into Enzymatic Smart Tattoos

The enzyme catalase has been used in previous work to consume hydrogen peroxide and increase the longevity of glucose oxidase.[193] More specifically, catalase (Cat) consumes hydrogen peroxide and produces water and oxygen as byproducts as indicated in the following reaction:

$$H_2O_2 \xrightarrow{Cat} \frac{1}{2}O_2 + H_2O$$
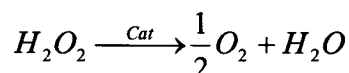
When coupled with GOx catalyzed consumption of glucose and oxygen, the overall reaction scheme may be written as:

$$glucose + \frac{1}{2}O_2 \xrightarrow{GOx/Cat} gluconic\ acid$$
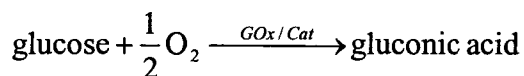
Therefore, incorporation of catalase into the sensing scheme of the devices presented in this work could reduce the effects of peroxide inactivation by the decreasing the hydrogen peroxide concentration within the sensor, as well as reducing the onset of oxygen-limited operation, thereby extending the glucose-limited range.

To test this hypothesis, catalase and glucose oxidase were simultaneously loaded into PtOEP-doped algilica particles using a solution of 0.05 M sodium acetate (pH = 4.0) comprising a 2 : 1 mass concentration ratio of GOx to Cat, such that the total concentrations of GOx and Cat were 23.3 and 11.65 mg/mL, respectively. The enzymes were subsequently crosslinked, followed by the adsorption of fluorescent nanofilms (10 PAH/PSS bilayers in total), as detailed in the previous chapter.

In order to determine if the simultaneous loading of both enzymes was possible, fluorescent variants were prepared (FITC-GOx and RITC-Cat) and imaged using confocal microscopy (Figure 95).
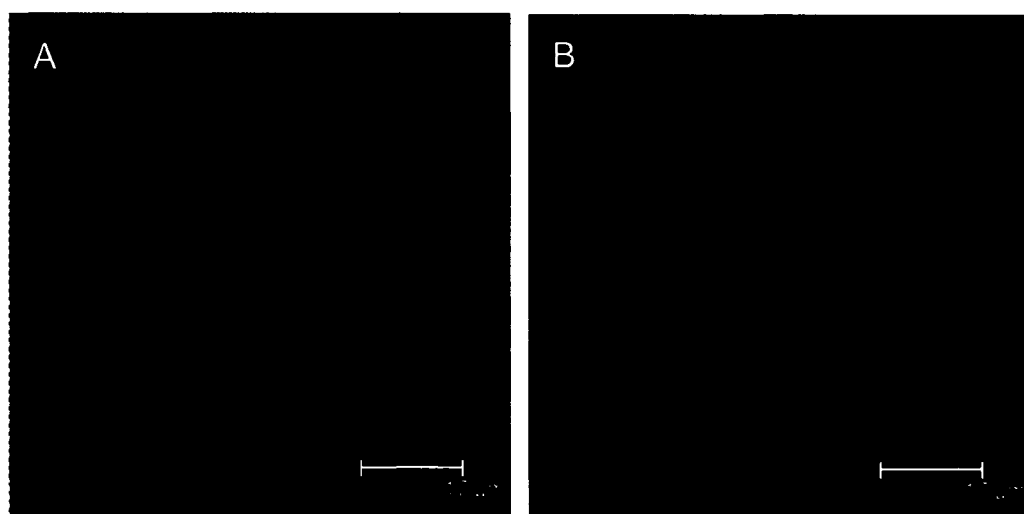
Figure 95. Confocal micrographs depicting the distribution of GOx (A) and Cat (B) within algilica particles after simultaneous loading.

From these images, it is important to note that the distribution index of GOx remains approximately 0.9 (as was in Figure 36), indicating near homogenous distribution, while the distribution index of Cat was determined to be approximately 0.7, indicating preferential adsorption to the sphere surface. Further experimentation would

be required to determine the optimum loading conditions, as well as immobilization ratio of both GOx and Cat.

The bienzymatic smart tattoos were exposed to dynamic testing under air-equilibrated conditions and the glucose response profile obtained and compared with the response profile for similar non-catalase containing sensors displayed in Figure 46.
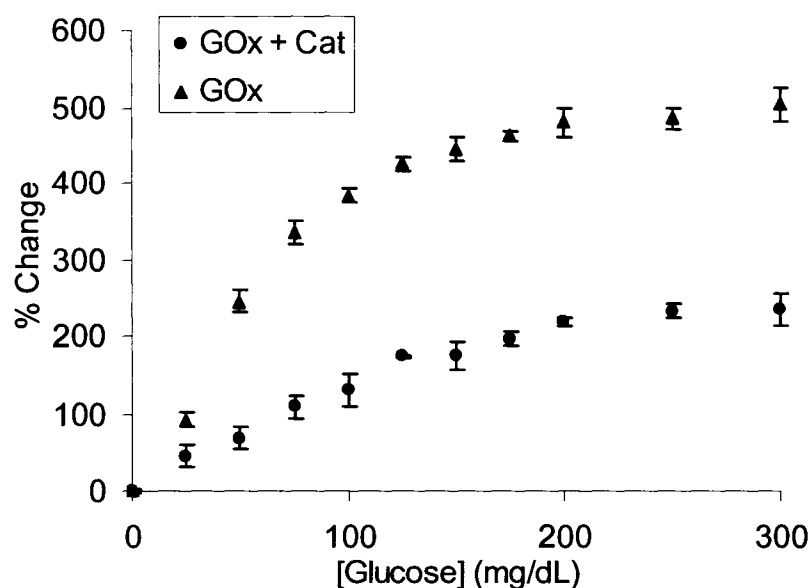
Figure 96. Comparison of glucose response profiles of sensors compromising immobilized GOx and co-immobilized GOx and Cat.

From these data, several important points are of note. The first of which is that sensors comprising co-immobilized GOx and Cat are indeed responsive to changes in bulk glucose concentration. Secondly, the maximum percent change in PtOEP/RITC peak ratio is approximately 500% and 230% for sensors containing immobilized GOx and those containing GOx and a Cat supplement, respectively. It is also important to note that the sensors containing co-immobilized enzymes have a more linear response over the

tested range of glucose concentrations. Using these data, the sensitivities and analytical

ranges for the respective response profiles can be acquired and displayed in the following

table:

Table 4. Comparison of sensitivity and analytical ranges of sensors loaded with GOx and both GOx and Catalase.

Enzyme Components	Sensitivity (% change/ mg dL^{-1})	Analytical Range (mg/dL)
GOx	4.16 ± 0.57	120 ± 10
GOx + Cat	1.15 ± 0.054	225 ± 20

As expected, the sensors containing co-immobilized GOx and Cat are less

sensitive than those containing solely GOx, such that an approximate 3.5 fold reduction

in sensitivity and 2 fold increase in analytical range is observed. This is a direct result of

oxygen production as a byproduct of peroxide breakdown, which causes elevated levels

of oxygen within the catalytic region of the sensor, thereby extending the glucose

sensitive range and reducing the percent change in PtOEP/RITC peak ratio. These results

could also be a product of a reduced concentration of immobilized GOx within the

particle, which would result in the reduced consumption of substrates, but may also result

in a reduced range (early onset of reaction-limited catalysis).

The results presented in Figure 96 are indeed intriguing, but the true efficacy of

co-immobilized Cat in the ability to reduce sensitivity drift due to enzyme inactivation

has yet to be demonstrated. To examine whether or not the incorporation of Cat could

reduce the effects of inactivation, an experiment similar to that used to acquire the data in

Figure 91 was performed, the results of which are presented in Figure 97.
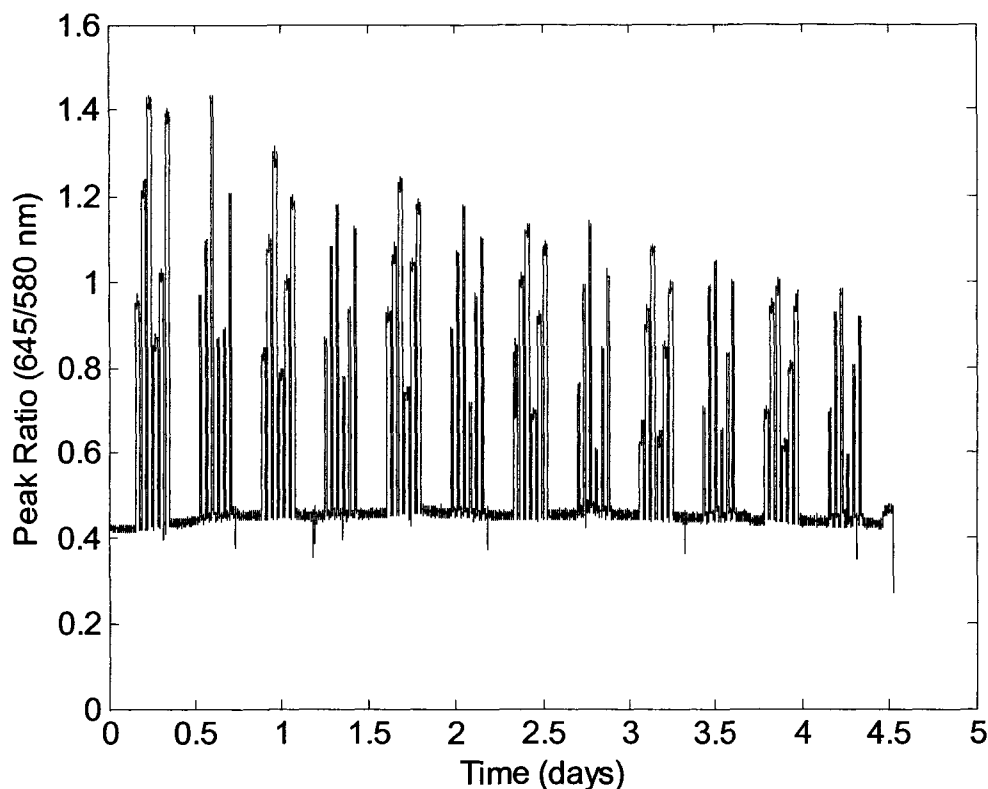
Figure 97. Glucose response under continuous operation conditions of sensors containing co-immobilized GOx and Cat.

From a visual comparison of the data presented in Figure 97 to those of Figure 91, it is apparent that the sensors containing catalase exhibit a decreased loss in sensitivity over time. To quantifiably compare the sensitivity drift over time, the sensitivity of each respective response profile over time was determined and directly compared with the data presented in Figure 92.
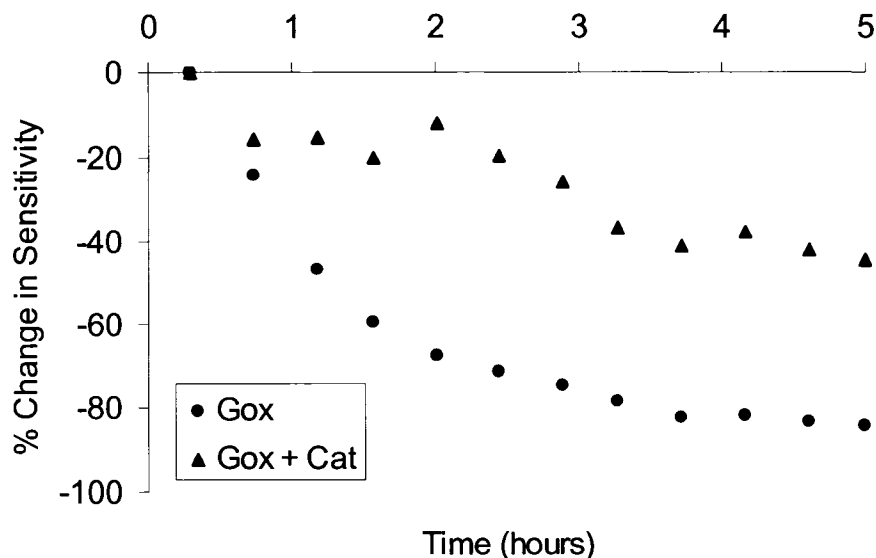
Figure 98. Drift in device sensitivity over time due to enzyme inactivation.

From these data, several important findings are observed, the first of which is that the incorporation of catalase into the sensing scheme does not completely eliminate sensitivity drift. This observation could be a result of several phenomena, such as the non-homogeneous distribution of catalase throughout the sensor (Figure 95). Since catalase is preferentially immobilized toward the surface, excess peroxide buildup within the sensor core, which was shown to be most catastrophic (Figure 86), could inactivate GOx and cause sensitivity drift. Also, it was shown in a previous report that catalase itself can be inactivated by hydrogen peroxide, which would ultimately result in the decreased ability to remove peroxide over time, thus leading to enzyme inactivation.[179] It is also highly likely that the ratio of immobilized GOx to catalase is non-optimized, such that the rate of peroxide produced from glucose oxidation eclipses that of consumption by catalase, resulting in enzyme inactivation and sensitivity drift.[179] Nonetheless, it is important to state that the *incorporation of catalase into the sensing scheme does indeed*

reduce sensitivity drift over time. Additionally, from the data presented in Figure 98, it is important to state that after 5 hours of continuous exposure to glucose approximately 40% of initial sensitivity was lost with GOx and Cat containing sensors, while 80% was lots with sensors containing solely GOx. This result is quite remarkable, as an approximate 2 fold-decrease in sensitivity loss is accomplished by simply co-immobilizing catalase. It is also important note that the rate of sensitivity drift is reduced approximately 3.5 fold as well when co-immobilizing catalase, approximately -47 % / hour with non-Cat containing sensors and approximately -14 % / hour with sensors containing co-immobilized enzyme.

Therefore, the refinement of the co-immobilization of catalase and glucose oxidase, such that both enzymes are homogeneously distributed and the rate of peroxide consumption is greater than the rate of production, is expected to produce sensors with increased longevity that will hopefully be suitable for long-term diabetic monitoring applications.

It is noteworthy to state that an attempt was made to incorporate catalase kinetics into the model, as such would have allowed an additional theoretical-experimental comparison. Moreover, such a model could enhance the design of sensors for use in long-term applications by systematically investigating the effect of physical parameter variations. More important, a model of this type could aid in the determination of an optimum catalase concentration, such that long-term stability as well as sensitivity are optimized, while reducing "trial and error" efforts. The incorporation of catalase into the model requires the addition of three partial differential equations, and since the three individual forms of catalase are susceptible to hydrogen peroxide poisoning, the pseudo

steady-state assumption cannot be made. Thus, the obtainment of a solution would require the simultaneous solution of a series of ten partial differential equations, a feat which was unobtainable given the accessible computation power and solver robustness.

5.4 Conclusion

A mathematical model describing reaction-diffusion-deactivation kinetics has been derived for spherical enzymatic smart tattoo systems and presented in this chapter. In this model, the effect of enzyme inactivation on sensor response properties over a defined operational time can be closely examined. Additionally, the model used experimentally determined calibration data to transform predicted substrate levels into predicted changes in PtOEP/RITC peak ratio, such that a direct comparison with experimental data could be performed. Model output predicted 98% loss of initial sensitivity over 5 days of continuous operation. Upon direct comparison with experimentally determined data, it was found that model output *underestimated* the effect of deactivation. Experimental data showed that after 5 hours of continuous operation, approximately 80% of initial sensitivity was loss, approximately 8-fold more than that predicted from the simulations. Given that these devices would ultimately be used for long-term continuous monitoring scenarios, the current design was deemed unacceptable.

Additional sensors were prepared containing co-immobilized glucose oxidase and catalase, in an attempt to reduce enzyme exposure to hydrogen peroxide and subsequently reduce the effects of enzyme inactivation. Results were indeed promising, at sensors containing catalase showed a marked decrease, approximately 2-fold, in sensitivity loss over time. Although these results are indeed encouraging, additional work is needed to optimize the bi-enzyme immobilization, namely enzyme distribution

and respective enzyme concentrations needed to minimize component interaction with hydrogen peroxide; these results should yield sensors with increased longevity, hopefully more suited for long-term applications. Additionally, significant disagreement between simulation and experimental data were observed, the majority of which was attributed the model only considering a single sensor. Therefore, a more complete understanding on how individual sensors function within a sensor population is desired to aid in the development of more accurate models. Thus, in the following chapter, an imaging technique with the ability to monitor individual sensor function within a population is presented.

CHAPTER 6

REAL-TIME IMAGING OF

SENSOR FUNCTION

6.1 Introduction

In chapter 4, the preparation and characterization of enzymatic smart tattoo concepts under dynamic conditions was demonstrated. The response properties of these sensors have been most notably shown to depend on bulk glucose levels, bulk oxygen levels, nanofilm coating thickness, and sensor concentration, the results of which indicated the importance of understanding how the response of individual sensors within a given population affects the overall response properties. Additionally, in chapter 5 a reaction-diffusion model was introduced that allowed response properties over time to be predicted. Simulation results grossly underestimated those experimentally obtained. It was hypothesized that the inconsideration of population dynamics (the model only simulates a single sensor) dominantly contributed to the observed experimental-theoretical disagreement. Therefore, is it critical to understand the effect of sensor group dynamics (i.e. how do individual sensors function within a population) on overall response properties, as such knowledge would be valuable in the *a priori* design of enzymatic smart tattoos implants. However, little information on sensor group dynamics

223

can be obtained using the device detailed in Figure 33, as this device optically interrogates a fixed volume of sensors and collects the subsequent emission, resulting in an *averaged response* over the illuminated volume. Thus, in order to investigate the dynamics of a sensor population, a device allowing selective analysis of individual sensors within a group is needed. Thereby, this chapter will focus on the development of such a device.

The most important requirement of this device is the ability to examine the behaviors of individual sensors within a population, thus a direct interface with fluorescence imaging instrumentation is required. Additionally, the device should allow dynamic testing of sensor properties, requiring the incorporation of a flow cell. With these basic requirements, an optically transparent microfluidic flow cell was envisioned. Interestingly, previous reports have shown that microfluidic devices can be designed such that two input streams remain partitioned throughout the length of the channel, assuming laminar flow properties, of course.[200] In these devices, the location of the fluidic partition (i.e. the junction between the inlet streams throughout the length of channel) can be moved by simply varying the flow-rate of one inlet relative to the other. By integrating this function into the proposed device, a selected region of an immobilized sensor population could be exposed to buffer while a separate region is exposed to glucose. Variations in inlet flow rate would allow the glucose-exposed region to be dynamically varied, while capturing the response properties of a group of sensors or individual sensors within a region of interest. Thus, this device will advance the understanding of how the response of individual sensors within a population contribute to overall response

properties, ultimately providing insight on designing clinically viable implantation schemes.

6.2 Experimental Details

6.2.1 Materials

Nano™ SU-8 50 and 100 and SU-8 Developer were purchased from MicroChem Corporation and used in conjunction with 4" silicon wafers obtained from Silicon Quest, Inc. during the photolithography process. Soft lithography was performed using PDMS (Sylgard® 184 Silicon Elastomer Base) and accompanying initiator (Sylgard® 184 Curing Agent), both of which were obtained from Dow Corning Corporation. Fluorescein isothiocyanate conjugated to dextran (FITC-dextran, Sigma), β-D-glucose (MP Biomedicals, Inc.), and phosphate buffered saline (PBS, Sigma) were used during device testing. Additionally, hydrochloric acid (HCl, Sigma), isopropyl alcohol (IPA, VWR), and acetone (VWR) were used as needed throughout the experimental procedures.

6.2.2 Microchannel Fabrication

The microchannel master mold was fabricated using conventional contact photolithography techniques.[201] The channel mask was designed with AutoCAD 2006 (Autodesk) and subsequently printed onto a transparency film with an emulsion printer (Linotronic, Linotype-Hell). The channel design is shown in Figure 99 with approximate dimensions.
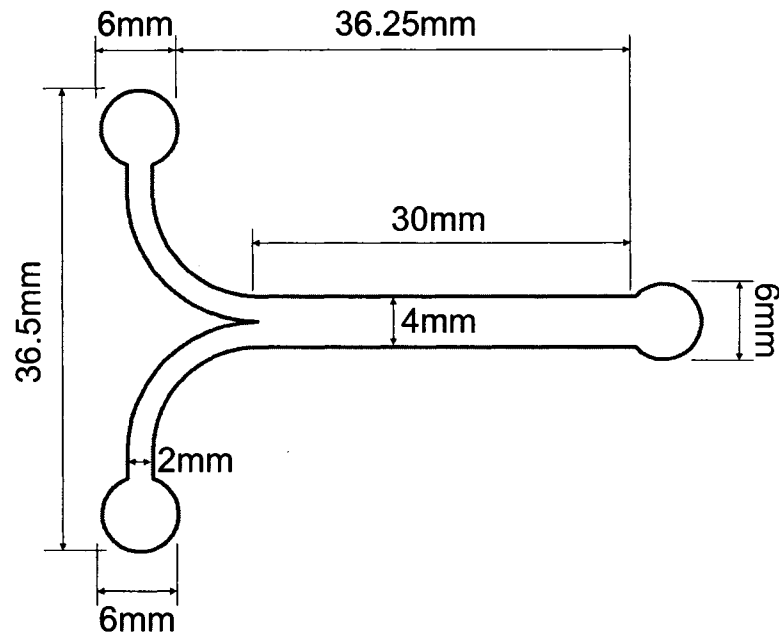
Figure 99. Mask layout used during channel preparation.

Because earlier results presented in chapter 4 were obtained with sensors immobilized on double-sided pressure-sensitive polyacrylate adhesive (3M), a channel with high aspect ratio features was desired to accommodate the adhesive/sensors. Therefore, a photoresist capable of producing feature heights > 200 μm was chosen, as a channel of this height would accommodate the thickness of the adhesive layer (~ 80 μm) and the average thickness of the sensor layer that was shown to contain approximately 3 layers of packed sensors (~ 50 μm, Figure 58), while still allowing fluid flow over the sample. For this reason, Nano™ SU-8 100, an epoxy-based, ultra-thick, negative tone photoresist, capable of producing structures with thicknesses > 200 μm, was chosen.

First, a silicon wafer was cleaned by rinsing in acetone and IPA, then dried by baking for 10 min at 250°C on a hot plate (PC-420D, Corning). After cooling to room temperature, SU-8 100 was slowly dispensed onto the center of the wafer and excess

bubbles were removed via desiccation (Bel-Art). A spin-coater (G3P-8, Specialty Coating Systems) set to 500 rpm, with a 10 rpm/second ramp, was used to spread the photoresist within 2 mm of the wafer edge. The wafer was subsequently desiccated to remove any remaining bubbles. Following the second desiccation, the wafer was reintroduced into the spin-coater, and spun at 500 rpm (100 rpm/second ramp) for 10 seconds to evenly spread the resist over the entire wafer surface. Finally, the speed was increased to 1000 rpm at 300 rpm/second for 30 seconds to attain an approximate thickness of 250 μm.

Soft baking, a process used to evaporate the solvent and densify the film, was performed in a two-step operation which has been shown to promote photoresist adhesion to the silicon substrate.[202] Prior to soft baking, the wafer was placed on a hot plate at 35°C for 15 minutes to minimize the edge-bead and promote film uniformity. The plate temperature was then increased (1°C / minute) until reaching 65°C, at which point baking ensued for 30 minutes. Following the initial baking step, the temperature was ramped (1°C / minute) to 95°C and the SU-8 100 coated wafer baked for an additional 90 minutes. After subsequent cooling to 50°C, the wafer was removed from the hot plate and cooled to room temperature. The mask depicted in Figure 99 was placed in direct contact with the coated wafer and exposed to UV illumination for 15 minutes via a mask aligner (EV420, Electronic Visions, Inc.).

A post-exposure bake was performed to crosslink the exposed photoresist region. Again a ramped, two-step baking process was used to minimize stress, wafer bowing, and resist cracking.[202] Using the same temperature ramp used in the soft bake procedure, the temperature was increased to 65°C for 1 minute, then 95°C for 20 minutes. Following

the post-exposure bake, the temperature was lowered in 5°C increments until room temperature was reached. This time-consuming process was instated to reduce the likelihood of catastrophic adhesion failure when developing the photoresist. The photoresist was developed in SU-8 Developer for 20 minutes, during which strong agitation was required to remove weakly-crosslinked SU-8 100 around the feature edges. After development, the wafer was thoroughly rinsed with IPA and dried under streaming nitrogen, thus marking the end of the master mold fabrication. Additionally, the feature thickness was quantified using a micrometer (ID-S1012E, Mitutoyo), with 15 random measurements over the feature surface.

Once the master mold was created, the channel design could be transferred to PDMS using conventional soft lithography techniques.[201, 202] Liquid PDMS was thoroughly mixed with its initiator in a 5:1 volumetric ratio. After that, the PDMS was desiccated to remove any bubbles, poured onto the wafer containing the positive relief channel pattern, and baked for 8 hours at 65°C in a convection oven (SW-11TA, Blue M Electric Company). Following removal of the wafer from the oven, care had to be taken to avoid rapid cooling, as this would likely result in catastrophic adhesion failure due to the difference in contraction rates of the wafer and the photoresist. After the wafer cooled to room temperature, the positive relief pattern was slowly removed from the wafer.

6.2.3 Preparation of Inlet Ports

Next, inlet and outlet ports were fabricated using a coring technique adapted from previous work as described in the following protocol.[203] A 16-gauge needle [VWR, 1.65 mm outer diameter, 1.19 mm inner diameter, Figure 100A] was modified by removing

the tip, as shown below in Figure 100B. The flat tip was subsequently beveled (Figure

100C) using a 5 μm roughness lapping film (LFG5P, ThorLabs).
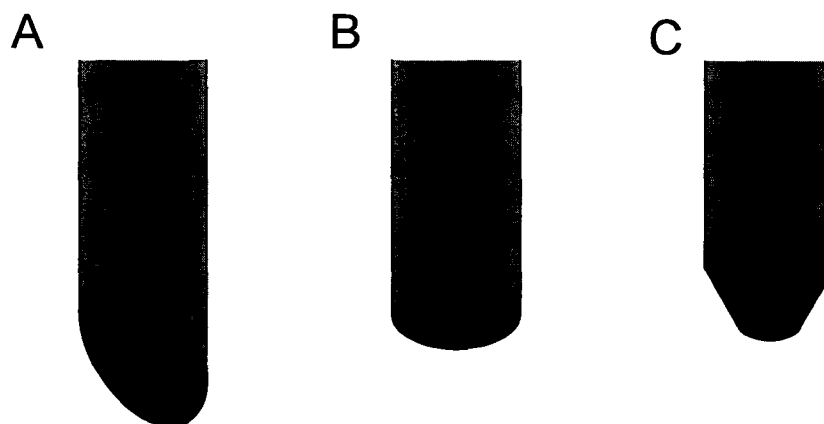
Figure 100. Fabrication of the coring tool. A.)Unmodified 16-gauge needle. B.) Needle following tip removal. C.) Beveled needle to be used as the coring tool. (Artwork courtesy Dustin Ritter.)

A 5-speed drill press (Homier Distributing Co.) containing the coring tool was

used to prepare the fluidic ports. When inserted into PDMS, the coring tool would

produce a port approximately 1.19 mm in diameter (Figure 101A – C), allowing the

insertion of a flat-tipped 16-gauge needle into the structure with minimal tearing.

Additionally, the difference between the inlet port and the needle diameter, ~ 460 μm,

would result in the formation of a compression seal between the needle and the inlet port

(Figure 101D), thereby minimizing leakage at the substrate-interconnect interface.

A   B   ☐ **PDMS**
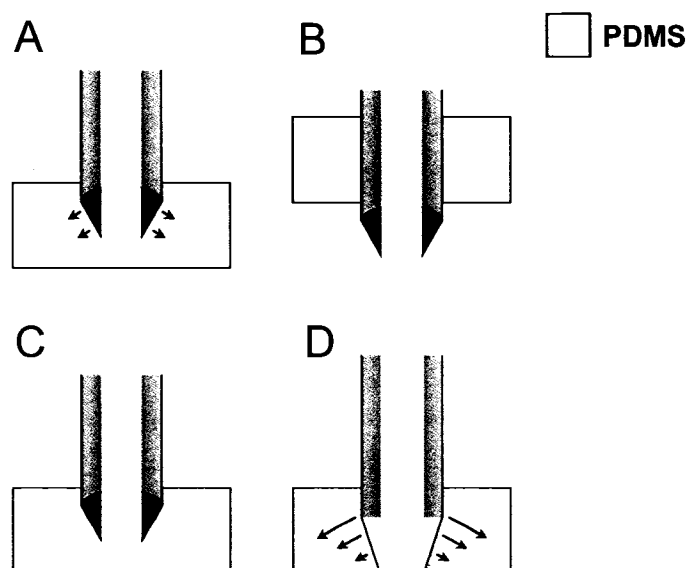
Figure 101. Coring procedure. A.) Insertion into the PDMS structure. B.) Coring tool advancement and collection of the core within the lumen. C.) Core extraction. D) Compression seal formation between port and inserted needle. (Artwork courtesy Dustin Ritter.)

It is important to state that to minimize tearing of the PDMS structure, the drill press was used at its lowest speed (760 rpm) and the coring tool was lowered steadily into the PDMS. It was also found that freezing the PDMS for 10 minutes prior to coring stiffened the PDMS and reduced the chance of tearing.

6.2.4 Flow Cell Assembly

Following preparation of the inlet and outlet ports, the PDMS substrate as well as a 4" glass wafer were stringently cleaned using the following procedures. The glass wafer was rinsed with acetone and IPA, dried with nitrogen and baked at 250°C for 10 minutes on a hot plate to ensure a dry surface. Subsequently, the PDMS substrate was soaked in 1 M HCl for 10 minutes, rinsed with DI water, and dried under streaming nitrogen. It should be noted that these two surfaces would ultimately be mated through oxygen plasma bonding, which requires a clean surface to produce high bonding strength.

After the glass substrate was cleaned, a 3 mm square of double-sided pressure-sensitive polyacrylate adhesive was cut and placed on the glass wafer. To ensure proper placement of the PDMS channel following oxygen plasma activation, the channel was positioned over the adhesive surface prior to oxygen plasma exposure and alignment marks were made on the bottom of the glass wafer. The PDMS substrate was removed and a droplet of sensors ranging from 2 to 5 µL (stock concentration ~ 10^7 particles/mL) was placed on the adhesive surface and dried under streaming nitrogen.

The surfaces of the PDMS substrate and glass wafer were activated using oxygen plasma (MicroRIE Series 800, Technics). During oxygen plasma exposure, a thin, highly-disordered oxide film is formed on and reacts with both the PDMS and the glass surfaces. Upon joining of the activated surfaces, covalent bonds are formed as the bonding interface dries, resulting in a stable junction of the two substrates.[204] Prior to surface activation, a microscope cover slip was cut to size with a diamond scribe (ThorLabs) and placed over the sensors during exposure, as an effort to reduce sensor exposure to the oxygen plasma. The glass wafer was subsequently exposed for 15 seconds at 70 W with the oxygen partial pressure at 75 mtorr. Similarly, the PDMS substrate was exposed at the same radio frequency (RF) power and oxygen partial pressure for 10 seconds.[205] Immediately, the two activated surfaces were joined, and allowed to sit for at least 2 hours. It should be noted that to promote uniform binding between the two substrates, an evenly-distributed weight (~ 1 kg) was applied.

6.2.5 Experimental Setup

Before sensor testing, experiments were performed to verify that the channel design would produce laminar flow characteristics. First, a 1 mm-wide by 50 µm-deep

channel of a similar profile as that depicted in Figure 99 was fabricated and tested for laminar flow as a proof of concept. The smaller dimensions were chosen in an effort to keep the Reynolds number below 2000, as is required to achieve laminar flow conditions. Furthermore, different channel designs could be fabricated much quicker and easier when the photolithography process was performed with a target thickness of 50 μm. The microchannel fabrication method was identical to that given for the 400 μm-deep channel, except that SU-8 50 was used instead of SU-8 100. Consequently the spin speeds and baking, exposure, and development times during the photolithography process were different.[202] After testing the small-scale channel, the laminar flow characteristics of the 4 mm-wide by 400 μm-deep channel (Figure 99) were examined. Additionally, experiments were performed to investigate the effect of varying inlet volumetric flow rates on the fluidic partition location.

For preliminary experiments where the laminar flow characteristics were quantified, two syringe pumps (KDS100 and KDS210, KD Scientific) equipped with 3 mL syringes containing FITC-dextran (1 mg/mL) and 0.01 M PBS were used. The interconnects consisted of three flat-tipped 16-gauge needles (VWR) inserted into the channel inlet ports. Syringes were connected to the interconnects by 1/8" outer diameter PEEK® tubing (Upchurch Scientific) equipped with standard Luer-Lock® fittings (VMR). Imaging was performed with a Nikon Eclipse TE2000-U epifluorescence microscope equipped with a long-pass FITC cube (Optical Insights, excitation filter: 455 ± 35 nm, dichroic mirror: 500 nm, emission filter: > 515 nm). Images were captured with a CoolSNAP ES CCD camera (Photometrics), and analysis was performed using

MetaMorph® Imaging software. An image depicting the completed experimental setup is given in Figure 102.

Figure 102. Image of experimental setup, depicting placement of the microfluidic flow cell on the microscope stage.

For sensor response imaging, a long-pass rhodamine cube (530 ± 15 nm excitation) in conjunction with a Dual-View® dual-emission filter (Optical Insights, equipped with 580 ± 12.5 and 640 ± 12.5 nm filters) was used to produce two simultaneous images projected onto equal portions of the CCD detector. Thus, the simultaneous acquisition of RITC and PtOEP images could be obtained. Additionally, a macro was written to collect a real-time *ratiometric* series, by dividing the respective PtOEP and RITC images. Macro practicality was tested by placing 4 μL droplet of sensors on a microscope slide, then introducing 2 μL of 600 mg/dL β-D-glucose, while collecting image frames every 3 seconds for a total of 2 minutes.

After the ability to collect real-time ratiometric images was demonstrated, the microfluidic device was subsequently tested using inlet solutions of 600 mg/dL glucose and 0.01 M PBS, respectively.

6.3 Results and Discussion

6.3.1 Microchannel Fabrication

An important concept in this device is the ability to examine the dynamic response of individual sensor behavior in a group setting, through exposure of varying flow rates. It is expected that eventual experiments using high flow rates will be performed, such that the flow cell would be exposed to high fluidic pressures; therefore, a reliable means of interconnecting fluidic inlets to the flow cell is needed. The interconnection method used in the work presented herein used a modified needle as a coring tool to remove a cylindrical core of the PDMS substrate in diameter to that of the inner lumen. A digital image of the coring tool fabricated for this work is given in the following figure.
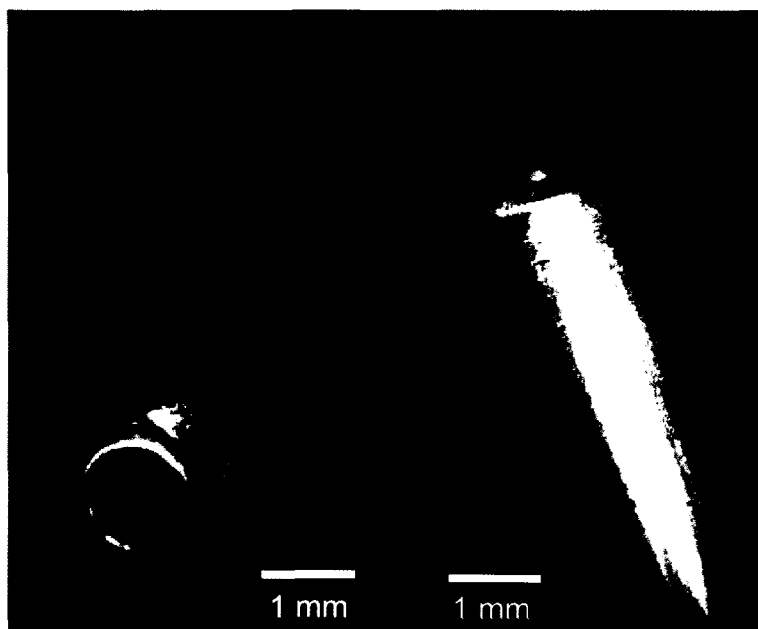
Figure 103. Images of coring tool profile. Top (left) and side (right) view.

From Figure 103, it is important to point out the beveled tip, which allows the formation of a compression seal between the flow cell and the fluidic inlets. Although no quantitative data was independently verified, from previous work it has been shown that the interconnection method produced devices which could withstand pressures up to 550 kPa, whereupon the failure occurred between the PDMS-glass bond.[203] It should be noted that throughout all testing described herein, leaking due to interconnection or bonding failure was not observed; thereby, indicating the efficacy of the interconnection/substrate-binding method to this application.

Following port fabrication, sensors were immobilized on the glass substrate and the surfaces of the two substrates joined using oxygen plasma bonding. The following image depicts the completed microfluidic device, including ports and immobilized sensors.

25 mm
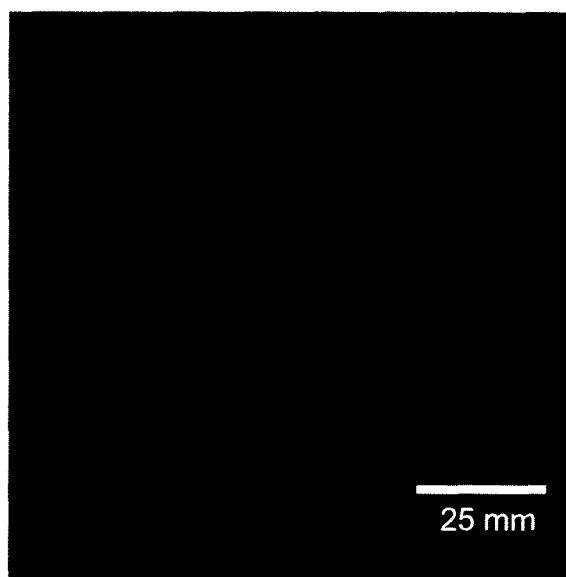
Figure 104. Competed microfluidic device.

It is important to note that prior to binding the substrates, the channel height was determined to be 408.6 ± 21.5 µm, which was approximately 1.5 fold greater than that which was expected. It is theorized that the room temperature during the lithography processes was below the temperature used by the photoresist manufacturer to characterize feature height, thus increasing viscosity and causing greater feature sizes than expected.

Additionally, an image of the sensors immobilized within the channel is given in the following figure.
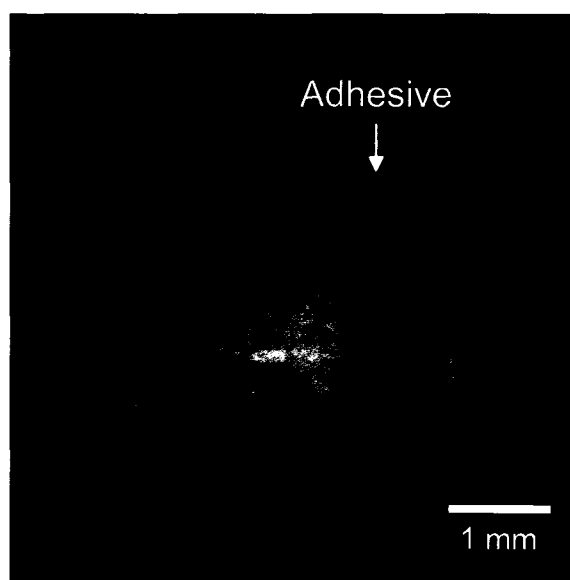
Figure 105. Image of immobilized sensors within the microchannel.

The image in Figure 105 was acquired by using UV illumination (Black Ray) and collecting subsequent emission via a digital camera. From this image, it is apparent that the adhesive is excited by UV illumination as well as the sensors. This image demonstrates the ability to immobilize sensors within the microfluidic device, thus completing device fabrication.

6.3.2   Laminar Flow Properties

An interesting design consideration of the microfluidic device presented in this work is to use inlet flow rate variation to controllably perturb a localized region of sensors with glucose. In order for this consideration to be obtained, the device must exhibit laminar flow properties. To characterize the flow properties of this device, a microchannel void of adhesive and sensors was prepared as described earlier. Using inlet solutions of PBS and PBS containing FITC-dextran, respectively, identical flow rates

(3mL/hr) were used and the fluorescent profile through the channel length was examined (Figure 106).
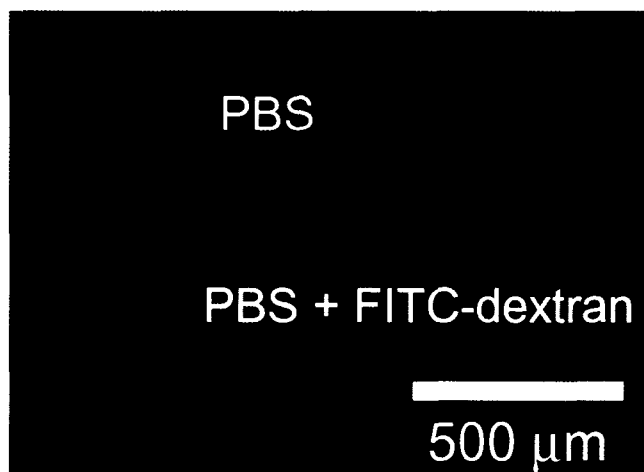
Figure 106. Channel flow profile using PBS and PBS containing FITC-dextran. Note inlet flow rates were both set to 3 mL/hr.

From this image, it is important to note that when inlet flow rates are equal, the partition is located at the center of the channel, as expected. In theory, by varying the relative inlet flow rates, the partition location could be shifted. To test this, the flow rate of the FITC-containing inlet (Q_{FITC}) was varied relative to the flow rate of the channel solely containing buffer (Q_{buffer}), such that the relative inlet flow rate ratio was defined as ($Q_r = Q_{FITC}/Q_{buffer}$).
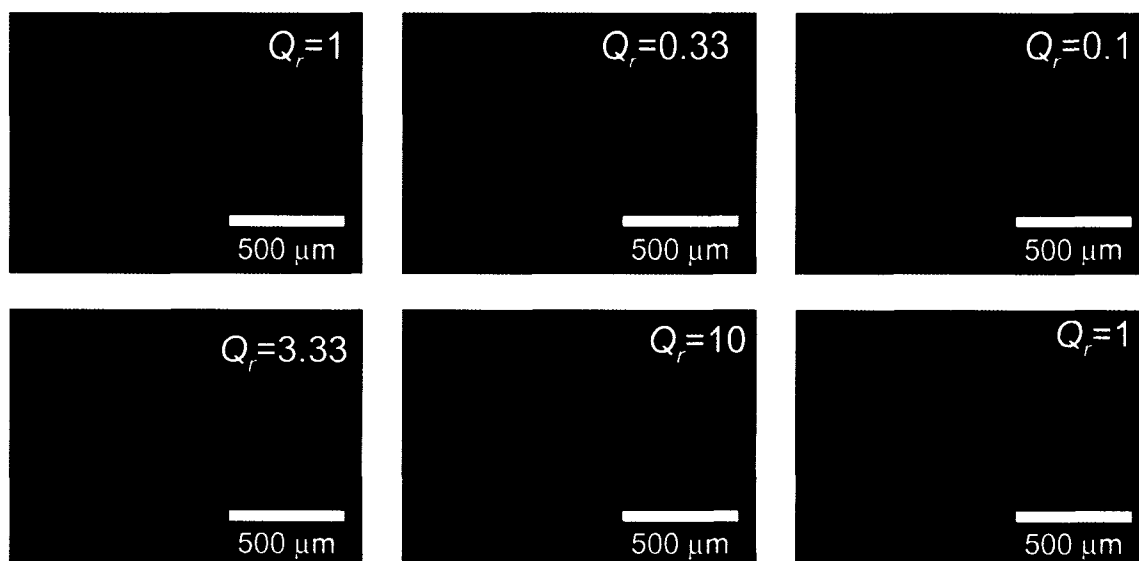
Figure 107. Fluorescence micrographs depicting shift in partition location by varying relative inlet flow rates. Note that Q_r = 1 = 3mL hr^{-1} / 3mL hr^{-1} magnification = 40X.

Figure 107 demonstrates the ability to control the partition location by simply altering the relative inlet flow rates. It should be noted that these data were acquired in a time sequence, indicating that the partition can be returned to its initial position, which in Figure 107 is center-channel.

6.3.3 Real-time Ratiometric Imaging

The most critical requirement in the device described in this chapter is the ability to analyze individual sensor response within a sensor population in order to understand how individual response properties contribute to the overall response. To accomplish this feat, fluorescence imaging techniques were employed. Given that the sensor response is ratiometric in nature, a method was needed to allow real-time ratiometric imaging, as such would allow the temporal ratiometric response of individual sensors within the field of view to be analyzed. However, in order to prepare an accurate ratiometric image, it is necessary to *simultaneously* obtain images containing PtOEP and RITC emission,

respectively. Therefore, a DualView® emission filter was used optically process the image prior to collection. With this device, the simultaneous acquisition of two emission images with a sole detector is possible through the projection of the images on the top and bottom half of the detector, respectively. A typical fluorescence micrograph containing separate PtOEP and RITC images of a sensor population is given in the following figure.
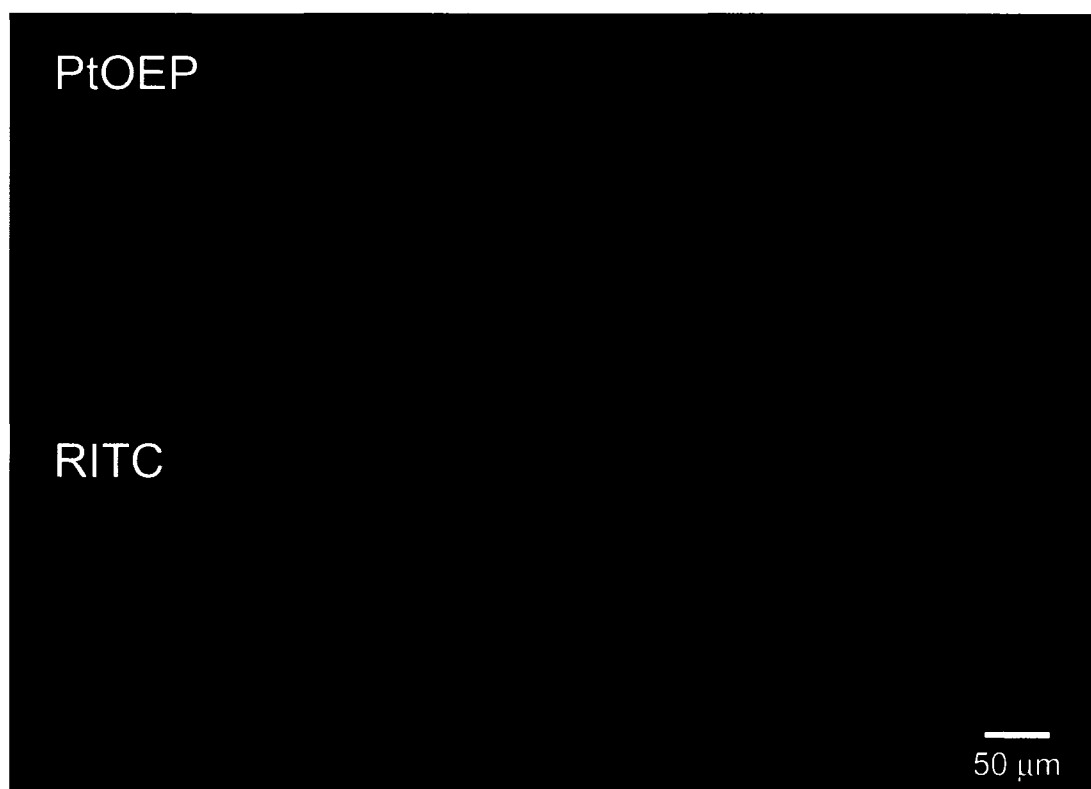
Figure 108. Typical fluorescence micrograph depicting PtOEP (top) and RITC (bottom) emission images acquired for an immobilized sensor population. Note total magnification = 100X.

It should be noted that PtOEP emission intensity is low relative to that of the RITC image. This observation is expected, as this image was collected under ambient conditions (air-equilibrated buffer). Additionally, the image presented in Figure 108 is as

exactly collected; therefore, in order to produce a ratiometric image, the respective images needed to be separated prior to division. Example ratiometric images will be given later in this section.

To acquire real-time ratiometric data, a macro was written to capture a series of time-lapse images implementing user-defined inputs (i.e. time of duration and frequency of acquisition). Following the time-lapse acquisition, the PtOEP and RITC images are separated and divided, resulting in a series of real-time ratiometric images. It is important to state that PtOEP images were not corrected for RITC contributions and should be addressed in future macro versions. To test the macro, a suspension of sensors was placed on a standard microscope slide, at which time the macro was executed. A droplet of glucose was added to the sensor suspension during image acquisition (total glucose concentration = 200 mg/mL), after which the setup remained undisturbed until acquisition was completed (120 second total acquisition time). The resulting temporal profile of ratiometric images was subsequently analyzed.
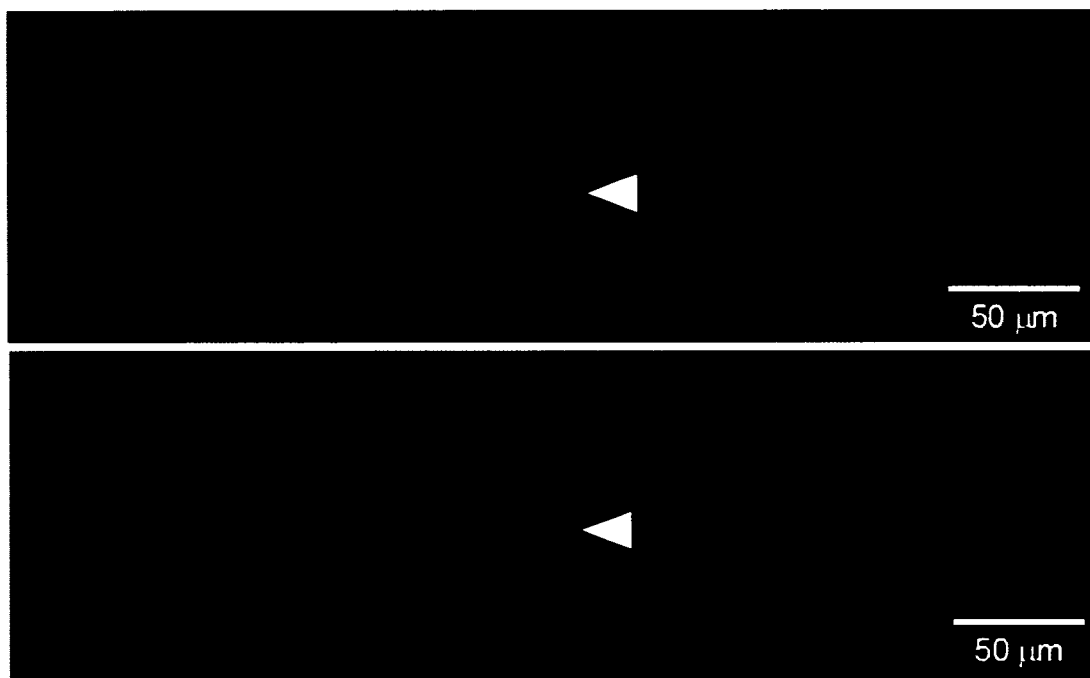
Figure 109. Ratiometric images of sensor prior to glucose exposure (top) and after exposure to a 200mg/mL initial concentration for 90 sec. Arrow highlights the same sensor before and after glucose exposure. Note total magnification = 100X.

From the image data presented in Figure 109, it is evident that an increase in ratiometric intensity is observed within individual sensors following exposure to 200 mg/dL initial bulk conditions. Thus, the ability to collect ratiometric images depicting the response properties of individual sensors over time has been demonstrated. In order to obtain dynamic data, the ratiometric time-lapse was subjected to region of interest (ROI) analysis. This method involves defining a common spatial ROI of circular geometry in the acquired images and analyzing the fluorescence emission intensity normalized to the total number of pixels within the ROI with respect to time. These data result in a graphical representation of the average temporal fluorescence intensity within the ROI. Four ROIs were used for analyzing the change in ratiometric intensity with

respect to time, three of which were within sensors and the fourth of which was that of

the entire image (i.e. average response of imaged population).
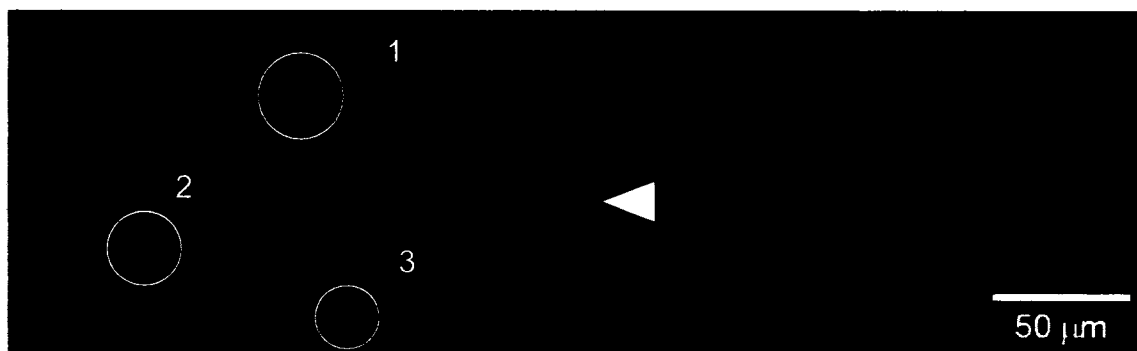
Figure 110. ROIs used to analyze change in ratiometric intensity within individual sensors during exposure to glucose. Note that ROI 4 contains the entire image. (Arrow used as reference).

Using the ROIs depicted in Figure 110, the time-dependent percent change in

ratiometric intensity within each ROI was determined and is presented in the following

plot.
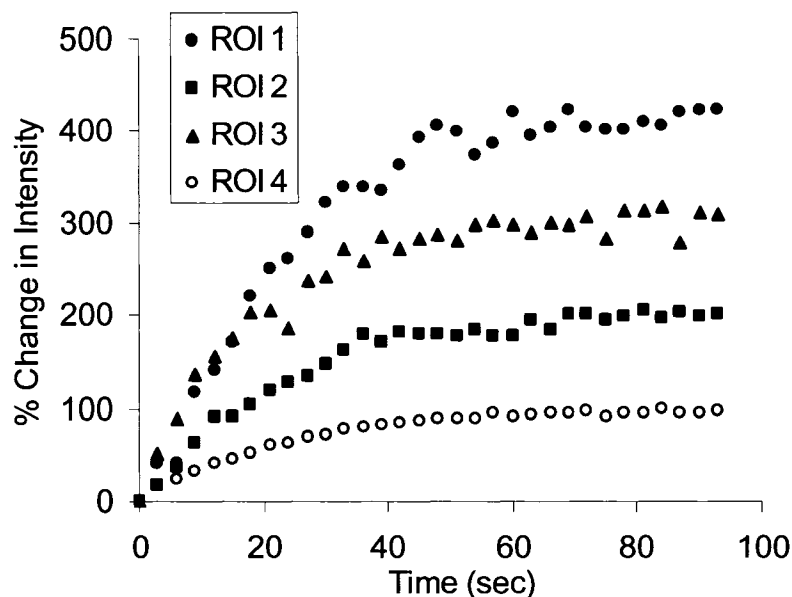
Figure 111. Percent change in ratiometric intensity of three individual sensors (ROIs 1 – 3) and all sensors within the viewing field (ROI 4).

It should be reiterated that this experiment was not conducted with sensors immobilized within the microfluidic device; in fact, the sensors were mobile throughout the experiment. Therefore, the sensors selected for analysis were those which exhibited less relative mobility throughout the course of the experiment. From these data, it is important to recognize that response time is approximately 30 seconds less than previous observations in the dynamic testing apparatus, which was shown in Chapter 4 to be approximately 80 seconds. In previous experiments where immobilized sensors were used for analysis, it was shown that the immobilized sensor layer was comprised of approximately three sensor layers, thus additional time may be required for underlying sensors to "see" bulk substrate levels and respond. Therefore, the total response time of the population would be a function of the time required for all sensors to equilibrate,

whereas in a suspension, sensors may be exposed to bulk conditions more rapidly, thus increasing response time.

Another point of interest is that total percent change observed in ROI 1-3 varies significantly. This observation could be explained by individual sensors being exposed to different bulk conditions, or more likely, varying physical parameters, such as immobilized enzyme concentration or particle diameter. Furthermore, previous simulations indicate that an increase in sensor radius from 10 to 20 μm, would result in a 6 % decrease in local oxygen concentration (larger sensor radii would increase the volume over which the oxygen concentration is at its lowest steady-state value) at glucose concentration of approximately 200 mg/dL.[41] Using the data presented in Figure 47, a 6 % reduction in steady-state oxygen levels observed at 200 mg/dL glucose would not significantly change steady-state peak ratio values, implicating that the stead-state intensity variation presented in Figure 111, may not be solely due to size variations. It is also important to consider that variations in sensor enzyme concentrations may also contribute to the discrepancies observed in the stead-state intensities. Although it is difficult to speculate whether or not the sensors analyzed containing significantly different enzyme concentrations, it is a useful exercise to consider the affect of variations in enzyme concentration on sensor function. Should immobilized enzyme concentrations fail to significantly reduce steady-state oxygen levels within the sensor or be such that catalysis occurs mainly at the outer region of the sensor, an insensitive response would be inevitable. Previous work has shown a distinct optimum enzyme concentration produces a highly sensitive response, and deviations on the order of μM concentrations could significantly affect response characteristics, an observation compounded when

considering variations in sensor radius as well.[41] Thus, it is plausible that the discrepancies observed in Figure 111 arise from variations in the physical properties of the sensor analyzed, supporting the notion that not all sensors within a population respond will equally to glucose levels, as expected.

Additionally, it is important to note that ROI 4, which contains the entire ratiometric image and presents an average response of all of the sensors within Figure 110, shows the lowest percent change in ratiometric intensity. Most likely, this low percent change is a result of high background noise from out-of-plane fluorescence, which significantly dampens the individual sensor contribution to overall signal. Nonetheless, these data support that individual sensors within a population display significant difference in response characteristics, which may be attributed to location and/or physical properties. To obtain a more concise understanding, a similar analysis of immobilized sensors exposed to dynamic conditions is needed.

6.3.4 Sensor Response Testing in Microchannel

The results presented in the previous section were of non-immobilized sensors operating under static conditions – a stark contrast to the experimental conditions used in chapters 4 and 5 to analyze sensor performance. Therefore, sensors were immobilized within the microfluidic device and exposed to a step change in glucose (200 mg/dL, 10mL/hr) during time-lapse imaging, a similar process to that used in previous chapters. A ratiometric series was subsequently obtained and the average ratiometric intensity within 3 random sensors was determined.
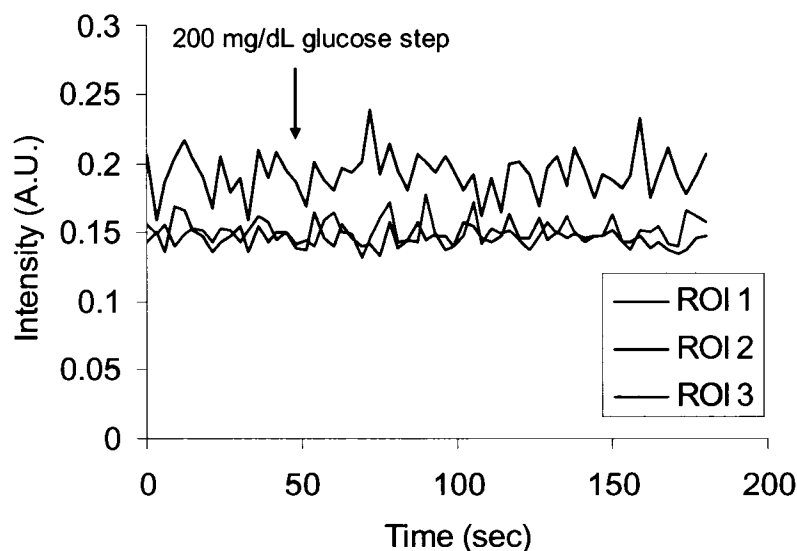
Figure 112. Change in ratiometric intensity within three random senor specimens immobilized within the microfluidic channel in response to a 200 mg/dL glucose step.

From these data, it is important to note that no significant change in ratiometric intensity was observed following sensor exposure to 200 mg/dL glucose. The experiment was repeated and the response of sensors at various locations within the immobilized population was performed with similar results. It was then hypothesized that the flow rates used may have dampened the response, possibly due to forced convection. Despite flow rate variations over the instrumentation range, no response was observed. An additional set of sensors was prepared and response properties were first validated using the dynamic testing apparatus, yet no response was obtained when tested in the microfluidic device. It is speculated that despite covering the immobilized sensors with a glass coverslip during oxygen plasma activation, that sensor exposure was not completely inhibited, the results of which could contribute to the lack of a discernable response. Therefore, an investigation of the effect of oxygen plasma on sensor behavior is indeed

warranted, the results of which may indicate alternative methods to bond the PDMS and glass substrates are needed.

6.4 Conclusion

The preparation of a microfluidic device for use in image analysis of smart tattoo function under dynamic testing conditions was described. The device was designed such that two inlet fluids would flow laminarly throughout the length of the channel. By varying the relative volumetric flow rate of the inlet fluids, buffer and glucose, respectively, the location at which the fluids converged within the channel can be precisely controlled, allowing a distinct region of sensors within an immobilized population to be exposed to glucose. The ability to acquire a real-time series of ratiometric images depicting the response characteristics of individual sensors within a population was demonstrated. Results indicated that individual sensors have significantly different response characteristics that ultimately contribute to overall response properties. More importantly, future work will investigate the effect of sample preparation procedures, namely oxygen plasma, with hopes of obtaining response data of sensors immobilized within the reported microfluidic devices.

CHAPTER 7

CONCLUSIONS AND FUTURE WORK

7.1 Conclusions

Smart tattoo type sensors are being investigated as a means to alleviate pain and discomfort associated with traditional finger-prick measurements. In this dissertation, enzymatic smart tattoos have been developed and characterized for potential use in minimally-invasive diabetic monitoring systems. While enzymatic smart tattoos comprising hydrogel supports and ruthenium-based oxygen indicators have been previously demonstrated, the efficacy of these prototypes was limited by low glucose sensitivity (~ 0.2 % change / mg dL^{-1}). Thus, this work was initially focused on increasing glucose sensitivity, which was addressed by selecting metalloporphyrin oxygen indicators and hybrid silicate (algilica) supports as platforms upon which to build highly sensitive devices.

Metalloporphyrin complexes exhibit higher excitation wavelengths, which reduce the effects of tissue scatter and absorption, increased photostability, and higher oxygen sensitivity than ruthenium-based indicators, and in conjunction with algilica matrices, which readily allow co-immobilization of hydrophilic (GOx) and hydrophobic (PtOEP) molecules, glucose sensitivities two orders of magnitude greater than previous enzymatic smart tattoos were achieved. These results indicate the importance of selecting an

249

oxygen indicator that is sensitive over the operational range of the sensor, as well as selecting a support matrix conducive to oxygen transport. Despite high sensitivities (~ 5 % change / mg dL^{-1}), these prototypes failed to be sensitive over the accepted monitoring range of 50 – 350 mg/dL, limiting diabetic monitoring applications. Therefore, an additional component of this work centered on developing a means to extend the sensing range by controlling substrate delivery into the sensor.

One of the more significant findings to emerge from this work is the ability to control device sensitivity and range through controlling substrate flux into the sensor via the application of surface adsorbed polyelectrolyte nanofilms. This simple, yet efficient technique (12 nm thick films were shown to significantly affect response properties) allowed the upper sensing range to be tuned over 90 – 250 mg/dL, indicating that polyelectrolyte nanofilms provide an effective means to control substrate flux. This finding suggests that applications requiring mass transport control of molecular species, including filtration technologies, may benefit from the use of polyelectrolyte nanofilms. Furthermore, it is important to highlight limitations of these results; particularly, the upper range limit achieved is still below that of the accepted monitoring range. While the range may be extended by simply increasing the nanofilms thickness, films comprised of alternative constituents may increase upper range limits while minimizing film thicknesses.

An additional study was performed to determine the long-term stability of sensor function under continuous operating conditions. The most obvious finding of this investigation was theoretical and experimental data indicated poor device longevity (90 % loss of sensitivity after 24 hours), suggesting that current prototypes are unfit for long-

term applications. Towards the goal of developing suitable long-term devices, first generation bi-enzyme smart tattoos containing co-immobilized catalase were developed to reduce enzyme inactivation from hydrogen peroxide. This design modification increased long-term stability by two-fold, suggesting that the incorporation of catalase enhances the operational life span of enzymatic smart tattoos and should be aggressively pursued in the next generation of prototypes. While this finding is indeed encouraging, additional work, which will be addressed later in this chapter, is required to optimize co-immobilization techniques. Nonetheless, results are promising, because with future developments these sensors could reduce the pain and bother associated with traditional diabetic monitoring techniques, which may increase patience compliance with suggested monitoring frequencies and aid in reducing the onset of complications.

Although this work represents a significant advancement in enzymatic smart tattoo technology, it is important to emphasize that the materials/techniques applied in this dissertation are broadly applicable to other areas of science and engineering. For example, the algilica support matrix used exclusively in this dissertation is comprised of hydrophilic polymer moieties, as well as silica domains, making this material attractive for the uniform entrapment of *both* hydrophobic and hydrophilic molecules. Thus, applications requiring molecular immobilization, bioencapsulation for example, may benefit from a similar approach. Additionally, the simple means of fabricating algilica supports lays the ground work for the future development of additional novel hybrid sol-gel materials whose future applications may be further widespread. Another and perhaps more important application which may benefit from the general approach detailed in this work is the area of biosensors. Using a similar approach, it may be possible to develop

additional enzymatic biosensors sensitive to lactate and glutamate, for example, through immobilization of their respective oxidation enzymes (lactate oxidase and glutamate oxidase, respectively). Such devices may prove useful in studying other aspects of physiology such as localized metabolic trends.

7.1.1 Novel Contributions to Engineering and Science

The novel contribution of the author to the field of engineering and science include:

1. Co-development of the novel immobilization matrix used in this dissertation – algilica.

2. Development of indicator and enzyme immobilization strategies for algilica; extensive characterization under dynamic testing conditions.

3. Demonstration of the ability to engineer device sensitivity and analytical range by varying nanofilm thickness.

4. Obtainment of transdermal spectra from implanted enzymatic smart tattoos (presented in the following section).

5. Development of a mathematical model to simulate the effect of continuous operation on sensor lifetime.

6. Preparation of bi-enzymatic smart tattoos more suitable for long-term applications.

7. Development of an imaging technique allowing real-time ratiometric monitoring of sensor dynamics.

7.2 Preliminary Acquisition of
Transdermal Spectra

Skin is a complex tissue comprised of many non-homogeneously distributed components that absorb and scatter light in a complex fashion, which in turn attenuates the propagating light.[62] These properties can in turn complicate the controlled delivery of excitation light to the sensor implants, as well as hinder the efficient collection of emission light. Independent of how well the sensors perform in bench top situations, the concept would be rendered useless should transdermal readouts be unobtainable. Therefore, *the ability to excite and collect transdermal emission data is of utmost importance to the ultimate success of this work.*

Sensor migration (i.e. sensor movement from the initial site of implantation) over time would result in decreased emission intensities as well as alterations in response properties (it was shown earlier in Chapter 4 that sensor concentration effects response dynamics). In an attempt to counteract this effect, the sensors were suspended in 20 wt% Pluronic F127. This unique material is classified as a low critical solution temperature (LCST) gel, such that it exists in sol (liquid) state *below* the transition temperature and in gel (solid) state at temperatures *above*. Previous work has shown that the transition temperature can be controlled by simply adjusting the concentration of Pluronic F127.[206] Exploiting this property, it was hypothesized that this material could be used as a delivery vessel for enzymatic smart tattoos, such that prior to implantation, the sensor suspension would exist in the sol state and transition to gel state would take place once implanted into the dermis. In theory, this *in vivo* transition would decrease sensor migration from the initial point of injection over time. It is important to note that immediately following injection, the implant did indeed solidify, as indicated by the presence of a bolus under

the skin surface. Following the 4-day recuperation period, the bolus remained clearly visible, indicating that the use of this material as a delivery vessel for smart tattoos is viable. Although this result was promising, it is out of the scope of this work to characterize the spatial and temporal distribution of the sensors after implantation, as well as the effect of Pluronic F127 on sensor function.

In vivo protocols were reviewed and approved by the Institutional Animal Care and Use Committee (IACUC) before initiation of *in vivo* experiments. Sensors were prepared using the previously described method. Implantation samples were prepared by suspending the sensors in a 20 wt% of Pluronic F127 (Aldrich) dissolved in 0.01 M PBS (pH = 7.4) to a final concentration of $\sim 10^8$ sensors/mL and stored at 4 °C until needed. Prior to implantation, approximately 100 μL of sensor suspension was loaded into 25 ½ gauge insulin syringes (Becton, Dickinson and Company) and sterilized under UV illumination (Black Ray) for approximately 10 minutes. As a control, a 20 wt% of Pluronic F127 dissolved in 0.01 M PBS (pH = 7.4) was also prepared and sterilized using the same procedure.

Sprague-Dawley rats ($\sim$300 g) were selected as the animal model for this preliminary work. A peritoneal injection of Nembutal® (50 mg/mL, Abbott) was administered at 1 μL/g of body weight to induce anesthesia, after which the dorsal region was shaved and sterilized with isopropyl alcohol (VWR). Prior to the implantation procedure, the animal was placed on a temperature regulating pad. Next, the respective samples were injected into the dermis of the dorsal region. Following the implantation procedure, the animal was allowed 4 days to recuperate, after which the animal was

inspected for localized irritation (redness, loss of hair, and scabbing), none of which was found.

Although no discomfort is associated with the acquisition of transdermal spectra, the animal was anesthetized using the same protocol described above, to eliminate excessive stress associated with handling. Transdermal spectra were acquired using a 6-around-1 optical fiber to deliver excitation light from a Hg-Xe arc lamp (Model 68811, Oriel) containing a 530 ± 5 nm interference filter (ThorLabs) to the injection site. Sensor emission was subsequently delivered to a diode array spectrometer (USB 2000, OceanOptics) through the collection bundle as depicted in Figure 113. Additionally, index matching gel (Thor labs) was used as a medium between the optical fiber and skin.
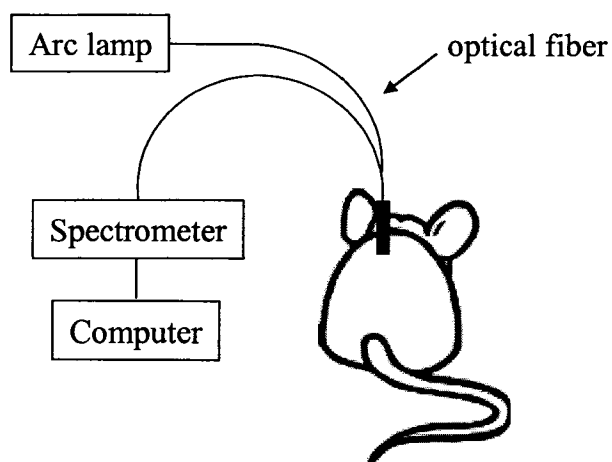
Figure 113. Schematic of instrumentation setup used to acquire in vivo transdermal spectra.

Following the recuperation period, transdermal spectra (10 per site) of the implantation sites containing the smart tattoos and the control were acquired (Figure 114).
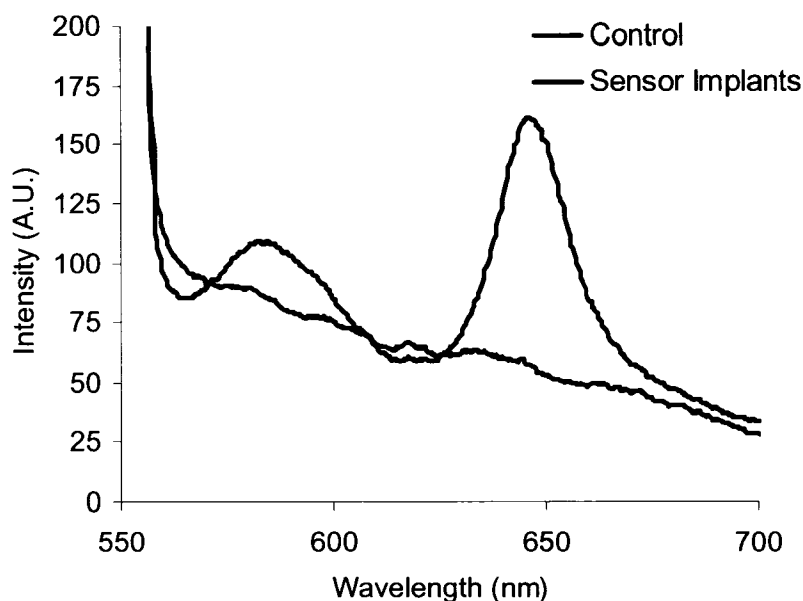
Figure 114. *In vivo* **transdermal sensor and control spectrum obtained in a rat model.**

The first point of note is that when compared to the control, the emission spectrum acquired for the site containing the smart tattoos are clearly similar to those obtained *in vitro* (Figure 39, RITC emission maximum at 580 nm and PtOEP emission maximum at 645 nm), indicating that it is achievable to collect transdermal spectra using the sensor concepts detailed in this work. To our knowledge, the ability to successfully interrogate and collect emission data from an implanted glucose sensor population has been published only once, further implicating the promise of the reported concepts.[207] It is important to state that the sole objective of this set of experiments was to determine if the acquisition of transdermal spectra was possible with the current sensor design (which it is); therefore, no attempt was made to obtain *in vivo* calibration data and assess *in vivo* function, and will be addressed in the following section.

.

7.3 Future Work

7.3.1 Algilica-Based Ratiometric Oxygen Sensors

In Chapter 3, self-referenced oxygen sensors based on PtOEP immobilization within algilica microspheres were presented. The results presented were obtained under steady-state conditions. Results depicting dynamic operation would be useful in determining response time, which would be instrumental in the future applications of such devices, as well as indicating if polyelectrolyte nanofilms affect oxygen diffusivity within the sensors.

7.3.2 Algilica-Based Ratiometric Glucose Sensors

In Chapter 4, enzymatic smart tattoos were fabricated using algilica particles, porphyrin indicators, and fluorescent nanofilms. Given the limited long-term stability of prototypes based only on glucose oxidase, of primary importance is the optimization of catalase incorporation into the sensing scheme. Initially, this would involve the development of immobilization strategies that allow the homogeneous distribution of both glucose oxidase and catalase into the sensor. Additionally, a significant amount of effort should be invested in determining the appropriate ratio of immobilized enzymes needed to decrease the affects of hydrogen peroxide while maximizing sensor performance, as unnecessarily high concentrations of catalase may minimize the concentration of immobilized glucose oxidase causing decreased sensitivity, while markedly low concentrations would result in decreased sensor longevity. Following the determination of these factors, the characterization of the bulk oxygen effect,

concentration effect, and most important, the effect of nanofilm thickness should be performed and compared with the results presented in Chapter 4.

Additional work should focus on testing sensor performance under increasingly physiological conditions, including testing under physiological temperature conditions, as well as testing under daily blood-glucose profiles of non-diabetics and diabetics (both compliants and non-compliants of the recommended testing frequencies).

In vivo experiments on multiple animals investigating host response on sensor function is also of considerable importance (preliminary results will be presented in the following section). Standard blood-draw measurements in conjunction with glucose infusions should be used to calibrate the implanted devices. After which, device accuracy is tracked over time, and the reduction of device sensitivity corroborated with histological finding (i.e. biodegradation and bioremediation). It would also be interesting to integrate the effect of bioremediation into Monte Carlo models, which simulate photon transport through skin tissue, to investigate the collection efficiency of transdermal spectra over time. Furthermore, given the implantation results reported in this work were obtained with hand injections, it is important to develop repeatable implantation strategies so that measurements across multiple implantation sites could be easily compared.

Of additional importance is the implementation of oxygen-sensing functionality with a population of smart tattoos. This functionality would allow the simultaneous measurement of the bulk oxygen levels within a sensor population and could be used to account for non-glucose specific shifts in bulk oxygen levels, such as altitude changes, illnesses, physical exertion, ect.

It would also be advantageous for future work to focus on the development of a dynamic test bed which more accurately simulates *in vivo* conditions, such as flow rates similar to those found in the dermis (mL/hr) as well as replicating the spatial distributions expected to be seen in *in vivo* implants. This would ultimately involve the development of skin phantom, through which glucose can readily flow at a similar rate observed *in vivo* (mL/hr). This in itself would be quite a feat to develop, but would provide the ability to collect response data under increasingly physiological conditions.

Additionally, of equal importance is the characterization of substrate diffusivities through the algilica. The author is aware that currently efforts are underway to develop a testing apparatus that allows substrate transport properties through various media to be determined, and awaits with great anticipation the results. Furthermore, this test bed could be used to test the effect of nanofilm coating on oxygen diffusion through algilica, the results of which could allow the proposition of additional theories as to why device sensitivity increases with the addition of the initial five nanofilm bilayers, as well as the development of more accurate models, as discussed in the following section.

7.3.3   Sensor Modeling

In Chapter 5, a model that simulated the continuous operation of sensors while considering the effects of enzyme inactivation was presented. Simulation results as well as experimentally obtained results in the implementation of a design change to produce sensors more suitable for long-term applications. This was accomplished through catalase incorporation into the sensing scheme; however, incorporation of catalase kinetics into the model was not successful, due to required addition of three partial differential equations. Further complications arise from the three individual forms of

catalase also being susceptible to hydrogen peroxide poisoning; thus, the pseudo steady-state assumption can not be made. Therefore, the obtainment of a solution would require the simultaneous solution of a series of ten partial differential equations. Various differential equation solves were used, and to no avail, a closed-loop solution was not obtained, due in part to the lack of computing power available at the time of the work. Nonetheless, future work should focus on integration of catalase kinetics into the model, as such a model could aid in the determining the optimal concentration of immobilized catalase needed to maximize long-term stability and device sensitivity.

Of more importance is the derivation of a model that considers the sensor function of an entire population. It is recommended that substrate diffusivities through algilica supports be determined (as described above) and used as model inputs, which should increase theoretical-experimental agreement. A particularly interesting paper detailing the derivation of a sorption kinetic model used to describe a population of polydispersed particles may be of particular use in expanding "group functionality" to the current model.[196] The results of which could be used to prepare a model that more accurately predicts experimental observations as well as be incorporated in to optimization algorithms which could elucidate optimum physical characteristics needed to develop sensors suited for long-term application.

7.3.4 Ratiometric Imaging of Sensor Performance

In Chapter 6, a microfluidic device was developed to allow imaging of individual sensor function under dynamic conditions. Unfortunately, little progress was made in acquiring data from the microfluidic device. It was hypothesized that oxygen plasma exposure to the sensor could have caused the loss of sensor function. This hypothesis

could be tested by exposing sensors to varying level of oxygen plasma characterizing the results under dynamic conditions. Results may require the development of additional immobilization schemes.

REFERENCES

1. National diabetes fact sheet: United States. http://www.cdc.gov/diabetes/pubs/pdf/ndfs_2005.pdf, April 5, 2006.

2. Alberti, K.G., Zimmet, P.Z., "Definition, diagnosis and classification of diabetes mellitus and its complications. Part 1: diagnosis and classification of diabetes mellitus. Provisional report of a WHO Consultation," *Diabetic Medicine* **1998,** 15, (7), 539-553.

3. MacFarlane, A.J., Burghardt, K.M., Kelly, J., Simell, T., Simell, O., Altosaar, I., Scott, F. W., "A type 1 diabetes-related protein from wheat (Triticum aestivum): cDNA clone of a wheat storage globulin, Glb1, linked to islet damage," *Journal of Biological Chemistry* **2003,** 278, (1), 54-63.

4. Drivsholm, T., de Fine Olivarius, N., Nielsen, A.B.S., Siersma, V., "Symptoms, signs and complications in newly diagnosed type 2 diabetic patients, and their relationship to glycaemia, blood pressure and weight," *Diabetologia* **2005,** 48, (2), 210-214.

5. Hu, F.B., Van Dam, R.M., Liu, S., "Diet and risk of Type II diabetes: the role of types of fat and carbohydrate," *Diabetologia* **2001,** 44, (7), 805-817.

6. Fagot-Campagna, A.P.D., Engelgau, M.M., Burrows, N.R., Geiss, L.S., Valdez, R., Beckles, G.L., Saaddine, J., Gregg, E.W., Williamson, D.F., Narayan, K.M., "Type 2 diabetes among North American children and adolescents: an epidemiologic review and a public health perspective," *Journal of Pediatrics* **2000,** 136, (5), 664-672.

7. Clark, C.M., Lee, D.A., "Prevention and treatment of the complications of diabetes mellitus," *New England Journal of Medicine* **1995,** 332, (18), 1210-1217.

8. The Diabetes Control and Complications Trial Research Group, "The effect of intensive treatment of diabetes on the development and progression of long-term complications in insulin-dependent diabetes mellitus," *New England Journal of Medicine* **1993,** 329, (14), 977-986.

9.   The Diabetes Control and Complications Trial Research Group, "Lifetime benefits and costs of intensive therapy as practiced in the diabetes control and complications trial," *Journal of the American Medical Association* **1996**, 276, (17), 1409-15.10.

10. American Diabetes Association, "Economic Costs of Diabetes in the U.S. in 2002," *Diabetes Care* **2003**, 26, (3), 917-932.

11. Evans, J.M.M., Newton, R.W., Ruta, D.A., MacDonald, T.M., Stevenson, R.J., Morris, A.D., "Frequency of blood glucose monitoring in relation to glycaemic control: observational study with diabetes database," *British Medical Journal* **1999**, 319, (7202), 83-86.

12. Harris, M.I., "Frequency of blood glucose monitoring in relation to glycemic control in patients with Type 2 diabetes," *Diabetes Care* **2001**, 24, (6), 979-982.

13. Kennedy, L., "Self-Monitoring of Blood Glucose in Type 2 Diabetes: Time for evidence of efficacy," *Diabetes Care* **2001**, 24, (6), 977-978.

14. Koschinsky, T., Heinemann, L., "Sensors for glucose monitoring: technical and clinical aspects,". *Diabetes/Metabolism Research and Reviews* **2001**, 17, (2), 113-123.

15. Louie, R.F., Tang, Z., Sutton, D.V, Lee, J.H., Kost, G.J., "Point-of-care glucose testing: effects of critical care variables, influence of reference instruments, and a modular glucose meter design," *Archives of Pathology and Laboratory Medicine* **2000**, 124, (2), 257-66.

16. Klonoff, D.C., "Current, emerging, and future trends in metabolic monitoring," *Diabetes Technology and Theraputics* **2002**, 4, (5), 583-8.

17. Buckingham, B., "Analysis: dawn of real-time continuous glucose sensing," *Diabetes Technology and Theraputics* **2003**, 5, (3), 381-3.

18. Potts, R.O., Tamada, J.A., Tierney, M.J., "Glucose monitoring by reverse iontophoresis," *Diabetes/Metabolism Research and Reviews* **2002**, 18, (S1), S49-S53.

19. Pickup, J. C., Hussain, F., Evans, N.D., Rolinski, O.J., Birch, D.J.S., "Fluorescence-based glucose sensors," *Biosensors and Bioelectronics* **2005**, 20, (12), 2555.

20. Amerov, A.K., Chen, J., Small,G.W., Arnold, M.A., "Scattering and absorption effects in the determination of glucose in whole blood by near-infrared spectroscopy," *Analytical Chemistry* **2005**, 77, (14), 4587-4594.

21. Stuart, D.A., Yonzon, C.R., Zhang, X., Lyandres, O., Shah, N.C. Glucksberg, M.R., Walsh, J.T., VanDuyne, R.P., "Glucose Ssnsing using near-infrared surface-enhanced raman spectroscopy: gold surfaces, 10-day stability, and improved accuracy," *Analytical Chemistry* **2005**, 77, (13), 4013-4019.

22. Wan, Q., Cote, G.L., Dixon, J.B., "Dual-wavelength polarimetry for monitoring glucose in the presence of varying birefringence," *Journal of Biomedical Optics* **2005**, 10, (2), 024029.

23. Russell, R.J., Pishko, M.V., Gefrides, C.C., McShane, M.J., Cote, G.L., "A fluorescence-based glucose biosensor using concanavalin A and dextran encapsulated in a poly(ethylene glycol) hydrogel," *Analytical Chemistry* **1999**, 71, (15), 3126-32.

24. McShane, M.J., "Potential for glucose monitoring with nanoengineered fluorescent biosensors," *Diabetes Technolgy and Theraputics* **2002**, 4, (4), 533-8.

25. McShane, M.J., Rastegar, S., Pishko, M., Cote, G.L., "Monte Carlo modeling for implantable fluorescent analyte sensors," *IEEE Transactions on Biomedical Engineering* **2000**, 47, (5), 624-32.

26. McShane, M.J., "Microcapsules as "smart tattoo" glucose sensors: engineering systems with enzymes and glucose-binding sensing elements," In *Topics in Fluorescence Spectroscopy*, Geddes, C. D.; Lakowicz, J. R., Eds. Springer: New York, 2006; Vol. 11.

27. Chinnayelka, S., McShane, M.J., "Microcapsule biosensors using competitive binding resonance energy transfer assays based on apoenzymes," *Analytical Chemistry* **2005**, 77, (17), 5501-5511.

28. D'Auria, S., DiCesare, N., Staiano, M., Gryczynski, Z., Rossi, M., Lakowicz, J.R., "A novel fluorescence competitive assay for glucose determinations by using a thermostable glucokinase from the thermophilic microorganism Bacillus stearothermophilus," *Analytical Biochemistry* **2002**, 303, (2), 138-44.

29. D'Auria, S., Herman, P., Rossi, M., Lakowicz, J.R., "The fluorescence emission of the apo-glucose oxidase from Aspergillus niger as probe to estimate glucose concentrations," *Biochemical and Biophysical Research Communications* **1999**, 263, (2), 550-3.

30. Barone, P.W., Baik, S., Heller, D.A., Strano, M.S., "Near-infrared optical sensors based on single-walled carbon nanotubes," *Nature Materials* **2005**, 4, (1), 86.

31. Ibey, B.L., Beier, H.T., Rounds, R.M., Cote, G.L., Yadavalli, V.K., Pishko, M.V., "Competitive binding assay for glucose based on glycodendrimer-fluorophore conjugates," *Analytical Chemistry* **2005**, 77, (21), 7039-7046.

32.	Ballerstadt, R., Polak, A., Beuhler, A., Frye, J., "In vitro long-term performance study of a near-infrared fluorescence affinity sensor for glucose monitoring," *Biosensors and Bioelectronics* **2004,** 19, (8), 905.

33.	Ballerstadt, R., Schultz, J.S., A fluorescence affinity hollow fiber sensor for continuous transdermal glucose monitoring. *Analytical Chemistry* **2000,** 72, (17), 4185.

34.	Moschou, E.A., Sharma, B.V., Deo, S.K., Daunert, S., "Fluorescence glucose detection: advances toward the ideal in vivo biosensor," *Journal of Fluorescence* **2004,** 14, (5), 535-47.

35.	Zhu, H., Srivastava, R., Brown, J.Q., McShane, M.J., "Combined physical and chemical immobilization of glucose oxidase in alginate microspheres improves stability of encapsulation and activity," *Bioconjugate Chemistry* **2005,** 16, (6), 1451-1458.

36.	Wolfbeis, O.S., Oehme, I., Papkovskaya, N., Klimant, I., "Sol-gel based glucose biosensors employing optical oxygen transducers, and a method for compensating for variable oxygen background," *Biosensors and Bioelectronics* **2000,** 15, (1), 69-76.

37.	Papkovsky, D.B., "Luminescent porphyrins as probes for optical (bio)sensors," *Sensors and Actuators, B: Chemical* **1993,** B11, (1-3), 293.

38.	Rosenzweig, Z., Kopelman, R., "Analytical properties and sensor size effects of a micrometer-sized optical fiber glucose biosensor," *Analytical Chemistry* **1996,** 68, (8), 1408-13.

39.	Xu, H., Aylott, J.W., Kopelman, R., "Fluorescent nano-PEBBLE sensors designed for intracellular glucose imaging," *The Analyst* **2002,** 127, 1471-1477.

40.	Decher, G., "Fuzzy nanoassemblies: toward layered polymeric multicomposites," *Science* **1997,** 277, (5330), 1232-1237.

41.	Brown, J.Q., McShane, M.J., "Modeling of spherical fluorescent glucose microsensor systems: Design of enzymatic smart tattoos," *Biosensors and Bioelectronics* **2006,** 21, (9), 1760-1769.

42.	Koo, Y.L., Cao, Y., Kopelman, R., Koo, S.M., Brasuel, M., Philbert, M.A., "Real-time measurements of dissolved oxygen inside live cells by organically modified silicate fluorescent nanosensors," *Analytical Chemistry* **2004,** 76, (9), 2498-2505.

43.	Wolfbeis, O.S., "Materials for fluorescence-based optical chemical sensors," *Journal of Materials Chemistry* **2005,** 15, (27-28), 2657-2669.

44.	Papkovsky, D.B., O'Riordan, T.C., "Emerging applications of phosphorescent metalloporphyrins," *Journal of Fluorescence* **2005,** 15, (4), 569-584.

45. Lu, X., Manners, I., Winnik, M.A., "Polymer/silica composite films as luminescent oxygen sensors," *Macromolecules* **2001**, 34, (6), 1917-1927.

46. Han, B.H., Manners, I., Winnik, M.A., "Oxygen sensors based on mesoporous silica particles on layer-by-layer self-assembled films," *Chemistry of Materials* **2005**, 17, (12), 3160-3171.

47. Sieg, A., Guy, R.H., Delgado-Charro, M.B., "Noninvasive and minimally invasive methods for transdermal glucose monitoring," *Diabetes Technology and Theraputics* **2005**, 7, (1), 174-97.

48. Sieg, A., Guy, R.H., Delgado-Charro, M.B., "Noninvasive glucose monitoring by reverse iontophoresis in vivo: application of the internal standard concept," *Clinical Chemistry* **2004**, 50, (8), 1383-90.

49. Sieg, A., Guy, R.H., Delgado-Charro, M.B., "Reverse iontophoresis for noninvasive glucose monitoring: the internal standard concept," *Journal of Pharmaceutical Sciences* **2003**, 92, (11), 2295-302.

50. Tierney, M.J., Tamada, J.A., Potts, R.O., Jovanovic, L., Garg, S., "Clinical evaluation of the GlucoWatch(R) biographer: a continual, non-invasive glucose monitor for patients with diabetes," *Biosensors and Bioelectronics* **2001**, 16, (9-12), 621-629.

51. Klonoff, D.C., "Continuous Glucose Monitoring: Roadmap for 21st century diabetes therapy," *Diabetes Care* **2005**, 28, (5), 1231-1239.

52. Bode, B., Gross, K., Rikalo, N., Schwartz, S., Wahl, T., Page, C., Gross, T., Mastrototaro, J., "Alarms based on real-time sensor glucose values alert patients to hypo- and hyperglycemia: the guardian continuous monitoring system," *Diabetes Technology and Theraputics* **2004**, 6, (2), 105-13.

53. Chee, F., Fernando, T., van Heerden, P.V., "Closed-loop glucose control in critically ill patients using continuous glucose monitoring system (CGMS) in real time," *IEEE Transactions on Information Technology in Biomedicine* **2003**, 7, (1), 43-53.

54. Clarke, W.L., "The original Clarke Error Grid Analysis (EGA)," *Diabetes Technology and Theraputics* **2005**, 7, (5), 776-9.

55. Clarke, W.L., Anderson, S., Farhy, L., Breton, M., Gonder-Frederick, L., Cox, D., Kovatchev, B., "Evaluating the clinical accuracy of two continuous glucose sensors using continuous glucose-error grid analysis," *Diabetes Care* **2005**, 28, (10), 2412-7.

56. Poscia, A., Mascini, M., Moscone, D., Luzzana, M., Caramenti, G., Cremonesi, P., Valgimigli, F., Bongiovanni, C., Varalli, M., "A microdialysis technique for continuous subcutaneous glucose monitoring in diabetic patients (part 1)," *Biosensors and Bioelectronics* **2003**, 18, (7), 891-898.

57. Varalli, M., Marelli, G., Maran, A., Bistoni, S., Luzzana, M., Cremonesi, P., Caramenti, G., Valgimigli, F., Poscia, A., "A microdialysis technique for continuous subcutaneous glucose monitoring in diabetic patients (part 2)," *Biosensors and Bioelectronics* **2003**, 18, (7), 899-905.

58. Heinemann, L., "Continuous glucose monitoring by means of the microdialysis technique: underlying fundamental aspects," *Diabetes Technology and Theraputics* **2003**, 5, (4), 545-61.

59. Mitragotri, S., Blankschtein, D., Langer, R., "Transdermal drug delivery using low-frequency sonophoresis," *Pharmaceutical Research* **1996**, 13, (3), 411-420.

60. Mitragotri, S., Kost, J., "Low-frequency sonophoresis: a review," *Advanced Drug Delivery Reviews* **2004**, 56, (5), 589-601.

61. Chuang, H., Taylor, E., Davison, T.W., "Clinical evaluation of a continuous minimally invasive glucose flux sensor placed over ultrasonically permeated skin," *Diabetes Technology and Theraputics* **2004**, 6, (1), 21-30.

62. Van Gemert, M.J.C., Jacques, S.L., Sterenborg, H.J., Star, W.M., "Skin optics," *IEEE Transactions on Biomedical Engineering* **1989**, 36, (12), 1146-1154.

63. Khalil, O.S., "Spectroscopic and clinical aspects of noninvasive glucose measurements," *Clinical Chemistry* **1999**, 45, (2), 165-177.

64. Malin, S.F., Ruchti, T.L., Blank, T.B., Thennadil, S.N., Monfre, S.L., "Noninvasive prediction of glucose by near-infrared diffuse reflectance spectroscopy," *Clinical Chemistry* **1999**, 45, (9), 1651-8.

65. Khalil, O.S., "Non-invasive glucose measurement technologies: an update from 1999 to the dawn of the new millennium," *Diabetes Technology and Theraputics* **2004**, 6, (5), 660-97.

66. Arnold, M.A., Burmeister, J.J., Small, G.W., "Phantom glucose calibration models from simulated noninvasive human near-infrared spectra," *Analytical Chemistry* **1998**, 70, (9), 1773-81.

67. Brown, C.D., Davis, H.T., Ediger, M.N., Fleming, C.M., Hull, E.L., Rohrscheib, M., "Clinical assessment of near-infrared spectroscopy for noninvasive diabetes screening," *Diabetes Technology and Theraputics* **2005**, 7, (3), 456-66.

68. Bruulsema, J.T., Hayward, J.E., Farrell, T.J., Patterson, M.S., Heinemann, L., Berger, M., Koschinsky, T., Sandahl-Christiansen, J., Orskov, H., Essenpreis, M., Schmelzeisen-Redeker, G., Bocker, D., "Correlation between blood glucose concentration in diabetics and noninvasively measured tissue optical scattering coefficient," *Optics Letters* **1997**, 22, (3), 190.

69. Heinemann, L., Kramer, U., Klotzer, H.M., Hein, M., Volz, D., Hermann, M., Heise, T., Rave, K., "Noninvasive glucose measurement by monitoring of scattering coefficient during oral glucose tolerance tests. Non-Invasive Task Force," *Diabetes Technology and Theraputics* **2000**, 2, (2), 211-20.

70. Heinemann, L., Schmelzeisen-Redeker, G., "Non-invasive continuous glucose monitoring in Type I diabetic patients with optical glucose sensors. Non-Invasive Task Force (NITF)," *Diabetologia* **1998**, 41, (7), 848-54.

71. Cohen, O., Fine, I., Monashkin, E., Karasik, A., "Glucose correlation with light scattering patterns--a novel method for non-invasive glucose measurements," *Diabetes Technology and Theraputics* **2003**, 5, (1), 11-7.

72. Fercher, A.F., Drexler, W., Hitzenberger, C.K., Lasser, T., "Optical coherence tomography - principles and applications," *Reports on Progress in Physics* **2003**, 66, (2), 239-303.

73. Schmitt, J.M., "Optical coherence tomography (OCT): a review," *Selected Topics in IEEE Journal of Quantum Electronics* **1999**, 5, (4), 1205-1215.

74. Hanlon, E.B., Manoharan, R., Koo, T.W., Shafer, K.E., Motz, J.T., Fitzmaurice, M., Kramer, J.R., Itzkan, I., Dasari, R.R., Feld, M.S., "Prospects for *in vivo* Raman spectroscopy," *Physics in Medicine and Biology* **2000**, 45, (2), R1-R59.

75. Pelletier, C.C., Lambert, J.L., Borchert, M., "Determination of glucose in human aqueous humor using Raman spectroscopy and designed-solution calibration," *Applied Spectroscopy* **2005**, 59, (8), 1024-1031.

76. Cote, G.L., Fox, M.D., Northrop, R.B., "Noninvasive optical polarimetric glucose sensing using a true phase measurement technique," *IEEE Transactions on Biomedical Engineering* **1992**, 39, (7), 752-6.

77. Cameron, B.D., Gorde, H.W., Satheesan, B., Cote, G.L., "The use of polarized laser light through the eye for noninvasive glucose monitoring," *Diabetes Technology and Theraputics* **1999**, 1, (2), 135-43.

78. Cameron, B.D., Cote, G.L., "Noninvasive glucose sensing utilizing a digital closed-loop polarimetric approach," *IEEE Transactions on Biomedical Engineering* **1997**, 44, (12), 1221-7.

79. Baba, J.S., Cameron, B.D., Theru, S., Cote, G.L., "Effect of temperature, pH, and corneal birefringence on polarimetric glucose monitoring in the eye," *Journal of Biomedical Optics* **2002,** 7, (3), 321-8.

80. MacKenzie, H.A., Ashton, H.S., Spiers, S., Shen, Y., Freeborn, S.S., Hannigan, J., Lindberg, J., Rae, P., "Advances in Photoacoustic Noninvasive Glucose Testing," *Clinical Chemistry* **1999,** 45, (9), 1587-1595.

81. Caduff, A., Dewarrat, F., Talary, M., Stalder, G., Heinemann, L., Feldman, Y., "Non-invasive glucose monitoring in patients with diabetes: A novel system based on impedance spectroscopy," *Biosensors and Bioelectronics* In Press, Corrected Proof.

82. Caduff, A., Hirt, E., Feldman, Y., Ali, Z., Heinemann, L., "First human experiments with a novel non-invasive, non-optical continuous glucose monitoring system," *Biosensors and Bioelectronics* **2003,** 19, (3), 209-217.

83. Weiss, S., "Fluorescence spectroscopy of single biomolecules," *Science* **1999,** 283, (5408), 1676-1683.

84. Fang, H., Kaur, G., Wang, B., "Progress in boronic acid-based fluorescent glucose sensors," *Journal of Fluorescence* **2004,** 14, (5), 481.

85. Yoon, J., Czarnik, A.W., "Fluorescent chemosensors of carbohydrates. A means of chemically communicating the binding of polyols in water based on chelation-enhanced quenching," *Journal of the American Chemical Society* **1992,** 114, (14), 5874.

86. James, T.D., Samankumara, K.R., Shinkai, S., "Novel photoinduced electron-transfer sensor for saccharides based on the interaction of boronic acid and amine," *Chemical Communications* **1994,** 4, 477-478.

87. James, T.D., Samankumara, K.R., Iguchi, R., Shinkai, S., "Novel saccharide-photoinduced electron transfer sensors based on the interaction of boronic acid and amine," *Journal of the American Chemical Society* **1995,** 117, (35), 8982.

88. Appleton, B., Gibson, T.D., "Detection of total sugar concentration using photoinduced electron transfer materials: development of operationally stable, reusable optical sensors," *Sensors and Actuators, B: Chemical* **2000,** 65, (1), 302-304.

89. Gurpreet, G., Lin, N., Fang, H., Wang, B., "Boronic acid-based fluorescence sensors for glucose monitroing," In *Topics in Fluorescence Spectroscopy,* Geddes, C.D., Lakowicz, J. R., Eds. Springer: New York, 2006, Vol. 11.

90. Phillips, M.D., James, T.D., "Boronic Acid Based Modular Fluorescent Sensors for Glucose," *Journal of Fluorescence* **2004,** 14, (5), 549-559.

91.   Heagy, M.D., "*N*-phenylboronic acid derivatives of arenecarboximides as saccharide probes with virtual spacer design," In *Topics in Fluorescence Spectroscopy*, Geddes, C.D., Lakowicz, J.R., Eds. Springer: New York, 2006, Vol. 11.

92.   Cao, H., Diaz, D.I., DiCesare, N., Lakowicz, J.R., Heagy, M.D., "Monoboronic acid sensor that displays anomalous fluorescence sensitivity to glucose," *Organic Letters* **2002**, 4, (9), 1503-5.

93.   Cordes, D.B., Suri, J.T., Cappuccio, F.E., Camara, J.N., Gamsey, S., Sharrett, Z., Thoniyot, P., Wessling, R.A., Singaram, B., "Two-component optical sugar sensing using boronic acid-substituted viologens with anionic fluorescent dyes," In *Topics in Fluorescence Spectroscopy*, Geddes, C.D., Lakowicz, J.R., Eds. Springer: New York, 2006, Vol. 11.

94.   Cordes, D.B., Miller, A., Gamsey, S., Sharrett, Z., Thoniyot, P., Wessling, R., Singaram, B., "Optical glucose detection across the visible spectrum using anionic fluorescent dyes and a viologen quencher in a two-component saccharide sensing system," *Organic and Biomolecular Chemistry* **2005**, 3, (9), 1708.

95.   Badugu, R., Lakowicz, J.R., Geddes, C.D., "Development of smart contact lenses for ophthalmic glucose monitoring," In *Topics in Fluorescence Spectroscopy*, Geddes, C.D., Lakowicz, J.R., Eds. Springer: New York, 2006, Vol. 11.

96.   Badugu, R., Lakowicz, J.R., Geddes, C.D. "A Glucose sensing contact lens: A new approach to non-invasive continuous physiological glucose monitoring," San Jose, CA, United States, 2004, International Society for Optical Engineering, Bellingham, WA 98227-0010, United States: San Jose, CA, United States, 2004, p 234.

97.   Badugu, R., Lakowicz, J.R., Geddes, C.D., "Ophthalmic glucose monitoring using disposable contact lenses - A review," *Journal of Fluorescence* **2004**, 14, (5), 617.

98.   Lakowicz, J.R., *Principles of fluorescence spectroscopy*. 2nd ed., Kluwer Academic/Plenium: New York, 1999.

99.   Schultz, J.S., Mansouri, S., Goldstein, I.J., "Affinity sensor: a new technique for developing implantable sensors for glucose and other metabolites," *Diabetes Care* **1982**, 5, (3), 245-253.

100.   Meadows, D.L., Schultz, J.S., "Design, manufacture and characterization of an optical fiber glucose affinity sensor based on an homogeneous fluorescence energy transfer assay system," *Analytica Chimica Acta* **1993**, 280, (1), 21-30.

101.   Lakowicz, J.R., Maliwal, B., "Optical sensing of glucose using phase-modulation fluorimetry," *Analytica Chimica Acta* **1993**, 271, (1), 155-164.

102. Tolosa, L., Malak, H., Raob, G., Lakowicz, J.R., "Optical assay for glucose based on the luminescence decay time of the long wavelength dye Cy5," *Sensors and Actuators, B: Chemical* **1997,** B45, (2), 93-99.

103. Tolosa, L., Szmacinski, H., Rao, G., Lakowicz, J.R., "Lifetime-based sensing of glucose using energy transfer with a long lifetime donor," *Analytical Biochemistry* **1997,** 250, (1), 102-108.

104. Ballerstadt, R., Evans, C., Gowda, A., McNichols, R., "In vivo performance evaluation of a transdermal near-infrared fluorescence resonance energy transfer affinity Sensor for Continuous Glucose Monitoring," *Diabetes Technology & Therapeutics* **2006,** 8, (3), 296-311.

105. Chinnayelka, S., McShane, M.J., "Resonance energy transfer nanobiosensors based on affinity binding between apo-enzyme and its substrate," *Biomacromolecules* **2004,** 5, (5), 1657.

106. Chinnayelka, S. Microcapsule biosensors based on competitive binding and fluorescence resonance energy transfer assays. Louisiana Tech University, 2005.

107. Trettnak, W., Wolfbeis, O.S., "Fully reversible fibre-optic glucose biosensor based on the intrinsic fluorescence of glucose oxidase," *Analytica Chimica Acta* **1989,** 221, 195-203.

108. Sierra, J.F., Galban, J., De Marcos, S., Castillo, J.R., "Direct determination of glucose in serum by fluorimetry using a labeled enzyme," *Analytica Chimica Acta* **2000,** 414, (1-2), 33-41.

109. Chinnayelka, S., McShane, M.J., "Glucose-sensitive nanoassemblies comprising affinity-binding complexes trapped in fuzzy microshells," *Journal of Fluorescence* **2004,** 14, (5), 585.

110. D'Auria, S., Di Cesare, N., Gryczynski, Z., Gryczynski, I., Rossi, M., Lakowicz, J.R., "A Thermophilic Apoglucose Dehydrogenase as Nonconsuming Glucose Sensor," *Biochemical and Biophysical Research Communications* **2000,** 274, (3), 727-731.

111. Maity, H., Maiti, N.C., Jarori, G.K., "Time-resolved fluorescence of tryptophans in yeast hexokinase-PI: effect of subunit dimerization and ligand binding," *Journal of Photochemistry and Photobiology B: Biology* **2000,** 55, (1), 20-26.

112. Maity, H., Kasturi, S.R., "Interaction of bis(1-anilino-8-naphthalenesulfonate) with yeast hexokinase: a steady-state fluorescence study," *Journal of Photochemistry and Photobiology. B* **1998,** 47, (2-3), 190-6.

113. Hussain, F., Birch, D.J.S., Pickup, J.C., "Glucose sensing based on the intrinsic fluorescence of sol-gel immobilized yeast hexokinase," *Analytical Biochemistry* **2005**, 339, (1), 137-143.

114. Marvin, J.S., Hellinga, H.W., "Engineering biosensors by introducing fluorescent allosteric signal transducers: construction of a novel glucose sensor," *Journal of the American Chemical Society* **1998**, 120, (1), 7-11.

115. Tolosa, L., Gryczynski, I., Eichhorn, L.R., Dattelbaum, J.D., Castellano, F.N., Rao, G., Lakowicz, J.R., "Glucose Sensor for Low-Cost Lifetime-Based Sensing Using a Genetically Engineered Protein," *Analytical Biochemistry* **1999**, 267, (1), 114-120.

116. Ye, K., Schultz, J.S., "Genetic engineering of an allosterically based glucose indicator protein for continuous glucose monitoring by fluorescence resonance energy transfer," *Analytical Chemistry* **2003**, 75, (14), 3451-3459.

117. Trettnak, W., Leiner, M.J.P., Wolfbeis, O.S., "Fibre-optic glucose sensor with a pH optrode as the transducer," *Biosensors* **1989**, 4, (1), 15-26.

118. McCurley, M.F., "Optical biosensor using a fluorescent, swelling sensing element," *Biosensors & Bioelectronics* **1994**, 9, (7), 527.

119. Mack, A.C., Jinshu, M., McShane, M.J., "Transduction of pH and glucose-sensitive hydrogel swelling through fluorescence resonance energy transfer," IEEE Sensors 2005 **2005**, 4.

120. Wolfbeis, O.S., Durkop, A., Wu, M., Lin, Z., "A europium-ion-based luminescent sensing probe for hydrogen peroxide," *Angewandte Chemie - International Edition* **2002**, 41, (23), 4495.

121. Wu, M., Lin, Z., Durkop, A., Wolfbeis, O.S., "Time-resolved enzymatic determination of glucose using a fluorescent europium probe for hydrogen peroxide," *Analytical and Bioanalytical Chemistry* **2004**, 380, (4), 619-626.

122. Duerkop, A., Schaeferling, M., Wolfbeis, O.S., "Glucose sensing and glucose determination using fluroescenct probes and molecular receptors," In *Topics in Fluorescence Spectroscopy*, Geddes, C.D., Lakowicz, J.R., Eds. Springer: New York, 2006, Vol. 11.

123. Lubbers, D.W., Opitz, N., "Optical fluorescence sensors for continuous measurement of chemical concentrations in biological systems," *Sensors and Actuators* **1983**, 4, 641-654.

124. Trettnak, W., Leiner, M.J.P., Wolfbeis, O.S., "Optical sensors. Part 34. Fibre optic glucose biosensor with an oxygen optrode as the transducer," *The Analyst* **1988**, 113, 1519-1523.

125. Moreno-Bondi, M.C., Wolfbeis, O.S., Leiner, M.J.P., Schaffar, B.P.H., "Oxygen optrode for use in a fiber-optic glucose biosensor," *Analytical Chemistry* **1990**, 62, 2377-2380.

126. Bronk, K.S., Walt, D.R., "Fabrication of patterned sensor arrays with aryl azides on a polymer-coated imaging optical fiber bundle," *Analytical Chemistry* **1994**, 66, (20), 3519-20.

127. Li, L., Walt, D.R., "Dual-analyte fiber-optic sensor for the simultaneous and continuous measurement of glucose and oxygen," *Analytical Chemistry* **1995**, 67, (20), 3746-52.

128. Rosenzweig, Z., Kopelman, R., "Analytical properties of miniaturized oxygen and glucose fiber optic sensors," *Sensors and Actuators, B: Chemical* **1996**, B36, (1-3 pt 2), 475.

129. Rosenzweig, Z., Kopelman, R., "Development of a submicrometer optical fiber oxygen sensor," *Analytical Chemistry* **1995**, 67, (15), 2650-4.

130. Wu, X.J., Choi, M.M.F., "Optical enzyme-based glucose biosensors," In *Topics in Fluorescence Spectroscopy*, Geddes, C.D., Lakowicz, J.R., Eds. Springer: New York, 2006, Vol. 11.

131. Clark, H.A., Kopelman, R., Tjalkens, R., Philbert, M.A., "Optical nanosensors for chemical analysis inside single living cells. 2. Sensors for pH and calcium and the intracellular application of PEBBLE sensors," *Analytical Chemistry* **1999**, 71, (21), 4837-4843.

132. Clark, H.A., Hoyer, M., Philbert, M.A., Kopelman, R., "Optical nanosensors for chemical analysis inside single living cells. 1. Fabrication, characterization, and methods for intracellular delivery of PEBBLE sensors," *Analytical Chemistry* **1999**, 71, (21), 4831-4836.

133. Brown, J.Q. *Modeling, design, and validation of fluorescent spherical enzymatic glucose microsensors using nanoengineered polyelectrolyte coatings.* Louisiana Tech university, 2005.

134. Guyton, A.C., Hall, J.E., *Textbook of Medical Physiology.* 10th ed., Saunders: Philadelphia, 2000.

135. Stucker, M., Struk, A., Altmeyer, P., Herde, M., Baumgartl, H., Lubbers, D.W., "The cutaneous uptake of atmospheric oxygen contributes significantly to the oxygen supply of human dermis and epidermis," *The Journal of Physiology* **2002**, 538, (3), 985-994.

136. Ibey, B.L., Cote, G.L., Yadavalli, V., Gant, V.A., Newmyer, K., Pishko, M.V. In "Analysis of Longer Wavelength AlexaFluor Dyes for Use in a Minimally Invasive Glucose Sensor," Cancun, Mexico, 2003, Institute of Electrical and Electronics Engineers Inc.: Cancun, Mexico, 2003, p 3446.

137. Brown, J.Q., Srivastava, R., McShane, M.J., "Encapsulation of glucose oxidase and an oxygen-quenched fluorophore in polyelectrolyte-coated calcium alginate microspheres as optical glucose sensor systems," *Biosensors and Bioelectronics* **2005**, 21, (1), 212-6.

138. Wolfbeis, O.S., Oehme, I., Papkovskaya, N., Klimant, I., "Sol-gel based glucose biosensors employing optical oxygen transducers, and a method for compensating for variable oxygen background," *Biosensors and Bioelectronics* **2000**, 15, (1-2), 69-76.

139. Choi, H.N., Kim, M.A., Lee, W.Y., "Amperometric glucose biosensor based on sol-gel-derived metal oxide/Nafion composite films," *Analytica Chimica Acta* **2005**, 537, (1-2), 179-187.

140. Wang, B., Li, B., Deng, Q., Dong, S., "Amperometric glucose biosensor based on sol-gel organic-inorganic hybrid material," *Analytical Chemistry* **1998**, 70, (15), 3170-3174.

141. Pandey, P.C., Upadhyay, S., Pathak, H.C., "New glucose sensor based on encapsulated glucose oxidase within organically modified sol-gel glass," *Sensors and Actuators, B: Chemical* **1999**, B60, (2-3), 83-89.

142. Lvov, Y., *Electrostatic layer-by-layer assembly of proteins and polyions.* M.Dekker: New York, 2000, p 125-167.

143. Schonhoff, M., "Self-assembled polyelectrolyte multilayers," *Current Opinion in Colloid & Interface Science* **2003**, 8, (1), 86-95.

144. Liu, X., Bruening, M.L., "Size-selective transport of uncharged solutes through multilayer polyelectrolyte membranes," *Chemistry of Materials* **2004**, 16, (2), 351-357.

145. Bruening, M.L., Sullivan, D.M., "Enhancing the ion-transport selectivity of multilayer polyelectrolyte membranes," *Chemistry - A European Journal* **2002**, 8, (17), 3832-3837.

146. Miller, M.D., Bruening, M.L., "Controlling the nanofiltration properties of multilayer polyelectrolyte membranes through variation of film composition," *Langmuir* **2004**, 20, (26), 11545-11551.

147. Stanton, B.W., Harris, J.J., Miller, M.D., Bruening, M.L., "Ultrathin, multilayered polyelectrolyte films as nanofiltration membranes," *Langmuir* **2003**, 19, (17), 7038-7042.

148.   Harris, J.J., Stair, J.L., Bruening, M.L., "Layered polyelectrolyte films as selective, ultrathin barriers for anion transport," *Chemistry of Materials* **2000**, 12, (7), 1941-1946.

149.   Miller, M.D., Bruening, M.L., "Correlation of the swelling and permeability of polyelectrolyte multilayer films," *Chemistry of Materials* **2005**, 17, (21), 5375-5381.

150.   Amao, Y., "Probes and polymers for optical sensing of oxygen," *Microchimica Acta* **2003**, 143, (1), 1-12.

151.   Grant, P.S., McShane, M.J., "Development of multilayer fluorescent thin film chemical sensors using electrostatic self-assembly," *IEEE Sensors Journal* **2003**, 3, (2), 139.

152.   Wolfbeis, O.S., Oehme, I., Papkovskaya, N., Klimant, I., "Sol-gel based glucose biosensors employing optical oxygen transducers, and a method for compensating for variable oxygen background," *Biosensors and Bioelectronics* **2000**, 15, (1), 69.

153.   Morin, A.M., Xu, W., Demas, J.N., DeGraff, B.A., "Oxygen sensors based on quenching of tris-(4,7-diphenyl-1,10-phenanthroline)ruthenium(II) in fluorinated polymers," *Journal of Fluorescence* **2000**, 10, (1), 7-12.

154.   Pickup, J.C., Hussain, F., Evans, N.D., Sachedina, N., "In vivo glucose monitoring: The clinical reality and the promise," *Biosensors and Bioelectronics* **2005**, 20, (10 SPEC ISS), 1897.

155.   Chinnayelka, S., McShane, M.J., "Glucose-sensitive nanoassemblies comprising affinity-binding complexes trapped in fuzzy microshells," *Journal of Fluorescence* **2004**, 14, (5), 585-95.

156.   Chinnayelka, S., McShane, M.J., "Resonance energy transfer nanobiosensors based on affinity binding between apo-enzyme and its substrate," *Biomacromolecules* **2004**, 5, (5), 1657-61.

157.   Brasuel, M., Kopelman, R., Miller, T.J., Tjalkens, R., Philbert, M.A., Fluorescent nanosensors for intracellular chemical analysis: decyl methacrylate liquid polymer matrix and ion-exchange-based potassium PEBBLE sensors with real-time application to viable rat C6 glioma cells. *Analytical Chemistry* **2001**, 73, (10), 2221-2228.

158.   Zhu, H., Stein, E.W., McShane, M.J., *Science* **2006**, Submitted.

159.   Stein, E.W., Zhu, H., McShane, M.J., *Journal of the American Chemical Society* **2006**, Submitted.

160. Sukhorukov, G., Dahne, L., Hartman, J. Donath, E., Mohwald, H.,L., "Controlled precipitation of dyes into hollow polyelectrolyte capsules based on colloids and biocolloids," *Advanced Materials* **2000**, 12, (2), 112-115.

161. Brinkley, M., A brief survey of methods for preparing protein conjugates with dyes, haptens, and cross-linking reagents. *Bioconjugate Chemistry* **1992**, 3, (1), 2-13.

162. Evans, N.T., Naylor, P.F., "The dynamics of changes in dermal oxygen tension," *Respiration Physiology* **1966**, 2, (1), 61-72.

163. Eaton, K., Douglas, B., Douglas, P., "Luminescent oxygen sensors: Time-resolved studies and modelling of heterogeneous oxygen quenching of luminescence emission from Pt and Pd octaethylporphyrins in thin polymer films," *Sensors and Actuators, B: Chemical* **2004**, 97, (1), 2.

164. Carraway, E.R., Demas, J.N., DeGraff, B.A., "Photophysics and oxygen quenching of transition-metal complexes on fumed silica," *Langmuir* **1991**, 7, (12), 2991-2998.

165. Chinnayelka, S., McShane, M.J., "Glucose sensors based on microcapsules containing an orange/red competitive binding resonance energy transfer assay," *Diabetes Technology and Theraputics* **2006**, 8, (3), 269-78.

166. Brown, J.Q., Srivastava, R., Zhu, H., McShane, M.J., "Enzymatic fluorescent microsphere glucose sensors:evaluation of response under dynamic conditions," *Diabetes Technology & Therapeutics* **2006**, 8, (3), 288-295.

167. Rosenzweig, Z., Kopelman, R., "Analytical properties and sensor size effects of a micrometer sized optical fiber glucose biosensor," *Analytical Chemistry* **1996**, 68, (8), 1408.

168. Lowry, O.H., Rosebrough, N.J., Farr, A.L., Randall, R.J., "Protein measurement with the folin phenol Rreagent," *Journal of Biological Chemistry* **1951**, 193, (1), 265-275.

169. Pazur, J.H., Kleppe, K., "The oxidation of glucose and related compounds by glucose oxidase from Aspergillus Niger," *Biochemistry* **1964**, 3, 578-83.

170. McDonagh, C., MacCraith, B.D., McEvoy, A.K., "Tailoring of sol-gel films for optical sensing of oxygen in gas and aqueous phase," *Analytical Chemistry* **1998**, 70, (1), 45-50.

171. Tohver, V., Smay, J.E., Braem, A., Braun, P.V., Lewis, J.A., "From the cover: nanoparticle halos: a new colloid stabilization mechanism," *Proceedings of the National Academy of Sciences of the United States of America* **2001**, 98, (16), 8950-8954.

172. Wirnsberger, G., Yang, P., Huang, H.C., Scott, B., Deng, T., Whitesides, G.M., Chmelka, B.F., Stucky, G.D., "Patterned block-copolymer-silica mesostructures as host media for the laser dye rhodamine 6G," *The Journal of Physical Chemistry. B* **2001**, 105, (27), 6307-6313.

173. Coppi, G., Iannuccelli, V., Leo, E., Bernabei, M.T., Cameroni, R., "Protein immobilization in crosslinked alginate microparticles," *Journal of Microencapsulation* **2002**, 19, (1), 37-44.

174. Kulcu, E., Tamada, J.A., Reach, G., Potts, R.O., Lesho, M.J., "Physiological differences between interstitial glucose and blood glucose measured in human subjects," *Diabetes Care* **2003**, 26, (8), 2405-2409.

175. Ben-Ami, H., Nagachandran, P., Mendelson, A., Edoute, Y., "Drug-induced hypoglycemic coma in 102 diabetic patients," *Archives of Internal Medicine* **1999**, 159, (3), 281-4.

176. Brunner, G.A., Ellmerer, M., Sendlhofer, G., Wutte, A., Trajanoski, Z., Schaupp, L., Quehenberger, F., Wach, P., Krejs, G.J., Pieber, T.R., "Validation of home blood glucose meters with respect to clinical and analytical approaches," *Diabetes Care* **1998**, 21, (4), 585-590.

177. Philip, E.C., "Hypoglycemia is the limiting factor in the management of diabetes," *Diabetes/Metabolism Research and Reviews* **1999**, 15, (1), 42-46.

178. Chen, T., Friedman, K.A., Lei, I., Heller, A., "In situ assembled mass-transport controlling micromembranes and their application in implanted amperometric glucose sensors," *Analytical Chemistry* **2000**, 72, (16), 3757-3763.

179. Tse, P. H. S., Gough, D. A., "Time-Dependent Inactivation of Immobilized Glucose Oxidase and Catalase," *Biotechnology and Bioengineering* **1987**, 29, (6), 705-713.

180. Malikkides, C.O., Weiland, R.H., "On the Mechanism of immobilized glucose oxidase deactivation by hydrogen peroxide," *Biotechnology and Bioengineering* **1982**, 24, (11), 2419-2439.

181. Flora, K.K., Brennan, J.D., "Effect of matrix aging on the behavior of human serum albumin entrapped in a tetraethyl orthosilicate-derived glass," *Chemistry of Materials* **2001**, 13, (11), 4170-4179.

182. Nguyen, D.T., Smit, M., Dunn, B., Zink, J.I., "Stabilization of creatine kinase encapsulated in silicate sol-gel materials and unusual temperature effects on its activity," *Chemistry of Materials* **2002**, 14, (10), 4300-4306.

183. Healey, B.G., Li, L., Walt, D.R., "Multianalyte biosensors on optical imaging bundles," *Biosensors & Bioelectronics* **1997**, 12, (6), 521.

184.   Ikomi, F., Hanna, G.K., Schmid-Schonbein, G.W., "Mechanism of colloidal particle uptake into the lymphatic system: basic study with percutaneous lymphography," *Radiology* **1995**, 196, (1), 107-113.

185.   Ai, H., Lvov, Y. M., Mills, D.K., Jennings, M., Alexander, J.S., Jones, S. A., "Coating and selective deposition of nanofilm on silicone rubber for cell adhesion and growth," *Cell Biochemistry and Biophysics* **2003**, 38, (2), 103-14.

186.   Netrabukkana, R., Lourvanij, K., Rorrer, G.L., "Diffusion of glucose and glucitol in microporous and mesoporous silicate/aluminosilicate catalysts," *Industrial and Engineering Chemistry Research* **1996**, 35, (2), 458-464.

187.   Wang, L., Schonhoff, M., Mohwald, H., "Lipids coupled to polyelectrolyte multilayers: ultraslow diffusion and the dynamics of electrostatic interactions," *Journal of Physical Chemistriy, B* **2002**, 106, (35), 9135-9142.

188.   Anderson, J.M., "Inflammatory response to implants," *ASAIO Transactions* **1988**, 34, (2), 101-7.

189.   Srivastava, R. *Application of self-assembled ultrathin film coatings to stabilize enzyme encapsulation and activity in alginate microspheres*. Louisiana Tech university, 2005.

190.   Gouda, M.D., Singh, S.A., Rao, A.G., Thakur, M.S., Karanth, N.G., "Thermal inactivation of glucose oxidase. Mechanism and stabilization using additives," *Journal of Biological Chemistry* **2003**, 278, (27), 24324-33.

191.   Tse, P.H.S., Leypoldt, J.K., Gough, D.A., "Determination of the intrinsic kinetic constants of immobilized glucose oxidase and catalase," *Biotechnology and Bioengineering* **1987**, 29, (6), 696-704.

192.   Kleppe, K., "The effect of hydrogen peroxide on glucose oxidase from Aspergillus niger," *Biochemistry* **1966**, 5, (1), 139-43.

193.   Miron, J., Gonzalez, M.P., Vazquez, J.A., Pastrana, L., Murado, M.A., "A mathematical model for glucose oxidase kinetics, including inhibitory, deactivant and diffusional effects, and their interactions," *Enzyme and Microbial Technology* **2004**, 34, (5), 513-522.

194.   Stewart, P.S., "Diffusion in biofilms," *Journal of Bacteriology* **2003**, 185, (5), 1485-91.

195.   Lei, C., Shin, Y., Liu, J., Ackerman, E.J., "Entrapping enzyme in a functionalized nanoporous support," *Journal of the American Chemical Society* **2002**, 124, (38), 11242-11243.

196.   Basagaoglu, H., McCoy, B.J., Ginn, T.R., Loge, F.J., Dietrich, J.P., "A diffusion limited sorption kinetics model with polydispersed particles of distinct sizes and shapes," *Advances in Water Resources* **2002**, 25, (7), 755-772.

197.   Stein, E.W., Volodkin, D.V., McShane, M.J., Sukhorukov, G.B., "Real-time assessment of spatial and temporal couple catalysis with polyelectrolyte microcapsules containing coimmobilized glucose oxidase and peroxidase," *Biomacromolecules* **2006**, 7, 710-719.

198.   Cryer, P.E., Davis, S.N., Shamoon, H., "Hypoglycemia in Diabetes," *Diabetes Care* **2003**, 26, (6), 1902-1912.

199.   Parkes, J.L., Slatin, S.L., Pardo, S., Ginsberg, B.H., "A new concensus error grid to evaluate the clinical significance of innaccuracies in the measurement of blood glucose," *Diabetes Care* **2000**, 23, 1143-1148.

200.   Kamholz, A.E., Yager, P., "Theoretical Analysis of Molecular Diffusion in Pressure-Driven Laminar Flow in Microfluidic Channels," *Biophysical Journal* **2001**, 80, (1), 155-160.

201.   Lorenz, H., Despont, M., Fahrni, N., Brugger, J., Vettiger, P., Renaud, P., "High-aspect-ratio, ultrathick, negative-tone near-UV photoresist and its applications for MEMS," *Sensors and Actuators A: Physical* **1998**, 64, (1), 33-39.

202.   Xia, Y., Whitesides, G.M., "Soft lithography," In Annual Reviews Inc, Palo Alto, CA, USA: 1998, Vol. 28, pp 153-184.

203.   Christensen, A.M., Chang-Yen, D.A., Gale, B.K., "Characterization of interconnects used in PDMS microfluidic systems," *Journal of Micromechanics and Microengineering* **2005**, 15, (5), 928-934.

204.   Jo, B.H., Van Lerberghe, L.M., Motsegood, K.M., Beebe, D.J., "Three-dimensional micro-channel fabrication in polydimethylsiloxane (PDMS) elastomer," *Journal of Microelectromechanical Systems* **2000**, 9, (1), 76-81.

205.   Amirfeiz, P., Bengtsson, S., Bergh, M., Zanghellini, E., Borjesson, L., "Formation of silicon structures by plasma-activated wafer bonding," *Journal of the Electrochemical Society* **2000**, 147, (7), 2693-2698.

206.   Oh, S.H., Kim, J.K., Song, K.S., Noh, S.M., Ghil, S.H., Yuk, S.H., Lee, J.H., "Prevention of postsurgical tissue adhesion by anti-inflammatory drug-loaded pluronic mixtures with sol-gel transition behavior," *Journal of Biomedical Materials Research, A* **2005**, 72, (3), 306-16.

207.   Ibey, B.L., Pishko, M., Cote, G.L., "Implantable Concanavlin A based sensors for interstitial fluid glucose sensing in diabetics," In *Topics in Fluorescence Spectroscopy*, Geddes, C. D., Lakowicz, J. R., Eds. Springer: New York, 2006, Vol. 11.